

What is the Milky Way outer halo made of? ★, ★★, ★★★

High resolution spectroscopy of distant red giants

G. Battaglia^{1,2}, P. North³, P. Jablonka^{3,4}, M. Shetrone⁵, D. Minniti^{6,7,8}, M. Díaz⁹, E. Starkenburg¹⁰, and M. Savoy³

¹ Instituto de Astrofísica de Canarias, calle Via Lactea s/n, E-38205 La Laguna, Tenerife, Spain
e-mail: gbattaglia@iac.es

² Universidad de La Laguna, Dpto. Astrofísica, E-38206 La Laguna, Tenerife, Spain

³ Institute of Physics, Laboratory of Astrophysics, École Polytechnique Fédérale de Lausanne (EPFL), Observatoire de Sauverny, CH-1290 Versoix, Switzerland

⁴ GEPI, Observatoire de Paris, CNRS, Université de Paris Diderot, F-92195 Meudon, Cedex, France

⁵ University of Texas at Austin, McDonald Observatory, USA

⁶ Instituto Milenio de Astrofísica, Santiago, Chile

⁷ Departamento de Física, Facultad de Ciencias Exactas, Universidad Andres Bello, Av. Fernandez Concha 700, Las Condes, Santiago, Chile

⁸ Vatican Observatory, V00120 Vatican City State, Italy

⁹ Departamento de Astronomía, Universidad de Chile, Camino el Observatorio 1515, Las Condes, Santiago, Chile, Casilla 36-D

¹⁰ Leibniz-Institut für Astrophysik Potsdam (AIP) An der Sternwarte 16, 14482 Potsdam, Germany

Received: 01/09/2017; accepted: 02/10/2017

ABSTRACT

In a framework where galaxies form hierarchically, extended stellar haloes are predicted to be an ubiquitous feature around Milky Way-like galaxies and to consist mainly of the shredded stellar component of smaller galactic systems. The type of accreted stellar systems are expected to vary according to the specific accretion and merging history of a given galaxy, and so is the fraction of stars formed in-situ versus accreted. Analysis of the chemical properties of Milky Way halo stars out to large Galactocentric radii can provide important insights into the properties of the environment in which the stars that contributed to the build-up of different regions of the Milky Way stellar halo formed. In this work we focus on the outer regions of the Milky Way stellar halo, by determining chemical abundances of halo stars with large present-day Galactocentric distances, >15 kpc. The data-set we acquired consists of high resolution HET/HRS, Magellan/MIKE and VLT/UVES spectra for 28 red giant branch stars covering a wide metallicity range, $-3.1 \lesssim [\text{Fe}/\text{H}] \lesssim -0.6$. We show that the ratio of α -elements over Fe as a function of $[\text{Fe}/\text{H}]$ for our sample of outer halo stars is not dissimilar from the pattern shown by MW halo stars from solar neighborhood samples. On the other hand, significant differences appear at $[\text{Fe}/\text{H}] \gtrsim -1.5$ when considering chemical abundance ratios such as $[\text{Ba}/\text{Fe}]$, $[\text{Na}/\text{Fe}]$, $[\text{Ni}/\text{Fe}]$, $[\text{Eu}/\text{Fe}]$, $[\text{Ba}/\text{Y}]$. Qualitatively, this type of chemical abundance trends are observed in massive dwarf galaxies, such as Sagittarius and the Large Magellanic Cloud. This appears to suggest a larger contribution in the outer halo of stars formed in an environment with high initial star formation rate and already polluted by asymptotic giant branch stars with respect to inner halo samples.

Key words. stars:abundances - Galaxy:halo - Galaxy:structure - Galaxy:formation - Galaxies:interaction

1. Introduction

Extended stellar haloes containing a significant amount of streams and substructures are observed around the Milky Way (MW), M31, and there are indications that they may be a ubiquitous component of galaxies down to the scale of Large Magellanic Cloud (LMC)-like objects (e.g., for recent works and reviews, see Helmi 2008; McConnachie et al. 2009; Martínez-Delgado et al. 2009; Mouhcine et al. 2011; Rich et al. 2012).

Within the Λ Cold Dark Matter (Λ CDM) framework, stellar haloes are a natural outcome of the hierarchical build-up of

structures (e.g., Bullock & Johnston 2005; Cooper et al. 2010). High resolution N-body and hydro-dynamical simulations (e.g., Zolotov et al. 2009; Tissera et al. 2012, 2013, 2014; Pillepich et al. 2014) show that stellar haloes are expected to consist both of stars formed within the virial radius of the main progenitor, for instance in a disk structure from the dissipative collapse of smoothly accreted cold gas at high-redshift and later on put on halo orbits by some violent event, and by the shredded stellar component of smaller galactic systems accreted onto the main progenitor¹. The relative dominance of these mechanisms depends upon the specific build-up history of a given galaxy, but there is general consensus that the outer parts of stellar haloes almost exclusively host accreted stars, whilst the inner regions

* Based on ESO program 093.B-0615(A)

** Based on observations obtained with the Hobby-Eberly Telescope, which is a joint project of the University of Texas at Austin, the Pennsylvania State University, Stanford University, Ludwig-Maximilians-Universität München, and Georg-August-Universität Göttingen.

*** This paper presents data gathered with the *Magellan* Telescopes at Las Campanas Observatory, Chile.

¹ Some of these systems will still be gas-rich when accreted and will continue forming stars, formally within the virial halo of the main progenitor; even though Tissera et al. (2013) treat them as a separate component, here we consider them as “accreted stars”, since their properties should reflect the chemical enrichment and star formation history of the accreted sub-galactic system.

might also contain an important component of stars originated within the main progenitor. Another expectation from simulations is that stars from early accretion events are to be preferentially found in the inner regions of haloes, while the outer parts are in general dominated by late accretion events.

Observational evidence for spatial variations in the properties of the MW stellar halo, likely related to different dominant formation mechanisms at play, was first put forward by Searle & Zinn (1978) on the basis of the metallicity and horizontal branch colors of MW globular clusters. The wealth of information brought about in the last years by very large area photometric and spectroscopic surveys, such as those within SDSS, has painted a complex observational picture, which confirms the existence of spatial variations in the kinematic, metallicity, abundance and age properties of the stellar halo, as well as the existence of a variety of substructures. The stellar halo of our Galaxy can be broadly described as consisting of at least two partially overlapping components: a flatter inner-halo population, with a small net prograde rotation and a metallicity distribution function peaking at $[Fe/H] \sim -1.6$, and a more extended and approximately spherical outer-halo population, showing no or little retrograde rotation (but see the recent work by Deason et al. 2017) and a metallicity distribution function peaking at $[Fe/H] \sim -2.3$ (e.g., Carollo et al. 2007, 2010; de Jong et al. 2010; Beers et al. 2012; Allende Prieto et al. 2014; Fernández-Alvar et al. 2015; Das & Binney 2016).

The shift in dominance between the inner- and outer- halo component occurs at Galactocentric distances of ~ 15 kpc, which is also the distance range in which such transition is seen in the simulations. The age distribution of field blue horizontal branch (BHB) stars (e.g., Santucci et al. 2015: 4700 stars with spectroscopic from SDSS; Carollo et al. 2016: 130,000 color-selected BHB stars from SDSS photometry), shows a decrease of 1-1.5 Gyr in its mean value and a larger age spread from the inner 15kpc to the outer regions probed by these studies (45-50kpc); an age difference between stars likely associated to the inner- and outer-halo population, with the former being older than the latter, was also pointed out by Schuster et al. (2012) with a much smaller sample of solar neighborhood stars with halo kinematics for which exquisite high resolution spectroscopic data were obtained. From the analysis of 100,000 main-sequence turn-off stars with spectroscopy from SDSS out to 15kpc from the Sun, Lee et al. (2017) show that the median $[C/Fe]$ increases as a function of height from the Galactic disk mid-plane, as so does the fraction of CEMP-no stars (those with no over-abundance of heavy neutron-capture elements) versus CEMP-s stars (those with over-abundance of heavy neutron-capture elements associated to the s-process); the authors argue this effect might be related to the mass function of the sub-haloes in which the stars in the inner- and outer-halo region formed. From an analysis of ~ 4500 K-giants likely belonging to the halo with spectroscopy from SEGUE and SEGUE-2, Janesh et al. (2016) conclude that a larger amount of substructure is seen at $[Fe/H] > -1.2$ with respect to the stars in the sample with lower metallicities, and for those located beyond 30kpc from the MW center with respect to those found at smaller Galactocentric distances (see also e.g., Xue et al. 2011); the Sagittarius (Sag) stream appears responsible for the increase in substructure seen in metallicity and distance, in particular at $[Fe/H] > -1.9$.

In general, the above observational picture appears consistent with the inner regions of the halo having been assembled earlier and in an environment experiencing a faster initial chemical enrichment than the outer halo; the outer halo containing the remnants of later accretion events, some of which have been

identified as substructures even when lacking the full 6D phase space information, due to the larger dynamical mixing times at those distances.

It is clear then that even though stellar haloes typically account for only a few percent of a galaxy stellar mass, studying their spatially varying properties allows us to retrieve crucial information on the galaxy build-up history, going back to its earliest phases.

Satellite galaxies are arguably the sub-haloes that escaped tidal disruption during the halo assembly and survived until present day. The comparison between the chemical abundance patterns of their stars to those of halo stars offers then a particularly illuminating and direct way of identifying in which type of environment halo stars formed, as well as for constraining the timescales of accretion events.

Until recently, this type of analysis, which requires high resolution spectroscopy, was by necessity restricted to samples of solar neighborhood stars, providing however already a wealth of information. The ratio of α - elements over Fe in solar neighborhood sample was found to be super-solar for the overwhelming majority of stars with halo kinematics (e.g., Venn et al. 2004). A dichotomy is present at intermediate metallicities (especially visible in the range $-1.5 \lesssim [Fe/H] \lesssim -0.8$), with a sequence of “high- α ” stars, showing an almost constant value at all metallicities (e.g., $[Mg/Fe]$, $[Si/Fe] \sim +0.3, +0.4$; NLTE $[O/Fe] \sim +0.5$) and a sequence of “low- α ” stars, at $0.1, 0.2$ dex lower values and with a slightly declining trend for increasing $[Fe/H]$ (e.g., Nissen & Schuster 1997, 2010; Ramírez et al. 2012; Hawkins et al. 2015); the “high- α ” and “low- α ” sequences can be also traced in a number of other elements, as $[Cu/Fe]$, $[Zn/Fe]$, $[Ba/Y]$, $[Na/Fe]$, $[Al/Fe]$, $[Ni/Fe]$, $[(C+N)/Fe]$ (e.g., Nissen & Schuster 2011; Hawkins et al. 2015). Such chemical patterns have been interpreted as “high- α ” stars likely forming in regions with a star formation rate high enough that only massive stars and type II supernovae contributed to the chemical enrichment; on the other hand, “low- α ” stars most likely originated in environments with a slower chemical evolution, experiencing enrichment also from type Ia supernovae and low-mass asymptotic giant branch (AGB) stars. Typically the “low-alpha” sequence is attributed to accreted systems.

Interestingly, the analysis of space velocities of a few dozen halo stars of the solar neighborhood shows that “low- α ” stars have on average more eccentric orbits than “high- α ” stars, allowing them to reach larger apocenter distances and larger heights above the Galactic plane. This essentially indicates that “low- α ” stars, possibly born in accreted systems, are likely to belong to the outer-halo population (e.g., Nissen & Schuster 1997; Fulbright 2002; Roederer 2009; Nissen & Schuster 2010). On the other hand, APOGEE spectra of 3200 giants have shown that the “high-alpha” sequence appears chemically indistinguishable from the canonical thick disk, with both components exhibiting a high degree of chemical homogeneity (Hawkins et al. 2015); an interpretation offered by Hawkins et al. for this finding is that the gas from which the inner regions of the MW halo formed was also the precursor of the thick disk. However, the aforementioned work does not carry out an analysis of how the chemical abundance properties of the various Galactic component might vary spatially, hence it is not possible to establish where the transition between “canonical thick disk & halo” to accreted halo occurs.

Fernández-Alvar et al. (2015) analyze the trends in Ca, Mg, and Fe abundances as a function of Galactocentric distance out to ~ 80 kpc for almost 4000 stars with low resolution spectroscopy from surveys within SDSS and, in the range

$-1.6 < [\text{Fe}/\text{H}] < -0.4$, find a decreasing trend for $[\text{Ca}/\text{Fe}]$ but an increasing trend for $[\text{Mg}/\text{Fe}]$. Fernández-Alvar et al. (2017) extend their previous analysis to several other chemical elements, but over a smaller range in Galactocentric distances ($5 < r_g[\text{kpc}] < 30$), using infrared spectroscopy of giants from APOGEE; the median $[\text{X}/\text{Fe}]$ for α elements is lower by 0.1dex (or more for O, Mg, S) for stars at $r_g > 15\text{kpc}$ at $[\text{M}/\text{H}] > -1.1$ with respect to closer by stars, and differences are also detected in other elements (Ni, K, Na and Al). This confirms that “low- α ” stars are found at large Galactocentric distances.

It should be pointed out that even the so-called “low- α ” stars have chemical abundance patterns that do not match those of stars in the early-type dwarf galaxy satellites of the MW when compared at the same metallicity; in other words, in MW early type satellites the decline (“knee”) in $[\alpha/\text{Fe}]$ (or individual α -elements over Fe) is detected at much lower metallicities than in the halo (e.g., in $[\text{Mg}/\text{Fe}]$: at $[\text{Fe}/\text{H}] \sim -2$ in the Fornax dwarf spheroidal galaxy [hereafter, dSph], Hendricks et al. 2014, Lemasle et al. 2014; $[\text{Fe}/\text{H}] \sim -1.6$ in the Sculptor dSph, Tolstoy, Hill & Tosi 2009; $[\text{Fe}/\text{H}] \sim -2.8$ in the Draco dSph, Cohen & Huang 2009). The surviving MW satellites are on orbits that make them unlikely to contribute halo stars passing through the Solar Neighborhood (Roederer 2009). The low metallicity part of the halo might then be compatible with having been assembled by the shredded ancient (prior to the time where SNIa started having a significant contribution to the Fe production) stellar component of systems resembling the MW early-type satellite progenitors; however, the super-solar values seen in the halo out to much larger metallicity most likely require the supposedly accreted component to have been formed in environments experiencing a higher initial SFR anyway (see e.g., Fulbright 2002; Venn et al. 2004). Recently, low resolution spectroscopic data from SDSS/SEGUE allowed to place the α -knee of likely Sag stream member stars at $[\text{Fe}/\text{H}] \sim -1.3$, only slightly more metal-poor than in the MW halo (de Boer et al. 2014): this might indicate that a small number of large systems experiencing an initial chemical enrichment like Sag stream stars might have contributed substantially to the build up of the MW stellar halo at old times.

Detailed chemical abundance properties of distant halo stars for a variety of elements with different nucleosynthetic origins allows to make a more refined comparison to the properties of MW satellites and of the inner versus outer halo. This requires time-consuming high resolution spectroscopy of typically faint stars. The only study in which detailed chemical abundance properties of the stellar halo have been analyzed as a function of distance from the Galactic center for a large number of elements derived from high resolution spectroscopy is the work by Fernández-Alvar et al. (2017) based on APOGEE infrared spectra. However, the authors do not carry out a comparison between the halo chemical abundance properties and those of MW satellites and do not take explicitly into account the possible presence of Sag stream stars and how this might affect the interpretation.

In this work, we derive chemical abundances from high resolution optical spectroscopy for a sample of 28 halo stars which can be considered as highly likely outer-halo objects, due to their large present-day Galactocentric distances $> 15\text{kpc}$ and heights from the MW mid-plane —z—>9kpc; we can in this way by-pass the typically large uncertainties in the measurements of space kinematics and related orbital properties in assigning stars presently found in the solar neighborhood to the inner- or outer-halo population. We then interpret the chemical abundance trends for this sample of outer halo stars in the light of what has been observed for solar neighborhood samples, MW

satellites, including the LMC, and factoring in the possible presence of Sag stream stars in our sample. Our sample is genuinely new, with only one star overlapping with APOGEE (Ahn et al. 2014) measurements, is competitive in size (e.g., there are ~ 50 stars beyond a Galactocentric distance of 15kpc in Fernandez-Alvar et al. 2017) and provides abundances for several elements which are not measured from APOGEE spectra (Sc, Cr, Co, Cu, Zn, Sc, Y, Zr, Ba, La, Ce, Pr, Nd, Sm, Eu) as well as a set of elements in common (C, Mg, Ti, Si, Ca, O, Al, Na, Ni, Mn, V), handy for comparisons of trends.

The article is organized as follows: in Sect. 2 we describe the sample selection, observing facilities used and data reduction procedure; Sects. 3 summarizes the method for equivalent widths and radial velocity determination, and in Sect. 4 we explain the analysis performed for deriving the elemental abundances. We proceed to comparing our radial velocities, metallicities and distances with results in the literature for the same stars in Sect. 5. In Sect. 6 we comment on the chemical abundance trends found for our sample of halo stars, and compare them with those of solar neighborhood samples and MW satellites, including Sag and the LMC. Sect. 7 is devoted to exploring whether the stars in our sample might belong to known substructures. We conclude with a discussion and summary in Sect. 8.

2. Sample, observations and data reduction

Our sample consists of 28 individual red giant branch (RGB) stars observed at high spectral resolution with HET/HRS, Magellan/MIKE and VLT/UVES. Their location on the sky is shown in Fig. 1. Three stars were observed both with HET/HRS and VLT/UVES to test the consistency of results from the different facilities. The details of the target selection, instrument set-ups and data-reduction will be given below. Table 1 lists the Julian dates of the observations, total exposure times per target and combined signal to noise per pixel, together with the adopted stellar parameters and radial velocities. Table 2 lists the equatorial and galactic coordinates provided by the Gaia satellite in the first data release, as well as the Gaia DR1 ID and the m_G magnitude (Gaia Collaboration et al. 2016a,b; Lindegren et al. 2016; van Leeuwen et al. 2017; Arenou et al. 2017; Evans et al. 2017; Carrasco et al. 2016).

2.1. The sample

Most of our target RGB stars were selected from the Spaghetti survey sample (e.g., Morrison et al. 2000, 2001; Dohm-Palmer et al. 2001; Morrison et al. 2003) as published in Starkenburg et al. 2010; 2011 (21 stars); of the remaining 7 stars, six targets were drawn from the catalog of distance determinations for the SEGUE K Giants by Xue et al. (2014) and one from the APOGEE sample. The main criterion for selection was for the giants to be placed at Galactocentric distances² $r_g > 15\text{kpc}$. Additionally, we preferred targets bright enough to be within the reach of high resolution spectroscopic observations on the chosen facilities in a reasonable exposure time ($V \lesssim 17.5$) and made sure that the selected targets would cover a large metallicity range, in particular the $[\text{Fe}/\text{H}]$ region where the abundances of α -elements in solar neighborhood halo samples differs the most from those of stars in classical dSphs, that is beyond $[\text{Fe}/\text{H}] = -1.6$.

² We assumed that the Sun is found at 8 kpc from the Galactic center.

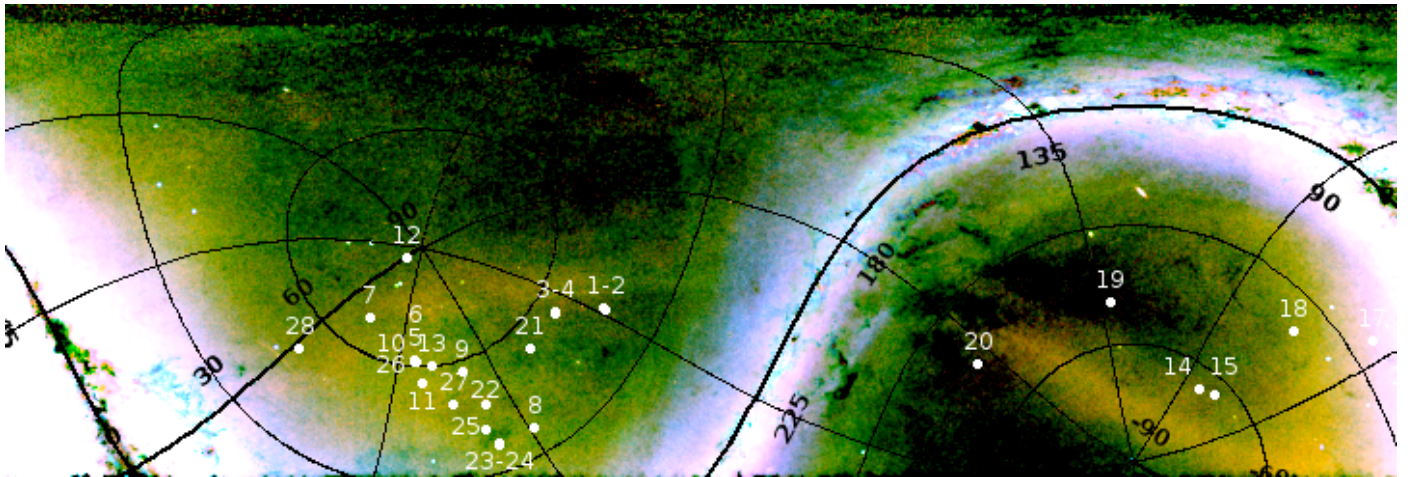


Fig. 1. Location of our targets overlaid on an RGB rendering of the distribution of Milky Way halo stars in an Equatorial- Carré view. The latter has been produced by combining the 8 (blue channel), 15 (green channel), 25 (red channel) kpc slices from the Pan-STARRS1 3π Survey data-set from <https://zenodo.org/record/60518#.WHTxMHqvLM>, obtained by applying to the Pan-STARRS1 3π Survey data-set matched-filter technique using an $[Fe/H] = -1.5$ and 12 Gyr old model in the g,r bands (for details, we refer the reader to Bernard et al. 2016). The grid is in Galactic coordinates.

2.2. Observations

The observations were carried out with three high resolution spectrographs:

- MIKE (Magellan Inamori Kyocera Echelle) attached to the 6.5m Magellan telescope at Las Campanas Observatory, Chile (Bernstein et al. 2003). Its blue and red arms cover simultaneously the wavelength ranges $\sim 3350 - 5060\text{\AA}$ and $4860 - 9400\text{\AA}$; however, we only use the portion of the spectra redder than 3700\AA due to the low signal to noise ratio (S/N) of the spectra of our cool target stars in the bluest regions of the wavelength range. With the chosen $1''$ slit, the resolving powers are $\sim 28\,000$ and $\sim 22\,000$ in the blue and red ranges respectively. A 2×2 pixels binning was adopted on the detectors. The total exposure times varied between 4400 and 5400 seconds, distributed into two or three successive exposures. Observations were carried out in visitor mode in 2 nights (Mar 8 and June 19, 2014) under program CN2014A-20 (PI: Minniti).
- UVES (UV-Visual Echelle Spectrograph) attached to the 8.2m Kueyen UT2 unit of the VLT telescope at Paranal Observatory operated by ESO, Chile (Dekker et al. 2000). It was used in the Dichroic #1 mode, providing a spectral coverage $\sim 3500 - 4525\text{\AA}$ in the blue, and $\sim 4784 - 5759\text{\AA}$ and $\sim 5838 - 6805\text{\AA}$ in the red, with a resolving power $R \sim 45\,000$ for a $1''$ slit. A 2×2 pixels binning was used, as for MIKE. The exposure time was either 5×3000 seconds (5 exposures) or 3×2400 seconds. Observations were carried out in service mode under program 093.B-0615 (PI: Battaglia, 45h), and the different exposures on a given star are often separated in time by as much as a whole year.
- HRS (High Resolution Spectrograph) attached to the 10m Hobby-Eberly Telescope (HET) at McDonald Observatory, Texas, USA (Tull 1998; Ramsey et al. 1998). The instrument was configured to HRS_15k_central_600g5822_2as_2sky_IS0_GC0_2x5 to achieve $R=18,000$ spectra covering 4825\AA to 6750\AA . The data were acquired as part of normal queue scheduled observing (Shetrone et al. 2007) under program UT13-2-007 (PI: Shetrone). The targets were observed between February

and June of 2013 for a total of 33.7 hours of shutter open time. Directly after each target a Th-Ar exposure was taken and on nearly every night (weather permitting) a radial velocity standard was observed during twilight. The total exposure times varied between 6000 and 12000 seconds, distributed into two to five exposures of 1800, 2400, or 3000 seconds spread over a few weeks.

2.3. Data reduction

2.3.1. MIKE

The spectra were reduced with the pipeline written by Dan Kelson³ and based on the Carnegie Python Distribution (CarPy)⁴. The pipeline provides flat-fielded, optimally extracted and wavelength calibrated 1-D spectra for the successive spectral orders. We normalized them to the continuum in a preliminary way and merged them following the method proposed by Aoki (2008), using the IRAF package⁵. The 1-dimensional spectra resulting from order merging were then visually examined and the remaining obvious cosmics removed by hand, using the IRAF splot subroutine.

2.3.2. UVES

The reduction was done with the ESO UVES pipeline (release 5.09) with optimal extraction. Cosmics and other anomalies (e.g., poorly subtracted telluric emission lines) were suppressed by hand, as for the MIKE spectra.

2.3.3. HRS

The spectra were reduced with IRAF ECHELLE scripts. The standard IRAF scripts for overscan removal, bias subtraction, flat

³ <http://code.obs.carnegiescience.edu/mike>

⁴ <http://code.obs.carnegiescience.edu/carnegie-python-distribution>

⁵ IRAF is distributed by the National Optical Astronomy Observatory (NOAO), which is operated by the Association of Universities for Research in Astronomy (AURA), Inc., under cooperative agreement with the U.S. National Science Foundation

fielding and scattered light removal were employed. For the HRS flat field we masked out the Li I, H I and Na D regions because the HET HRS flat field lamp suffered from faint emission lines. The sky fibers were extracted in the same manner as the star fibers. We also extracted the spectra of a sky flat and used that to determine the throughput differences between the sky fibers and the object fibers. The sky fibers were then scaled by this value and subtracted from the star flux. The spectra were combined into a single long spectrum for the blue and red chips.

3. Equivalent widths and radial velocity measurements

3.1. MIKE

To normalize the spectra to the continuum and determine line equivalent widths (EW), we have applied the 4DAO avatar (Mucciarelli 2013) of the DAOSPEC code⁶ (Stetson & Pancino 2008, 2010) to each of the blue and red spectral ranges, after masking the numerous telluric lines that plague the red range. In some cases we have divided the blue range in two portions, typically below and above 4200 Å, because of the very poor S/N of the bluer side, whose contribution is penalized with a low weight. The code also computes the radial velocity (RV) for each identified line and gives the mean RV and its rms scatter for each spectral range. The RVs given in Table 1 are weighted means of the RVs determined for each spectral range treated by the 4DAO code. The weights are the reciprocal of the squared respective errors, the latter being defined as the rms scatter given by DAOSPEC divided by the square root of the number of identified lines. The errors on the mean RV values correspond to their rms scatter divided by the square root of the number of spectral ranges (only 2 or 3 in practice).

The DAOSPEC code fits saturated Gaussians to the line profiles and succeeds well for faint lines, but its EW estimate is biased for strong lines (Kirby & Cohen 2012). The limiting EW above which the DAOSPEC determination becomes significantly biased depends on spectral resolution: the higher the resolution, the sooner a bias appears with increasing EW. To evaluate the bias, we have determined manually the EWs of a set of well isolated lines in the star #13, using both direct integration and Gaussian fit. Both methods give similar results, and due to the modest spectral resolution used here, the bias appears only for $EW > 160 \text{ m}\AA$, as shown in Fig. 2. Therefore, we decided to keep only lines with $EW \leq 160 \text{ m}\AA$ for our analysis.

The DAOSPEC code provides formal errors on EWs, that do not include systematic effects like uncertain continuum level. To make them more realistic, we arbitrarily add a 5% error in a quadratic way to the error computed by DAOSPEC. This avoids assigning too contrasted weights to some lines when computing mean abundances.

3.2. UVES

We applied the same method as for MIKE to determine the continuum and EWs. However, because of the higher resolving power of UVES, we had to correct all EWs for the bias that we determined in the same way as above, but here for all stars of our UVES sample. The difference between EWs determined with DAOSPEC and manually is shown on Fig. 3. We still ex-

⁶ DAOSPEC has been written by P. B. Stetson for the Dominion Astrophysical Observatory of the Herzberg Institute of Astrophysics, National Research Council, Canada.

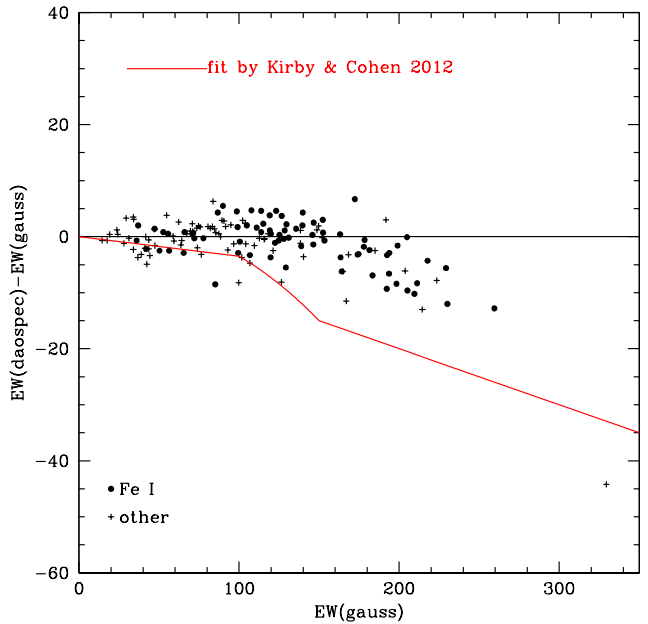


Fig. 2. Comparison of the EWs determined by DAOSPEC with those obtained by “manual” Gaussian fits for clean lines, for star #13, of the MIKE sample. The red curve shows the bias found by Kirby & Cohen (2012) for their spectra with a resolution $R \gtrsim 60\,000$.

clude very strong lines ($EW > 210 \text{ m}\AA$) and adopt the following correction to the EWs given by 4DAO:

$$EW = 1.0044 \cdot EW(4DAO) + 0.5 \text{ for } EW < 100 \text{ m}\AA, \quad (1)$$

$$EW = 1.11 \cdot EW(4DAO) - 10.06 \text{ for } 100 < EW < 210 \text{ m}\AA. \quad (2)$$

This function is continuous at $EW = 100 \text{ m}\AA$. The correction being small, we keep the same error on EW as provided by DAOSPEC, after adding quadratically a 5% error to them, as for the MIKE sample.

The RVs were determined in the same way as for MIKE, and the values given in Table 1 are averaged over three determinations corresponding to the three UVES spectral ranges. The table lists also the velocities from the individual exposures, since some were observed as much as a whole year apart. However, we did not find any sign of evident RV variability in any of the ten UVES stars.

3.3. HRS

We have used the same method as for MIKE and UVES to determine the continuum and EWs. The resolution is lower than that of MIKE spectra, and we verified that the EWs given by the 4DAO code do not need any correction. The S/N is lower on average for this sample than for the MIKE and UVES ones, so we used the UVES data rather than the HRS ones for the three stars that were observed with both instruments. For the sake of completeness and for comparison purposes, we have nevertheless determined independently the stellar parameters and abundances of these three objects (designated #21 UVES, #26 UVES, and #28 UVES in the tables) on the basis of HRS spectra alone. We note that the spectrum of #28 UVES has a very poor S/N, so the corresponding results must be taken with caution.

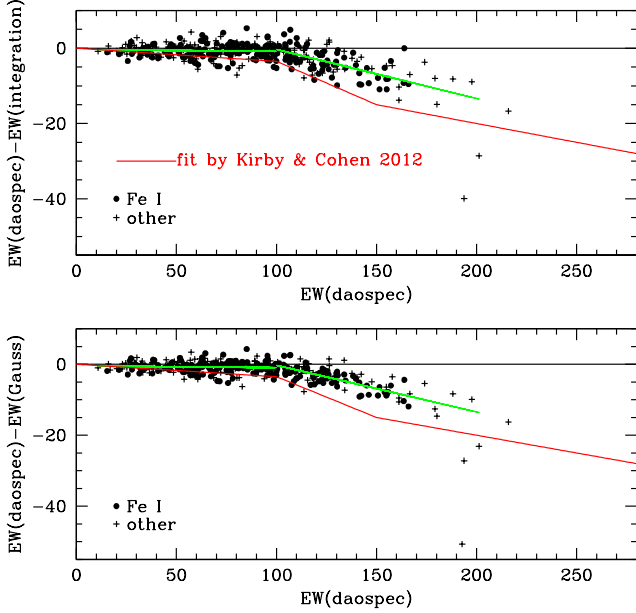


Fig. 3. Comparison of the EWs determined by DAOSPEC with those obtained by manual direct integration (top panel) and Gaussian fits (bottom panel) for clean lines, for all ten stars of the UVES sample. The red curve shows the bias found by Kirby & Cohen (2012) for their own spectra ($R \gtrsim 60\,000$). The green lines show the linear regressions below and above 100 mÅ.

The EWs are provided in Tables 5, 6, 7, 8, 9, 10, and 11.

Radial velocities were determined from cross-correlation using the IRAF task fxcor using the Arcturus spectra (Hinkle et al. 2000). The heliocentric correction was made using the IRAF task rvcorrect. A correction for zero points was made based on the radial velocity standard taken in twilight. The final heliocentric velocities are given in Table 1; also in this case we list radial velocities from the individual exposures, due to the different dates of observation in some cases. In this sample, star #03 is found to be a RV variable. The spectra were then shifted and combined using the IRAF tasks dopcor and scombine.

4. Analysis

4.1. Models

We used the MARCS 1-D spherical atmosphere models with standard abundances, downloaded from the MARCS web site⁷ (Gustafsson et al. 2008), and interpolated using Thomas Masseron's `interp1_modeles` code available on the same site. “Standard composition” means that the abundances are scaled solar, except for the α elements that are overabundant relative to solar by 0.4 dex for $[\text{Fe}/\text{H}] \leq -1.0$, by 0.3 dex for $[\text{Fe}/\text{H}] = -0.75$, by 0.2 dex for $[\text{Fe}/\text{H}] = -0.5$ and by 0.1 dex for $[\text{Fe}/\text{H}] = -0.25$. We adopted those computed for a microturbulence velocity $v_{\text{turb}} = 2 \text{ km s}^{-1}$ and for 1 solar mass.

4.2. Codes

All abundances were computed with the `turbospectrum` code (Alvarez & Plez 1998; Plez 2012). It assumes local thermody-

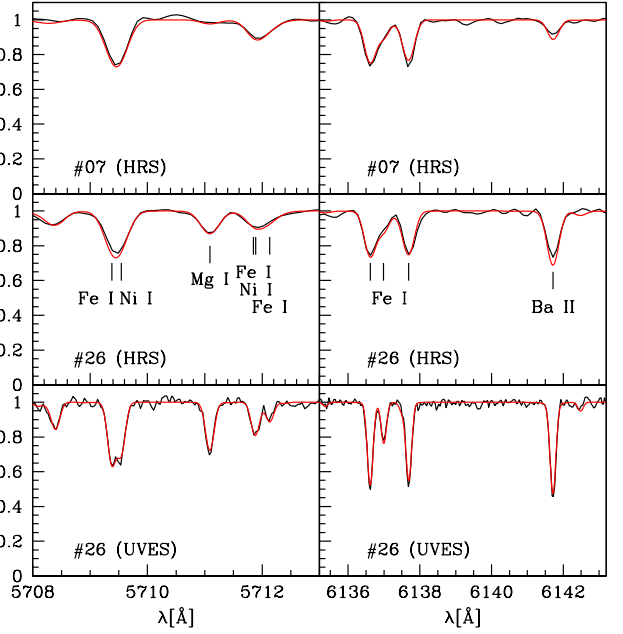


Fig. 4. Examples of observed spectra and best-fitting models over a wavelength region encompassing absorption lines from different elements (see labels). The first row refers to star #7, observed with HET/HRS. The second and last rows show star #26, observed with HET/HRS and VLT/UVES, respectively.

namic equilibrium (LTE) but is able to compute the line transfer in spherical geometry, and includes continuum scattering in the source function. We used this code in the ABFIND mode to get abundances from the EWs.

In a few cases we also used `turbospectrum` to compute synthetic spectra and determine abundances through a fit to the observed spectrum, especially for blended zirconium lines. For this we developed a python routine `fitspec.py` which generates synthetic spectra with `turbospectrum` for various abundances of the element of interest, and convolves them with Gaussians with various FWHMs, and finds the optimal abundance, FWHM and λ shift in the relevant short spectral range. The convolution is done with the `fa1tb03` utility code provided with `turbospectrum`. This code was also used to determine the carbon abundance, based on part of the CH molecular G band, in the 4322–4325 Å spectral range. As in Jablonka et al. (2015), we assumed a solar [N/Fe] ratio, a carbon isotopic ratio $^{12}\text{C}/^{13}\text{C} = 6$ typical of the tip of the RGB, and we adopted the [Mg/Fe] ratio as a proxy for [O/Fe] when the latter was not measured. To compute hyperfine structure (HFS) corrections of some lines, we used Chris Sneden’s MOOG code⁸ (2010 version) with the blend driver. More details are given below. Examples of observed spectra, with overlaid the best-fitting models, are shown in Fig. 4.

4.3. Line list and solar abundances

We adopted the line list of Roederer et al. (2008, 2010), and complemented it with data from the VALD database (Piskunov et al. 1995; Ryabchikova et al. 1997; Kupka et al. 1999, 2000; Ryabchikova et al. 2015). The line wavelengths and oscillator

⁷ marcs.astro.uu.se

⁸ <http://www.as.utexas.edu/~chris/moog.html>

strengths are given in Table 5, 6, 7, 8, 9, 10, and 11. The adopted solar abundances are taken from Anders & Grevesse (1989) and Grevesse & Sauval (1998) and displayed in Table 4.

4.4. Preliminary stellar parameters

In order to derive the stars' atmospheric parameters, we feed the spectroscopic analysis with first guesses for the effective temperature T_{eff} , gravity $\log g$, microturbulent velocity v_{turb} and $[\text{Fe}/\text{H}]$. As initial $[\text{Fe}/\text{H}]$ values we adopt those given in the original works from which the targets were selected (that have low spectral resolution, except for the star drawn from APOGEE); T_{eff} and $\log g$ are instead derived photometrically, and v_{turb} follows from the empirical relation $v_{\text{turb}} = 2.0 - 0.2 \times \log g$ by Anthony-Twarog et al. (2013).

The majority of the stars have SDSS ugriz and JHK photometry from the UKIDSS large area spectroscopic survey⁹, which allows us to constrain the star' photometric effective temperature $T_{\text{eff,p}}$ by using several of the Ramírez & Meléndez (2005) effective temperature-color-[Fe/H] calibrations $T_{\text{eff,p,col}}$ (specifically T_{VI} , T_{VJ} , T_{VH} and T_{VK}); on the other hand, for stars #20, 22, 23, 24, 25, 27, we have used only $T_{\text{eff,p,VI}}$, due to the availability of only Washington photometry, transformed into V & $V-I$ using the relation in Morrison et al. 2003.

We transformed the SDSS photometry into Johnson-Cousins B , V and I using the transformations involving gri in Lupton (2005)¹⁰. The $B-V$, $V-I$, $V-J$, $V-H$, $V-K$ colors are dereddened using the E(B-V) reddening from the Schlegel et al. (1998) maps, with the Schlafly & Finkbeiner (2011) recalibration.

$T_{\text{eff,p}}$ is determined as the weighted average of the individual $T_{\text{eff,p,col}}$ relations with the error given by the scatter between $T_{\text{eff,p,col}}$ to which we add in quadrature the average error in $T_{\text{eff,p,col}}$.¹¹ The error in $T_{\text{eff,p}}$ typically ranges between 60 & 80K. We exclude T_{BV} as it is the most sensitive to uncertainties in $[\text{Fe}/\text{H}]$.

The first guess $\log g$ is obtained by finding the point along the RGB locus ($\log g \leq 3.5$) with the closest matching T_{eff} and $[\text{Fe}/\text{H}]$ in a set of Dartmouth isochrones (Dotter et al. 2008) of different ages, $[\text{Fe}/\text{H}]$ and $[\alpha/\text{Fe}]$ (age= 4, 8, 12 Gyr; $-2.4 < [\text{Fe}/\text{H}] < -0.60$, with a spacing of 0.2dex; $[\alpha/\text{Fe}]=0, 0.2, 0.4$); we explore different values for the ages and $[\alpha/\text{Fe}]$ because these quantities are in practice unknown (at this stage) and we wish not to fix them a priori. We derive the error in $\log g_p$ by repeating N=100 times the search for the best-matching isochrone, where each time the effective temperature and $[\text{Fe}/\text{H}]$ are randomly drawn from a Gaussian distribution centered on the input $T_{\text{eff,p}}$ and $[\text{Fe}/\text{H}]$ and with σ given by the corresponding errors.

⁹ The only exception is star #21 that lacks a measurement of the J-magnitude in the UKIDSS survey and for which we used the 2MASS value.

¹⁰ <http://www.sdss3.org/dr8/algorithms/sdssUBVRITransform.php#Lupton2005>

¹¹ The error in each of the $T_{\text{eff,p,col}}$ is derived by propagating the error in $[\text{Fe}/\text{H}]$ (assumed to be a conservative 0.2dex) and in color, where the latter includes the scatter in the transformations between SDSS and Johnson-Cousin bands. To this we add in quadrature the scatter found by Ramirez & Meléndez (2005) around their T_{eff} -[Fe/H]-color relations (40, 38, 32, 28K for T_{VI} , T_{VJ} , T_{VH} , T_{VK} respectively). Finally, other 50K are added in quadrature to the average $T_{\text{eff,p,col}}$ to account for the scatter between direct temperatures and those from the infrared flux method.

4.5. Adopted spectroscopic stellar parameters

We started from the photometrically estimated effective temperatures, surface gravities and microturbulent velocities as described in the previous section, and applied the usual spectroscopic diagnostics by plotting the Fe I abundance as a function of excitation potential to constrain T_{eff} and of EW to constrain v_{turb} . Following Tafelmeyer et al. (2010) and Jablonka et al. (2015), we discarded the Fe lines with $\chi_{\text{exc}} < 1.4$ eV in order to minimize NLTE effects as much as possible, as well as lines fainter than ~ 20 mÅ and stronger than ~ 200 mÅ (160 mÅ for the MIKE sample). In the Fe I abundance vs. EW diagram, we used the predicted rather than observed EWs to avoid any bias on the v_{turb} determination, following Magain (1984).

The surface gravity was determined as usual from the ionization balance, by requiring the equality of the Fe I and Fe II abundances.

When a change in T_{eff} and $\log g$ was required by the relevant spectroscopic diagnostic, we tried to remain within 2σ of the photometric estimate, allowing the slopes of the diagnostic plots to differ from zero by no more than 2σ either. In only three cases we had to lower T_{eff} by as much as $\sim 2.5\sigma$ in order to fulfill the spectroscopic diagnostic (#7, 9, 19). Regarding $\log g$, it was possible to maintain it within 2σ of the photometric estimate in all case but one (#6).

This trade-off between photometric and spectroscopic criteria often implies a spectroscopic T_{eff} slightly lower than the photometric one (and/or a slightly negative slope in the Fe I versus excitation potential plot) and a larger Fe II abundance relative to the Fe I one. The latter difference Δ_{II-I} does not exceed 2σ in most cases (σ being defined as the rms dispersion of the individual Fe II abundances divided by the square root of the number of lines), especially in the MIKE sample (where the only exception is star #9: 3σ) and in the HRS one (except for star #7: 2.3σ). In the UVES sample, which benefits from the best resolution and S/N, half the stars show differences larger than 2σ (between 2.2 and 4.3σ). This indicates a higher visibility of systematics like NLTE effects in this high quality data.

We chose to be more tolerant regarding ionization equilibrium in the case of very metal poor stars ($[\text{Fe}/\text{H}] \lesssim -2$), because there are indications in the literature that NLTE effects are more pronounced for them than at solar metallicity. For instance, Merle et al. (2012) compute the NLTE correction for both Fe I and Fe II abundances for two models with $T_{\text{eff}} = 4500$ K, $\log g = 1.0$, $[\text{Fe}/\text{H}] = -1.50$ and $[\text{Fe}/\text{H}] = -2.00$; they find $\Delta_{II-I} = 0.13$ for $[\text{Fe}/\text{H}] = -1.50$ and $\Delta_{II-I} = 0.15$ for $[\text{Fe}/\text{H}] = -2.00$, when the stars are analyzed assuming LTE. This is consistent with our empirical $-0.02 < \Delta_{II-I} < 0.20$ range for UVES. $\Delta_{II-I} = 0.24$ in two HRS stars, but the S/N of their spectra is poor and this represents no more than 2σ .

Disregarding the photometric $\log g$ estimate and strictly forcing ionization equilibrium would imply decreasing $\log g$ but also T_{eff} because these quantities are correlated. We preferred to remain not too far from the photometric estimates, which are physically sound.

The final stellar parameters are given in Table 1. The typical error on T_{eff} is about 100 K, that on $\log g$ about 0.2 dex and that on v_{turb} about 0.2 km s^{-1} .

4.6. Hyperfine structure

The hyperfine structure (HFS) mainly affects elements with an odd atomic mass, namely Sc, Mn, Co, Cu, and Eu, but also odd isotopes of Ba. It broadens the line, thereby alleviating its sat-

uration, so that estimating the abundance directly from the EW results in an overestimate, if one does not take into account the HFS structure. For a given EW, the HFS correction increases in absolute value as v_{turb} decreases, because both tend to desaturate the line. Faint lines remain unaffected, being far from saturation, but for strong lines on the plateau of the curve of growth, the HFS correction may exceed 1.5 dex in absolute value (the HFS correction is always negative).

As mentioned before, we estimated HFS corrections to the raw EW abundances using the MOOG code, running it with both the `bblend` driver and the `abfind` driver and computing the abundance difference, as described in North et al. (2012) and Jablonka et al. (2015). We used the HFS components with their oscillator strengths given in the Kurucz web site¹² for Co, Cu, most Ba lines and Eu, and by Prochaska & McWilliam (2000) for Sc and Mn.

For Ba II (and especially for the $\lambda 4934$ line which has a wide HFS), which has both odd and even isotopes, we assumed a solar mix with an 18% fraction of odd isotopes (Lodders et al. 2009). For Eu, we assumed equal abundances of the $A = 151$ and 153 isotopes (Zhang et al. 2010).

4.7. Abundances

The final abundances given in Table 4 are the weighted mean of the individual line abundances, the weights being the inverse variances of the single line abundances. These variances were propagated by `turbospectrum` from the errors on the corresponding EWs. We also give in the same table some upper limits evaluated from the small EW of marginally identified lines, for stars #10 (O), #12 (Pr), and #23 (Mn). Such upper limits concern only abundances given by one or two lines and are indicated in the relevant tables by a < sign before their value.

The carbon abundances are given in Table 3. They are given only for the stars measured with MIKE and with UVES, because the spectral range of HRS does not include the CH G band. The spectrum of star #12 is too noisy in the wavelength range of interest to provide a reliable estimate of the C abundance.

For species represented by only one line, the errors indicated have to be considered as lower limits, because they include only the formal error given by the 4DAO code (plus 5%), but not the uncertainty on the continuum level, oscillator strength, possible blend with a small telluric line (especially in the case of oxygen), or faint unrecognized cosmic hit. For the stars measured with HET/HRS, we did not discard very strong lines, and the abundance of some elements like Na, Mg, and Ba sometimes rely on lines with $EW > 200 \text{ m}\AA$ and must be taken with caution: the Gaussian fit may not be quite appropriate for such lines, and abundances depend more critically on broadening parameters that may be uncertain.

4.7.1. Errors

As mentioned in Sect. 3.1, we added quadratically a 5% error to the EW error estimated by the DAOSPEC code to make the errors on EW more realistic; thus, no EW has an error smaller than 5%. These errors are generally larger than those obtained from the Cayrel (1988) formula revised by Battaglia et al. (2008). They are listed in Tables 5 to 11.

The errors listed in Table 4 are defined in the same way as in Jablonka et al. (2015).

¹² <http://kurucz.harvard.edu/linelists.html>

5. Comparison to previous works

Both the Spaghetti survey (e.g., Morrison et al. 2000; Dohm-Palmer et al. 2001, see also Starkenburg et al. 2010 for additional constraints onto the luminosity classification) and the SDSS-SEGUE survey are carried out at relatively low spectral resolution ($\sim 2.5\text{--}3.5 \text{ \AA}$). Here we compare the heliocentric velocity and [Fe/H] estimates from these original sources with our determinations at ~ 10 x larger spectral resolving power. Similarly, we revise the stars's distance determinations on the basis of the stellar gravity, temperature, [Fe/H] and $[\alpha/\text{Fe}]$ from our analysis.

5.1. Heliocentric velocity and [Fe/H]

Figure 5 shows the comparison of the heliocentric radial velocities (left) and metallicities [Fe/H] (right) obtained in this work to those obtained in the original sources. As mentioned before, the sample contains two stars detected as radial velocity binaries (star #3 as determined from our HET observations and #11, also known as 2M12490495-0743456, with the binarity detected by APOGEE multiple visits), however their velocities happen to agree well with the measurements in the literature; there are only a few cases for which the velocities disagree beyond the 3σ level, and we cannot exclude that these velocity differences are due to the stars being unidentified radial velocity binaries. As for the metallicity, the comparison can be deemed satisfactory. As expected, the high resolution observations have more precise [Fe/H] determinations with respect to the original measurements at low spectral resolution. There is only one star with clearly discrepant [Fe/H] (#28): its Spaghetti survey metallicity was derived from the Mg triplet index, but was found to be very (and unusually) discrepant from the metallicity derived from the Ca K line index, which returned [Fe/H] = -1.30 , much closer to the high-resolution spectrum value (Starkenburg, priv. communication).

Star 2M12490495-0743456 was also observed by APOGEE and its SDSS DR13 abundances are in excellent agreement with our determinations, except for [Co/Fe] and [Ni/Fe], which anyway agree within 2σ ; the abundance of [Al/Fe] and [V/Fe] is undetermined in our data (SDSS DR13 : [Fe/H] = -0.97 ± 0.04 ; [O/Fe] = 0.21 ± 0.06 ; [Mg/Fe] = 0.18 ± 0.05 ; [Al/Fe] = -0.05 ± 0.14 ; [Si/Fe] = 0.17 ± 0.05 ; [Ca/Fe] = 0.27 ± 0.07 ; [V/Fe] = 0.57 ± 0.24 ; [Mn/Fe] = -0.39 ± 0.05 ; [Co/Fe] = 0.32 ± 0.23 ; [Ni/Fe] = -0.01 ± 0.04 . This work: [Fe/H] = -0.96 ± 0.11 ; [O/Fe] = 0.25 ± 0.04 ; [Mg/Fe] = 0.24 ± 0.11 ; [Al/Fe] = ND; [Si/Fe] = 0.12 ± 0.07 ; [Ca/Fe] = 0.30 ± 0.13 ; [V/Fe] = ND; [Mn/Fe] = -0.49 ± 0.12 ; [Co/Fe] = -0.23 ± 0.19 ; [Ni/Fe] = -0.17 ± 0.09).

5.2. Distances

In both the Spaghetti survey and Xue et al. (2014) the distance modulus (and hence, the heliocentric distance d_h) to a star is found by comparing the star's apparent magnitude with the absolute magnitude of globular clusters giant-branch color-luminosity fiducials, interpolated at the observed star color and spectroscopic [Fe/H].

In the Spaghetti survey the distance errors are obtained from Montecarlo simulations in which the effect of the color and metallicity error are factored in; to the latter is added in quadrature 0.25dex to account for possible systematic calibration errors. On the other hand, Xue et al. (2014) adopt a probabilistic approach to propagate the errors in metallicities, magnitudes, and colors into distance uncertainties, and be able to fold in also prior information about the giant-branch luminosity function and

the different metallicity distributions of the SEGUE K-giant targeting sub-categories.

This type of determination implicitly assumes that the age and $[\alpha/\text{Fe}]$ of halo stars compare well to those of the globular clusters fiducials, which might not hold for the whole sample: for instance, a few halo stars are known to have sub-solar $[\alpha/\text{Fe}]$ and we also want to account for the possibility of the late accretion of stars originated in satellites with prolonged star formation histories (e.g., Sag).

Hence we relax the above assumption and revise the stars' distance determinations by applying the same method as in Sect. 4.4 but using the stars's $\log g$, T_{eff} , $[\text{Fe}/\text{H}]$ and $[\alpha/\text{Fe}]$ ($=([\text{Ca}/\text{Fe}] + [\text{Mg}/\text{Fe}] + [\text{Ti}/\text{Fe}])/3$) derived in our spectroscopic analysis and repeating the fit for different ages (4, 8 and 12 Gyr); the range of values for the isochrones $[\alpha/\text{Fe}]$ grid goes now from -0.2 to +0.6, with steps of 0.2dex. Figure 6 shows that our revised distances are typically larger than those in the literature, placing the great majority of the objects in the sample beyond the nominal separation between inner and outer halo. Assuming an age of 4 Gyr rather than 12 Gyr results in a 20-30% distance increase for most of the stars.

The determination of the distance errors is non-trivial: at face value, the 68% confidence level obtained by repeating the fit with hundreds MonteCarlo realizations of the stars's $\log g$, T_{eff} , $[\text{Fe}/\text{H}]$ and $[\alpha/\text{Fe}]$ drawn from Gaussian distributions centered around the spectroscopically determined values would yield relative errors of 30-40%. However, this is likely to be an overestimate, because in practice several combinations of the randomly drawn $\log g$, T_{eff} , $[\text{Fe}/\text{H}]$ and $[\alpha/\text{Fe}]$ would be rejected by the spectroscopic analysis because not compatible with the spectroscopic diagnostics. Since in the following the distance estimates are only used as additional, possible indicators of the stars's belonging to known substructures, we will consider as error the range of values due to the different ages assumed.

6. Chemical trends

In this section we compare the chemical abundances of our sample of distant MW halo stars to those of MW halo stars from solar neighborhood samples (Venn et al. 2004; Barklem et al. 2005; Nissen & Schuster 2010, 2011; Ishigaki et al. 2012, 2013) and a set of MW satellite galaxies, that is Sculptor (Tolstoy et al. 2009), Fornax (Letarte et al. 2010; Hendricks et al. 2014; Lemasle et al. 2014), LMC (inner disk and bar: Van der Swaelmen et al. 2013), the core of Sag (McWilliam & Smecker-Hane 2005; Carretta et al. 2010) and a sample of Sag stream stars by Chou et al. (2010). For the MW comparison samples, given that our purpose is to compare chemical trends, we specifically focus on studies dealing with halo samples (or studies that allow to select halo stars by providing a membership probability to the various Galactic components) covering a large range in $[\text{Fe}/\text{H}]$ and containing elemental abundances for a large number of elements and stars.

It should be kept in mind that solar neighborhood samples of (kinematically selected) halo stars typically contain a mix of stars belonging to the inner- and outer-halo population, in different proportions, whose orbits are such to place them at present day in the vicinity of the Sun (for the outer-halo population this implies highly elongated orbits), with the inner-halo population dominating at $[\text{Fe}/\text{H}] > -2$ (Carollo et al. 2007; An et al. 2013, 2015). For example, Schuster et al. (2012) computed the orbital properties of the “high” and “low”- α halo stars detected in Nissen & Schuster (2010, 2011) and showed the former to be essentially confined within the inner-halo region (the orbits reach

at most a maximum Galactocentric distance of ~ 15 kpc and a maximum height from the plane of 6-8 kpc), while the latter reaches out to the outer-halo region (spanning a range of maximum Galactocentric distances from ~ 5 kpc to 30-40 kpc and a maximum height from the plane of $\lesssim 18$ kpc). In the case of Ishigaki et al. (2013) the halo sample is estimated to have maximum apocentric distances within 30-40kpc, with the majority belonging to the inner-halo region.

Although the large errors on the proper motion measurements of our sample of distant halo stars, which are typically as large as the proper motions themselves in UCAC5, prevents us from reconstructing their orbital properties, the stars in our sample have large present-day Galactocentric distances (from 12kpc to 73kpc, with a median value of 32kpc). Since the present-day distance is smaller than, or can at most be equal to, the apocentric distance, this implies that our sample probes on average much farther out in the MW outer-halo region with respect to our comparison MW halo samples.

In this section, we display only the figures most relevant to highlight the main results, while the abundance ratios for the full set of elements derived in this work are shown in the Appendix. We will dedicate a separate subsection to discussing star #7, since its chemical properties appear distinct from the bulk of the sample in several elements.

- **Carbon** Figure 7 shows that our measurements compare well with the decreasing trend of $[\text{C}/\text{Fe}]$ as a function of increasing luminosity observed by Kirby et al. (2015) in four MW dwarf spheroidals and in three Galactic globular clusters. Clearly none of the stars in our sample is enhanced in $[\text{C}/\text{Fe}]$, when comparing to the criterion of Aoki et al. (2007) which takes into account evolutionary effects after the first dredge up. If we were to adopt the corrections by Placco et al. (2014) as a function of stellar gravity and metallicity (see their Fig. 9), the $[\text{C}/\text{Fe}]$ of our sample would increase to approximately solar, overlapping the distribution of MW halo stars by Lee et al. (2013) for the same metallicity but landing on its lower envelope. Probing out to $R \sim 20$ kpc and $|z| \sim 15$ kpc, Lee et al. (2017) used SDSS spectra to map the carbonicity of MW stars and found it to increase when moving away from the plane of the Galaxy, with the median $[\text{C}/\text{Fe}]$ being $\gtrsim +0.3$ -0.4 beyond $r_g \sim 20$ kpc. The increase in carbonicity is accompanied by a decrease in the median $[\text{Fe}/\text{H}]$, with the Lee et al. (2017) sample being dominated by stars more metal-poor than $[\text{Fe}/\text{H}] = -1.7$ at those distances. In this work we selected most of our stars from the Spaghetti survey, which targeted stars with relative featureless spectra in the Washington C and M photometric bands. Since these bands include the G-band Carbon feature, we do not claim to have an unbiased sample in $[\text{C}/\text{Fe}]$. Additionally, since more than half of our sample has $[\text{Fe}/\text{H}] > -1.7$ and the fraction of carbon-enhanced stars is known to increase with decreasing metallicity, these have a small chance of being carbon-rich anyway. When not distinguishing between CEMP-no and -s,-r/s and adopting a criterion of $[\text{C}/\text{Fe}] > +0.7$, the fraction of CEMP stars at $[\text{Fe}/\text{H}] < -2$ was found to be 13% by Lee et al. (2013) and 30% by Placco et al. (2014). In that regime our sample contains 7 stars; hence we cannot exclude our non-detection of carbon-enhanced metal-poor stars being due to small number statistics.

- **α -elements** The ratio of α -elements (O, Mg, Si, S, Ca, Ti) over Fe is typically used to trace the relative importance of the ISM chemical enrichment by SN II and SN Ia ejecta. At early times massive stars, which conclude their life as SNe II, are the main players in the chemical enrichment of the ISM. SNe II contribute mainly α -elements and little Fe-peak elements, on time-scales closely tracking star formation, due to the short life-times

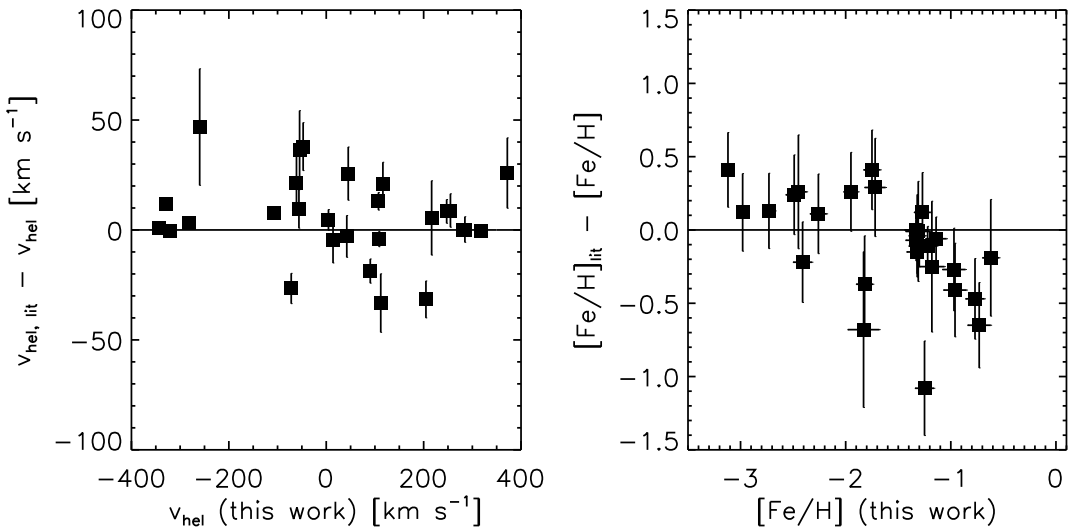


Fig. 5. Comparison between the heliocentric radial velocities (left) and metallicities $[\text{Fe}/\text{H}]$ (right) obtained in this work to those obtained in the original sources.

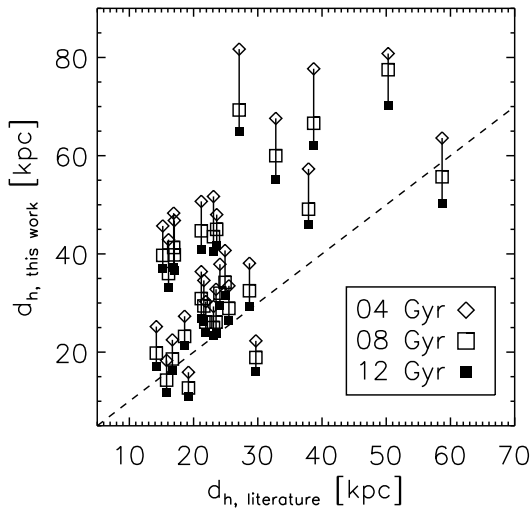


Fig. 6. Comparison between the heliocentric distances derived in the literature and in this work; the different symbols indicate the different ages assumed in the isochrone fitting (see legend).

of SN II progenitors. On the other hand, SNe Ia are the main producers of Fe and their progenitors can have long lifetimes (e.g., Tinsley 1979). Under the assumption of an homogeneously chemically enriched ISM, a decline (“knee”) in $[\alpha/\text{Fe}]$ is then typically interpreted as a consequence of this time-delay (e.g., Gilmore et al. 1989), with stars more metal-poor than the metallicity of the “knee” being born in an environment whose chemical enrichment was largely driven by SN II ejecta.

As visible in Fig. 8, our distant halo stars display enhancements in the ratio of α -elements over Fe with respect to the Solar values and, given the errors on our measurements, do not show significant differences from those of solar neighborhood halo (SoNH) stars over the full range of metallicities explored. Although we cannot state robustly whether, for example, the $[\alpha/\text{Fe}]$ are more compatible with the “high”- α population (possibly formed in-situ) or the “low”- α population (possibly accreted)

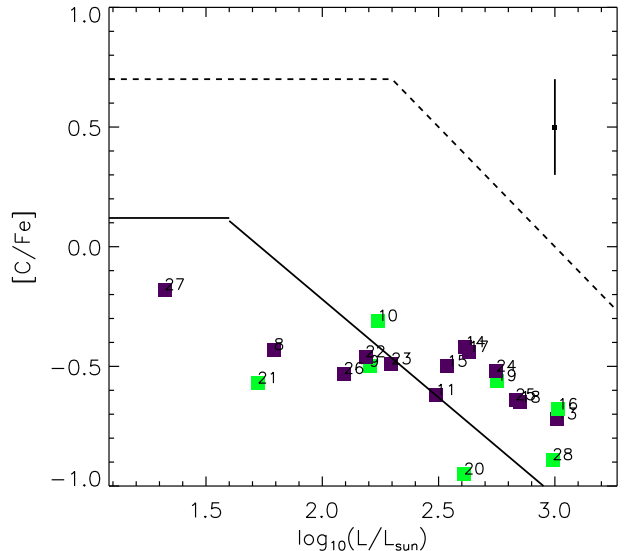


Fig. 7. $[\text{C}/\text{Fe}]$ as a function of luminosity for our sample (squares), split in stars that have spatial and kinematic properties compatible with membership to the Sag stream (green) and not compatible (purple), as described in Sect. 7 (see also Fig. 14). The dashed line indicates the Aoki et al. (2007) criterion for identifying carbon-enhanced metal-poor stars when taking into account evolutionary effects after the first dredge up; the solid line shows the trend of declining $[\text{C}/\text{Fe}]$ with increasing stellar luminosity in three MW globular clusters as in (see Kirby et al. 2015), which also agrees with the trends observed in that same work for the MW classical dSphs Ursa Minor, Draco, Sculptor and Fornax. In the corner we give a representative error-bar.

detected by Nissen & Schuster (2010), in general we can say that these outer halo stars do not appear to have formed from an ISM in which chemical enrichment from SN Ia ejecta was dominant.

As for SoNH stars, at $[\text{Fe}/\text{H}] \lesssim -1.5$ the abundance ratios of our targets overlap those of red giant branch stars in MW satellite

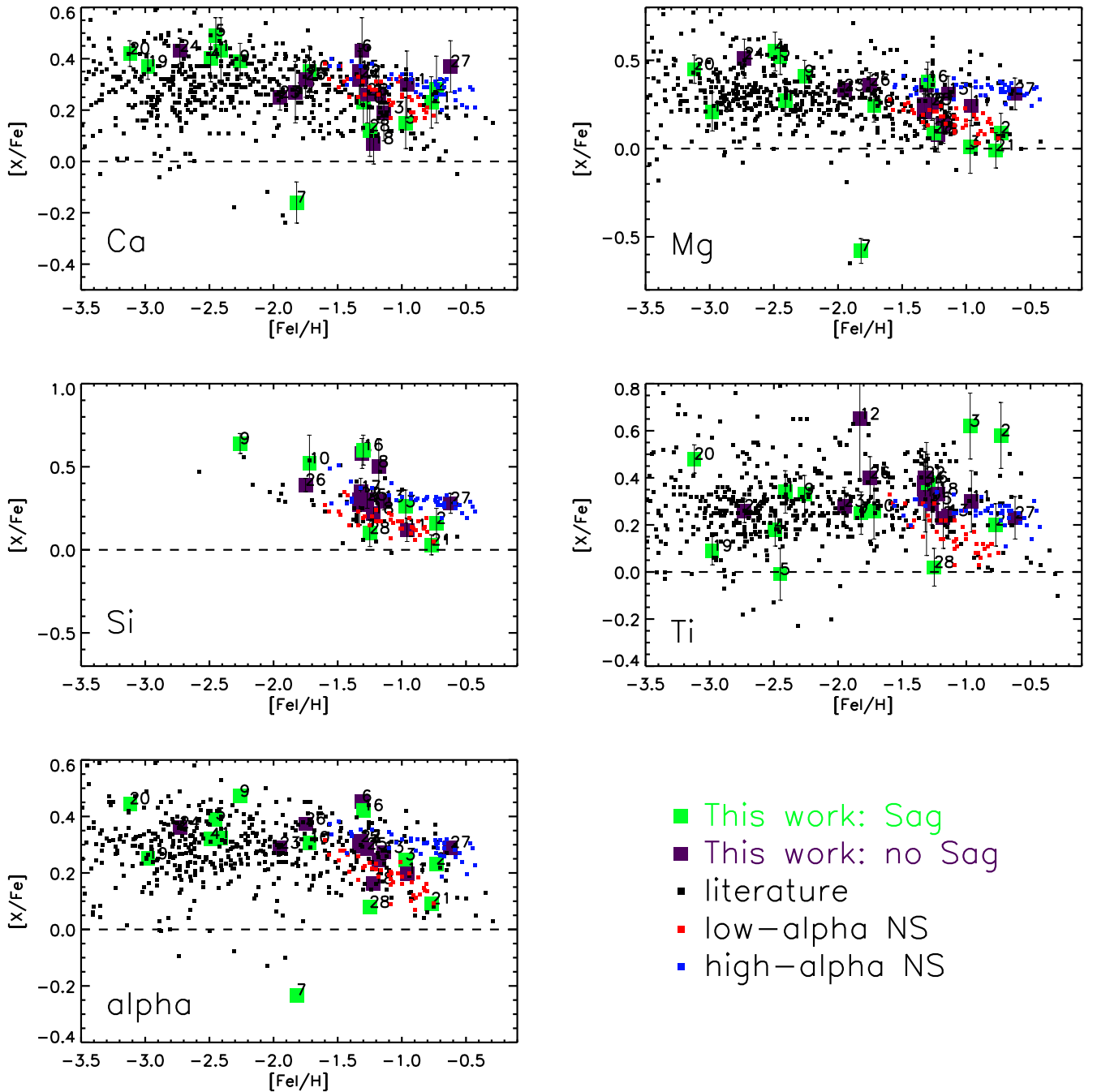


Fig. 8. Abundance of the α elements Ca, Mg, Si, Ti and combined α relative to iron (Fe I) as a function of [Fe I/H]. The sample is split in stars that have spatial and kinematic properties compatible with membership to the Sagittarius stream (green) and not compatible (purple). The small squares indicate the chemical abundances for literature samples of MW halo stars (black ones: Venn et al. (2004), Barklem et al. (2005), Ishigaki et al. (2012, 2013); red and blue: “low- α ” and “high- α ” populations as identified in Nissen & Schuster 2010, 2011). We warn the reader that the global $[\alpha/\text{Fe}]$ shown here and in Figs. 9, 13 has been calculated as the average of the abundance ratio of the individual α -elements to Fe that were available in each of the catalogs.

galaxies (Fig. 9). At higher metallicities their chemical trends depart from those of systems like Sculptor and Fornax, whose stars exhibit solar or even sub-solar ratios of α -elements to iron; however, if we extend the comparison to massive dwarf galaxies such as Sag (from samples in the core) or even the LMC, then we find a good agreement with the values measured for our distant halo stars. Recent work based on APOGEE data by Hasselquist et al. (2017) on larger samples of Sag stars suggests that for this

dwarf galaxy the change from halo-like “high” α -abundances to distinctly lower abundances is happening in the metallicity regime of our most metal-rich targets. Tentatively, we find indeed in this metallicity regime a “low- α ” population, in particular in Mg. As discussed in Sect. 7, a few of these might be genuine Sag stars from their position and velocity, others might be originating from a Sagittarius-like system.

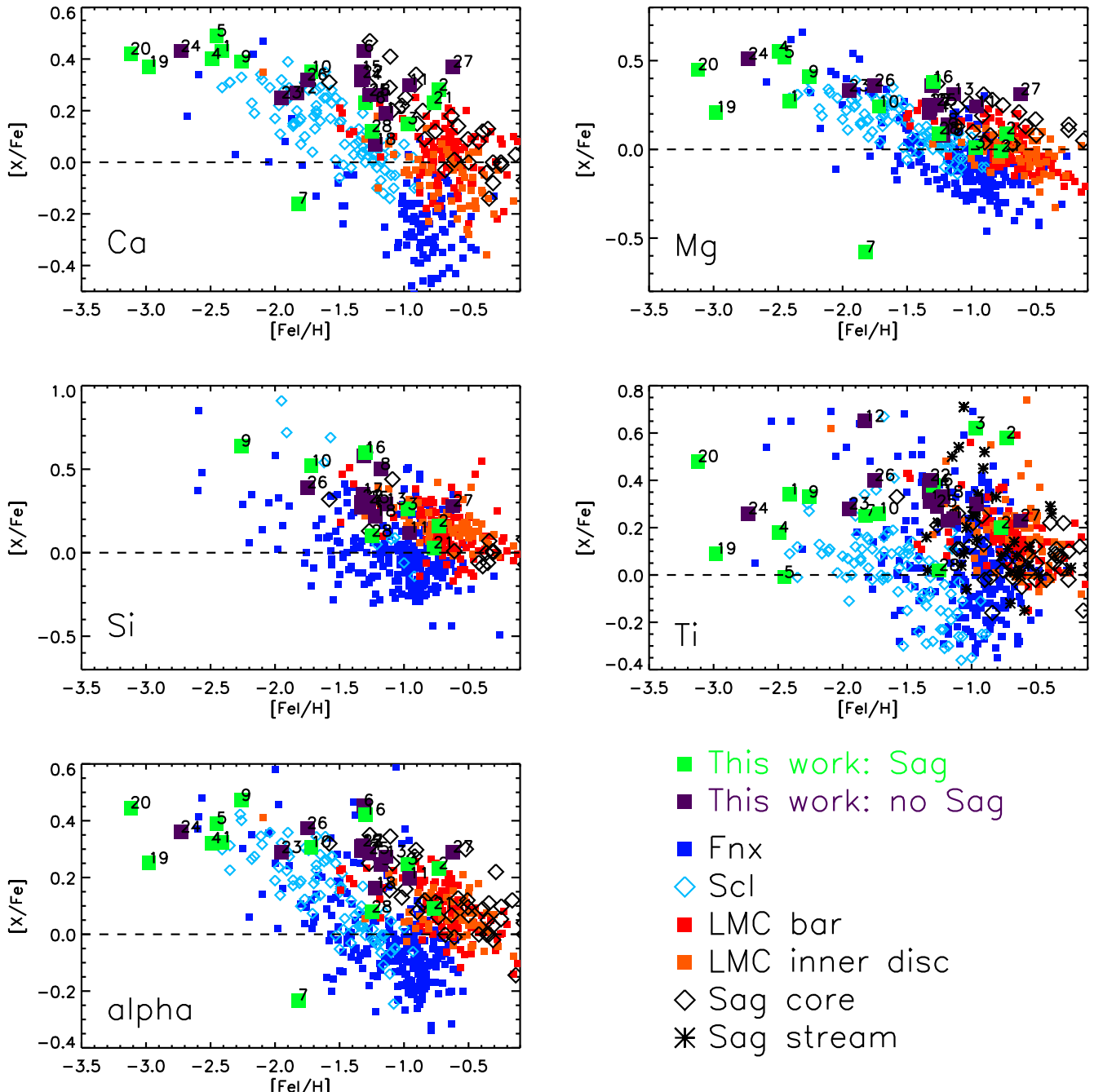


Fig. 9. Abundance of the α elements Ca, Mg, Si, Ti II and combined α relative to iron (Fe I) as a function of [Fe I/H]. The sample is split into stars that have spatial and kinematic properties compatible with membership to the Sag stream (green) and those unlikely to be compatible (purple). The other symbols indicate the chemical abundances for samples of stars in MW satellites, as described in the legend (Fnx = Fornax, Scl = Sculptor).

We point out that we limit the comparison to systems as luminous as, or more luminous (massive) than, the Sculptor dSph, because a) fainter systems have metallicity distribution functions (MDFs) that barely, or do not, reach the largest [Fe/H] of our targets (see e.g., Kirby et al. 2013); b) at a given [Fe/H], the $[\alpha/\text{Fe}]$ of fainter systems is even lower than in Sculptor, which already exhibits clearly solar or sub-solar values (depending on the α -element) at $[\text{Fe}/\text{H}] \sim -1$.

• **Fe-peak elements** The iron-peak elements (see Fig. 10 for Sc, Mn, Ni and Fig. 16 in the Appendix for V, Cr, Co, Cu,

Zn) are mainly formed in explosive nucleosynthesis (but see e.g., Karakas et al. 2008; Karakas 2010, for production of small amounts of Cu and Zn in massive AGB stars). Among them, Scandium is not synthesized in SNe Ia (Woosley et al. 2002), and indeed in MW dwarf galaxies $[\text{Sc}/\text{Fe}]$ appears to show a similar behavior as the ratio of α -elements to Fe, with a “knee”. In our sample, $[\text{Sc}/\text{Fe}]$ appears to be fairly constant, around the Solar value, at all metallicities, exhibiting a range of values again compatible with those of massive dwarf galaxies at $[\text{Fe}/\text{H}] \gtrsim -1.5$, as well as with SoNH samples.

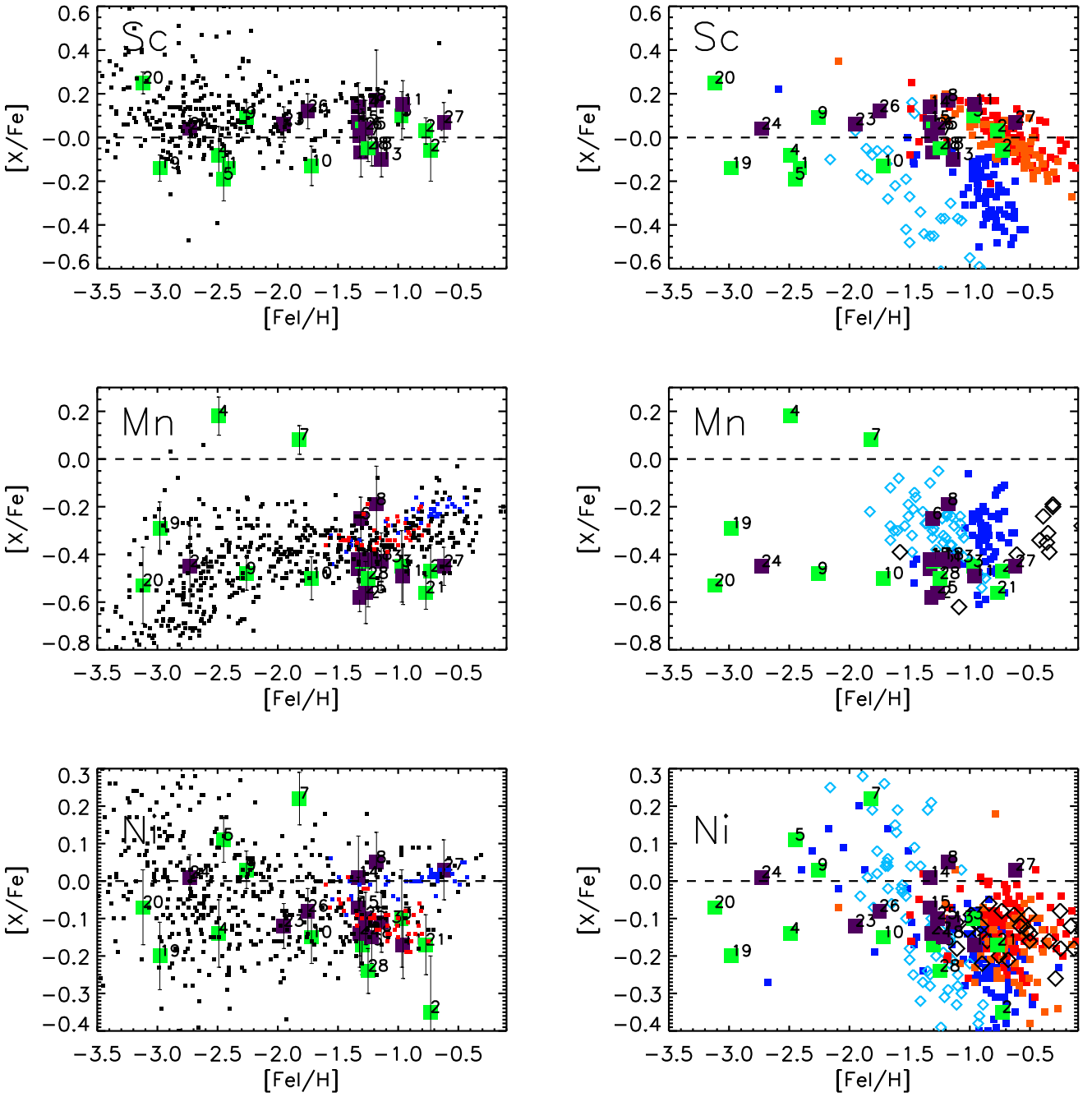


Fig. 10. As previous figure but for iron-peak elements Sc, Mn, Ni relative to iron (Fe I) as a function of [Fe I/H] (left: compared to MW halo samples; right: compared to samples of RGB stars in MW dwarf galaxies). The [Mn/Fe] abundances for MW dwarf galaxies are from North et al. (2012).

We find [Mn/Fe] to be sub-solar, around -0.5dex , for the bulk of our sample, even at the largest metallicities we probe, while in SoNH samples [Mn/Fe] starts increasing at $[\text{Fe}/\text{H}] \gtrsim -1$ (this is clearly seen in Nissen & Schuster 2011, and to a lesser extent in Sobeck et al. 2006, using stars from Fulbright 2000 and Simmerer et al. 2004). This increasing trend of [Mn/Fe] continues to higher metallicities for thick and thin disk stars, see for example Battistini & Bensby (2015). As these authors comment, below $[\text{Fe}/\text{H}] \lesssim -1$, the low [Mn/Fe] ratios are mainly determined by the SN II yields from massive stars (Tsujimoto & Shigeyama 1998), while the increase seen with increasing metal-

licities is interpreted as a contribution from SNe Ia (Kobayashi et al. 2006), with suggestions in the literature that a dependence of Mn yields from SNe Ia with metallicity may contribute to the increase in the [Mn/Fe] ratios (Cescutti et al. 2008). Within this context, the constant sub-solar values shown by our sample, which are lower than in Sculptor and Fornax but at a similar level as in the Sag core (measurements are not available for the LMC in the van der Swaelmen et al. 2013 work), could again point to a lack of strong contribution of SN Ia ejecta to the enrichment of the ISM from which these stars were born. However, Battistini & Bensby (2015) also show that, when applying NLTE correc-

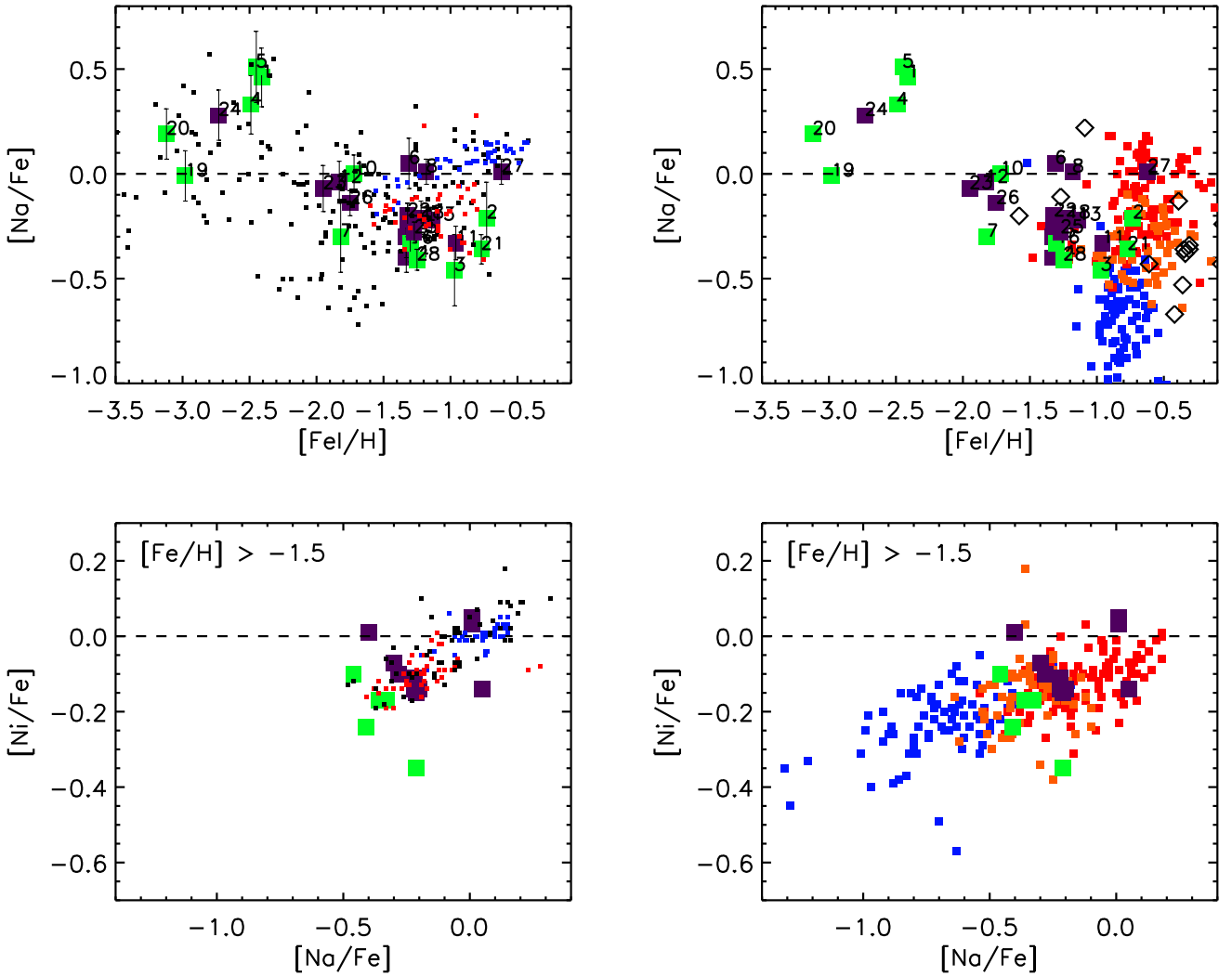


Fig. 11. Top: Abundance of Na relative to iron (Fe I) as a function of [Fe I/H]. Bottom: [Ni/Fe] vs [Na/Fe] for stars more metal-rich than [Fe/H] = -1.5. Left: compared to MW halo samples; right: compared to samples of RGB stars in MW dwarf galaxies.

tions to their sample of thin and thick disk stars, the corresponding Mn trend changes quite drastically, becoming essentially flat and pointing toward Mn sharing the same production site as Fe. Since we are not applying NLTE corrections, we then prefer not to over-interpret the results.

Even though star #4 exhibits super-solar values, it appears compatible with the large scatter in [Mn/Fe] found at low metallicities for SoNH stars.

• **Nickel and sodium** As for the other elements analyzed, also in [Ni/Fe] our outer halo stars cannot be distinguished from SoNH stars of similar metallicities at $[\text{Fe}/\text{H}] \lesssim -1.5$; at larger metallicities, while remaining compatible with the range of values exhibited by SoNH samples, our stars preferentially occupy the sub-solar values end. The same behavior is seen in [Na/Fe]. When considering [Ni/Fe] vs [Na/Fe] (Fig. 11), the “low- α ” and “high- α ” population of Nissen & Schuster (2010) occupy distinct regions of the diagram, with our targets mostly sharing a similar location to the “low- α ” population. However, this does not appear a particularly compelling diagnostic of whether a star is born in a dwarf galaxy: the RGB stars of similar metallicities in massive MW dwarf galaxies show a very broad range of val-

ues on this plane - smoothly transitioning from negative [Ni/Fe] and [Na/Fe] to solar (or almost solar) values when moving from Fornax to the LMC inner disk and then bar - hence almost overlapping with the region occupied by the “high- α ” stars.

• **n-capture elements** We now move on to consider the light neutron-capture element Y- and the heavy n-capture elements Ba- and Eu- (Figure 12; see Figure 15 in the Appendix for Sr, Zr, La and values in the Tables for Ce, Pe, Nd, Sm). Neutron-capture elements are produced by adding neutrons to iron or iron-peak elements; depending on the rate of the captures, the process is called *rapid*, *r* or *slow*, *s*. While the contribution of core collapse supernova from massive stars and compact objects to the *r*-process is still debated (e.g., Arnould et al. 2007), the main *s*-process is constrained to occur in thermally pulsating AGB stars ($1-4 M_{\odot}$) (see e.g., Busso et al. 1999; Travaglio et al. 2004). As discussed in Venn et al. (2004), helium burning in massive stars (the *weak s*-process), only contributes elements lighter than or up to Zr. Hence the *r*-process contributes to the chemical enrichment of the ISM with very little delay with respect to the formation time of the sites of production, while the *s*-process contributes with a delay of a few 100s Myrs with respect to when

the stars were born, therefore tracing chemical enrichment on a slightly longer timescales. Importantly, while Y and Ba can be produced both via the *r*- and *s*- process, Eu is considered as an almost purely *r*- process element (e.g., Truran 1981; Travaglio et al. 1999).

At $[Fe/H] \lesssim -1.5$ the [Y, Ba, Eu / Fe] ratios of our sample overlaps completely with the range of values exhibited by SoNH samples, with [Y/Fe] however occupying the lower end of the SoNH stars [Y/Fe] distribution. On the other hand, significant differences are seen at higher metallicities: most of the stars with $[Fe/H] \sim -1.3$ group at similar values of [Y/Fe], [Ba/Fe] and [Eu/Fe], with the [Y/Fe] and [Eu/Fe] concentrating on the low and high end, respectively, of the range of values exhibited by SoNH samples at similar metallicity, while the [Ba/Fe] is clearly above the approximately solar values of SoNH samples ($+0.4 \lesssim [Ba/Fe] \lesssim +1.0$). The departure of distant halo stars from the chemical abundances of SoNH samples becomes even more evident at $[Fe/H] \gtrsim -1$ in these 3 abundance ratios.

When we compare to RGB stars in dwarf galaxies, [Y/Fe] does not provide much information, due to the large scatter shown by measurements in dwarf galaxies. On the other hand, an increase of [Ba/Fe] to super-solar values similar to those observed in these distant halo stars ($+0.4 \lesssim [Ba/Fe] \lesssim +1.0$) is observed for massive systems such as Fornax and the LMC but not in a relatively small galaxy such as the Sculptor dSph ($L_V \sim 2.3 \times 10^6 L_\odot$, as compared to $L_V \sim 2 \times 10^7 L_\odot$ of Fornax and $\sim 1.5 \times 10^9 L_\odot$ of the LMC, see compilation by McConnachie 2012). In Fornax and the LMC the increase is seen at about 0.3dex higher metallicity than in our sample stars, and at these metallicities RGB stars in these galaxies also show similar enhancements of [Eu/Fe]. This difference in the metallicity at which the high [Ba/Fe] and [Eu/Fe] values kick in are likely a consequence of a difference in the initial star formation rate of the various systems. We remind the reader that, while one might be tempted to interpret the trends observed for the outer halo stars in terms of chemical enrichment within one galactic environment, there is no evidence that these stars belong all to one, disrupted massive system (see next section); hence what we are seeing here is likely stars formed in environments each following a separate evolutionary path; this should caution against providing an interpretation within one single chemical enrichment history.

In Fig. 13 we consider the ratios of [Y/Eu] and [Ba/Eu] in order to gain some insight into the relative contribution of the *s*- and *r*- process. [Ba/Eu] for a pure *r*-process is predicted to be at $[Ba/Eu]_r = -0.69$ (Arlandini et al. 1999) or ~ -0.8 dex (Sneden et al. 2008; Bisterzo et al. 2014), while the pure *s*-process $[Ba/Eu]_s = +1$ (Arlandini et al. 1999) or $+1.15$ (Bisterzo et al. 2014); our stars are within these values, therefore it is likely that the ISM from which they were born was enriched through both the *r*- and *s*- process and that we are likely detecting a component of enrichment from AGB stars. No particular differences are seen with respect to the behavior of SoNH stars or MW dwarf galaxies stars at similar metallicities, which are also thought to have been polluted by AGBs material at $[Fe/H] \gtrsim -2.0$ as witnessed by the rise in [Ba/Eu].

As discussed in Venn et al. (2004), a possible interpretation for a low [Y/Eu] is contributions from metal-poor AGB stars: Y belongs to the first peak that builds through rapid captures around neutron number N=50, while Ba (and La) belong to the second peak that builds around N=82, and at low-metallicity first-peak elements would be bypassed in favor of second-peak elements, because there are fewer nuclei to absorb the available neutrons. They also argue that a high [Ba/Y] would be compat-

ible with the yields of low-metallicity AGB stars. Interestingly, Fenner et al. (2006) show the [Ba/Y] yields of AGB stars of different metallicities as a function of the stellar mass and lifetime (see references therein): at metallicity $[M/H] \sim -1.5$, $[Ba/Y] \sim +0.5$ would be contributed by AGB stars with lifetimes between 150-300Myr, while at the upper end ($[Ba/Y] \sim +0.8$) would be contributed by AGB stars with lifetimes from 800 Myr to several Gyrs. It is beyond the scope of this paper to trace the nucleosynthetic site of the various elements: what we point out though is that, once again, at $[Fe/H] \gtrsim -1.5$ the chemical signature of our outer halo stars departs from the one of SoNH stars, showing a $[Ba/Y] \sim +0.5$, while the latter are scattered around Solar values; also in this case, our sample resembles the pattern exhibited by massive MW dwarf galaxies, thought to show enrichment by low-metallicity AGB stars. It is then possible that our distant targets formed in an environment where pollution of the ISM by AGB stars played a more dominant role with respect to the environment where inner halo stars formed. Due to the delayed contribution of AGB stars, this might imply that our distant halo stars formed in an environment with a slower chemical enrichment than those in the SoNH samples. We note that even the Nissen & Schuster (2011) “low- α ” stars at $[Fe/H] > -1.5$, which the authors argue to have originated in accreted systems, have a much lower [Ba/Y] than we measure at similar metallicity (see also Fishlock et al. 2017): this would suggest a different chemical enrichment path of the systems that deposited their tidal debris in the outskirts of the MW halo.

Finally, the bottom right panel of Fig. 13 shows the location of our targets on the [Ba/Fe] vs $[\alpha/Fe]$ plane to summarize some of the main similarities and differences with respect to MW satellites and SoNH stars at $[Fe/H] > -1.5$. As previously mentioned, at these metallicities, only systems more massive than Sculptor show enhancements in [Ba/Fe] as large as those we detect, which can tentatively point to a lower limit in the mass of the accreted satellite galaxies in which our $[Fe/H] > -1.5$ outer halo stars formed. Since the high [Ba/Fe] (and high [Ba/Y]) can be explained by enrichment of low-metallicity AGB stars with lifetimes from 150Myr to several billion years, these massive accreted systems must have experienced a slower chemical enrichment with respect to MW halo stars found in the more central regions, which have solar [Ba/Fe] and [Ba/Y] at the same metallicity. This might translate into a slightly later accretion time of these massive systems whose shredded stellar component deposited debris at the Galactocentric distances we are probing (at $[Fe/H] > -1.5$: $12 \leq r_g [\text{kpc}] \leq 60$, with a median of 25.5kpc) with respect to the putative accreted population of Nissen & Schuster (2010) whose maximum apocenter reaches to 30-40kpc. Looking at $[\alpha/Fe]$, the bulk of our outer halo stars with $[Fe/H] \sim -1.5$ does not appear to have formed from an ISM dominated by pollution from SNe Ia, hence not long after the “knee”, with the possible exception of #21 and #28, which show the lowest $[\alpha/Fe]$ and among the highest [Ba/Fe]; even though this does not provide a stringent upper limit on the accretion time, it would exclude accretion after several Gyrs from the start of star formation, because in that case we would have expected to detect lower values of $[\alpha/Fe]$. Nonetheless it is interesting to notice that the range of combined $[\alpha/Fe]$ and [Ba/Fe] of RGB stars in massive MW satellites does overlap those of stars in our samples, while this is not the case for the majority of SoNH stars; not only does this highlight again a significant difference in the chemical abundance of halo stars when moving to the outskirts of the halo, but also tells us that chemical abundances as those we are detecting are not “unheard of” among the MW satellites when comparing to systems such as the LMC.

Further comparison to the chemical evolution of the massive MW satellites would need to take into account the age distribution of the stars in the various spectroscopic samples, which not only varies according to the specific star formation history of the dwarf galaxy, but also depends on the spatial location where the spectroscopic samples were gathered, due to the age gradients generally present in dwarf galaxies. However, our findings appear to point to the fact that the MW outer halo could be at least partially made by accretion of systems experiencing a similar chemical enrichment to those of massive MW satellites. This is in agreement with the conclusions reached by Zinn et al. (2014); Fiorentino et al. (2015) on the basis of the period distribution of RR Lyrae stars in the MW halo and MW satellite galaxies.

6.1. Star 07

The elemental abundance ratios of star #07 stand out with respect to the rest of the sample, exhibiting a much lower $[\alpha/\text{Fe}]$ and $[\text{Ba}/\text{Fe}]$, higher $[\text{Mn}/\text{Fe}] \sim +0.1$ and marginally higher $[\text{Ni}/\text{Fe}]$ ($[\text{Mg}/\text{Fe}] \sim -0.6$, $[\text{Ca}/\text{Fe}] \sim -0.15$), $[\text{Ba}/\text{Fe}] \sim -1.6$, $[\text{Mn}/\text{Fe}] \sim +0.1$). The differences in the abundances of star #07 are large enough to be seen visually in the spectrum. Figure 4 exhibits two regions of the HET spectrum of star #07 and a star with similar stellar parameters, star #26. We note that the Fe and Ni features have roughly the same strength while the Ba and Mg features are much weaker in Star #07.

A rise in $[\text{Mn}/\text{Fe}]$ is seen in dSph galaxies at lower metallicities than in the MW (North et al. 2012), which can be explained by a metallicity dependent yield from SNe Ia. This would point to the low $[\alpha/\text{Fe}]$ and low $[\text{Ba}/\text{Fe}]$ being due to a high Fe abundance, perhaps from having originated in/close to a SN Ia pocket.

7. Possible relation to known substructures

Although our targets are not associated to any known MW satellite galaxy or globular cluster, Fig. 1 shows that several of them project onto known MW halo substructures, such as the bright and faint Sag streams, the Orphan stream, the Virgo Overdensity and approximately in the Tri/And region. This raises the question of whether the chemical abundance trends that we have traced, which are distinct from those of halo stars in solar neighborhood samples at $[\text{Fe}/\text{H}] > -1.5$, are due to stars belonging to known MW halo substructures, or are to be ascribed to other features.

7.1. Sagittarius stream

The tidal shredding of the Sag dwarf galaxy (Ibata et al. 1994) has produced the most impressive substructure visible in the halo of our Galaxy. While the inner regions (“core”) of the Sag dwarf galaxy are still gravitationally bound and form a spatially and kinematically confined structure, its stellar tidal debris are spread across a very large area on the sky and strongly overlap with halo stars both in distance, radial velocity and metallicity. To date the Sag stream has been traced both in the northern and southern hemisphere, with the various wraps encompassing heliocentric distances from ~ 25 to 100 kpc, and Galactic Standard of Rest (GSR) velocities¹³ about ± 150 km s $^{-1}$ (e.g., Koposov et al. 2012, Belokurov et al. 2014 and references therein; see Fig. 14). Recently, Hasselquist et al. (2017) have compared Sag

core and MW stars in the metallicity range $-1.2 < [\text{Fe}/\text{H}] < 0$, showing that at $[\text{Fe}/\text{H}] \lesssim -0.8$ Sag core stars exhibit similar chemical patterns than MW stars at high latitude (mostly consistent of halo stars); this makes a distinction based on chemistry alone difficult in the metallicity regime of our targets.

Given the complexity of the Sag system, N-body simulations modeling its orbital evolution in a MW-like gravitational potential offer a useful aid for a first order identification of which stars are most unlikely to be part of the stream. It should be kept in mind though that associating stars with substructures via comparison with models in various phase space parameters inherits the models’ limitations, for example with respect to modeling older wraps of streams and parts of the stream that are far from the main body. The shape of the dark matter halo assumed will influence the modeling of the Sag stream, and in reality such a shape might be complex, time-variable and show variation at different radii (e.g., Vera-Ciro et al. 2011). Additionally, the influence from large perturbers, like the LMC, can not always be ignored (Vera-Ciro & Helmi 2013).

Here we compare the location on the sky and radial velocities of our targets with the predictions from the Law & Majewski (2010, hereafter LM10) model (Fig. 14), following their recommendation of using only particles stripped in the most recent five pericentric passages. We transform the equatorial coordinates of the stars in our sample to a heliocentric coordinate system aligned with the Sag stream; in particular, in this reference frame, the equator is defined by the mid-plane of the Sag trailing tail debris as proposed by Majewski et al. (2003). We follow the convention of Belokurov et al. (2014) where the Sag longitude Λ_\odot increases in the direction of Sag’ motion and the Sag latitude axis B_\odot points to the North Galactic pole.

Due to the known mismatches between the predictions of Sag stream N-body models and some sets of observables (see Fig. 14), we let our comparison be guided also by the observed signatures of portions of the stream, as traced in distance by BHB and red clump (RC) stars and in kinematics by SDSS spectroscopy of giants (using the estimates given in Koposov et al. 2012, Belokurov et al. 2014).

According to the LM10 model, Sag debris can be found at different heights above the mid-plan of the trailing tail, with some dependence on the longitude Λ_\odot range under consideration, with 99.4% of the particles having $-23^\circ < B_\odot < +21^\circ$, approximately. We then adopt a very conservative cut of $|B_\odot| > 23\text{deg}$ to tag which stars in our sample have a location on the sky that makes them unlikely to be associated with the Sag stream (see Fig. 14). Eight of the stars with $|B_\odot| \leq 23\text{deg}$ have GSR velocities well beyond the range of values expected for the stream at the corresponding Λ_\odot , both in terms of predictions from the LM10 model and of the observations, and therefore we also consider them as unlikely to belong to the Sag stream (see Fig. 14): this leaves us with 13 stars being possibly associated and 15 unlikely to belong to the stream.

Of the stars in our sample, none was classified as belonging to the Sag stream (nor other groups) by Janesh et al. (2016); on the other hand, Starkenburg et al. (2010) tag #28 as part of Sag stream, #20 possibly of early stripped Sag tidal debris (if the MW dark matter halo is prolate), while #10 and #26 are most likely associated to the Virgo overdensity, although it cannot be excluded that they belong to the Sag northern leading arm, in particular if the MW DM halo is oblate.

Both samples of unlikely Sag stream members (purple) and possible Sag stream members (green) contain stars in the metallicity regime where we detect differences with SoNH stars (see e.g., Figs. 8-13). Nonetheless, it is evident that the group of stars

¹³ These are line-of-sight heliocentric velocities corrected for the Sun motion and Local Standard of Rest motion, where we use the values from Dehnen & Binney (1998) and $v_{\text{LSR}} = 220$ km s $^{-1}$, respectively.

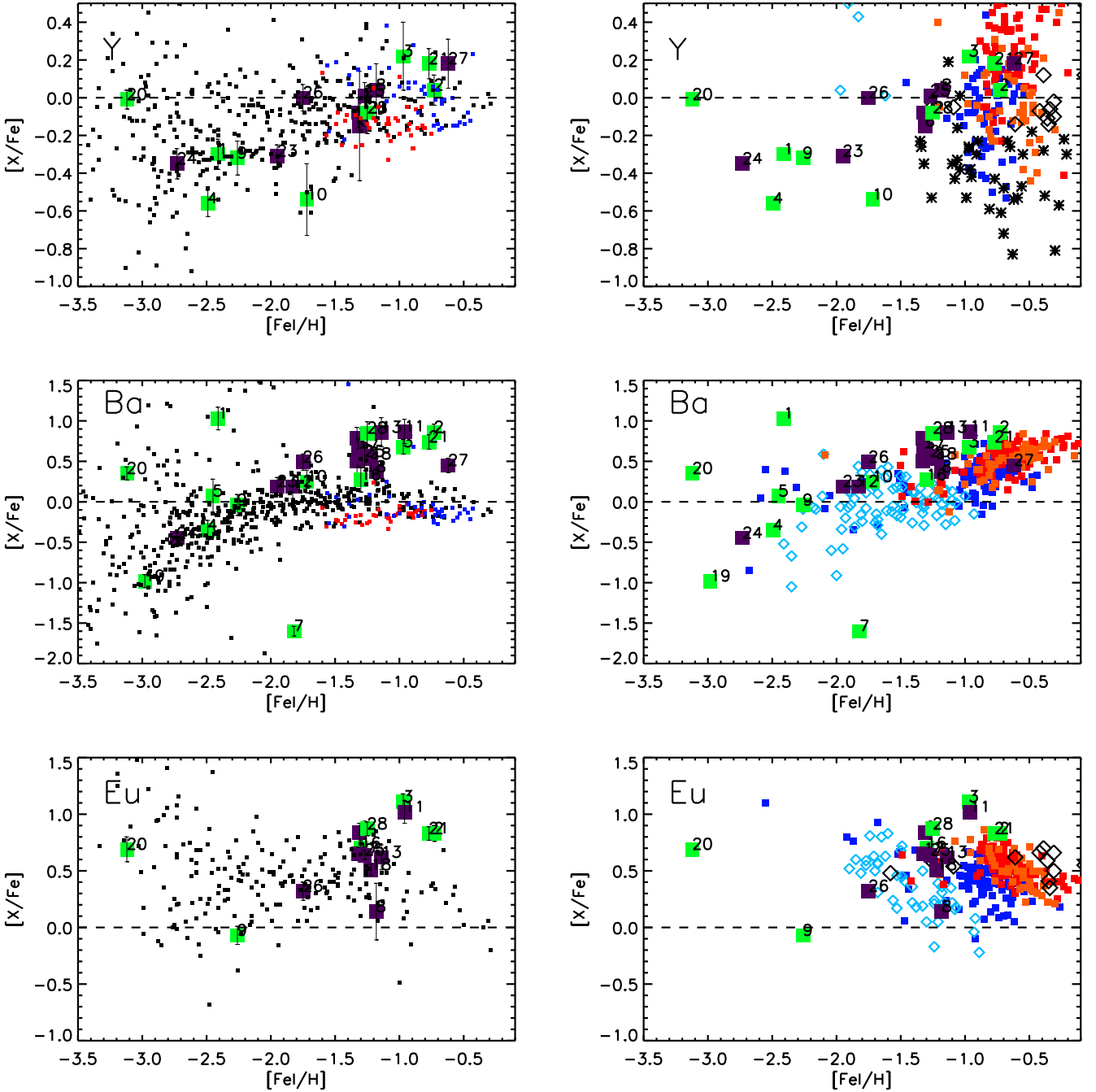


Fig. 12. As previous figure but for n-capture elements Y, Ba, Eu (left: compared to MW halo samples; right: compared to samples of RGB stars in MW dwarf galaxies).

which show the most distinct chemical patterns with respect to SoNH stars, in particular those with $[\text{Fe}/\text{H}] \sim -1.3$ that “clump” in $[\text{Mg}, \text{Si}, \text{Ti}, \text{Mn}, \text{Ni}, \text{Na}, \text{Ba}, \text{Eu}/\text{Fe}]$ and mildly in $[\text{Co}/\text{Fe}]$ are not due to possible Sag stream members.

We emphasize that with our selection we are likely to have overestimated the number of stars possibly belonging to the Sag stream, due to our very conservative Sag latitude selection. For example, the 5th and 95th percentiles of B_\odot for the particles lost in the most recent five pericentric passages in the LM10 model are -11° and 9° ; if we were to adopt this selection, only stars #7 and #28 would have position and kinematics compatible with membership to the stream. Hence, assuming that the LM10

model is not missing any important Sag feature in the regime of sky locations, distances and velocities we are exploring, it seems unlikely that the distinct chemical trends we are detecting at $[\text{Fe}/\text{H}] > -1.5$ between our distant outer halo stars and halo samples in the solar neighborhood are due to “contamination” by Sag stream stars. Therefore, it appears we might be probing the signature of other massive systems accreted by the MW in the outer parts of the stellar halo. In the next section, we will explore possible membership to other known MW halo substructures.

It is noteworthy that the only clearly chemically peculiar star in our sample (#7) would survive as Sag stream member also to the most stringent selection cut in B_\odot ; however, its chemical

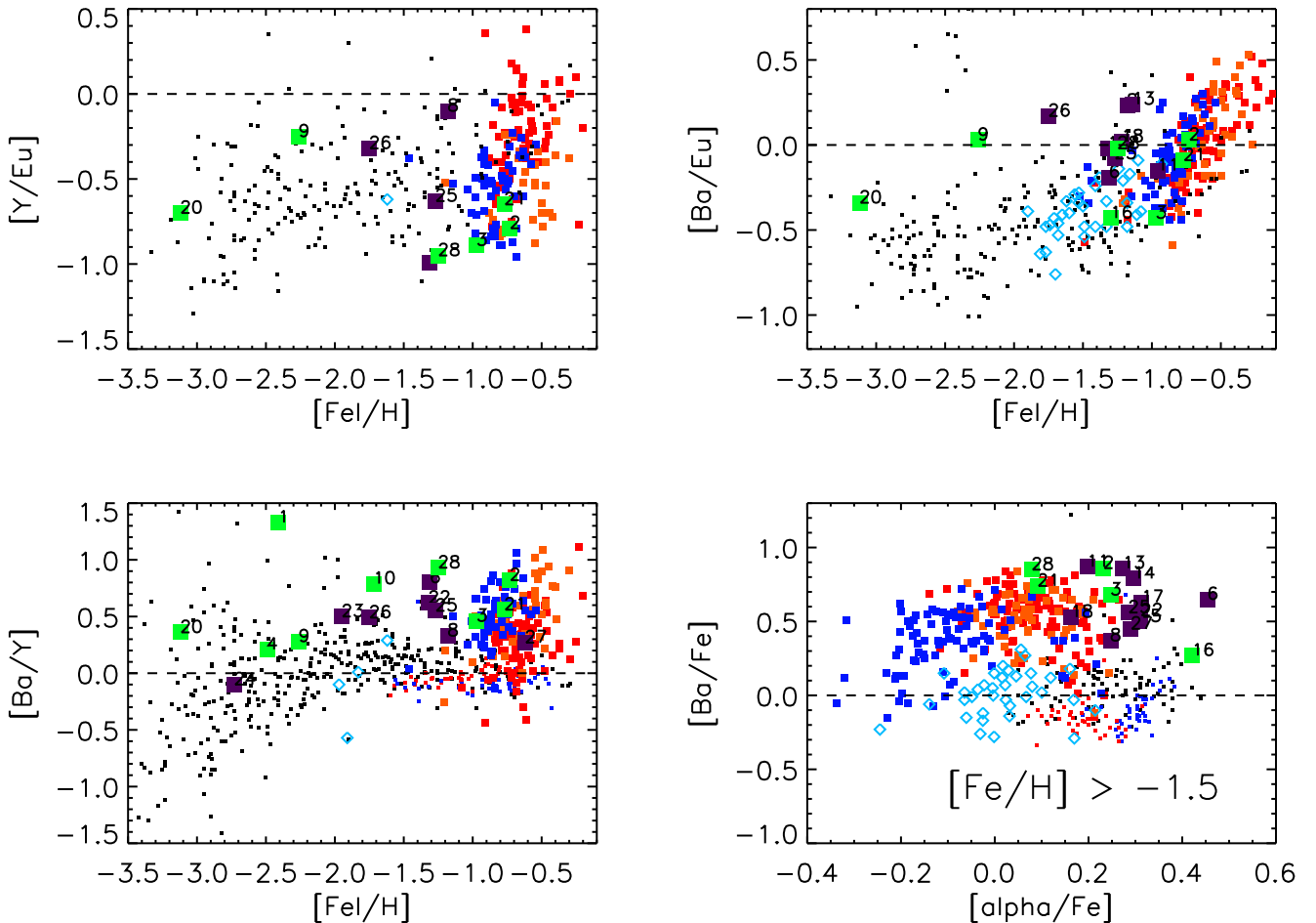


Fig. 13. $[Y/Eu]$, $[Ba/Eu]$, $[Ba/Y]$ vs $[Fe/H]$ at all metallicities, and $[Ba/Fe]$ vs $[a/Fe]$ of stars more metal-rich than $[Fe/H] = -1.5$ in our sample compared to literature samples of MW halo stars and of stars in MW dwarf galaxies (for the symbols see legend in Fig. 8 and 9).

properties do not resemble those of any Sag core stars studied at high resolution to date.

7.2. Other known substructures

Substructures in the MW halo have been detected in a wealth of works in the literature, surveying different portions of the visible sky and using a variety of stellar tracers (M-giants, horizontal branch stars, RR Lyrae, main-sequence-turn-off etc.). This sometimes has led to detections of supposedly different structures, which only later have been linked back to the same features. Reviewing all these studies is clearly beyond the scope of the present work, hence we have taken the review article by Grillmair & Carlin (2016) as reference for the location and general properties of streams and clouds that are known to-date. For those stars in our sample whose location on the sky broadly coincides with any of the substructures listed in that article, we have explored further their possible physical association considering the velocity, and (to a less extent, due to the large uncertainties) the distance, information, going back to the original sources to check more in detail the expected trends in distance and line-of-sight (l.o.s.) velocity as a function of, for instance, galactic coordinates.

The region that encompasses the range $150 < RA [\text{deg}] < 220$, $-20 < DEC [\text{deg}] < +20$, where the majority of our targets falls, is a complex one, being home to the features generally known as the “Virgo Overdensity” (VOD), including the Virgo Stellar Stream (VSS) and partially projecting also onto the Sag stream. The VOD is a poorly understood overdensity with (tentatively) associated to it many different components (e.g., Duffau et al. 2014, and references therein). The heliocentric velocities typically associated to substructures in this area span the range $(200, 360)$ km s^{-1} for the VOD and ~ 130 km s^{-1} for the VSS, while distances of stars associated to these substructures are expected to be approximately less than 20 kpc.

Another part of the sky rich in substructures is in the Triangulum-Andromeda region, where several features have been detected: the Segue 2 ultra-faint object (Belokurov et al. 2009), the Triangulum Stream (Bonaca et al. 2012), and a number of other features detected as overdensities of main sequence (MS) stars, main sequence turn-off (MSTO) stars, or K- and M-giants, dubbed Tri-And 1 and Tri-And 2 (Majewski et al. 2004; Rocha-Pinto et al. 2004; Martin et al. 2007), where some of them may be related to each other and have their origin in the disruption of the same small galactic system (see e.g., Deason et al. 2014; Sheffield et al. 2014).

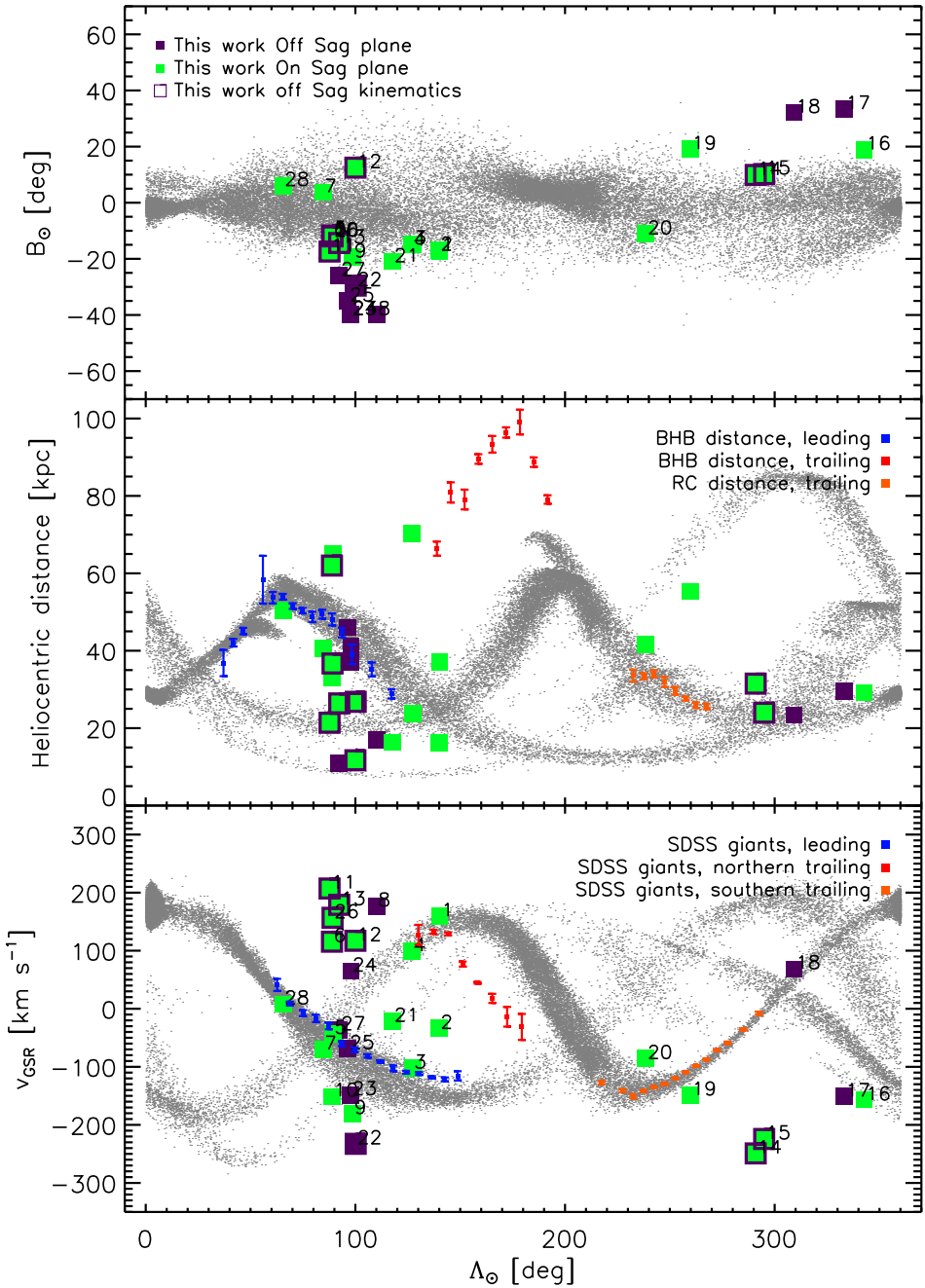


Fig. 14. Location and kinematics of our sample stars (green and purple squared) compared to expectations for the Sag stream from the Law & Majewski (2010) model (gray points; only particles either still bound or stripped in the most recent five pericentric passages are plotted) and from various sources of observations (see legend and main text). The top panel shows the distribution as a function of longitude Λ_\odot and latitude B_\odot in a reference system where the equator is aligned with the Sag stream trailing tail (see Majewski et al. 2003) but with modifications proposed by Belokurov et al. (2014), that is Λ increasing in the direction of the Sag motion and latitude axis pointing to the North Galactic Pole. Middle: Heliocentric distance versus Λ_\odot . Bottom: Galactic standard of Rest velocities versus Λ_\odot . Our targets are shown with large filled squares (green and purple squared having latitude $|B_\odot|$ smaller and larger than 30deg, respectively; green squares with purple border show the sample stars with v_{GSR} incompatible with the expectations/observations of the Sag stream), while the trend derived in the literature using the tracers as in the legend are shown with small (red, blue, and orange) squares with errorbars (see main text for the references to the original articles). We note that our v_{GSR} and those for the Sag particles in the LM10 model have been calculated assuming $R_\odot=8\text{kpc}$, a Local Standard of Rest (LSR) velocity of 220 km s^{-1} and the Solar motion from Dehnen & Binney (1998); in this figure, a factor has been applied to both our velocities and those from the particles in the LM10 model to correct for the different solar motion and v_{LSR} used in Belokurov et al. (2014).

Only a handful of our targets appears to possibly belong to any of the 25 streams and clouds listed in Grillmair & Carlin (2016). Star #18 has position, distance, line-of-sight (l.o.s.) velocity and metallicity that make it compatible with membership to the Hercules-Aquila Cloud. Stars #8,11,13 position, distance, l.o.s. velocity and metallicity fall well within the range of values listed for the VOD, hence they might be members of this structure; on the other hand, stars #1,24,26 have positions, l.o.s. velocities and literature distance estimates compatible with those of VOD stars, but our revised distance values place them beyond 35kpc, making membership to the VOD unlikely. The metallicity does not provide a very tight constrain, as stars in the VOD have been measured to have a broad range of values, within $-2 \lesssim [\text{Fe}/\text{H}] \lesssim -1$; the metallicity of #1 & 24 could be considered too low ($[\text{Fe}/\text{H}] = -2.4$ and -2.7 , respectively), but one cannot exclude that the MDF of VOD stars extends to lower values, in particular if the VOD is all or in part the result of the accretion of a dwarf galaxy.

In any case, of the stars with $[\text{Fe}/\text{H}] \sim -1.3$ clumping in $[\text{Mg}, \text{Si}, \text{Ti}, \text{Y}, \text{Ba}, \text{Eu}, \text{Na}$ and Ni/Fe] and $[\text{Co}/\text{Fe}]$, only #13 and #18 would appear to belong to known MW halo substructures other than Sag (VOD and Hercules-Aquila, respectively). Hence, overall, the aforementioned chemical trend does not appear to be due to stars belonging to known MW substructures.

8. Summary and conclusions

We have obtained VLT/UVES, Magellan/MIKE and HET/HRS high resolution optical spectroscopy for a sample of 28 halo stars with heliocentric distances $12 \leq d_h [\text{kpc}] \leq 73$ (median $d_h = 32\text{kpc}$), for which we have derived chemical abundances for 27 elements.

The large present-day distances of the stars in our sample place them in the outer-halo region of the MW and allow us to explore the chemical properties of MW halo stars over a considerably larger volume than literature studies based on high resolution spectroscopy of larger samples of halo stars currently found in the solar neighborhood. The sample size is even competitive with respect to what is currently provided by high resolution spectroscopic surveys such as APOGEE at similar distances and provides abundances for 11 elements in common and 16 not available from APOGEE.

At $[\text{Fe}/\text{H}] \lesssim -1.5$ the chemical properties of our sample stars mostly overlap those exhibited by SoNH stars. However, at $[\text{Fe}/\text{H}] \gtrsim -1.5$ differences are seen in particular for $[\text{Mn}, \text{Ni}, \text{Na}, \text{Ba}, \text{Eu}/\text{Fe}], [\text{Ba}/\text{Y}]$ and $[\text{Ba}/\text{Eu}]$, either as the chemical properties of our sample departing from those of SoNH stars or “clumping” in a restricted region of values with respect to the broader distribution shown by SoNH stars of similar metallicities (this can also be appreciated in $[\text{Mg}, \text{Si}, \text{Ti}/\text{Fe}]$). For the majority of stars at high metallicity the detected trends do not appear to be due to stars belonging to known MW substructures, including the Sag stream.

We analyze this behavior in the light of the chemical abundances measured for RGB stars in MW dwarf galaxies, including in the comparison also massive systems such as Sag and the LMC. Super-solar values of $[\text{Ba}/\text{Fe}]$ as those measured at $[\text{Fe}/\text{H}] \gtrsim -1.5$ in our sample appear only in the most luminous (massive) satellites (Fornax, Sag and the LMC), but not in the Sculptor dSph ($L_V \sim 2.3 \times 10^6 L_\odot$), for which $[\text{Ba}/\text{Fe}]$ remains constant to a solar-value in the high metallicity regime. On the other hand, the ratio of α -elements to iron do not resemble those observed for RGB stars of similar metallicity in the Fornax dSph, while compare well to Sag and LMC stars. We find that

the elemental abundances of stars in the most luminous dwarf galaxies show similar trends to those seen in our data for the elements for which we see differences with respect to SoNH stars at $[\text{Fe}/\text{H}] \gtrsim -1.5$. We conclude that, if MW outer halo stars have originated in the shredded stellar component of accreted dwarf galaxies, then the MW outer halo is partially formed by massive accreted systems. The large super-solar values we measure for $[\text{Ba}/\text{Fe}]$ and $[\text{Ba}/\text{Y}]$, which can be interpreted as the result of pollution by metal-poor AGB stars over time-scales of few 100s Myr to almost 1Gyr, compared to the solar values of SoNH samples at similar metallicities, might indicate that star formation in the accreted systems was able to proceed on longer time-scales than the accreted systems that possibly contributed to the build-up of the more internal halo regions, possibly because of later accretion times.

Due to our target selection (see Sect. 2), half of our targets have $[\text{Fe}/\text{H}] > -1.6$, which is the regime where we detect the most interesting differences with SoNH samples. Data from SDSS low resolution optical spectroscopy (Fernández-Alvar et al. 2015) suggest that at large Galactocentric distances, in particular at $r_g \gtrsim 30\text{kpc}$, stars with $-1.5 \lesssim [\text{Fe}/\text{H}] \lesssim -0.8$, are not very common and essentially occupy the high metallicity tail of the metallicity distribution of MW stars. If stars in the MW outer halo originated in accreted dwarf galaxies, this would imply that this metallicity regime is sampling the end point of their chemical evolution. We note that the metallicity distribution function of MW satellite stars are very wide, encompassing a few dex in $[\text{Fe}/\text{H}]$ even for the systems that have stopped star formation at $z > 2$; hence if we are probing the high metallicity tail of accreted systems, these will have carried with them a significant, or even larger, portion of more metal-poor stars that are now spread out in the outer halo. It will be interesting to see if just a few massive systems might have formed a considerable fraction of the MW outer halo.

Acknowledgements. The authors are indebted to the International Space Science Institute (ISSI), Bern, Switzerland, for supporting and funding the international team “First stars in dwarf galaxies”, where the idea for this project was born. The authors acknowledge the referee, T. Beers, for useful comments and H. Morrison for providing clarification about possible selection effects in the Spaghetti survey with respect to the star’s Carbon abundances. GB gratefully acknowledges financial support by the Spanish Ministry of Economy and Competitiveness (MINECO) under the Ramon y Cajal Programme (RYC-2012-11537) and the grant AYA2014-56795-P. ES gratefully acknowledges funding by the Emmy Noether program from the Deutsche Forschungsgemeinschaft (DFG). The Hobby-Eberly Telescope (HET) is a joint project of the University of Texas at Austin, the Pennsylvania State University, Stanford University, Ludwig-Maximilians-Universität München, and Georg-August-Universität Göttingen. The HET is named in honor of its principal benefactors, William P. Hobby and Robert E. Eberly. This work has made use of data from the European Space Agency (ESA) mission *Gaia* (<https://www.cosmos.esa.int/gaia>), processed by the *Gaia* Data Processing and Analysis Consortium (DPAC, <https://www.cosmos.esa.int/web/gaia/dpac/consortium>). Funding for the DPAC has been provided by national institutions, in particular the institutions participating in the *Gaia* Multilateral Agreement.

References

- Ahn, C. P., Alexandroff, R., Allende Prieto, C., et al. 2014, ApJS, 211, 17
- Allende Prieto, C., Fernández-Alvar, E., Schlesinger, K. J., et al. 2014, A&A, 568, A7
- Alvarez, R. & Plez, B. 1998, A&A, 330, 1109
- An, D., Beers, T. C., Johnson, J. A., et al. 2013, ApJ, 763, 65
- An, D., Beers, T. C., Santucci, R. M., et al. 2015, ApJ, 813, L28
- Anders, E. & Grevesse, N. 1989, Geochim. Cosmochim. Acta, 53, 197
- Anthony-Twarog, B. J., Deliyannis, C. P., Rich, E., & Twarog, B. A. 2013, ApJ, 767, L19
- Aoki, W. 2008, Data reduction of echelle spectra with IRAF, Report Version 1.1, National Astronomical Observatory of Japan
- Aoki, W., Beers, T. C., Christlieb, N., et al. 2007, ApJ, 655, 492

- Arenou, F., Luri, X., Babusiaux, C., et al. 2017, A&A, 599, A50
- Arlandini, C., Käppeler, F., Wissak, K., et al. 1999, ApJ, 525, 886
- Arnould, M., Goriely, S., & Takahashi, K. 2007, Phys. Rep., 450, 97
- Barklem, P. S., Christlieb, N., Beers, T. C., et al. 2005, A&A, 439, 129
- Battaglia, G., Irwin, M., Tolstoy, E., et al. 2008, MNRAS, 383, 183
- Battistini, C. & Bensby, T. 2015, A&A, 577, A9
- Beers, T. C., Carollo, D., Ivezić, Ž., et al. 2012, ApJ, 746, 34
- Belokurov, V., Koposov, S. E., Evans, N. W., et al. 2014, MNRAS, 437, 116
- Belokurov, V., Walker, M. G., Evans, N. W., et al. 2009, MNRAS, 397, 1748
- Bernard, E. J., Ferguson, A. M. N., Schlafly, E. F., et al. 2016, MNRAS, 463, 1759
- Bernstein, R., Shectman, S. A., Gunnels, S. M., Mochnacki, S., & Athey, A. E. 2003, in Proc. SPIE, Vol. 4841, Instrument Design and Performance for Optical/Infrared Ground-based Telescopes, ed. M. Iye & A. F. M. Moorwood, 1694–1704
- Bisterzo, S., Travaglio, C., Gallino, R., Wiescher, M., & Käppeler, F. 2014, ApJ, 787, 10
- Bonaca, A., Jurić, M., Ivezić, Ž., et al. 2012, AJ, 143, 105
- Bullock, J. S. & Johnston, K. V. 2005, ApJ, 635, 931
- Busso, M., Gallino, R., & Wasserburg, G. J. 1999, ARA&A, 37, 239
- Carollo, D., Beers, T. C., Chiba, M., et al. 2010, ApJ, 712, 692
- Carollo, D., Beers, T. C., Lee, Y. S., et al. 2007, Nature, 450, 1020
- Carollo, D., Beers, T. C., Placco, V. M., et al. 2016, Nature Physics, 12, 1170
- Carrasco, J. M., Evans, D. W., Montegriffo, P., et al. 2016, A&A, 595, A7
- Carretta, E., Bragaglia, A., Gratton, R. G., et al. 2010, A&A, 520, A95
- Cayrel, R. 1988, in IAU Symposium, Vol. 132, The Impact of Very High S/N Spectroscopy on Stellar Physics, ed. G. Cayrel de Strobel & M. Spite, 345
- Cescutti, G., Matteucci, F., Lanfranchi, G. A., & McWilliam, A. 2008, A&A, 491, 401
- Chou, M.-Y., Cunha, K., Majewski, S. R., et al. 2010, ApJ, 708, 1290
- Cohen, J. G. & Huang, W. 2009, ApJ, 701, 1053
- Cooper, A. P., Cole, S., Frenk, C. S., et al. 2010, MNRAS, 406, 744
- Das, P. & Binney, J. 2016, MNRAS, 460, 1725
- de Boer, T. J. L., Belokurov, V., Beers, T. C., & Lee, Y. S. 2014, MNRAS, 443, 658
- de Jong, J. T. A., Yanny, B., Rix, H.-W., et al. 2010, ApJ, 714, 663
- Deason, A. J., Belokurov, V., Hamren, K. M., et al. 2014, MNRAS, 444, 3975
- Deason, A. J., Belokurov, V., Koposov, S. E., et al. 2017, MNRAS, 470, 1259
- Dehnen, W. & Binney, J. J. 1998, MNRAS, 298, 387
- Dekker, H., D'Odorico, S., Kaufer, A., Delabre, B., & Kotzlowski, H. 2000, in Proc. SPIE, Vol. 4008, Optical and IR Telescope Instrumentation and Detectors, ed. M. Iye & A. F. Moorwood, 534–545
- Dohm-Palmer, R. C., Helmi, A., Morrison, H., et al. 2001, ApJ, 555, L37
- Dotter, A., Chaboyer, B., Jevremović, D., et al. 2008, ApJS, 178, 89
- Duffau, S., Vivas, A. K., Zinn, R., Méndez, R. A., & Ruiz, M. T. 2014, A&A, 566, A118
- Evans, D. W., Riello, M., De Angeli, F., et al. 2017, A&A, 600, A51
- Fenner, Y., Gibson, B. K., Gallino, R., & Lugaro, M. 2006, ApJ, 646, 184
- Fernández-Alvar, E., Allende Prieto, C., Schlesinger, K. J., et al. 2015, A&A, 577, A81
- Fernández-Alvar, E., Carigi, L., Allende Prieto, C., et al. 2017, MNRAS, 465, 1586
- Fiorentino, G., Bono, G., Monelli, M., et al. 2015, ApJ, 798, L12
- Fishlock, C. K., Yong, D., Karakas, A. I., et al. 2017, MNRAS, 466, 4672
- Fulbright, J. P. 2000, AJ, 120, 1841
- Fulbright, J. P. 2002, AJ, 123, 404
- Gaia Collaboration, Brown, A. G. A., Vallenari, A., et al. 2016a, A&A, 595, A2
- Gaia Collaboration, Prusti, T., de Bruijne, J. H. J., et al. 2016b, A&A, 595, A1
- Gilmore, G., Wyse, R. F. G., & Kuijken, K. 1989, ARA&A, 27, 555
- Grevesse, N. & Sauval, A. J. 1998, Space Science Reviews, 85, 161
- Grillmair, C. J. & Carlin, J. L. 2016, Tidal Streams in the Local Group and Beyond, 420, 87
- Gustafsson, B., Edvardsson, B., Eriksson, K., et al. 2008, A&A, 486, 951
- Hasselquist, S., Shetrone, M., Smith, V., et al. 2017, ArXiv e-prints
- Hawkins, K., Jofré, P., Masseron, T., & Gilmore, G. 2015, MNRAS, 453, 758
- Helmi, A. 2008, A&A Rev., 15, 145
- Hendricks, B., Koch, A., Lanfranchi, G. A., et al. 2014, ApJ, 785, 102
- Hinkle, K., Wallace, L., Harmer, D., Ayres, T., & Valenti, J. 2000, in IAU Joint Discussion, Vol. 1, IAU Joint Discussion
- Ibata, R. A., Gilmore, G., & Irwin, M. J. 1994, Nature, 370, 194
- Ishigaki, M. N., Aoki, W., & Chiba, M. 2013, ApJ, 771, 67
- Ishigaki, M. N., Chiba, M., & Aoki, W. 2012, ApJ, 753, 64
- Jablonska, P., North, P., Mashonkina, L., et al. 2015, A&A, 583, A67
- Janesh, W., Morrison, H. L., Ma, Z., et al. 2016, ApJ, 816, 80
- Karakas, A. I. 2010, MNRAS, 403, 1413
- Karakas, A. I., Lee, H. Y., Lugaro, M., Görres, J., & Wiescher, M. 2008, ApJ, 676, 1254
- Kirby, E. N. & Cohen, J. G. 2012, AJ, 144, 168
- Kirby, E. N., Cohen, J. G., Guhathakurta, P., et al. 2013, ApJ, 779, 102
- Kirby, E. N., Guo, M., Zhang, A. J., et al. 2015, ApJ, 801, 125
- Kobayashi, C., Umeda, H., Nomoto, K., Tominaga, N., & Ohkubo, T. 2006, ApJ, 653, 1145
- Koposov, S. E., Belokurov, V., Evans, N. W., et al. 2012, ApJ, 750, 80
- Kupka, F., Piskunov, N., Ryabchikova, T. A., Stempels, H. C., & Weiss, W. W. 1999, A&AS, 138, 119
- Kupka, F. G., Ryabchikova, T. A., Piskunov, N. E., Stempels, H. C., & Weiss, W. W. 2000, Baltic Astronomy, 9, 590
- Law, D. R. & Majewski, S. R. 2010, ApJ, 714, 229
- Lee, Y. S., Beers, T. C., Kim, Y. K., et al. 2017, ApJ, 836, 91
- Lee, Y. S., Beers, T. C., Masseron, T., et al. 2013, AJ, 146, 132
- Lemasle, B., de Boer, T. J. L., Hill, V., et al. 2014, A&A, 572, A88
- Letarte, B., Hill, V., Tolstoy, E., et al. 2010, A&A, 523, A17
- Lindgren, L., Lammers, U., Bastian, U., et al. 2016, A&A, 595, A4
- Lodders, K., Palme, H., & Gail, H.-P. 2009, Landolt Börnstein
- Magain, P. 1984, A&A, 134, 189
- Majewski, S. R., Ostheimer, J. C., Rocha-Pinto, H. J., et al. 2004, ApJ, 615, 738
- Majewski, S. R., Skrutskie, M. F., Weinberg, M. D., & Ostheimer, J. C. 2003, ApJ, 599, 1082
- Martin, N. F., Ibata, R. A., & Irwin, M. 2007, ApJ, 668, L123
- Martínez-Delgado, D., Pohlen, M., Gabany, R. J., et al. 2009, ApJ, 692, 955
- McConnachie, A. W. 2012, AJ, 144, 4
- McConnachie, A. W., Irwin, M. J., Ibata, R. A., et al. 2009, Nature, 461, 66
- McWilliam, A. & Smecker-Hane, T. A. 2005, ApJ, 622, L29
- Merle, T., Fabrizio, M., Thévenin, F., Nonino, M., & Bono, G. 2012, in SF2A-2012: Proceedings of the Annual meeting of the French Society of Astronomy and Astrophysics, ed. S. Boissier, P. de Laverny, N. Nardetto, R. Samadi, D. Valls-Gabaud, & H. Wozniak, 97–101
- Morrison, H. L., Mateo, M., Olszewski, E. W., et al. 2000, AJ, 119, 2254
- Morrison, H. L., Norris, J., Mateo, M., et al. 2003, AJ, 125, 2502
- Morrison, H. L., Olszewski, E. W., Mateo, M., et al. 2001, AJ, 121, 283
- Mouhcine, M., Ibata, R., & Rejkuba, M. 2011, MNRAS, 415, 993
- Mucciarelli, A. 2013, ArXiv e-prints
- Nissen, P. E. & Schuster, W. J. 1997, A&A, 326, 751
- Nissen, P. E. & Schuster, W. J. 2010, A&A, 511, L10
- Nissen, P. E. & Schuster, W. J. 2011, A&A, 530, A15
- North, P., Cescutti, G., Jablonka, P., et al. 2012, A&A, 541, A45
- Pillepich, A., Vogelsberger, M., Deason, A., et al. 2014, MNRAS, 444, 237
- Piskunov, N. E., Kupka, F., Ryabchikova, T. A., Weiss, W. W., & Jeffery, C. S. 1995, A&AS, 112, 525
- Placco, V. M., Frebel, A., Beers, T. C., & Stancliffe, R. J. 2014, ApJ, 797, 21
- Plez, B. 2012, Turbospectrum: Code for spectral synthesis, astrophysics Source Code Library
- Prochaska, J. X. & McWilliam, A. 2000, ApJ, 537, L57
- Ramírez, I. & Meléndez, J. 2005, ApJ, 626, 465
- Ramírez, I., Meléndez, J., & Chanamé, J. 2012, ApJ, 757, 164
- Ramsey, L. W., Adams, M. T., Barnes, T. G., et al. 1998, in Proc. SPIE, Vol. 3352, Advanced Technology Optical/IR Telescopes VI, ed. L. M. Stepp, 34–42
- Rich, R. M., Collins, M. L. M., Black, C. M., et al. 2012, Nature, 482, 192
- Rocha-Pinto, H. J., Majewski, S. R., Skrutskie, M. F., Crane, J. D., & Patterson, R. J. 2004, ApJ, 615, 732
- Roederer, I. U. 2009, AJ, 137, 272
- Roederer, I. U., Frebel, A., Shetrone, M. D., et al. 2008, ApJ, 679, 1549
- Roederer, I. U., Sneden, C., Thompson, I. B., Preston, G. W., & Shectman, S. A. 2010, ApJ, 711, 573
- Ryabchikova, T., Piskunov, N., Kurucz, R. L., et al. 2015, Phys. Scr, 90, 054005
- Ryabchikova, T. A., Piskunov, N. E., Kupka, F., & Weiss, W. W. 1997, Baltic Astronomy, 6, 244
- Santucci, R. M., Beers, T. C., Placco, V. M., et al. 2015, ApJ, 813, L16
- Schlafly, E. F. & Finkbeiner, D. P. 2011, ApJ, 737, 103
- Schlegel, D. J., Finkbeiner, D. P., & Davis, M. 1998, ApJ, 500, 525
- Schuster, W. J., Moreno, E., Nissen, P. E., & Pichardo, B. 2012, A&A, 538, A21
- Searle, L. & Zinn, R. 1978, ApJ, 225, 357
- Sheffield, A. A., Johnston, K. V., Majewski, S. R., et al. 2014, ApJ, 793, 62
- Shetrone, M., Cornell, M. E., Fowler, J. R., et al. 2007, PASP, 119, 556
- Simmerer, J., Sneden, C., Cowan, J. J., et al. 2004, ApJ, 617, 1091
- Sneden, C., Cowan, J. J., & Lugaro, M. 2008, ARA&A, 46, 241
- Sobeck, J. S., Ivans, I. I., Simmerer, J. A., et al. 2006, AJ, 131, 2949
- Starkenburg, E. 2011, PhD thesis, Kapteyn Astronomical Institute, University of Groningen
- Starkenburg, E., Hill, V., Tolstoy, E., et al. 2010, A&A, 513, A34
- Stetson, P. B. & Pancino, E. 2008, PASP, 120, 1332
- Stetson, P. B. & Pancino, E. 2010, DAOSPEC: An Automatic Code for Measuring Equivalent Widths in High-resolution Stellar Spectra, astrophysics Source Code Library
- Tafelmeyer, M., Jablonka, P., Hill, V., et al. 2010, A&A, 524, A58+

- Tinsley, B. M. 1979, ApJ, 229, 1046
 Tissera, P. B., Beers, T. C., Carollo, D., & Scannapieco, C. 2014, MNRAS, 439,
 3128
 Tissera, P. B., Scannapieco, C., Beers, T. C., & Carollo, D. 2013, MNRAS, 432,
 3391
 Tissera, P. B., White, S. D. M., & Scannapieco, C. 2012, MNRAS, 420, 255
 Tolstoy, E., Hill, V., & Tosi, M. 2009, ARA&A, 47, 371
 Travaglio, C., Galli, D., Gallino, R., et al. 1999, ApJ, 521, 691
 Travaglio, C., Gallino, R., Arnone, E., et al. 2004, ApJ, 601, 864
 Truran, J. W. 1981, A&A, 97, 391
 Tsujimoto, T. & Shigeyama, T. 1998, ApJ, 508, L151
 Tull, R. G. 1998, in Proc. SPIE, Vol. 3355, Optical Astronomical
 Instrumentation, ed. S. D'Odorico, 387–398
 Van der Swaelmen, M., Hill, V., Primas, F., & Cole, A. A. 2013, A&A, 560, A44
 van Leeuwen, F., Evans, D. W., De Angeli, F., et al. 2017, A&A, 599, A32
 Venn, K. A., Irwin, M., Shetrone, M. D., et al. 2004, AJ, 128, 1177
 Vera-Ciro, C. & Helmi, A. 2013, ApJ, 773, L4
 Vera-Ciro, C. A., Sales, L. V., Helmi, A., et al. 2011, MNRAS, 416, 1377
 Woosley, S. E., Heger, A., & Weaver, T. A. 2002, Reviews of Modern Physics,
 74, 1015
 Xue, X.-X., Ma, Z., Rix, H.-W., et al. 2014, ApJ, 784, 170
 Xue, X.-X., Rix, H.-W., Yanny, B., et al. 2011, ApJ, 738, 79
 Zhang, J., Cui, W., & Zhang, B. 2010, MNRAS, 402, 956
 Zinn, R., Horowitz, B., Vivas, A. K., et al. 2014, ApJ, 781, 22
 Zolotov, A., Willman, B., Brooks, A. M., et al. 2009, ApJ, 702, 1058

Appendix: Additional figures on chemical abundance trends

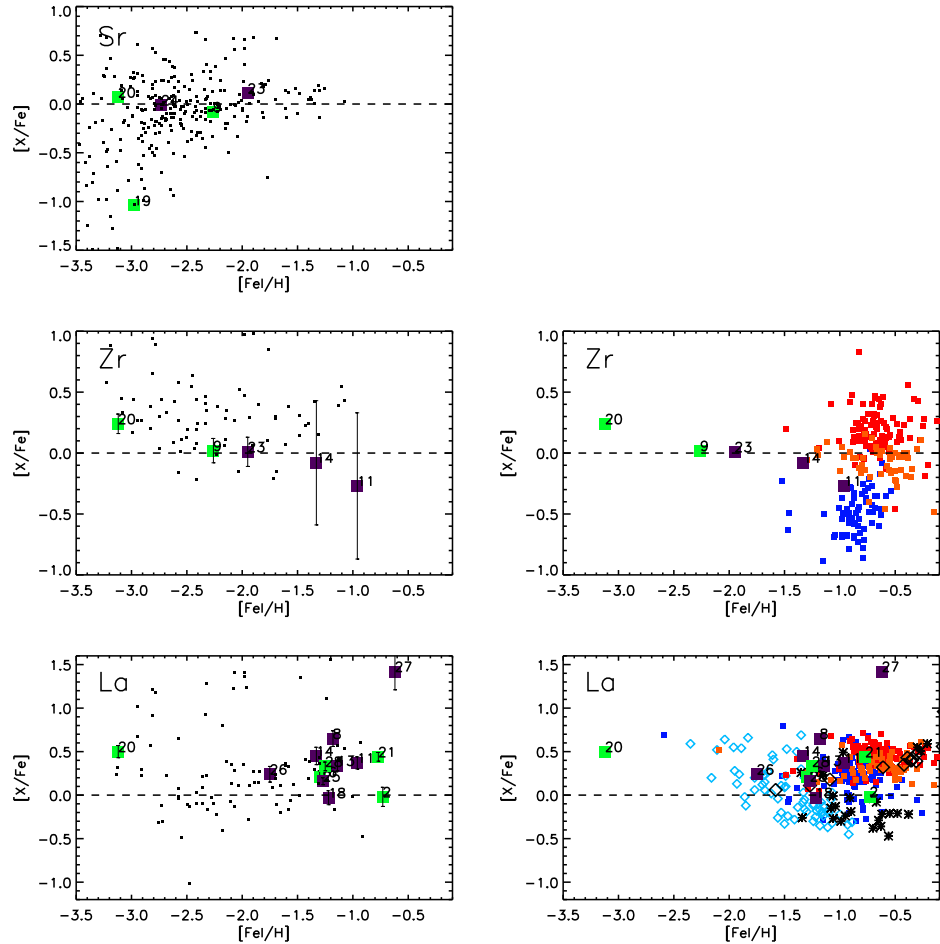


Fig. 15. Abundance of the n-capture elements Sr, Zr, La relative to iron (Fe I) as a function of [Fe I/H].

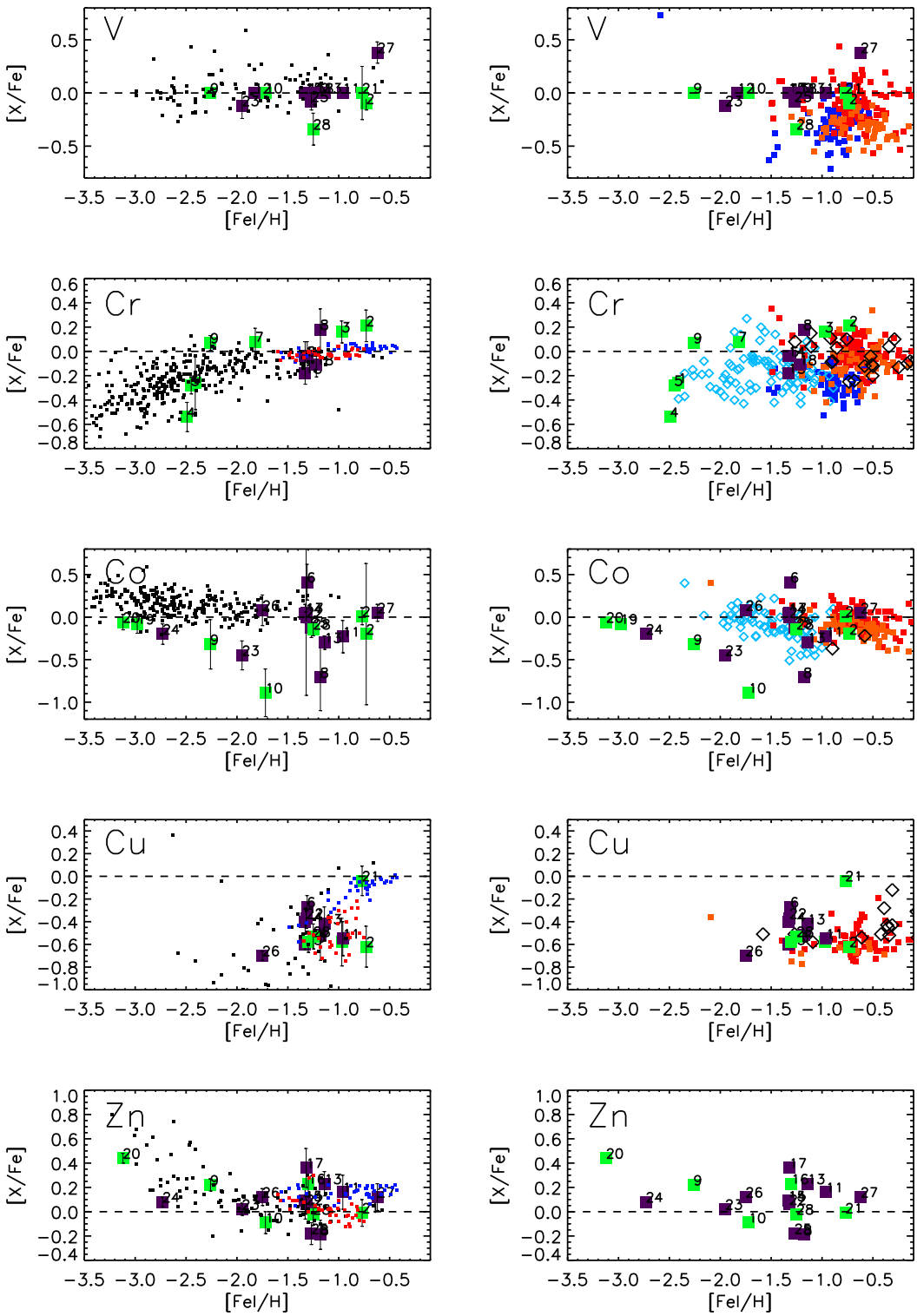
**Fig. 16.** Abundance of the Fe-peak elements VI, CrI, Co, Cu, Zn relative to iron (Fe I) as a function of $[\text{Fe I}/\text{H}]$.

Table 1. Atmospheric stellar parameters and details of observations for the sample stars. The table format is the following: (1) ID; (2), (3), (4) & (5): spectroscopic T_{eff} and $\log g$, [Fe/H] of the atmosphere model, microturbulence velocity; (6) photometric $\log g$; (7) Julian day for the middle of the exposure (in case of single exposures, otherwise we give the days of the first and last exposures); (8) total exposure time; (9) radial velocity and error; (10) signal-to-noise ratios at $\sim 4000 \text{ \AA}$, $\sim 4900 \text{ \AA}$, and $\sim 6700 \text{ \AA}$; (11) instrument. For the HET and UVES stars, the first line gives the average radial velocity of all exposures, while the following lines give the Julian day and heliocentric radial velocity of each exposure. The photometric $\log g$ of most HRS stars had asymmetric error bars; the error quoted here is the larger one of the upper and lower errors. Sources: All stars observed with HRS and UVES, and stars #8, 9, 10 & 12 with MIKE, were selected from the Spaghetti survey, as listed in (Starkenburg 2011); star #11 comes from the APOGEE survey; stars from #13-18 were drawn from the Xue et al.(2014) catalog.

ID	$T_{\text{eff}}^{\text{sp}}$ [K]	$\log g$ [cgs]	[Fe/H] model	$v_{\text{turb}}^{\text{sp}}$ [km s $^{-1}$]	$\log g_{\text{pho}}$ [cgs]	JD – 2456000	t_{exp} [s]	V_{rad} [km s $^{-1}$]	S/N			Instrument, Remark
									4000	4900	6700	
01	4750	1.5	−2.40	1.10	1.7 ± 0.2	358 – 414 357.650 358.665 369.617 413.671	7200	284.70 ± 0.17 284.39 ± 0.77 285.17 ± 0.77 284.60 ± 1.30 284.62 ± 0.72	–	36	59	HRS
02	4654	1.5	−0.75	1.30	1.5 ± 0.5	339 – 398 338.716 388.754 397.722	7200	90.48 ± 0.15 90.18 ± 0.32 90.52 ± 0.35 90.69 ± 0.26	–	27	44	HRS
03	4800	2.2	−0.95	1.10	1.7 ± 0.3	365 – 424 364.671 397.757 423.676	9000	13.95 ± 7.59 2.57 ± 0.26 10.69 ± 0.29 28.30 ± 0.26	–	27	42	HRS, spectroscopic binary
04	4486	0.7	−2.50	1.70	0.9 ± 0.1	341 – 386 340.910 363.681 383.629 385.617	9600	216.43 ± 0.42 214.94 ± 1.80 216.45 ± 1.16 216.79 ± 0.77 216.53 ± 0.29	–	32	50	HRS
4600	1.6	−1.00	1.10	1.9 ± 0.4	366 – 412 365.719 387.660 411.709	7200	117.00 ± 0.18 117.04 ± 0.27 116.63 ± 0.51 117.22 ± 0.38	–	27	52	HRS, #21 UVES	
4700	1.8	−1.70	1.10	1.8 ± 0.5	357 – 445 356.851 364.824 365.827 420.747 444.672	12000	247.88 ± 0.19 248.31 ± 0.34 248.39 ± 0.74 248.01 ± 0.64 247.43 ± 0.31 247.63 ± 0.32	–	54	75	HRS, #26 UVES	
05	4650	0.7	−2.45	1.90	1.1 ± 0.5	391 – 444 390.841 427.730 428.724 442.685 443.682	12000	45.16 ± 0.39 45.64 ± 1.06 44.36 ± 1.18 45.28 ± 0.96 44.19 ± 0.74 46.23 ± 0.76	–	34	63	HRS
06	4350	0.8	−1.30	1.50	1.1 ± 0.6	395 – 417 394.739 413.762 416.682	9000	204.69 ± 0.15 204.93 ± 0.32 204.40 ± 0.37 204.70 ± 0.67	–	18	41	HRS
07	4700	1.3	−1.80	1.40	1.7 ± 0.2	387 – 445 386.744 412.844 427.807 429.790 444.751	12000	−47.41 ± 0.15 −46.95 ± 0.52 −47.85 ± 0.27 −47.45 ± 0.34 −47.27 ± 0.26 −47.23 ± 0.44	–	54	96	HRS
4529	1.1	−0.85	1.40	0.8 ± 0.2	392 – 398 391.805 397.798	6000	4.75 ± 0.36 4.46 ± 0.29 5.18 ± 0.44	–	12	21	HRS, #28 UVES	

Table 1. (continued)

ID	$T_{\text{eff}}^{\text{sp}}$ [K]	$\log g$ [cgs]	[Fe/H] model	$v_{\text{turb}}^{\text{sp}}$ [km s $^{-1}$]	$\log g_{\text{pho}}$ [cgs]	JD – 2456000	t_{exp} [s]	V_{rad} [km s $^{-1}$]	4000	4900	6700	Instrument, Remark
08	5000	2.3	-1.20	1.25	2.2 ± 0.4	725.573	10800	371.81 ± 0.11	20	30	65	MIKE
09	4748	1.8	-2.30	1.50	1.9 ± 0.3	725.712	10800	-56.04 ± 0.51	45	60	150	MIKE
10	4842	1.8	-1.70	1.50	1.8 ± 0.4	725.851	10800	-61.13 ± 0.36	30	50	80	MIKE
11	4444	1.4	-0.90	1.10	1.5 ± 0.4	828.537	4400	317.78 ± 0.03	20	50	110	MIKE
12	5264	3.1	-1.80	0.70	2.5 ± 0.4	828.597	5400	111.95 ± 0.15	–	12	45	MIKE
13	4243	0.8	-1.15	1.50	1.0 ± 0.3	828.476	5400	281.00 ± 0.04	30	60	90	MIKE
14	4513	1.3	-1.30	1.14	1.6 ± 0.3	828.898	4800	-342.89 ± 0.09	25	45	70	MIKE
15	4570	1.4	-1.30	1.20	1.5 ± 0.3	828.847	3600	-320.57 ± 0.08	25	50	75	MIKE
16	4253	0.8	-1.25	1.40	0.9 ± 0.2	828.677	5400	-282.22 ± 0.18	20	40	80	MIKE
17	4550	1.3	-1.30	1.15	1.3 ± 0.2	828.750	5400	-328.43 ± 0.13	25	35	80	MIKE
18	4350	1.0	-1.20	1.35	0.9 ± 0.3	828.804	3600	-107.42 ± 0.14	25	45	95	MIKE
19	4603	1.2	-2.95	1.70	1.4 ± 0.2	873 – 889 872.888 877.884 888.798 888.835 888.872	15000	-259.91 ± 0.22 -259.65 ± 0.06 -260.30 ± 0.12 -259.85 ± 0.39 -260.14 ± 0.25 -260.38 ± 0.36	35	75	120	UVES
20	4500	1.3	-3.10	1.75	1.1 ± 0.2	875 – 896 874.900 893.890 895.878	7200	-54.67 ± 0.22 -54.23 ± 0.22 -54.98 ± 0.15 -54.88 ± 0.09	32	60	80	UVES
21	4800	2.3	-0.75	0.90	2.0 ± 0.4	747 – 1071 746.604 746.640 826.505 1070.793 1070.829	15000	116.40 ± 0.13 117.12 ± 0.26 117.26 ± 0.27 116.57 ± 0.21 115.81 ± 0.10 115.07 ± 0.07	35	50	85	UVES, also observed with HRS
22	4700	1.8	-1.30	1.15	1.6 ± 0.3	837 – 1070 837.500 1042.843 1069.679 1069.715 1069.751	15000	-71.88 ± 0.10 -72.36 ± 0.04 -72.08 ± 0.05 -71.71 ± 0.14 -71.17 ± 0.12 -72.29 ± 0.13	35	55	80	UVES
23	4730	1.7	-1.90	1.40	1.7 ± 0.3	1128 – 1158 1127.544 1127.580 1128.586 1157.561 1157.601	15000	42.22 ± 0.13 41.40 ± 0.28 40.51 ± 0.12 42.07 ± 0.11 42.93 ± 0.11 43.77 ± 0.16	38	65	90	UVES
24	4600	1.2	-2.70	1.55	1.3 ± 0.3	780 – 1129 779.611 1070.866 1128.549	7200	255.05 ± 0.18 254.29 ± 0.12 255.65 ± 0.16 255.18 ± 0.19	32	55	75	UVES

Table 1. (continued)

ID	$T_{\text{eff}}^{\text{sp}}$ [K]	$\log g$ [cgs]	[Fe/H] model	$v_{\text{turb}}^{\text{sp}}$ [km s $^{-1}$]	$\log g_{\text{pho}}$ [cgs]	JD – 2456000	t_{exp} [s]	V_{rad} [km s $^{-1}$]	S/N 4000	S/N 4900	S/N 6700	Instrument, Remark
25	4300	1.0	-1.25	1.40	1.2 ± 0.2	742 – 785 741.580 774.661 779.646 784.539 784.575	15000	107.25 ± 0.13 106.80 ± 0.22 108.04 ± 0.08 106.66 ± 0.03 107.38 ± 0.09 107.37 ± 0.10	30	60	80	UVES
26	4720	1.9	-1.70	1.15	2.0 ± 0.3	858 – 1126 858.503 859.505 1069.839 1125.606 1125.642	15000	247.26 ± 0.14 247.05 ± 0.27 246.91 ± 0.14 247.29 ± 0.13 247.91 ± 0.20 247.01 ± 0.16	40	60	80	UVES, also observed with HRS
27	4800	2.7	-0.65	0.75	2.1 ± 0.3	784 – 1128 784.499 838.509 1127.621 1127.657 1127.693	15000	108.42 ± 0.10 108.44 ± 0.13 108.49 ± 0.15 109.19 ± 0.13 107.39 ± 0.05 108.43 ± 0.12	30	45	65	UVES
28	4450	0.9	-1.25	1.50	0.7 ± 0.2	742 – 841 741.851 775.797 830.598 830.637 840.574	15000	4.60 ± 0.11 4.23 ± 0.17 5.06 ± 0.04 4.03 ± 0.17 4.22 ± 0.14 5.29 ± 0.20	40	45	80	UVES, also observed with HRS

Table 2. Coordinates, magnitude, distance and velocity of the stars in the sample. Column (1): ID; (2)-(3)-(4)-(5)-(6): first release Gaia coordinates and G magnitude; (7)-(8)-(9): heliocentric distance, Galactocentric distance and Galactic Standard of Rest velocity; (10)-(11) longitude and latitude in a system aligned with the Sag stream; (12) name of the known MW substructure to which the star is possibly associated. The coordinates are given in the International Celestial Reference System (ICRS) and correspond approximately to the equatorial J2000.0 coordinates, while the reference year is 2015. The errors on the equatorial coordinates vary between 0.1 and 30 milliarcseconds (mas), depending on the number of measurements.

ID	Gaia ID	α (J2000) [decimal °]	δ (J2000) [decimal °]	ℓ [decimal °]	b [decimal °]	m_G [mag]	d_h [kpc]	r_{gal} [kpc]	v_{GSR} km s^{-1}	Λ_\odot [decimal °]	B_\odot [decimal °]	Substructure	Comment
HRS-01	612887125855203968	145.722736176	11.064412509	223.454513677	42.974341222	16.282	37.2	42.0	170.9	140.2182	-17.2112	Sag	
02	612943888143412096	146.141816105	11.279705430	223.446107779	43.438397170	16.393	16.1	21.4	-22.3	139.8422	-16.9177	Sag	
03	3870240041683456000	158.659559972	10.347341776	233.831860702	53.709170985	17.099	23.8	27.6	-91.4	127.2325	-14.7064	Sag	
04	3870165687209304192	158.695828606	9.973295653	234.395945105	53.538110317	16.558	70.2	73.4	109.9	127.0807	-15.0523	Sag	
#21 UVES	3805383905209904768	165.104636554	1.395482629	252.281919882	52.983728567	16.664							
#26 UVES	3682458195986672640	193.727319152	-2.341630089	304.694033858	60.518242433	16.637							
05	3688559970125163904	193.960593490	-1.613468534	305.219928945	61.238713105	16.987	65.0	63.2	-34.3	89.2721	-11.2485	Sag	
06	3688452286707840640	194.119215967	-2.199181707	305.500614133	60.647434102	17.181	62.0	60.2	123.9	88.8395	-11.6827		clump
07	3724956004027595392	205.560857699	9.019925634	338.848956766	68.273464814	16.446	40.5	38.5	-67.4	84.4498	3.7067	Sag	
#28 UVES	3652114389480042880	223.211492264	1.496296732	356.701963111	51.228426070	16.883							
MIKE-08	3555759031576592000	163.824823166	-18.508049407	268.066167485	36.380672547	16.921	17.0	19.0	194.5	110.0752	-39.8714	VOD	[Fe/H] of clump but Eu,Mn,Ni off
09	3597524083837476864	182.062459753	-4.416150382	283.001779175	56.775105125	15.667	26.2	26.4	-169.1	98.7544	-19.3433	Sag	
10	3688450087681660416	194.035314734	-2.273345489	305.324070376	60.576556987	16.659	33.1	31.8	-142.3	88.8772	-11.7883	Sag	
11	3675598136782397824	192.270660520	-7.729364732	301.911128674	55.137716988	15.590	21.4	20.5	217.4	87.6893	-17.4041	VOD	
12	3957130734774308736	196.207779183	24.320979562	350.727065501	85.879785221	16.970	11.7	13.7	117.2	99.9986	12.4984		
13	368294973032975744	189.870793093	-2.916219697	296.987047134	59.817468183	15.135	26.4	25.8	188.6	92.2963	-14.3636	VOD	clump
14	2435815144861784832	355.468325584	-9.188827808	77.182067445	-65.674537158	16.213	31.5	31.8	-258.0	290.9595	9.8968	clump	
15	2436884729157603840	351.627842024	-10.473751039	68.661339153	-63.980925733	15.787	24.0	24.1	-233.4	295.0057	10.2066		
16	6880970854429743232	303.805525046	-11.519145229	31.805016791	-23.753969365	15.847	29.2	23.5	-168.7	342.7682	18.9589	Sag	
17	1733990241423159936	311.867125660	3.229578126	50.168829709	-23.903942909	16.132	29.5	25.6	-167.3	333.0929	33.3503	clump	
18	2720307593796059136	331.814984733	5.764033021	66.378274064	-38.465250833	15.196	23.3	22.1	52.8	309.2599	32.1026	Her-Aqu	clump
UVES-19	2583930459319327872	18.041523460	12.998214278	130.729521882	-49.559449053	16.365	55.2	59.0	-158.9	259.7272	19.0744	Sag	
20	3261503881461950208	51.549431319	-2.494533042	186.031431352	-45.549794858	15.556	41.7	47.6	-83.3	238.6173	-11.1438	Sag	
21	3805383905209904768	165.104636554	1.395482629	252.281919882	52.983728567	16.664	16.3	19.4	-8.9	117.7666	-21.0405	Sag	
22	3585463609511300864	176.168096220	-12.897982785	278.781672081	46.819132340	16.595	26.8	27.2	-217.9	100.1554	-29.5518		clump
23	3540980289631278208	172.801776544	-22.909035199	279.841303528	36.339371983	16.413	37.0	36.8	-130.9	97.7173	-39.8698		
24	3541034852893925632	172.784730895	-22.767590125	279.756572860	36.464282297	15.999	41.0	40.7	82.1	97.8268	-39.7552		
25	3543472882489394304	176.277546542	-19.199845600	282.021491710	40.963207478	16.546	45.9	45.3	-52.8	96.4867	-35.0405		clump
26	3682458195986672640	193.727319152	-2.341630089	304.694033858	60.518242433	16.637	36.7	35.3	165.2	89.1178	-11.9979		
27	3576989398518840576	184.185698087	-13.077444623	290.013749161	48.922114525	16.926	11.0	12.1	-23.0	92.2993	-25.9764		
28	3652114389480042880	223.211492264	1.496296732	356.701963111	51.228426070	16.883	50.3	45.7	8.3	65.4251	6.1280	Sag	

Table 3. Carbon abundance obtained from the CH G band, for stars observed with MIKE (except for star #12, see text) and UVES. The error given is the formal one provided by the fit and should be considered as an indication of its quality. A more realistic error would amount to $\sim 0.2dex$, taking into account the uncertainties on the continuum, oxygen abundance, and stellar parameters (especially T_{eff}). The adopted C- solar abundance is 8.55 as in Jablonka et al. (2015).

Star #	[C/H]	[C/Fe]	Star #	[C/H]	[C/Fe]
08	6.92 ± 0.04	-0.43	19	5.01 ± 0.01	-0.56
09	5.79 ± 0.01	-0.50	20	4.48 ± 0.02	-0.95
10	6.52 ± 0.03	-0.31	21	7.21 ± 0.02	-0.57
11	6.97 ± 0.04	-0.62	22	6.77 ± 0.02	-0.46
13	6.69 ± 0.05	-0.72	23	6.12 ± 0.01	-0.49
14	6.80 ± 0.03	-0.42	24	5.30 ± 0.01	-0.52
15	6.72 ± 0.02	-0.50	25	6.64 ± 0.03	-0.64
16	6.57 ± 0.04	-0.68	26	6.27 ± 0.01	-0.53
17	6.79 ± 0.02	-0.44	27	7.75 ± 0.03	-0.18
18	6.68 ± 0.03	-0.65	28	6.41 ± 0.02	-0.89

Table 4. Average abundance ratios. Column (1) gives the star identification (after the instrument name at the head of each block); columns (2) and (3) give the neutral and ionized iron abundance relative to solar, respectively; the remaining columns give the abundance ratios for each of the species listed in the Table header relative to neutral iron and normalized to solar ($[X/\text{FeI}]$). For each star, the abundance ratios are given in the first line and the corresponding errors in the second line. Below each of the elements, we list the corresponding solar abundance according to Grevesse & Sauval (1998), on the usual scale where the H abundance is 12. For reasons of space only TiII, VI, and CrI are given in this table.

ID	[Fe/H]		O	Na	Mg	Al	Si	Ca	Sc	TiII	VI	CrI	Mn	Co	Ni	Cu	Zn	Sr	Y	Zr	Ba	La	Ce	Pr	Nd	Sm	Eu				
	7.50	7.50	8.83	6.33	7.58	6.47	7.55	6.36	3.17	5.02	4.00	5.67	5.39	4.92	6.25	4.21	4.60	2.97	2.24	2.60	2.13	1.17	1.58	0.71	1.50	1.01	0.51				
HRS:																															
01	-2.41	-2.25	—	0.46	0.27	—	—	0.43	-0.14	0.34	—	-0.26	—	—	—	—	—	-0.30	—	1.03	—	—	—	0.64	—	—	—				
	0.09	0.16	—	0.14	0.08	—	—	0.13	0.08	0.09	—	0.22	—	—	—	—	—	0.08	—	0.14	—	—	—	0.06	—	—	—				
02	-0.73	-0.72	0.42	-0.21	0.09	—	0.16	0.28	-0.07	0.58	-0.10	0.21	-0.47	—	-0.36	-0.63	—	—	0.04	—	0.86	-0.02	—	—	0.33	—	—	0.83			
	0.11	0.09	0.13	0.17	0.11	—	0.09	0.13	0.14	0.14	0.06	0.13	0.11	—	0.15	0.18	—	—	0.08	—	0.10	0.11	—	—	0.08	—	—	0.07			
03	-0.97	-0.98	—	-0.46	0.01	—	0.26	0.15	0.10	0.62	—	0.16	-0.45	—	-0.10	-0.58	—	—	0.22	—	0.68	—	—	—	1.24	—	G. Battaglia et al.: What is the Milky Way	1.11			
	0.11	0.08	—	0.17	0.15	—	0.10	0.10	0.11	0.14	—	0.09	0.15	—	0.13	0.21	—	—	0.18	—	0.09	—	—	—	0.10	—	—	0.07			
04	-2.49	-2.33	—	0.33	0.55	—	—	0.40	-0.08	0.18	—	-0.54	0.18	—	-0.14	—	—	—	-0.56	—	-0.35	—	—	—	1.28	—	—	—			
	0.08	0.07	—	0.14	0.11	—	—	0.09	0.13	0.07	—	0.12	0.08	—	0.09	—	—	—	0.07	—	0.12	—	—	—	0.04	—	—	—			
#21	-1.01	-0.99	—	—	—	—	—	0.31	—	—	—	-0.11	—	—	—	-0.56	—	—	—	—	0.80	0.49	—	—	—	—	1.25	—	—	—	
UVES	0.11	0.08	—	—	—	—	—	0.11	—	—	—	0.15	—	—	—	0.18	—	—	—	—	0.09	0.05	—	—	—	—	0.07	—	—	—	
#26	-1.66	-1.53	—	-0.20	0.27	—	—	0.36	0.37	0.45	—	-0.19	—	—	-0.19	—	—	—	0.13	—	0.63	—	—	—	—	—	—	—	—		
UVES	0.10	0.08	—	0.08	0.06	—	—	0.08	0.19	0.10	—	0.12	—	—	0.09	—	—	—	0.18	—	0.10	—	—	—	—	—	—	—	—		
05	-2.45	-2.25	—	0.51	0.52	—	—	0.49	-0.19	-0.01	—	-0.28	—	—	0.11	—	—	—	—	—	0.07	—	—	—	—	—	—	—	—	—	
	0.08	0.07	—	0.17	0.10	—	—	0.07	0.10	0.11	—	0.07	—	—	0.06	—	—	—	—	—	0.21	—	—	—	—	—	—	—	—	—	
06	-1.31	-1.23	—	0.06	0.36	—	0.58	0.43	-0.07	0.31	—	-0.04	-0.25	—	-0.14	-0.27	—	—	-0.15	—	0.65	—	—	—	0.60	—	0.84	—	—		
	0.12	0.10	—	0.12	0.09	—	0.09	0.13	0.11	0.24	—	0.12	0.09	—	0.10	0.10	—	—	0.29	—	0.17	—	—	—	0.12	—	0.08	—	—		
07	-1.82	-1.72	—	-0.30	-0.58	—	—	-0.16	—	0.25	—	0.08	0.08	—	0.22	—	—	—	—	—	1.60	—	—	—	—	—	—	—	—	—	
	0.08	0.06	—	0.17	0.07	—	—	0.08	—	0.09	—	0.11	0.06	—	0.07	—	—	—	—	—	0.06	—	—	—	—	—	—	—	—	—	
#28	-0.84	-0.81	—	—	-0.16	—	0.04	0.01	-0.03	0.21	0.49	0.01	-0.07	—	-0.01	-0.45	—	—	-0.20	—	0.81	0.73	—	—	0.65	—	1.42	—	—		
UVES	0.13	0.13	—	—	0.31	—	0.23	0.15	0.13	0.14	0.20	0.23	0.18	—	0.16	0.11	—	—	0.21	—	0.18	0.12	—	—	0.08	—	—	—	0.18		
MIKE:																															
08	-1.18	-1.20	—	0.01	0.14	—	0.50	0.26	0.17	0.23	—	-0.06	-0.19	-0.71	0.05	-0.52	-0.19	—	0.04	—	0.37	0.66	0.35	1.74	0.34	outer halo made of P _{II} ,	0.14	—			
	0.12	0.12	—	0.06	0.11	—	0.17	0.17	0.23	0.13	—	0.20	0.16	0.39	0.08	0.22	0.12	—	0.14	—	0.17	0.09	0.12	0.31	0.14	—	0.25	—			
09	-2.26	-2.18	—	—	0.41	—	0.64	0.39	0.09	0.33	—	-0.29	-0.48	-0.32	0.03	—	0.22	-0.08	-0.32	0.02	-0.04	—	—	—	—	—	—	—	—	0.07	
	0.08	0.07	—	—	0.09	—	0.06	0.06	0.07	0.08	—	0.09	0.07	0.29	0.05	—	0.05	0.10	0.09	0.10	0.13	—	—	—	—	—	—	—	—	0.08	
10	-1.72	-1.67	< 0.79	0.00	0.24	—	0.52	0.36	-0.13	0.26	—	-0.07	-0.51	-0.89	-0.15	—	-0.09	—	-0.54	—	0.25	—	-0.03	0.42	0.26	0.26	—	—			
	0.10	0.10	0.15	0.09	0.09	—	0.17	0.17	0.09	0.12	—	0.13	0.09	0.28	0.07	—	0.09	—	0.19	—	0.14	—	0.05	0.13	0.12	0.15	—	—			
11	-0.96	-0.90	0.25	-0.33	0.24	—	0.12	0.30	0.15	0.30	—	-0.16	-0.49	-0.23	-0.17	-0.55	0.16	—	—	1.84	0.87	0.37	0.54	0.76	0.59	0.71	0.12	0.10			
	0.11	0.08	0.04	0.08	0.11	—	0.07	0.13	0.11	0.13	—	0.12	0.12	0.19	0.09	0.15	0.14	—	0.15	0.07	0.14	0.10	0.25	0.12	0.10	0.11	0.10	0.10			
12	-1.83	-1.84	—	-0.04	—	—	1.67	0.27	—	0.65	—	0.21	—	—	—	—	—	—	—	—	0.19	—	< 2.53	—	—	—	—	—	—	—	—
	0.15	0.28	—	0.10	—	—	0.12	0.12	—	0.26	—	0.16	—	—	—	—	—	—	—	—	0.15	—	0.20	—	—	—	—	—	—	—	
13	-1.14	-1.11	0.36	-0.22	0.31	-0.20	0.29	0.19	-0.10	0.24	—	-0.26	-0.43	-0.30	-0.11	-0.42	0.23	—	—	—	0.86	0.34	0.08	0.56	0.36	0.59	0.62	—	—		
	0.10	0.07	0.04	0.06	0.10	0.04	0.05	0.11	0.08	0.10	—	0.12	0.12	0.08	0.08	0.15	0.10	—	—	0.18	0.06	0.13	0.08	0.06	0.10	0.11	—	—			
14	-1.33	-1.25	0.65	-0.40	0.21	—	0.27	0.32	0.14	0.38	—	-0.01	-0.46	0.04	0.01	-0.40	0.09	—	—	0.84	0.79	0.45	0.40	—	0.39	0.46	—	—			
	0.11	0.09	0.04	0.07	0.10	—	0.12	0.11	0.11	0.10	—	0.18	0.08	0.11	0.11	0.11	0.11	—	—	0.45	0.13	0.10	0.12	—	0.16	0.08	—	—			
15	-1.33	-1.27	0.69	-0.30	0.25	—	0.30	0.35	0.07	0.35	—	-0.12	-0.42	—	-0.07	-0.60	0.09	—	—	—	0.50	—	0.24	—	0.21	0.22	—	—			
	0.10	0.08	0.07	0.10	0.12	—	0.07	0.11	0.08	0.13	—	0.13	0.08	—	0.08	0.05	0.15	—	—	0.17	—	0.11	—	0.10	0.08	—	—	—			
16	-1.30	-1.29	0.21	-0.33	0.38	—	0.60	0.23	0.04	0.38	—	-0.24	-0.43	—	-0.17	-0.58	0.23	—	—	—	0.27	0.21	—	0.22	0.54	0.52	0.71	—			
	0.10	0.08	0.04	0.09	0.11	—	0.09	0.11	0.09	0.12	—	0.11	0.09	—	0.08	0.09	0.14	—	—	0.15	0.07	—	0.09	0.16	0.16	0.07	—	—			
17	-1.32	-1.28	0.53	-0.22	0.23	—	0.35	0.33	0.01	0.31	—	-0.20	-0.42	0.05	-0.14	—	0.36	—	—	—	0.63	—	0.30	—	0.19	0.35	0.65	—	—		
	0.10	0.08	0.09	0.08	0.11	—	0.08	0.11	0.10	0.14	—	0.20	0.09	0.97	0.09	—	0.16	—	—	0.15	—	0.11	—	0.11	0.07	0.06	—	—			
18	-1.22	-1.18	0.33	-0.21	0.08	—	0.22	0.07	-0.05	0.33	—	-0.30	-0.42	—	-0.15	—	—	—	—	—	0.53	-0.03	0.02	—	0.24	0.26	0.51	—	—		
	0.09	0.08	0.05	0.08	0.10	—	0.08	0.08	0.08	0.11	—	0.09	0.08	—	0.07	—	—	—	—	0.15	0.08	0.10	—	0.10	0.09	0.05	—	—			

Table 4. (continued)

ID	$\frac{\text{FeI}}{\text{H}}$	$\frac{\text{FeII}}{\text{H}}$	O	Na	Mg	Al	Si	Ca	Sc	TiII	VI	CrI	Mn	Co	Ni	Cu	Zn	Sr	Y	Zr	Ba	La	Ce	Pr	Nd	Sm	Eu	
	7.50	7.50	8.83	6.33	7.58	6.47	7.55	6.36	3.17	5.02	4.00	5.67	5.39	4.92	6.25	4.21	4.60	2.97	2.24	2.60	2.13	1.17	1.58	0.71	1.50	1.01	0.51	
UVES:																												
19	-2.98 0.05	-2.84 0.05	-0.01 0.12	0.21 0.11	-0.58 0.15	-0.37 -0.05	-0.14 0.06	0.09 0.06	-	-0.26 0.07	-0.29 0.11	-0.08 0.11	-0.20 0.09	-	-	-1.04 0.17	-	-	-0.98 0.08	-	-	-	-	-	-	-		
20	-3.12 0.05	-2.92 0.08	-0.19 -0.12	0.45 0.08	-	-0.42 -0.05	0.25 0.05	0.48 0.06	-	-0.32 -0.06	-0.53 -0.06	-0.06 -0.07	-	0.44 0.10	0.07 0.12	-0.01 0.05	0.23 0.06	0.35 0.08	0.50 0.07	0.64 0.04	-	-	-	-	-	-	0.69 0.11	
21	-0.77 0.09	-0.74 0.07	-0.36 -0.07	-0.01 0.10	-	0.03 -0.06	0.23 0.10	0.03 0.06	0.20 0.09	0.00 0.25	-0.11 0.09	-0.57 0.07	0.01 0.10	-0.17 0.08	-0.04 0.13	-0.01 0.11	-	0.18 0.08	-	0.74 0.09	0.44 0.05	0.24 0.06	-	0.70 0.10	-	0.83 0.06		
22	-1.32 0.08	-1.33 0.06	0.56 0.04	-0.20 0.06	0.25 0.08	-	0.31 -0.05	0.33 0.08	-	0.40 -0.11	-	-0.11 -0.09	-0.58 0.06	0.00 0.06	-0.14 0.06	-0.37 0.09	0.06 0.08	-	-0.08 -0.08	-	0.54 0.11	-	-	-	0.32 0.08	-	-	
23	-1.95 0.07	-1.82 0.06	-	-0.07 0.11	0.33 0.05	-	-0.25 -0.05	0.06 0.08	0.28 0.12	-0.12 0.08	-0.20 -0.20	< -0.27 0.05	-0.45 0.17	-0.12 0.06	-	0.02 0.05	0.11 0.08	-0.31 0.06	0.27 0.08	0.19 0.11	-	-	-	-	-	-	-	0.21 0.09
24	-2.73 0.06	-2.62 0.08	-	0.28 0.12	0.51 0.11	-	-0.43 -0.05	0.04 0.06	0.26 0.05	-	-0.27 -0.06	-0.45 0.17	-0.20 0.12	0.01 0.06	-	0.08 0.04	-0.01 0.14	-0.35 0.08	-	-0.45 0.07	-	-	-	-	-	-	-	
25	-1.27 0.08	-1.23 0.06	0.44 0.03	-0.28 0.05	0.25 0.09	-	0.30 -0.05	0.26 0.11	0.04 0.13	0.29 0.09	-0.08 0.08	-0.16 0.10	-0.56 0.13	-0.12 0.12	-0.10 0.07	-	-0.18 0.09	-	0.01 0.07	-	0.56 0.14	0.16 0.04	0.07 0.12	0.53 0.04	0.22 0.07	-	0.64 0.04	
26	-1.75 0.08	-1.67 0.06	-	-0.14 -0.06	0.36 0.07	-	0.39 -0.04	0.32 0.07	0.12 0.08	0.40 0.09	-	-0.24 -0.08	-	0.08 0.18	-0.08 0.06	-0.71 0.04	0.12 0.07	-	-0.00 0.07	-	0.49 0.10	0.24 0.09	-	-	0.65 0.16	-	0.32 0.08	
27	-0.62 0.08	-0.64 0.07	0.49 0.04	0.01 0.06	0.31 0.09	0.13 0.05	0.28 0.06	0.37 0.10	0.07 0.09	0.23 0.10	0.38 0.09	0.01 0.03	-0.45 0.08	0.05 0.08	0.03 0.11	-	0.12 0.13	-	0.18 0.13	-	0.45 0.09	1.42 0.21	-	-	0.09 0.07	-	-	
28	-1.25 0.09	-1.25 0.06	-	-0.41 -0.05	0.09 0.08	-	0.10 0.10	0.12 0.06	-0.05 0.08	0.02 0.15	-0.34 0.13	-0.22 0.09	-0.50 0.12	-0.14 0.08	-0.24 0.06	-0.53 0.11	-0.02 0.09	-	-0.08 0.11	-	0.85 0.14	0.33 0.05	0.19 0.07	0.63 0.05	0.57 0.09	-	0.87 0.06	

Table 5. Line parameters, observed equivalent widths and corresponding abundances of stars 01, 02, 03, 04, and #21 UVES observed with HRS.

El.	λ	χ_{ex}	$\log(gf)$	EW $\pm\sigma$ (EW) log $\epsilon(X) + 12$ [dex]							#21 UVES
				01	02	03	04				
O 1	6363.776	0.02	-10.260	-	-	25.7 \pm 5.9	8.53	-	-	-	-
Na 1	5682.633	2.10	-0.706	-	-	-	-	28.8 \pm 3.3	4.76	-	-
Na 1	5688.205	2.10	-0.452	-	-	-	-	-	-	21.7 \pm 3.4	4.23
Na 1	5889.951	0.00	0.108	-	-	344.3 \pm 24.7	5.08	-	-	-	-
Na 1	5895.924	0.00	-0.194	174.8 \pm 13.3	4.38	306.0 \pm 22.5	5.22	286.5 \pm 18.4	5.11	189.2 \pm 13.3	3.88
Na 1	6154.226	2.10	-1.547	-	-	35.5 \pm 3.5	5.61	-	-	-	-
Mg 1	5172.684	2.71	-0.450	210.1 \pm 12.8	5.44	-	-	-	-	242.2 \pm 13.7	5.41
Mg 1	5183.604	2.72	-0.239	-	-	-	-	-	-	269.9 \pm 16.3	5.37
Mg 1	5528.405	4.35	-0.498	-	-	191.1 \pm 9.9	6.84	148.6 \pm 10.1	6.47	107.8 \pm 6.3	5.73
Mg 1	5711.088	4.35	-1.724	-	-	112.0 \pm 5.7	7.07	84.5 \pm 6.1	6.76	37.5 \pm 3.3	5.81
Si 1	5690.425	4.93	-1.870	-	-	46.2 \pm 3.9	6.94	-	-	-	-
Si 1	5708.399	4.95	-1.470	-	-	-	-	48.0 \pm 3.2	6.72	-	-
Si 1	5948.541	5.08	-1.230	-	-	80.7 \pm 6.1	7.09	74.4 \pm 9.8	7.11	-	-
Si 1	6243.814	5.62	-1.244	-	-	-	-	36.5 \pm 3.8	6.99	-	-
Ca 1	5265.556	2.52	-0.113	66.4 \pm 4.3	4.83	-	-	-	-	-	-
Ca 1	5349.465	2.71	-0.310	-	-	101.4 \pm 5.6	5.67	95.0 \pm 5.7	5.80	-	-
Ca 1	5581.965	2.52	-0.555	-	-	-	-	-	-	110.1 \pm 6.2	5.97
Ca 1	5588.749	2.53	0.358	53.9 \pm 3.4	4.04	169.7 \pm 10.7	6.05	138.2 \pm 7.3	5.72	81.7 \pm 4.7	4.24
Ca 1	5590.114	2.52	-0.571	-	-	109.8 \pm 9.5	5.87	-	-	21.7 \pm 2.8	4.01
Ca 1	5601.277	2.53	-0.523	-	-	118.4 \pm 6.4	6.01	98.7 \pm 5.2	5.86	47.0 \pm 3.7	4.48
Ca 1	5857.451	2.93	0.240	-	-	170.8 \pm 11.3	6.31	-	-	44.8 \pm 5.1	4.17
Ca 1	6102.723	1.88	-0.793	53.3 \pm 4.2	4.35	-	-	-	-	-	-
Ca 1	6122.217	1.89	-0.316	83.6 \pm 6.7	4.55	187.3 \pm 12.1	5.88	142.8 \pm 8.9	5.44	100.8 \pm 7.6	4.33
Ca 1	6161.297	2.52	-1.266	-	-	78.3 \pm 7.3	5.81	-	-	-	67.7 \pm 5.5
Ca 1	6162.173	1.90	-0.090	103.4 \pm 7.0	4.73	195.7 \pm 11.0	5.74	160.4 \pm 9.6	5.42	122.7 \pm 8.4	4.49
Ca 1	6166.439	2.52	-1.142	-	-	-	-	49.6 \pm 4.4	5.32	-	72.4 \pm 5.0
Ca 1	6169.042	2.52	-0.797	-	-	-	-	-	-	-	91.8 \pm 5.3
Ca 1	6169.563	2.53	-0.478	-	-	-	-	-	-	-	113.9 \pm 6.3
Ca 1	6439.075	2.53	0.390	67.5 \pm 5.3	4.27	167.3 \pm 9.6	5.83	154.4 \pm 9.0	5.80	90.6 \pm 5.4	4.27
Ca 1	6455.598	2.52	-1.340	-	-	70.1 \pm 5.5	5.71	37.4 \pm 3.3	5.27	-	55.1 \pm 3.8
Ca 1	6499.650	2.52	-0.818	-	-	107.4 \pm 5.8	5.92	75.9 \pm 5.3	5.54	-	90.1 \pm 5.3
Ca 1	6717.681	2.71	-0.524	-	-	125.6 \pm 6.6	6.13	91.8 \pm 6.9	5.73	-	-
Sc 2	5031.021	1.36	-0.400	-	-	124.6 \pm 7.0	2.79	-	-	84.6 \pm 8.7	1.04
Sc 2	5526.790	1.77	0.024	35.0 \pm 3.7	0.62	105.3 \pm 5.7	2.40	88.8 \pm 5.1	2.40	54.4 \pm 3.0	0.56
Sc 2	5657.896	1.51	-0.603	-	-	-	-	74.7 \pm 4.2	2.34	-	-
Sc 2	6309.920	1.50	-1.618	-	-	-	-	39.2 \pm 3.9	2.57	-	-
Sc 2	6604.601	1.36	-1.399	-	-	61.5 \pm 4.4	2.25	39.3 \pm 2.9	2.11	-	-
Ti 1	4991.066	0.84	0.450	76.8 \pm 5.6	3.16	-	-	137.2 \pm 11.5	4.38	94.8 \pm 8.2	2.71
Ti 1	4999.503	0.83	0.320	66.0 \pm 5.2	2.97	-	-	-	-	78.7 \pm 6.5	2.53
Ti 1	5016.161	0.85	-0.480	-	-	122.9 \pm 9.6	4.65	85.7 \pm 5.2	4.17	35.9 \pm 5.5	2.61
Ti 1	5039.958	0.02	-1.080	-	-	-	-	-	-	49.6 \pm 4.1	2.33
Ti 1	5064.653	0.05	-0.940	-	-	-	-	-	-	61.4 \pm 5.8	2.41
Ti 1	5173.743	0.00	-1.060	33.3 \pm 4.0	2.54	-	-	-	-	97.5 \pm 8.1	3.04
Ti 1	5192.969	0.02	-0.950	-	-	-	-	-	-	91.3 \pm 5.1	2.85
Ti 1	5210.384	0.05	-0.820	43.3 \pm 4.3	2.58	136.6 \pm 7.7	4.30	106.9 \pm 9.4	4.04	85.2 \pm 5.7	2.65
Ti 1	5978.541	1.87	-0.496	-	-	-	-	52.8 \pm 4.4	4.54	-	-
Ti 1	6126.216	1.07	-1.425	-	-	55.0 \pm 3.2	4.20	48.3 \pm 5.0	4.38	-	-
Ti 2	5129.156	1.89	-1.340	-	-	-	-	-	-	63.0 \pm 3.6	2.68
Ti 2	5154.068	1.57	-1.750	46.6 \pm 3.9	2.83	-	-	-	-	61.0 \pm 3.2	2.63
Ti 2	5185.902	1.89	-1.410	-	-	-	-	90.3 \pm 6.5	4.52	-	-
Ti 2	5188.687	1.58	-1.050	85.8 \pm 5.0	3.15	-	-	-	-	112.4 \pm 6.2	2.99
Ti 2	5336.786	1.58	-1.600	54.3 \pm 4.0	2.86	-	-	92.9 \pm 6.7	4.40	-	-
Ti 2	5381.021	1.57	-1.970	46.1 \pm 3.2	3.02	109.2 \pm 6.8	4.74	98.9 \pm 5.8	4.88	61.4 \pm 4.8	2.83
Ti 2	5418.768	1.58	-2.130	-	-	111.8 \pm 5.9	4.97	86.2 \pm 5.7	4.75	43.7 \pm 2.9	2.70
V 1	6216.364	0.28	-1.330	-	-	61.6 \pm 3.8	3.18	-	-	-	-
Cr 1	5206.023	0.94	0.020	89.9 \pm 4.8	3.26	-	-	-	-	120.7 \pm 7.5	2.95
Cr 1	5208.409	0.94	0.170	-	-	-	-	259.2 \pm 13.3	4.92	-	-
Cr 1	5296.691	0.98	-1.360	-	-	-	-	97.2 \pm 6.0	4.67	-	103.6 \pm 7.0
Cr 1	5345.796	1.00	-0.896	-	-	162.5 \pm 8.4	5.19	-	-	-	140.4 \pm 8.1
Cr 1	5348.314	1.00	-1.210	-	-	143.5 \pm 7.2	5.16	-	-	-	97.9 \pm 5.9
Cr 1	5409.784	1.03	-0.670	44.0 \pm 4.8	2.81	172.6 \pm 8.7	5.12	129.6 \pm 7.5	4.72	59.1 \pm 3.2	2.59
Mn 1	5407.417	2.14	-1.743	-	-	74.3 \pm 4.6	4.28	48.7 \pm 3.6	4.24	-	-
Mn 1	5432.539	0.00	-3.795	-	-	-	-	41.9 \pm 3.8	3.68	-	-
Mn 1	6013.510	3.07	-0.352	-	-	75.8 \pm 7.1	4.20	47.3 \pm 5.1	4.00	-	-
Mn 1	6021.820	3.08	-0.054	-	-	76.4 \pm 5.6	4.06	78.0 \pm 11.3	4.29	23.5 \pm 3.1	3.08
Fe 1	4859.741	2.88	-0.764	-	-	-	-	-	-	79.6 \pm 7.1	4.91
Fe 1	4871.318	2.87	-0.363	-	-	-	-	143.6 \pm 12.9	6.21	122.2 \pm 12.1	5.36
Fe 1	4872.138	2.88	-0.567	-	-	187.9 \pm 12.5	6.82	164.4 \pm 15.4	6.63	105.4 \pm 6.9	5.26
Fe 1	4890.755	2.88	-0.394	79.7 \pm 8.3	5.18	-	-	-	-	-	176.1 \pm 12.7
Fe 1	4891.492	2.85	-0.112	87.8 \pm 7.4	5.07	-	-	184.3 \pm 14.7	6.29	122.9 \pm 9.1	5.10
Fe 1	4903.310	2.88	-0.926	-	-	-	-	155.5 \pm 13.1	6.90	-	202.9 \pm 14.2
Fe 1	4918.994	2.87	-0.342	-	-	-	-	152.3 \pm 13.0	6.27	-	-

Table 5. continued.

El.	λ	χ_{ex}	$\log(gf)$	EW $\pm\sigma$ (EW) $\log \varepsilon(X) + 12$ [dex]					#21 UVES
				01	02	03	04		
Fe 1	4924.770	2.28	-2.241	-	-	-	-	-	109.7 \pm 8.8
Fe 1	5001.863	3.88	0.010	-	-	-	-	-	-
Fe 1	5006.119	2.83	-0.638	-	-	-	-	-	-
Fe 1	5041.756	1.49	-2.203	-	-	-	-	-	-
Fe 1	5044.211	2.85	-2.038	-	-	-	-	-	97.7 \pm 6.3
Fe 1	5049.820	2.28	-1.355	-	-	171.7 \pm 14.0	6.74	-	6.92
Fe 1	5068.766	2.94	-1.042	43.0 \pm 2.6	4.93	135.2 \pm 7.7	6.71	126.1 \pm 10.8	6.36
Fe 1	5074.748	4.22	-0.200	-	-	103.6 \pm 7.6	6.34	-	6.57
Fe 1	5079.223	2.20	-2.067	48.3 \pm 5.4	5.19	-	-	-	97.5 \pm 6.8
Fe 1	5131.468	2.22	-2.515	36.3 \pm 2.7	5.35	-	-	44.1 \pm 2.7	6.60
Fe 1	5141.739	2.42	-1.964	-	-	117.4 \pm 6.3	6.64	-	6.09
Fe 1	5159.058	4.28	-0.820	-	-	68.4 \pm 3.6	6.65	-	-
Fe 1	5162.272	4.18	0.020	-	-	-	-	45.8 \pm 4.8	6.63
Fe 1	5165.410	4.22	-0.003	-	-	96.3 \pm 5.2	6.39	-	-
Fe 1	5171.596	1.49	-1.793	101.9 \pm 7.0	5.56	-	-	126.0 \pm 8.1	6.34
Fe 1	5191.455	3.04	-0.551	72.9 \pm 4.1	5.30	174.3 \pm 9.4	6.79	-	-
Fe 1	5192.344	3.00	-0.421	-	-	229.5 \pm 11.6	7.01	-	-
Fe 1	5198.711	2.22	-2.135	-	-	127.9 \pm 10.8	6.75	88.7 \pm 5.0	6.84
Fe 1	5202.336	2.18	-1.838	-	-	184.5 \pm 9.3	7.15	146.0 \pm 10.4	6.61
Fe 1	5215.180	3.27	-0.871	36.3 \pm 2.8	4.97	-	-	-	6.58
Fe 1	5216.274	1.61	-2.150	-	-	162.4 \pm 9.7	7.01	-	7.03
Fe 1	5217.389	3.21	-1.070	-	-	-	-	44.9 \pm 4.7	6.30
Fe 1	5232.940	2.94	-0.058	86.3 \pm 5.8	5.02	225.6 \pm 11.5	6.56	195.2 \pm 11.5	-
Fe 1	5242.491	3.63	-0.967	-	-	96.1 \pm 6.5	6.69	120.4 \pm 7.9	6.41
Fe 1	5266.555	3.00	-0.386	-	-	-	-	-	-
Fe 1	5281.790	3.04	-0.834	41.7 \pm 2.3	4.79	151.8 \pm 10.4	6.80	120.8 \pm 6.5	6.51
Fe 1	5283.621	3.24	-0.432	49.3 \pm 4.5	4.81	167.5 \pm 9.2	6.87	-	-
Fe 1	5302.300	3.28	-0.720	53.1 \pm 3.4	5.24	168.7 \pm 10.5	7.21	-	-
Fe 1	5307.361	1.61	-2.987	-	-	-	-	68.3 \pm 4.3	5.10
Fe 1	5322.041	2.28	-2.803	-	-	78.9 \pm 4.0	6.35	50.4 \pm 3.2	6.72
Fe 1	5324.179	3.21	-0.103	-	-	-	-	33.6 \pm 2.0	6.67
Fe 1	5328.531	1.56	-1.850	-	-	-	-	93.3 \pm 6.5	-
Fe 1	5332.899	1.56	-2.777	-	-	-	-	139.7 \pm 7.5	-
Fe 1	5339.929	3.27	-0.647	-	-	-	-	5.31	-
Fe 1	5364.871	4.45	0.228	33.3 \pm 2.8	5.19	108.4 \pm 7.1	6.67	-	-
Fe 1	5365.399	3.57	-1.020	-	-	96.7 \pm 6.1	6.65	77.9 \pm 4.1	6.44
Fe 1	5367.466	4.41	0.443	-	-	127.1 \pm 6.8	6.76	-	6.44
Fe 1	5369.961	4.37	0.536	-	-	-	-	47.5 \pm 3.2	6.31
Fe 1	5379.574	3.69	-1.514	-	-	-	-	-	-
Fe 1	5383.369	4.31	0.645	-	-	129.5 \pm 7.3	6.49	-	6.30
Fe 1	5389.479	4.41	-0.410	-	-	84.1 \pm 5.0	6.74	107.4 \pm 6.1	-
Fe 1	5393.167	3.24	-0.715	-	-	158.7 \pm 9.0	7.02	58.1 \pm 4.8	-
Fe 1	5400.501	4.37	-0.160	-	-	116.2 \pm 6.4	7.12	111.4 \pm 7.7	6.66
Fe 1	5410.910	4.47	0.398	-	-	138.7 \pm 7.4	7.05	100.5 \pm 7.2	-
Fe 1	5415.199	4.39	0.642	44.9 \pm 2.9	4.98	130.7 \pm 7.7	6.58	124.0 \pm 7.6	6.61
Fe 1	5424.068	4.32	0.520	47.2 \pm 3.1	5.08	-	-	110.8 \pm 6.7	6.79
Fe 1	5445.042	4.39	-0.020	-	-	-	-	61.3 \pm 4.5	6.48
Fe 1	5560.211	4.43	-1.190	-	-	-	-	-	-
Fe 1	5569.618	3.42	-0.486	-	-	133.8 \pm 8.6	6.59	131.3 \pm 6.8	6.25
Fe 1	5572.842	3.40	-0.275	-	-	-	-	-	6.39
Fe 1	5576.089	3.43	-1.000	-	-	122.3 \pm 6.2	6.91	177.1 \pm 9.4	6.74
Fe 1	5586.755	3.37	-0.120	62.9 \pm 5.6	4.95	189.6 \pm 9.7	6.83	-	-
Fe 1	5615.644	3.33	0.050	85.5 \pm 5.5	5.29	-	-	-	-
Fe 1	6003.011	3.88	-1.120	-	-	91.0 \pm 5.3	6.88	-	-
Fe 1	6024.058	4.55	-0.120	-	-	105.6 \pm 6.5	6.99	92.1 \pm 5.8	6.70
Fe 1	6027.051	4.08	-1.089	-	-	62.4 \pm 5.6	6.47	-	-
Fe 1	6056.004	4.73	-0.460	-	-	68.4 \pm 6.5	6.77	42.5 \pm 5.6	6.48
Fe 1	6065.482	2.61	-1.530	49.1 \pm 4.0	5.08	166.7 \pm 9.4	7.05	123.7 \pm 8.1	-
Fe 1	6078.491	4.80	-0.321	-	-	-	-	79.5 \pm 5.5	6.65
Fe 1	6082.710	2.22	-3.573	-	-	61.6 \pm 4.4	6.60	70.3 \pm 10.1	-
Fe 1	6136.615	2.45	-1.400	60.2 \pm 6.1	5.03	-	-	6.69	-
Fe 1	6137.691	2.59	-1.403	61.3 \pm 5.9	5.22	-	-	96.5 \pm 7.0	-
Fe 1	6151.617	2.18	-3.299	-	-	79.1 \pm 4.7	6.58	-	6.81
Fe 1	6157.728	4.08	-1.260	-	-	80.4 \pm 5.0	7.01	-	-
Fe 1	6165.360	4.14	-1.474	-	-	51.6 \pm 4.1	6.71	-	6.26
Fe 1	6173.334	2.22	-2.880	-	-	119.5 \pm 7.3	7.03	-	6.57
Fe 1	6180.203	2.73	-2.586	-	-	87.6 \pm 6.4	6.76	62.2 \pm 5.1	-
Fe 1	6187.989	3.94	-1.720	-	-	58.7 \pm 3.8	6.85	-	-
Fe 1	6191.558	2.43	-1.417	79.9 \pm 7.1	5.52	-	-	-	-
Fe 1	6200.312	2.61	-2.437	-	-	121.0 \pm 7.1	7.16	80.8 \pm 7.4	-
Fe 1	6213.429	2.22	-2.482	-	-	119.5 \pm 8.5	6.63	45.0 \pm 2.7	-
Fe 1	6219.280	2.20	-2.433	-	-	-	-	30.3 \pm 4.7	-
Fe 1	6230.722	2.56	-1.281	58.9 \pm 4.2	4.99	-	-	55.6 \pm 5.2	6.50
Fe 1	6246.318	3.60	-0.733	26.8 \pm 2.8	4.95	128.1 \pm 13.7	6.83	109.4 \pm 7.1	-
						97.0 \pm 10.4	6.49	-	6.54

Table 5. continued.

El.	λ	χ_{ex}	$\log(gf)$	EW $\pm\sigma$ (EW) $\log \varepsilon(X) + 12$ [dex]								#21 UVES	
				01	02	03	04						
Fe 1	6252.555	2.40	-1.687	60.7 \pm 5.4	5.25	155.3 \pm 9.4	6.76	122.0 \pm 9.0	6.54	71.1 \pm 5.1	4.84	130.9 \pm 7.0	6.44
Fe 1	6265.132	2.18	-2.550	-	-	148.6 \pm 8.6	7.12	-	-	-	-	133.5 \pm 7.1	6.97
Fe 1	6290.965	4.73	-0.774	-	-	57.2 \pm 4.3	6.83	27.4 \pm 3.1	6.34	-	-	-	-
Fe 1	6297.792	2.22	-2.740	-	-	-	-	97.5 \pm 8.0	6.85	-	-	-	-
Fe 1	6301.500	3.65	-0.718	-	-	116.8 \pm 7.6	6.66	113.8 \pm 6.6	6.82	-	-	114.3 \pm 10.0	6.69
Fe 1	6302.494	3.69	-0.973	-	-	88.6 \pm 6.0	6.38	77.0 \pm 6.8	6.40	-	-	68.7 \pm 6.4	6.02
Fe 1	6311.500	2.83	-3.141	-	-	-	-	-	-	-	-	32.2 \pm 2.8	6.33
Fe 1	6322.685	2.59	-2.426	-	-	104.0 \pm 6.8	6.75	97.8 \pm 6.6	7.01	-	-	87.6 \pm 5.1	6.50
Fe 1	6335.330	2.20	-2.177	-	-	130.5 \pm 10.9	6.46	-	-	61.7 \pm 4.2	4.89	-	-
Fe 1	6344.148	2.43	-2.923	-	-	99.5 \pm 5.7	6.95	69.3 \pm 5.7	6.67	-	-	-	-
Fe 1	6355.028	2.85	-2.350	-	-	104.6 \pm 6.5	7.00	-	-	-	-	97.4 \pm 7.2	6.96
Fe 1	6380.743	4.19	-1.376	-	-	-	-	32.5 \pm 3.2	6.43	-	-	43.3 \pm 3.4	6.49
Fe 1	6393.601	2.43	-1.432	-	-	171.8 \pm 12.5	6.72	145.0 \pm 9.5	6.64	86.5 \pm 7.2	4.86	145.9 \pm 7.9	6.42
Fe 1	6400.000	3.60	-0.290	-	-	-	-	-	-	91.0 \pm 7.8	5.36	-	-
Fe 1	6408.018	3.69	-1.018	-	-	-	-	-	-	-	-	69.6 \pm 4.8	6.07
Fe 1	6411.648	3.65	-0.595	36.1 \pm 4.2	5.08	109.8 \pm 6.8	6.38	105.6 \pm 6.4	6.55	-	-	111.7 \pm 5.8	6.50
Fe 1	6419.949	4.73	-0.240	-	-	70.7 \pm 4.5	6.57	63.5 \pm 5.6	6.60	-	-	-	-
Fe 1	6421.350	2.28	-2.027	57.3 \pm 5.1	5.35	157.6 \pm 8.3	7.12	126.7 \pm 9.4	6.87	68.6 \pm 6.8	4.96	135.3 \pm 7.2	6.80
Fe 1	6430.845	2.18	-2.006	63.1 \pm 4.5	5.33	153.2 \pm 8.3	6.61	128.4 \pm 8.2	6.60	96.6 \pm 5.7	5.24	133.2 \pm 7.1	6.38
Fe 1	6494.980	2.40	-1.273	80.2 \pm 5.7	5.31	-	-	-	-	107.8 \pm 5.9	5.01	180.2 \pm 11.3	6.63
Fe 1	6518.366	2.83	-2.460	-	-	-	-	50.1 \pm 5.6	6.26	-	-	83.7 \pm 6.9	6.73
Fe 1	6581.209	1.49	-4.679	-	-	50.9 \pm 4.3	6.52	-	-	-	-	-	-
Fe 1	6592.913	2.73	-1.473	50.4 \pm 3.1	5.16	147.7 \pm 7.9	6.75	102.5 \pm 6.9	6.29	-	-	120.5 \pm 6.8	6.38
Fe 1	6593.870	2.43	-2.422	25.2 \pm 1.8	5.18	123.4 \pm 6.4	6.88	101.0 \pm 6.6	6.84	32.5 \pm 2.4	4.95	97.5 \pm 7.8	6.47
Fe 1	6677.985	2.69	-1.418	-	-	175.7 \pm 10.3	7.02	119.8 \pm 8.2	6.51	-	-	131.4 \pm 7.0	6.46
Fe 1	6750.151	2.42	-2.621	-	-	106.7 \pm 7.7	6.74	85.4 \pm 5.3	6.69	-	-	85.5 \pm 4.9	6.39
Fe 2	4923.921	2.89	-1.320	-	-	-	-	160.6 \pm 11.9	6.64	-	-	158.5 \pm 9.3	6.50
Fe 2	5018.436	2.89	-1.220	-	-	242.0 \pm 13.1	6.87	185.8 \pm 11.3	6.72	120.3 \pm 8.7	4.99	-	-
Fe 2	5197.567	3.23	-2.100	40.5 \pm 3.0	4.96	-	-	87.4 \pm 6.5	6.71	82.6 \pm 7.9	5.47	-	-
Fe 2	5234.623	3.22	-2.230	42.2 \pm 3.5	5.12	-	-	-	-	-	-	-	-
Fe 2	5264.802	3.23	-3.120	-	-	-	-	-	-	23.3 \pm 2.2	5.25	-	-
Fe 2	5275.997	3.20	-1.940	45.1 \pm 3.7	4.87	-	-	-	-	69.4 \pm 4.4	4.98	-	-
Fe 2	5284.103	2.89	-2.990	-	-	-	-	66.3 \pm 6.8	6.67	-	-	-	-
Fe 2	5325.552	3.22	-3.120	-	-	58.2 \pm 9.4	6.73	-	-	36.2 \pm 3.1	5.52	-	-
Fe 2	5425.249	3.20	-3.160	-	-	-	-	37.9 \pm 2.0	6.49	-	-	40.1 \pm 2.6	6.40
Fe 2	5534.838	3.24	-2.730	-	-	90.3 \pm 4.8	7.10	-	-	26.1 \pm 2.7	4.93	-	-
Fe 2	6149.246	3.89	-2.720	-	-	54.3 \pm 3.8	7.02	26.1 \pm 1.7	6.51	-	-	40.5 \pm 4.7	6.79
Fe 2	6247.557	3.89	-2.310	-	-	53.9 \pm 4.2	6.61	37.3 \pm 4.4	6.41	23.6 \pm 4.4	5.21	49.2 \pm 2.9	6.61
Fe 2	6416.919	3.89	-2.650	-	-	36.7 \pm 3.1	6.53	-	-	-	-	52.7 \pm 4.8	7.03
Fe 2	6432.676	2.89	-3.520	-	-	-	-	55.4 \pm 4.4	6.90	-	-	42.6 \pm 3.1	6.44
Fe 2	6456.379	3.90	-2.100	27.0 \pm 3.8	5.36	61.4 \pm 4.5	6.58	36.3 \pm 2.6	6.19	-	-	-	-
Fe 2	6516.077	2.89	-3.320	38.2 \pm 2.6	5.64	68.2 \pm 4.0	6.72	-	-	28.8 \pm 2.1	5.09	43.7 \pm 3.2	6.27
Co 1	5483.354	1.71	-1.490	-	-	76.3 \pm 38.2	4.00	-	-	-	-	-	-
Ni 1	5081.110	3.85	0.300	-	-	-	-	83.0 \pm 9.3	5.39	-	-	-	-
Ni 1	5084.096	3.68	0.030	-	-	88.7 \pm 12.1	5.38	-	-	-	-	-	-
Ni 1	5155.764	3.90	0.074	-	-	58.5 \pm 3.8	4.87	-	-	-	-	-	-
Ni 1	5476.904	1.83	-0.780	-	-	-	-	-	-	108.2 \pm 8.0	3.71	-	-
Ni 1	6128.973	1.68	-3.430	-	-	56.1 \pm 4.0	5.47	38.4 \pm 4.2	5.40	-	-	-	-
Ni 1	6327.599	1.68	-3.170	-	-	-	-	43.8 \pm 4.1	5.24	-	-	-	-
Ni 1	6482.798	1.93	-2.630	-	-	49.8 \pm 3.4	4.85	-	-	-	-	-	-
Ni 1	6586.310	1.95	-2.780	-	-	78.5 \pm 4.6	5.56	-	-	-	-	-	-
Ni 1	6643.630	1.68	-2.220	-	-	128.3 \pm 7.4	5.61	71.3 \pm 4.2	4.85	37.7 \pm 4.2	3.59	-	-
Cu 1	5105.537	1.39	-1.542	-	-	101.2 \pm 7.0	2.77	76.8 \pm 7.7	2.66	-	-	93.0 \pm 6.9	2.63
Cu 1	5700.237	1.64	-2.583	-	-	31.7 \pm 8.6	2.96	-	-	-	-	-	-
Y 2	4883.682	1.08	0.070	29.8 \pm 3.2	-0.44	101.1 \pm 8.1	1.62	79.2 \pm 7.0	1.50	-	-	-	-
Y 2	4900.119	1.03	-0.090	-	-	-	-	-	-	30.2 \pm 3.4	-0.81	-	-
Y 2	5087.419	1.08	-0.170	20.0 \pm 2.3	-0.49	-	-	-	-	-	-	-	-
Y 2	5200.410	0.99	-0.570	-	-	76.3 \pm 5.2	1.48	-	-	-	-	-	-
Y 2	5402.774	1.84	-0.630	-	-	33.7 \pm 2.3	1.56	-	-	-	-	-	-
Ba 2	4934.076	0.00	-0.150	169.7 \pm 16.1	0.69	286.3 \pm 16.7	2.29	224.1 \pm 14.0	1.83	165.5 \pm 10.9	-0.17	246.7 \pm 14.5	1.89
Ba 2	5853.668	0.60	-1.000	67.4 \pm 7.3	0.45	135.5 \pm 14.5	2.34	102.9 \pm 10.2	2.01	55.0 \pm 4.9	-0.65	124.8 \pm 12.9	2.25
Ba 2	6141.713	0.70	-0.076	118.6 \pm 8.1	0.84	177.4 \pm 12.2	2.11	147.2 \pm 7.6	1.84	83.9 \pm 6.5	-0.93	165.4 \pm 10.4	1.93
Ba 2	6496.897	0.60	-0.377	113.7 \pm 6.5	0.84	182.3 \pm 11.1	2.26	-	-	84.0 \pm 5.3	-0.82	-	-
La 2	5290.820	0.00	-1.650	-	-	24.7 \pm 4.2	0.43	-	-	-	-	-	-
La 2	6320.376	0.17	-1.610	-	-	-	-	-	-	-	-	29.2 \pm 2.0	0.65
Nd 2	5319.810	0.55	-0.140	24.2 \pm 2.2	-0.27	63.8 \pm 3.3	1.04	66.4 \pm 6.5	1.57	-	-	-	-
Nd 2	5431.520	1.12	-0.470	-	-	-	-	38.8 \pm 2.8	1.80	25.1 \pm 1.8	0.30	-	-
Nd 2	5533.820	0.56	-1.230	-	-	23.3 \pm 2.9	1.16	-	-	-	-	-	-
Eu 2	6645.103	1.38	0.121	-	-	35.5 \pm 3.1	0.61	27.8 \pm 2.6	0.65	-	-	43.7 \pm 2.6	0.75

Table 6. Line parameters, observed equivalent widths and corresponding abundances of stars #26 UVES, 05, 06, 07, and #28 UVES observed with HRS.

El.	λ	χ_{ex}	$\log(gf)$	EW $\pm\sigma$ (EW) log $\varepsilon(X) + 12$ [dex]								
				#26 UVES		05		06		07		#28 UVES
Na 1	5688.205	2.10	-0.452	27.0 \pm 2.6	4.43	-	-	84.7 \pm 7.3	5.08	-	-	-
Na 1	5889.951	0.00	0.108	239.9 \pm 18.0	4.40	221.5 \pm 15.8	4.24	-	-	210.7 \pm 19.7	4.25	-
Na 1	5895.924	0.00	-0.194	229.4 \pm 15.0	4.64	218.6 \pm 14.7	4.51	-	-	178.8 \pm 11.6	4.19	-
Mg 1	5172.684	2.71	-0.450	-	-	233.5 \pm 13.4	5.57	-	-	197.9 \pm 10.8	5.29	-
Mg 1	5183.604	2.72	-0.239	-	-	261.9 \pm 14.7	5.56	-	-	213.4 \pm 11.2	5.21	-
Mg 1	5528.405	4.35	-0.498	132.7 \pm 7.0	6.22	109.0 \pm 6.1	5.82	197.2 \pm 10.2	6.63	63.5 \pm 3.2	5.13	207.6 \pm 11.5
Mg 1	5711.088	4.35	-1.724	52.8 \pm 3.1	6.18	-	-	104.1 \pm 6.7	6.64	-	-	69.3 \pm 6.0
Si 1	5645.613	4.93	-2.140	-	-	-	-	43.0 \pm 3.3	6.97	-	-	-
Si 1	5690.425	4.93	-1.870	-	-	-	-	38.3 \pm 3.0	6.61	-	-	59.5 \pm 5.5
Si 1	5708.399	4.95	-1.470	-	-	-	-	86.3 \pm 6.7	7.09	-	-	-
Si 1	5948.541	5.08	-1.230	-	-	-	-	84.5 \pm 6.0	6.97	-	-	42.2 \pm 4.0
Si 1	6243.814	5.62	-1.244	-	-	-	-	-	-	-	-	60.0 \pm 7.5
Si 1	6244.465	5.62	-1.091	-	-	-	-	40.6 \pm 6.3	6.72	-	-	51.2 \pm 7.3
Ca 1	5349.465	2.71	-0.310	78.8 \pm 6.5	5.43	-	-	110.8 \pm 7.3	5.52	-	-	-
Ca 1	5581.965	2.52	-0.555	62.4 \pm 4.3	5.01	-	-	99.1 \pm 5.9	5.19	-	-	-
Ca 1	5588.749	2.53	0.358	98.6 \pm 5.0	4.96	79.2 \pm 4.2	4.27	-	-	81.7 \pm 4.2	4.45	-
Ca 1	5590.114	2.52	-0.571	61.5 \pm 3.3	5.00	-	-	120.1 \pm 7.3	5.63	-	-	91.2 \pm 6.3
Ca 1	5601.277	2.53	-0.523	60.9 \pm 3.1	4.95	-	-	-	-	35.4 \pm 2.4	4.39	114.5 \pm 9.4
Ca 1	5857.451	2.93	0.240	96.2 \pm 6.8	5.37	-	-	160.8 \pm 10.2	5.85	59.6 \pm 6.4	4.56	-
Ca 1	6102.723	1.88	-0.793	-	-	64.6 \pm 6.0	4.33	-	-	-	-	-
Ca 1	6122.217	1.89	-0.316	124.4 \pm 7.4	5.11	98.0 \pm 6.9	4.42	184.5 \pm 12.7	5.36	90.3 \pm 5.2	4.43	189.1 \pm 10.4
Ca 1	6161.297	2.52	-1.266	30.7 \pm 2.8	5.00	-	-	-	-	-	-	-
Ca 1	6162.173	1.90	-0.090	159.8 \pm 8.8	5.30	120.8 \pm 8.9	4.61	204.9 \pm 11.8	5.37	96.9 \pm 7.1	4.34	193.6 \pm 14.7
Ca 1	6166.439	2.52	-1.142	-	-	-	-	84.2 \pm 5.3	5.41	-	-	82.4 \pm 10.2
Ca 1	6169.563	2.53	-0.478	-	-	42.9 \pm 3.4	4.45	-	-	-	-	-
Ca 1	6439.075	2.53	0.390	128.3 \pm 6.5	5.38	94.0 \pm 5.8	4.42	175.2 \pm 9.7	5.46	83.5 \pm 4.3	4.37	157.5 \pm 9.9
Ca 1	6455.598	2.52	-1.340	28.5 \pm 2.1	5.02	-	-	76.6 \pm 6.7	5.45	-	-	-
Ca 1	6499.650	2.52	-0.818	48.3 \pm 2.9	4.92	25.4 \pm 2.1	4.43	118.0 \pm 6.7	5.66	-	-	-
Ca 1	6717.681	2.71	-0.524	64.5 \pm 3.9	5.14	25.1 \pm 3.0	4.34	-	-	24.2 \pm 2.1	4.31	-
Sc 2	5031.021	1.36	-0.400	-	-	64.3 \pm 4.0	0.68	110.1 \pm 9.0	1.95	-	-	-
Sc 2	5526.790	1.77	0.024	69.0 \pm 3.5	1.60	47.5 \pm 2.7	0.46	102.1 \pm 7.0	1.84	-	-	111.6 \pm 6.6
Sc 2	6309.920	1.50	-1.618	30.3 \pm 2.5	2.00	-	-	29.5 \pm 5.1	1.71	-	-	-
Sc 2	6604.601	1.36	-1.309	-	-	-	-	62.5 \pm 4.6	1.79	-	-	-
Ti 1	4840.874	0.90	-0.430	-	-	-	-	-	-	39.0 \pm 3.2	2.99	-
Ti 1	4913.613	1.87	0.220	30.4 \pm 3.2	3.34	-	-	-	-	-	-	-
Ti 1	4981.730	0.85	0.570	111.6 \pm 6.8	3.69	-	-	-	-	108.6 \pm 6.6	3.43	-
Ti 1	4997.097	0.00	-2.070	-	-	-	-	107.9 \pm 10.4	3.85	-	-	-
Ti 1	4999.503	0.83	0.320	111.3 \pm 8.1	3.90	-	-	167.1 \pm 12.8	3.97	87.1 \pm 5.8	3.14	-
Ti 1	5016.161	0.85	-0.480	61.9 \pm 4.3	3.48	-	-	120.5 \pm 11.5	3.78	47.2 \pm 3.8	3.11	-
Ti 1	5039.958	0.02	-1.080	-	-	44.6 \pm 4.3	2.58	-	-	75.1 \pm 4.9	3.23	-
Ti 1	5173.743	0.00	-1.060	-	-	49.0 \pm 5.2	2.59	-	-	75.2 \pm 4.6	3.16	-
Ti 1	5192.969	0.02	-0.950	90.2 \pm 5.4	3.62	67.0 \pm 4.2	2.79	-	-	84.4 \pm 5.1	3.28	181.6 \pm 11.6
Ti 1	5210.384	0.05	-0.820	92.2 \pm 4.9	3.57	57.7 \pm 4.3	2.55	164.9 \pm 9.9	4.08	91.5 \pm 5.0	3.34	161.0 \pm 14.3
Ti 1	5978.541	1.87	-0.496	-	-	-	-	59.0 \pm 5.3	3.88	-	-	-
Ti 1	6126.216	1.07	-1.425	-	-	-	-	68.4 \pm 6.1	3.80	-	-	54.8 \pm 5.3
Ti 1	6258.102	1.44	-0.390	37.1 \pm 2.9	3.47	-	-	-	-	-	-	-
Ti 1	6554.223	1.44	-1.150	-	-	-	-	61.3 \pm 6.8	3.91	-	-	-
Ti 2	4865.610	1.12	-2.700	-	-	-	-	-	-	53.4 \pm 4.8	3.35	-
Ti 2	5129.156	1.89	-1.340	-	-	62.4 \pm 4.9	2.65	-	-	-	-	-
Ti 2	5154.068	1.57	-1.750	-	-	-	-	-	-	82.9 \pm 5.4	3.56	-
Ti 2	5185.902	1.89	-1.410	72.4 \pm 4.0	3.73	-	-	128.7 \pm 7.3	4.50	68.3 \pm 4.3	3.28	116.3 \pm 9.9
Ti 2	5336.786	1.58	-1.600	92.4 \pm 5.2	4.03	51.3 \pm 4.5	2.33	118.3 \pm 6.3	4.05	92.4 \pm 5.9	3.61	-
Ti 2	5381.021	1.57	-1.970	72.6 \pm 4.0	3.88	51.4 \pm 3.8	2.67	-	-	71.6 \pm 4.0	3.49	-
Ti 2	5418.768	1.58	-2.130	59.4 \pm 3.5	3.73	-	-	75.4 \pm 5.6	3.67	63.7 \pm 3.3	3.50	95.4 \pm 5.2
V 1	6216.364	0.28	-1.330	-	-	-	-	-	-	-	-	108.6 \pm 10.6
Cr 1	5206.023	0.94	0.020	-	-	118.4 \pm 6.8	3.16	-	-	157.5 \pm 8.1	4.19	-
Cr 1	5208.409	0.94	0.170	-	-	-	-	314.0 \pm 16.4	4.61	-	-	-
Cr 1	5296.691	0.98	-1.360	65.2 \pm 5.7	3.78	34.9 \pm 2.6	3.06	-	-	74.5 \pm 3.8	3.88	-
Cr 1	5345.796	1.00	-0.896	85.3 \pm 4.7	3.86	41.5 \pm 2.8	2.74	172.3 \pm 8.9	4.63	93.2 \pm 5.1	3.87	168.6 \pm 9.1
Cr 1	5348.314	1.00	-1.210	71.6 \pm 4.1	3.81	34.6 \pm 3.3	2.93	138.4 \pm 7.9	4.26	71.9 \pm 5.0	3.69	128.6 \pm 10.1
Cr 1	5409.784	1.03	-0.670	-	-	71.5 \pm 4.1	3.03	185.4 \pm 9.9	4.61	111.8 \pm 5.7	4.08	-
Cr 1	6330.091	0.94	-2.920	-	-	-	-	55.2 \pm 3.0	4.12	-	-	-
Mn 1	5407.417	2.14	-1.743	-	-	-	-	67.7 \pm 4.8	3.79	-	-	-
Mn 1	5420.351	2.14	-1.462	-	-	-	-	-	-	31.3 \pm 1.8	3.64	-
Mn 1	5516.766	2.18	-1.847	-	-	-	-	57.1 \pm 4.9	3.84	-	-	-
Mn 1	6013.510	3.07	-0.352	-	-	-	-	79.0 \pm 5.3	3.86	27.9 \pm 4.0	3.61	109.5 \pm 8.3
Mn 1	6021.820	3.08	-0.054	-	-	-	-	89.7 \pm 6.4	3.85	48.7 \pm 4.1	3.72	117.8 \pm 9.0
Fe 1	4859.741	2.88	-0.764	-	-	90.5 \pm 11.3	5.27	-	-	-	-	-
Fe 1	4871.318	2.87	-0.363	123.7 \pm 11.9	5.81	-	-	-	-	118.9 \pm 7.2	5.69	-
Fe 1	4872.138	2.88	-0.567	-	-	-	-	-	-	110.6 \pm 7.1	5.75	-
Fe 1	4890.755	2.88	-0.394	128.9 \pm 9.9	5.92	111.1 \pm 8.1	5.32	228.5 \pm 20.4	6.50	131.8 \pm 9.6	5.94	-
Fe 1	4891.492	2.85	-0.112	133.0 \pm 9.1	5.66	-	-	215.7 \pm 15.2	6.11	124.7 \pm 8.1	5.52	-

Table 6. continued.

El.	λ	χ_{ex}	$\log(gf)$	EW $\pm\sigma$ (EW) log $\varepsilon(X) + 12$ [dex]								
				#26 UVES		05		06		07		#28 UVES
Fe 1	4903.310	2.88	-0.926	-	-	93.8 \pm 5.8	5.50	-	-	105.3 \pm 5.5	5.99	-
Fe 1	4918.994	2.87	-0.342	145.3 \pm 10.4	6.03	-	-	-	-	-	-	-
Fe 1	4920.502	2.83	0.068	-	-	139.7 \pm 11.2	5.33	-	-	-	-	-
Fe 1	4924.770	2.28	-2.241	80.4 \pm 5.7	6.17	50.8 \pm 8.0	5.25	103.9 \pm 9.8	5.88	71.5 \pm 4.8	5.77	-
Fe 1	4966.088	3.33	-0.871	-	-	59.5 \pm 4.1	5.32	-	-	79.8 \pm 5.4	5.89	-
Fe 1	5001.863	3.88	0.010	-	-	35.4 \pm 4.1	4.67	-	-	68.7 \pm 4.1	5.41	-
Fe 1	5006.119	2.83	-0.638	-	-	78.1 \pm 6.0	4.81	-	-	-	-	-
Fe 1	5014.942	3.94	-0.303	85.4 \pm 5.2	6.33	42.4 \pm 2.4	5.18	-	-	61.4 \pm 4.0	5.63	-
Fe 1	5028.126	3.57	-1.123	38.1 \pm 3.9	5.55	-	-	-	-	-	-	-
Fe 1	5041.756	1.49	-2.203	-	-	-	-	-	-	125.8 \pm 6.7	6.08	-
Fe 1	5044.211	2.85	-2.038	35.4 \pm 3.6	5.52	-	-	-	-	43.3 \pm 6.0	5.65	112.5 \pm 13.1
Fe 1	5049.820	2.28	-1.355	-	-	-	-	175.7 \pm 9.7	6.25	105.7 \pm 5.7	5.67	168.8 \pm 12.0
Fe 1	5068.766	2.94	-1.042	95.3 \pm 7.2	6.05	68.8 \pm 5.5	5.16	-	-	87.4 \pm 5.0	5.73	138.1 \pm 12.4
Fe 1	5074.748	4.22	-0.200	-	-	-	-	96.7 \pm 10.4	6.25	61.1 \pm 5.0	5.84	-
Fe 1	5079.223	2.20	-2.067	-	-	83.2 \pm 5.8	5.53	-	-	-	-	-
Fe 1	5131.468	2.22	-2.515	69.8 \pm 6.3	6.05	-	-	-	-	53.3 \pm 4.9	5.55	134.7 \pm 9.1
Fe 1	5141.739	2.42	-1.964	-	-	50.4 \pm 5.7	5.12	112.8 \pm 11.7	5.93	-	-	-
Fe 1	5159.058	4.28	-0.820	-	-	-	-	-	-	24.6 \pm 2.2	5.75	-
Fe 1	5162.272	4.18	0.020	73.7 \pm 4.4	5.96	-	-	-	-	67.0 \pm 3.8	5.69	129.7 \pm 9.6
Fe 1	5171.596	1.49	-1.793	136.1 \pm 7.7	6.03	116.0 \pm 6.8	4.98	-	-	127.3 \pm 7.2	5.65	-
Fe 1	5191.455	3.04	-0.551	109.6 \pm 5.7	5.92	78.9 \pm 5.4	4.97	185.2 \pm 11.3	6.46	113.5 \pm 7.5	5.90	179.2 \pm 13.4
Fe 1	5192.344	3.00	-0.421	-	-	80.4 \pm 4.7	4.81	-	-	110.9 \pm 6.0	5.67	218.3 \pm 12.9
Fe 1	5194.941	1.56	-2.090	107.5 \pm 6.0	5.82	-	-	168.9 \pm 9.0	6.29	111.2 \pm 5.8	5.64	-
Fe 1	5198.711	2.22	-2.135	-	-	52.9 \pm 3.4	5.08	-	-	83.8 \pm 4.5	5.83	-
Fe 1	5202.336	2.18	-1.838	114.5 \pm 5.9	6.33	86.5 \pm 5.0	5.31	189.9 \pm 10.7	6.66	100.9 \pm 6.8	5.87	-
Fe 1	5215.180	3.27	-0.871	85.2 \pm 4.9	6.02	-	-	-	-	-	-	130.0 \pm 10.2
Fe 1	5216.274	1.61	-2.150	109.4 \pm 7.3	5.98	-	-	154.5 \pm 9.6	6.07	119.8 \pm 6.2	5.97	-
Fe 1	5217.389	3.21	-1.070	66.5 \pm 4.5	5.70	-	-	111.1 \pm 7.0	6.06	68.5 \pm 3.8	5.64	130.9 \pm 14.7
Fe 1	5232.940	2.94	-0.058	141.6 \pm 7.7	5.74	113.7 \pm 6.2	5.03	215.2 \pm 11.8	6.08	135.2 \pm 6.9	5.65	245.7 \pm 15.8
Fe 1	5242.491	3.63	-0.967	62.2 \pm 3.5	6.04	-	-	91.9 \pm 7.1	6.12	50.5 \pm 3.8	5.67	-
Fe 1	5266.555	3.00	-0.386	-	-	103.7 \pm 7.0	5.22	184.3 \pm 11.0	6.21	111.9 \pm 5.9	5.64	195.6 \pm 10.3
Fe 1	5281.790	3.04	-0.834	87.0 \pm 4.9	5.74	53.8 \pm 5.0	4.79	129.5 \pm 7.2	5.94	90.0 \pm 4.8	5.67	-
Fe 1	5302.300	3.28	-0.720	78.0 \pm 4.5	5.71	-	-	-	-	71.4 \pm 4.1	5.43	155.4 \pm 12.1
Fe 1	5307.361	1.61	-2.987	78.5 \pm 4.2	5.98	-	-	118.6 \pm 8.6	5.93	71.4 \pm 4.6	5.62	-
Fe 1	5322.041	2.28	-2.803	43.0 \pm 3.3	5.74	-	-	-	-	-	-	96.4 \pm 6.8
Fe 1	5324.179	3.21	-0.103	124.6 \pm 6.7	5.89	104.8 \pm 7.0	5.22	184.4 \pm 9.7	6.25	-	-	-
Fe 1	5332.899	1.56	-2.777	-	-	53.1 \pm 3.9	4.88	150.8 \pm 9.3	6.46	-	-	-
Fe 1	5339.929	3.27	-0.647	95.8 \pm 5.2	6.01	53.4 \pm 5.0	4.87	-	-	89.1 \pm 4.7	5.73	155.7 \pm 9.7
Fe 1	5364.871	4.45	0.228	61.2 \pm 4.0	5.74	33.6 \pm 2.6	5.07	-	-	58.2 \pm 2.9	5.60	-
Fe 1	5365.399	3.57	-1.020	-	-	-	-	-	-	-	-	106.7 \pm 13.3
Fe 1	5367.466	4.41	0.443	68.4 \pm 4.7	5.66	39.6 \pm 2.2	4.93	87.9 \pm 5.0	5.62	-	-	123.9 \pm 8.2
Fe 1	5369.961	4.37	0.536	-	-	36.8 \pm 2.9	4.73	-	-	-	-	-
Fe 1	5379.574	3.69	-1.514	-	-	-	-	69.6 \pm 4.2	6.24	26.0 \pm 1.8	5.76	-
Fe 1	5383.369	4.31	0.645	87.2 \pm 5.0	5.78	75.5 \pm 4.5	5.25	-	-	-	-	153.8 \pm 13.6
Fe 1	5389.479	4.41	-0.410	38.7 \pm 2.3	5.83	-	-	72.8 \pm 6.4	6.15	28.8 \pm 2.2	5.58	-
Fe 1	5393.167	3.24	-0.715	81.4 \pm 4.1	5.72	-	-	148.5 \pm 7.8	6.42	76.9 \pm 4.0	5.48	-
Fe 1	5400.501	4.37	-0.160	-	-	26.5 \pm 2.9	5.21	105.7 \pm 5.7	6.54	40.1 \pm 3.0	5.52	-
Fe 1	5410.910	4.47	0.398	65.2 \pm 3.7	5.69	36.9 \pm 3.5	4.99	-	-	-	-	120.9 \pm 8.0
Fe 1	5415.199	4.39	0.642	75.3 \pm 4.3	5.59	-	-	125.1 \pm 7.3	6.13	-	-	151.1 \pm 9.7
Fe 1	5424.068	4.32	0.520	90.9 \pm 6.6	5.98	51.2 \pm 5.6	4.94	124.4 \pm 6.9	6.15	76.4 \pm 3.9	5.55	145.3 \pm 7.9
Fe 1	5445.042	4.39	-0.020	-	-	-	-	75.7 \pm 5.4	5.78	46.9 \pm 3.1	5.54	-
Fe 1	5569.618	3.42	-0.486	92.7 \pm 4.8	5.92	75.2 \pm 5.2	5.26	134.5 \pm 7.4	6.13	80.7 \pm 4.4	5.53	-
Fe 1	5572.842	3.40	-0.275	-	-	65.2 \pm 4.6	4.84	-	-	103.7 \pm 5.4	5.79	-
Fe 1	5576.089	3.43	-1.000	68.6 \pm 3.8	5.90	-	-	118.6 \pm 6.3	6.35	67.3 \pm 3.7	5.76	-
Fe 1	5586.755	3.37	-0.120	113.0 \pm 5.9	5.86	79.2 \pm 5.1	4.90	-	-	102.0 \pm 5.5	5.57	182.7 \pm 10.4
Fe 1	5701.544	2.56	-2.216	-	-	-	-	-	-	57.6 \pm 2.9	5.69	-
Fe 1	6003.011	3.88	-1.120	42.0 \pm 4.5	5.94	-	-	-	-	37.8 \pm 2.5	5.81	-
Fe 1	6024.058	4.55	-0.120	60.2 \pm 4.4	6.15	-	-	89.2 \pm 6.3	6.30	47.3 \pm 3.1	5.81	-
Fe 1	6027.051	4.08	-1.089	-	-	-	-	80.3 \pm 8.2	6.46	-	-	-
Fe 1	6056.004	4.73	-0.460	-	-	-	-	68.1 \pm 5.6	6.46	-	-	81.0 \pm 5.3
Fe 1	6065.482	2.61	-1.530	93.4 \pm 6.4	5.98	-	-	156.5 \pm 11.4	6.32	94.9 \pm 7.0	5.82	164.7 \pm 14.4
Fe 1	6078.491	4.80	-0.321	-	-	-	-	-	-	-	-	71.4 \pm 6.2
Fe 1	6082.710	2.22	-3.573	-	-	-	-	82.7 \pm 6.3	6.44	-	-	-
Fe 1	6136.615	2.45	-1.400	-	-	88.2 \pm 6.9	5.13	-	-	-	-	-
Fe 1	6137.691	2.59	-1.403	110.9 \pm 8.0	6.05	-	-	-	-	114.0 \pm 10.1	6.05	-
Fe 1	6151.617	2.18	-3.299	-	-	-	-	86.5 \pm 6.5	6.14	-	-	-
Fe 1	6165.360	4.14	-1.474	-	-	-	-	30.6 \pm 4.9	5.99	-	-	-
Fe 1	6173.334	2.22	-2.880	47.8 \pm 3.9	5.77	-	-	136.3 \pm 7.3	6.69	46.0 \pm 3.4	5.68	111.9 \pm 6.3
Fe 1	6180.203	2.73	-2.586	-	-	-	-	88.8 \pm 5.0	6.25	-	-	-
Fe 1	6191.558	2.43	-1.417	-	-	100.9 \pm 6.5	5.34	-	-	-	-	-
Fe 1	6200.312	2.61	-2.437	53.8 \pm 3.9	5.94	-	-	114.5 \pm 8.5	6.43	-	-	-
Fe 1	6213.429	2.22	-2.482	78.1 \pm 4.8	6.06	37.8 \pm 4.9	5.09	-	-	56.2 \pm 3.9	5.47	-
Fe 1	6219.280	2.20	-2.433	70.7 \pm 4.8	5.80	-	-	-	-	69.2 \pm 4.5	5.64	141.4 \pm 8.2
Fe 1	6229.226	2.85	-2.805	-	-	-	-	63.6 \pm 6.4	6.17	-	-	84.6 \pm 7.4

Table 6. continued.

El.	λ	χ_{ex}	$\log(gf)$	EW $\pm\sigma$ (EW) log $\varepsilon(X) + 12$ [dex]									
				#26 UVES		05		06		07		#28 UVES	
Fe 1	6230.722	2.56	-1.281	108.5 \pm 7.0	5.96	98.7 \pm 5.7	5.31	194.5 \pm 12.6	6.46	-	-	184.9 \pm 11.0	6.68
Fe 1	6240.646	2.22	-3.233	28.7 \pm 2.1	5.71	-	-	-	-	-	-	97.5 \pm 7.8	6.69
Fe 1	6246.318	3.60	-0.733	65.9 \pm 4.6	5.72	35.0 \pm 2.7	4.99	129.5 \pm 7.2	6.37	61.2 \pm 3.4	5.53	-	-
Fe 1	6252.555	2.40	-1.687	99.8 \pm 6.6	6.00	88.3 \pm 5.7	5.34	-	-	107.3 \pm 5.8	5.95	179.4 \pm 12.0	6.83
Fe 1	6265.132	2.18	-2.550	-	-	35.4 \pm 3.8	5.05	132.3 \pm 8.5	6.21	70.1 \pm 4.1	5.74	-	-
Fe 1	6297.792	2.22	-2.740	-	-	-	-	111.1 \pm 7.3	6.08	56.7 \pm 3.1	5.73	-	-
Fe 1	6301.500	3.65	-0.718	-	-	29.1 \pm 3.1	4.92	103.7 \pm 5.8	5.93	-	-	-	-
Fe 1	6302.494	3.69	-0.973	43.0 \pm 3.2	5.55	-	-	-	-	35.2 \pm 2.8	5.36	96.0 \pm 7.7	6.32
Fe 1	6311.500	2.83	-3.141	-	-	-	-	-	-	-	-	70.8 \pm 5.2	6.87
Fe 1	6322.685	2.59	-2.426	49.0 \pm 3.6	5.79	-	-	100.7 \pm 8.1	6.10	56.5 \pm 4.1	5.87	-	-
Fe 1	6335.330	2.20	-2.177	89.3 \pm 5.9	5.96	57.8 \pm 4.7	5.06	156.7 \pm 10.4	6.24	82.0 \pm 4.4	5.62	142.8 \pm 7.8	6.38
Fe 1	6344.148	2.43	-2.923	-	-	-	-	63.2 \pm 4.4	5.70	-	-	-	-
Fe 1	6355.028	2.85	-2.350	-	-	-	-	112.0 \pm 7.2	6.59	-	-	112.2 \pm 7.5	6.89
Fe 1	6380.743	4.19	-1.376	-	-	-	-	43.4 \pm 2.8	6.18	-	-	-	-
Fe 1	6393.601	2.43	-1.432	110.7 \pm 5.8	5.97	82.7 \pm 5.2	5.01	170.9 \pm 11.2	6.11	111.1 \pm 6.7	5.78	-	-
Fe 1	6400.000	3.60	-0.290	-	-	72.8 \pm 4.6	5.17	-	-	-	-	-	-
Fe 1	6408.018	3.69	-1.018	50.6 \pm 3.3	5.76	-	-	95.6 \pm 7.3	6.10	61.7 \pm 3.9	5.91	121.5 \pm 7.5	6.85
Fe 1	6411.648	3.65	-0.595	-	-	-	-	114.3 \pm 6.7	6.00	65.9 \pm 4.1	5.53	119.7 \pm 6.8	6.35
Fe 1	6419.949	4.73	-0.240	-	-	-	-	74.1 \pm 5.3	6.32	25.3 \pm 4.1	5.66	-	-
Fe 1	6421.350	2.28	-2.027	100.3 \pm 5.0	6.20	-	-	162.9 \pm 8.7	6.51	92.0 \pm 4.9	5.80	-	-
Fe 1	6430.845	2.18	-2.006	108.9 \pm 6.3	6.05	84.8 \pm 6.0	5.28	-	-	96.2 \pm 5.3	5.70	171.5 \pm 9.1	6.57
Fe 1	6494.980	2.40	-1.273	118.4 \pm 6.2	5.90	96.2 \pm 5.9	5.03	-	-	132.7 \pm 7.3	5.96	182.9 \pm 9.4	6.40
Fe 1	6592.913	2.73	-1.473	89.4 \pm 6.0	5.91	-	-	-	-	78.5 \pm 5.0	5.50	157.6 \pm 9.5	6.63
Fe 1	6593.870	2.43	-2.422	63.9 \pm 4.9	5.90	-	-	103.1 \pm 7.1	5.88	-	-	-	-
Fe 1	6609.110	2.56	-2.692	33.4 \pm 2.5	5.67	-	-	-	-	36.3 \pm 2.7	5.70	-	-
Fe 1	6677.985	2.69	-1.418	96.0 \pm 4.8	5.95	-	-	151.0 \pm 8.0	6.08	95.2 \pm 6.0	5.74	169.6 \pm 8.8	6.69
Fe 1	6750.151	2.42	-2.621	60.8 \pm 4.2	6.01	-	-	-	-	53.3 \pm 2.8	5.77	112.0 \pm 9.5	6.56
Fe 2	4923.921	2.89	-1.320	135.5 \pm 8.1	6.08	111.2 \pm 12.2	4.78	-	-	143.6 \pm 8.2	5.90	189.9 \pm 20.0	6.56
Fe 2	5018.436	2.89	-1.220	-	-	131.0 \pm 8.0	5.04	-	-	164.9 \pm 9.8	6.01	-	-
Fe 2	5197.567	3.23	-2.100	71.7 \pm 4.8	6.00	56.9 \pm 5.3	4.86	-	-	80.0 \pm 4.8	5.81	108.9 \pm 9.9	6.72
Fe 2	5234.623	3.22	-2.230	87.6 \pm 5.9	6.51	84.3 \pm 5.3	5.49	-	-	92.6 \pm 4.9	6.22	117.0 \pm 8.9	6.99
Fe 2	5264.802	3.23	-3.120	-	-	35.4 \pm 2.3	5.49	42.0 \pm 9.2	6.08	-	-	-	-
Fe 2	5275.997	3.20	-1.940	-	-	86.2 \pm 5.8	5.20	-	-	-	-	-	-
Fe 2	5284.103	2.89	-2.990	41.5 \pm 3.5	5.71	-	-	-	-	-	-	-	-
Fe 2	5325.552	3.22	-3.120	21.8 \pm 1.9	5.72	21.4 \pm 2.1	5.16	44.5 \pm 2.7	6.13	33.0 \pm 2.2	5.76	54.4 \pm 3.4	6.50
Fe 2	5425.249	3.20	-3.160	25.4 \pm 2.2	5.83	-	-	-	-	25.8 \pm 1.6	5.60	-	-
Fe 2	5534.838	3.24	-2.730	-	-	-	-	-	-	41.7 \pm 2.5	5.58	-	-
Fe 2	5991.371	3.15	-3.540	-	-	-	-	-	-	34.1 \pm 2.2	6.09	-	-
Fe 2	6149.246	3.89	-2.720	31.8 \pm 2.5	6.35	-	-	-	-	-	-	-	-
Fe 2	6247.557	3.89	-2.310	-	-	-	-	60.4 \pm 6.8	6.51	36.2 \pm 3.6	5.78	75.0 \pm 7.5	6.95
Fe 2	6432.676	2.89	-3.520	28.2 \pm 1.9	5.88	33.2 \pm 4.2	5.37	52.2 \pm 6.7	6.26	34.1 \pm 2.0	5.75	77.2 \pm 6.7	6.95
Fe 2	6456.379	3.90	-2.100	51.9 \pm 2.9	6.23	-	-	-	-	49.8 \pm 3.0	5.87	-	-
Fe 2	6516.077	2.89	-3.320	-	-	29.0 \pm 2.5	5.08	77.9 \pm 5.1	6.58	43.0 \pm 2.6	5.73	-	-
Co 1	5483.354	1.71	-1.490	-	-	-	-	109.8 \pm 9.4	4.01	-	-	-	-
Ni 1	4904.412	3.54	-0.170	-	-	-	-	-	-	68.0 \pm 5.6	4.91	-	-
Ni 1	5081.110	3.85	0.300	43.4 \pm 4.5	4.32	-	-	-	-	66.2 \pm 4.1	4.82	-	-
Ni 1	5084.096	3.68	0.030	43.3 \pm 3.5	4.38	-	-	-	-	-	-	-	-
Ni 1	5115.392	3.83	-0.110	27.2 \pm 1.7	4.33	-	-	-	-	-	-	-	-
Ni 1	5155.764	3.90	0.074	29.1 \pm 2.2	4.26	-	-	-	-	-	-	-	-
Ni 1	6128.973	1.68	-3.430	-	-	-	-	-	-	-	-	70.8 \pm 12.0	5.50
Ni 1	6176.812	4.09	-0.260	-	-	-	-	-	-	-	-	72.2 \pm 7.7	5.50
Ni 1	6327.599	1.68	-3.170	39.9 \pm 4.2	4.97	-	-	77.2 \pm 7.6	5.01	25.5 \pm 1.8	4.61	-	-
Ni 1	6482.798	1.93	-2.630	-	-	-	-	69.6 \pm 4.7	4.68	-	-	85.6 \pm 7.4	5.28
Ni 1	6586.310	1.95	-2.780	-	-	-	-	-	-	24.5 \pm 2.5	4.53	-	-
Ni 1	6643.630	1.68	-2.220	65.5 \pm 3.8	4.55	41.4 \pm 3.6	3.90	125.8 \pm 6.7	4.89	89.4 \pm 5.3	4.88	-	-
Cu 1	5105.537	1.39	-1.542	-	-	-	-	101.0 \pm 9.9	2.20	-	-	128.6 \pm 10.3	3.01
Cu 1	5700.237	1.64	-2.583	-	-	-	-	44.4 \pm 2.9	2.66	-	-	42.6 \pm 4.5	2.91
Y 2	4883.682	1.08	0.070	64.5 \pm 6.4	0.71	-	-	-	-	-	-	95.7 \pm 8.9	1.21
Y 2	5087.419	1.08	-0.170	-	-	-	-	82.6 \pm 12.5	0.78	-	-	-	-
Ba 2	4934.076	0.00	-0.150	190.9 \pm 11.9	1.07	185.0 \pm 10.2	0.24	257.0 \pm 14.6	1.57	79.5 \pm 4.2	-1.28	244.5 \pm 15.5	1.91
Ba 2	5853.668	0.60	-1.000	72.5 \pm 5.4	0.80	67.8 \pm 6.4	-0.38	99.3 \pm 11.8	0.68	-	-	161.4 \pm 12.2	2.54
Ba 2	6141.713	0.70	-0.076	117.0 \pm 6.7	0.97	103.9 \pm 9.7	-0.56	157.9 \pm 11.0	1.11	37.4 \pm 2.1	-1.29	230.8 \pm 18.6	2.41
Ba 2	6496.897	0.60	-0.377	136.5 \pm 7.9	1.37	-	-	-	-	-	-	-	-
La 2	6390.480	0.32	-1.410	-	-	-	-	-	-	-	-	62.3 \pm 6.0	1.06
Nd 2	5319.810	0.55	-0.140	-	-	-	-	82.2 \pm 4.9	0.79	-	-	-	-
Nd 2	5431.520	1.12	-0.470	-	-	-	-	-	-	-	-	42.3 \pm 3.9	1.32
Eu 2	6049.513	1.28	-0.800	-	-	-	-	-	-	-	-	32.3 \pm 7.8	1.16
Eu 2	6645.103	1.38	0.121	-	-	-	-	32.4 \pm 3.6	0.04	-	-	71.1 \pm 8.0	1.03

Table 7. Line parameters, observed equivalent widths and corresponding abundances of stars 08, 09, 10, 11, and 12 observed with MIKE.

El.	λ	χ_{ex}	$\log(gf)$	EW $\pm\sigma$ (EW) $\log \varepsilon(X) + 12$ [dex]							
				08		09		10		11	
Li 1	6707.764	0	-0.036	-	-	19.3 ± 2.0	1.01	-	-	-	-
O 1	6300.304	0	-9.750	-	-	-	-	-	37.9 ± 2.7	8.13	-
O 1	6363.776	0.02	-10.260	-	-	-	9.7 ± 3.0	< 7.90	-	-	-
Na 1	5682.633	2.10	-0.706	43.3 ± 3.8	5.16	-	-	20.5 ± 3.4	4.61	63.5 ± 5.6	5.11
Na 1	5895.924	0	-0.194	-	-	-	-	-	-	-	159.9 ± 11.0
Na 1	6160.747	2.10	-1.246	-	-	-	-	-	27.5 ± 3.6	5.00	-
Mg 1	4571.096	0.00	-5.623	112.7 ± 10.1	6.62	94.1 ± 6.3	5.77	108.0 ± 8.9	6.15	-	-
Mg 1	4702.991	4.35	-0.440	134.8 ± 9.3	6.31	101.0 ± 6.3	5.68	116.8 ± 7.7	6.00	-	-
Mg 1	5528.405	4.35	-0.498	153.8 ± 12.0	6.60	106.7 ± 6.3	5.82	126.9 ± 7.1	6.17	-	-
Mg 1	5711.088	4.35	-1.724	69.8 ± 5.0	6.63	24.6 ± 3.0	5.69	44.0 ± 3.5	6.10	104.6 ± 6.6	6.86
Si 1	4102.936	1.91	-3.140	112.0 ± 10.1	6.46	-	-	120.8 ± 12.1	6.33	158.0 ± 12.8	6.84
Si 1	5665.555	4.92	-2.040	31.2 ± 4.1	6.94	-	-	-	34.2 ± 3.5	6.87	45.4 ± 6.1
Si 1	5690.425	4.93	-1.870	-	-	-	-	-	37.1 ± 2.7	6.77	-
Si 1	5701.104	4.93	-2.050	-	-	-	-	-	19.1 ± 2.4	6.52	-
Si 1	5708.399	4.95	-1.470	-	-	18.3 ± 2.0	5.93	35.4 ± 6.5	6.36	-	-
Si 1	5772.146	5.08	-1.750	-	-	-	-	-	37.6 ± 3.7	6.84	-
Si 1	5948.541	5.08	-1.230	-	-	-	-	40.0 ± 11.2	6.35	63.2 ± 3.6	6.83
Si 1	6243.814	5.62	-1.244	-	-	-	-	-	26.4 ± 3.0	6.73	-
Si 1	6244.465	5.62	-1.091	-	-	-	-	-	23.2 ± 2.2	6.49	-
Ca 1	4318.651	1.90	-0.139	112.9 ± 11.9	5.45	-	-	-	-	-	-
Ca 1	4425.437	1.88	-0.358	110.4 ± 8.3	5.41	78.7 ± 5.3	4.46	111.5 ± 6.7	5.23	-	-
Ca 1	4435.679	1.89	-0.517	-	-	81.5 ± 6.0	4.69	-	-	-	-
Ca 1	4454.779	1.90	-0.258	-	-	-	-	127.0 ± 10.5	4.90	-	-
Ca 1	4455.887	1.90	-0.518	105.6 ± 10.4	5.49	74.0 ± 4.7	4.54	-	140.0 ± 10.6	5.77	-
Ca 1	5265.556	2.52	-0.113	-	-	68.5 ± 6.2	4.69	-	-	-	-
Ca 1	5349.465	2.71	-0.310	68.2 ± 7.8	5.31	-	-	-	-	-	-
Ca 1	5581.965	2.52	-0.555	-	-	34.2 ± 2.5	4.44	61.1 ± 5.5	5.00	103.3 ± 6.6	5.63
Ca 1	5588.749	2.53	0.358	119.7 ± 9.7	5.51	84.5 ± 4.3	4.53	98.8 ± 6.0	4.87	151.0 ± 8.8	5.67
Ca 1	5590.114	2.52	-0.571	64.9 ± 5.4	5.26	32.4 ± 2.2	4.42	56.7 ± 4.4	4.93	104.9 ± 6.2	5.68
Ca 1	5601.277	2.53	-0.523	89.3 ± 7.6	5.76	36.9 ± 2.4	4.47	49.7 ± 6.7	4.75	118.7 ± 7.5	5.95
Ca 1	5857.451	2.93	0.240	88.3 ± 6.4	5.34	-	-	82.5 ± 5.3	5.06	-	45.2 ± 4.2
Ca 1	6102.723	1.88	-0.793	106.5 ± 6.1	5.50	65.1 ± 4.4	4.44	101.9 ± 5.7	5.20	144.7 ± 7.8	5.63
Ca 1	6122.217	1.89	-0.316	137.7 ± 8.3	5.50	97.0 ± 5.1	4.56	119.5 ± 7.5	5.04	-	78.5 ± 5.8
Ca 1	6161.297	2.52	-1.266	32.8 ± 2.4	5.27	-	-	29.1 ± 3.8	5.07	75.9 ± 4.8	5.63
Ca 1	6162.173	1.90	-0.090	-	-	114.1 ± 7.2	4.64	132.4 ± 8.3	5.02	-	94.3 ± 11.5
Ca 1	6166.439	2.52	-1.142	-	-	-	-	-	89.6 ± 4.9	5.79	-
Ca 1	6169.042	2.52	-0.797	68.8 ± 6.2	5.50	27.6 ± 2.2	4.51	47.7 ± 3.0	4.96	106.7 ± 6.0	5.81
Ca 1	6169.563	2.53	-0.478	102.1 ± 6.5	5.84	42.6 ± 3.2	4.49	-	122.9 ± 7.4	5.82	-
Ca 1	6439.075	2.53	0.390	128.0 ± 6.9	5.53	88.8 ± 5.0	4.51	119.4 ± 6.5	5.16	-	70.3 ± 4.3
Ca 1	6455.598	2.52	-1.340	-	-	-	-	-	70.7 ± 5.2	5.58	-
Ca 1	6499.650	2.52	-0.818	68.3 ± 4.8	5.53	24.7 ± 2.4	4.46	31.4 ± 7.6	4.66	101.1 ± 6.1	5.70
Ca 1	6717.681	2.71	-0.524	75.5 ± 4.2	5.54	31.1 ± 2.6	4.51	-	-	-	-
Sc 2	4246.822	0.31	0.242	-	-	127.2 ± 7.5	0.82	142.1 ± 9.2	1.29	-	-
Sc 2	4415.557	0.60	-0.668	89.7 ± 9.5	1.77	82.8 ± 6.2	0.97	107.9 ± 10.5	1.68	-	-
Sc 2	4670.407	1.36	-0.576	-	-	40.0 ± 3.3	0.96	-	-	-	-
Sc 2	5526.790	1.77	0.024	89.6 ± 6.9	2.30	47.3 ± 3.2	0.92	61.0 ± 4.9	1.30	102.6 ± 6.8	2.44
Sc 2	5657.896	1.51	-0.603	-	-	41.1 ± 2.6	1.09	-	-	100.2 ± 9.0	2.59
Sc 2	6604.601	1.36	-1.309	-	-	-	-	21.5 ± 2.1	1.31	66.1 ± 3.6	2.32
Ti 1	3998.636	0.05	0.020	112.1 ± 13.7	4.03	81.9 ± 5.5	2.73	-	-	-	-
Ti 1	4512.734	0.84	-0.400	-	-	-	-	53.4 ± 4.3	3.37	107.2 ± 8.8	4.19
Ti 1	4518.022	0.83	-0.250	75.7 ± 9.8	4.00	35.8 ± 3.5	2.77	-	-	-	-
Ti 1	4533.239	0.85	0.540	-	-	75.8 ± 5.2	2.85	-	-	-	-
Ti 1	4534.776	0.84	0.350	90.4 ± 6.8	3.80	60.4 ± 5.0	2.68	79.7 ± 6.3	3.19	128.3 ± 8.2	3.92
Ti 1	4535.568	0.83	0.140	-	-	-	-	89.9 ± 6.9	3.64	-	-
Ti 1	4548.764	0.83	-0.280	75.5 ± 6.0	4.02	36.6 ± 2.2	2.82	60.7 ± 4.1	3.38	111.6 ± 7.9	4.16
Ti 1	4555.483	0.85	-0.400	62.8 ± 5.6	3.84	30.8 ± 2.4	2.84	50.0 ± 5.0	3.31	104.0 ± 6.8	4.10
Ti 1	4623.097	1.74	0.160	-	-	-	-	-	81.7 ± 4.8	4.09	-
Ti 1	4645.188	1.73	-0.510	-	-	-	-	-	66.7 ± 5.1	4.34	-
Ti 1	4656.468	0.00	-1.290	74.9 ± 5.8	4.04	-	-	64.8 ± 4.1	3.47	-	-
Ti 1	4681.909	0.05	-1.030	-	-	48.3 ± 2.8	2.84	72.6 ± 5.5	3.43	-	-
Ti 1	4840.874	0.90	-0.430	54.3 ± 6.2	3.70	26.3 ± 2.4	2.81	-	-	-	-
Ti 1	4913.613	1.87	0.220	-	-	-	-	-	75.9 ± 5.0	3.97	-
Ti 1	4981.730	0.85	0.570	-	-	77.6 ± 4.9	2.78	102.4 ± 8.6	3.43	-	-
Ti 1	4999.503	0.83	0.320	-	-	68.4 ± 4.1	2.80	-	-	-	-
Ti 1	5016.161	0.85	-0.480	72.6 ± 6.7	4.08	27.1 ± 3.3	2.80	-	-	115.0 ± 8.9	4.28
Ti 1	5039.958	0.02	-1.080	-	-	49.3 ± 3.9	2.83	-	-	129.1 ± 8.2	4.26
Ti 1	5173.743	0.00	-1.060	88.8 ± 9.3	4.05	48.2 ± 3.3	2.75	73.5 ± 6.6	3.34	-	-
Ti 1	5192.969	0.02	-0.950	98.6 ± 9.5	4.21	53.0 ± 4.1	2.75	-	-	-	-
Ti 1	5210.384	0.05	-0.820	-	-	57.5 ± 3.3	2.74	-	-	-	-
Ti 1	5490.147	1.46	-0.840	-	-	-	-	-	44.8 ± 5.1	3.70	-
Ti 1	5978.541	1.87	-0.496	-	-	-	-	-	53.6 ± 3.6	4.03	-
Ti 1	6126.216	1.07	-1.425	-	-	-	-	-	62.6 ± 3.6	4.02	-

Table 7. continued.

El.	λ	χ_{ex}	$\log(gf)$	EW $\pm\sigma$ (EW) $\log \varepsilon(X) + 12$ [dex]								12
				08		09		10		11		
Ti 1	6258.102	1.44	-0.390	51.8 \pm 4.1	4.12	-	-	21.2 \pm 1.6	3.29	91.2 \pm 5.5	4.05	-
Ti 1	6554.223	1.44	-1.150	-	-	-	-	-	-	40.0 \pm 3.2	3.80	-
Ti 1	6556.062	1.46	-1.060	-	-	-	-	-	-	52.8 \pm 3.4	3.97	-
Ti 1	6743.122	0.90	-1.630	-	-	-	-	-	-	59.1 \pm 3.1	3.87	-
Ti 2	4395.839	1.24	-1.930	-	-	58.8 \pm 4.9	2.98	-	-	-	-	-
Ti 2	4399.765	1.24	-1.200	127.8 \pm 10.8	4.37	-	-	-	-	-	-	-
Ti 2	4417.713	1.16	-1.190	110.0 \pm 12.3	4.01	103.0 \pm 6.1	3.22	-	-	-	-	-
Ti 2	4418.331	1.24	-1.990	-	-	61.5 \pm 6.0	3.09	78.6 \pm 5.8	3.60	106.3 \pm 6.8	4.60	-
Ti 2	4443.801	1.08	-0.710	139.4 \pm 9.4	3.96	119.9 \pm 7.5	3.02	-	-	-	-	-
Ti 2	4444.554	1.12	-2.200	74.1 \pm 5.7	4.02	58.5 \pm 3.4	3.08	70.1 \pm 4.9	3.47	-	-	-
Ti 2	4450.482	1.08	-1.520	-	-	97.0 \pm 6.3	3.29	-	-	-	-	-
Ti 2	4464.449	1.16	-1.810	-	-	74.4 \pm 5.2	3.10	97.7 \pm 6.6	3.81	-	-	-
Ti 2	4468.493	1.13	-0.630	139.5 \pm 13.5	3.93	123.3 \pm 9.2	3.05	133.7 \pm 7.4	3.40	-	-	-
Ti 2	4470.853	1.16	-2.020	-	-	-	-	-	-	99.9 \pm 7.3	4.44	-
Ti 2	4493.522	1.08	-2.780	58.1 \pm 3.9	4.15	-	-	46.9 \pm 4.3	3.51	78.6 \pm 5.5	4.46	-
Ti 2	4501.270	1.12	-0.770	133.1 \pm 10.8	3.95	117.6 \pm 7.1	3.05	143.9 \pm 8.8	3.68	-	-	-
Ti 2	4563.757	1.22	-0.690	136.7 \pm 10.1	4.02	111.3 \pm 7.5	2.93	135.1 \pm 8.0	3.55	-	-	-
Ti 2	4571.971	1.57	-0.310	-	-	117.3 \pm 7.2	3.08	140.5 \pm 9.9	3.62	-	-	-
Ti 2	4583.409	1.16	-2.840	-	-	27.7 \pm 2.5	3.15	40.8 \pm 4.3	3.55	57.8 \pm 6.6	4.06	-
Ti 2	4636.320	1.16	-3.230	44.1 \pm 5.4	4.37	-	-	-	-	53.8 \pm 4.8	4.35	-
Ti 2	4708.663	1.24	-2.350	-	-	44.7 \pm 3.1	3.07	-	-	84.4 \pm 6.8	4.35	-
Ti 2	4798.531	1.08	-2.660	-	-	37.1 \pm 2.8	3.04	-	-	-	-	-
Ti 2	4865.610	1.12	-2.700	47.8 \pm 4.3	3.84	-	-	-	-	83.7 \pm 5.5	4.48	-
Ti 2	5129.156	1.89	-1.340	-	-	57.4 \pm 3.8	3.05	-	-	-	-	53.8 \pm 9.7
Ti 2	5154.068	1.57	-1.750	-	-	-	-	80.3 \pm 8.5	3.66	-	-	-
Ti 2	5185.902	1.89	-1.410	-	-	52.0 \pm 5.3	3.01	-	-	95.9 \pm 6.3	4.42	-
Ti 2	5336.786	1.58	-1.600	-	-	63.8 \pm 3.6	3.04	-	-	-	-	-
Ti 2	5381.021	1.57	-1.970	-	-	51.4 \pm 4.5	3.15	-	-	-	-	-
Ti 2	5418.768	1.58	-2.130	-	-	42.5 \pm 2.6	3.16	58.9 \pm 4.6	3.60	85.9 \pm 5.6	4.47	-
Ti 2	6559.563	2.05	-2.175	-	-	-	-	-	-	52.1 \pm 3.6	4.26	-
V 2	4005.702	1.82	-0.450	-	-	51.7 \pm 4.0	2.01	-	-	-	-	-
Cr 1	4254.352	0	-0.090	-	-	123.4 \pm 8.2	2.96	-	-	-	-	-
Cr 1	4274.812	0	-0.220	-	-	129.1 \pm 7.6	3.19	-	-	-	-	-
Cr 1	4545.953	0.94	-1.370	-	-	-	-	60.4 \pm 4.4	3.80	112.5 \pm 7.4	4.86	-
Cr 1	4646.162	1.03	-0.740	-	-	60.1 \pm 5.3	3.18	-	-	-	-	-
Cr 1	4651.284	0.98	-1.460	66.5 \pm 7.8	4.35	22.7 \pm 1.9	3.05	-	-	-	-	-
Cr 1	5206.023	0.94	0.020	-	-	102.3 \pm 6.3	3.19	-	-	-	-	98.1 \pm 8.8
Cr 1	5208.409	0.94	0.170	-	-	-	-	-	-	-	-	115.0 \pm 15.8
Cr 1	5296.691	0.98	-1.360	-	-	-	-	65.0 \pm 4.9	3.83	129.7 \pm 8.4	4.85	-
Cr 1	5298.271	0.98	-1.140	-	-	-	-	77.9 \pm 9.0	3.89	-	-	-
Cr 1	5345.796	1.00	-0.896	100.1 \pm 8.8	4.51	59.2 \pm 5.6	3.20	101.6 \pm 7.0	4.20	149.8 \pm 9.6	4.78	-
Cr 1	5348.314	1	-1.210	-	-	-	-	76.7 \pm 9.3	3.95	128.9 \pm 9.4	4.69	-
Cr 1	5409.784	1.03	-0.670	-	-	71.7 \pm 4.7	3.26	95.7 \pm 6.1	3.86	-	-	-
Cr 1	6330.091	0.94	-2.920	-	-	-	-	-	-	57.6 \pm 3.3	4.45	-
Cr 2	4558.650	4.07	-0.449	71.5 \pm 6.0	4.67	37.7 \pm 2.2	3.51	-	-	-	-	-
Cr 2	4588.199	4.07	-0.627	-	-	26.3 \pm 2.8	3.42	-	-	-	-	-
Mn 1	4033.060	0	-0.644	-	-	130.0 \pm 9.6	2.70	-	-	-	-	-
Mn 1	4034.480	0.00	-0.842	155.8 \pm 12.3	4.08	-	-	-	-	-	-	-
Mn 1	4041.350	2.11	0.277	126.2 \pm 16.1	4.34	65.3 \pm 4.9	2.66	-	-	-	-	-
Mn 1	4754.040	2.28	-0.088	90.4 \pm 5.9	3.87	31.8 \pm 2.1	2.64	59.9 \pm 4.4	3.17	131.7 \pm 8.4	4.09	-
Mn 1	4823.520	2.32	0.121	-	-	-	-	64.8 \pm 4.1	3.17	-	-	-
Mn 1	5407.417	2.14	-1.743	-	-	-	-	-	-	77.2 \pm 6.3	3.99	-
Mn 1	5420.351	2.14	-1.462	-	-	-	-	-	-	88.7 \pm 6.0	3.77	-
Mn 1	5432.539	0	-3.795	-	-	-	-	-	-	113.0 \pm 6.0	3.80	-
Mn 1	6013.510	3.07	-0.352	-	-	-	-	-	-	73.1 \pm 4.0	3.95	-
Mn 1	6021.820	3.08	-0.054	-	-	-	-	-	-	84.7 \pm 5.0	4.00	-
Fe 1	3997.392	2.73	-0.479	131.7 \pm 12.4	6.80	89.6 \pm 6.0	5.40	-	-	143.9 \pm 12.9	6.74	-
Fe 1	4021.866	2.76	-0.729	-	-	77.0 \pm 6.2	5.30	-	-	-	-	-
Fe 1	4062.441	2.85	-0.862	-	-	-	-	73.7 \pm 6.8	5.46	-	-	-
Fe 1	4067.978	3.21	-0.472	-	-	60.7 \pm 4.3	5.07	86.3 \pm 9.7	5.78	-	-	-
Fe 1	4107.488	2.83	-0.879	-	-	72.0 \pm 5.6	5.34	-	-	-	-	-
Fe 1	4132.058	1.61	-0.675	-	-	142.3 \pm 7.9	5.19	-	-	-	-	-
Fe 1	4132.899	2.85	-1.006	-	-	61.6 \pm 4.7	5.20	-	-	-	-	-
Fe 1	4136.998	3.41	-0.453	-	-	45.0 \pm 3.7	4.94	73.7 \pm 7.6	5.70	-	-	-
Fe 1	4143.868	1.56	-0.511	-	-	142.4 \pm 9.4	4.97	-	-	-	-	-
Fe 1	4147.668	1.49	-2.104	-	-	84.7 \pm 6.3	5.29	-	-	-	-	-
Fe 1	4156.799	2.83	-0.809	-	-	72.4 \pm 5.8	5.27	-	-	-	-	-
Fe 1	4157.780	3.42	-0.403	-	-	58.6 \pm 5.0	5.18	-	-	121.7 \pm 7.7	6.70	-
Fe 1	4175.636	2.85	-0.827	98.2 \pm 7.5	6.40	80.9 \pm 6.4	5.54	-	-	-	-	-
Fe 1	4176.566	3.37	-0.805	-	-	-	-	-	-	105.6 \pm 8.1	6.69	-
Fe 1	4182.382	3.02	-1.180	69.6 \pm 7.7	6.12	42.4 \pm 3.8	5.14	58.6 \pm 5.9	5.56	-	-	-
Fe 1	4184.892	2.83	-0.869	-	-	66.9 \pm 4.6	5.18	78.1 \pm 8.7	5.54	-	-	-
Fe 1	4187.039	2.45	-0.548	114.1 \pm 9.9	5.83	100.3 \pm 6.0	5.16	111.3 \pm 9.7	5.50	-	-	-
Fe 1	4195.329	3.33	-0.492	-	-	73.0 \pm 4.6	5.51	94.1 \pm 7.2	6.10	-	-	-

Table 7. continued.

El.	λ	χ_{ex}	$\log(gf)$	EW $\pm\sigma$ (EW) log $\varepsilon(X) + 12$ [dex]						
				08	09	10	11	12		
Fe 1	4199.095	3.05	0.155	—	—	93.0 \pm 6.1	5.13	111.7 \pm 9.4	5.68	—
Fe 1	4202.029	1.49	-0.708	—	—	141.5 \pm 10.0	5.07	—	—	—
Fe 1	4222.213	2.45	-0.967	125.3 \pm 10.4	6.41	—	—	—	—	—
Fe 1	4233.603	2.48	-0.604	121.5 \pm 12.9	6.02	94.8 \pm 6.3	5.12	—	—	—
Fe 1	4238.810	3.40	-0.233	—	—	—	—	96.7 \pm 8.2	5.96	136.7 \pm 9.5
Fe 1	4250.119	2.47	-0.405	144.9 \pm 10.8	6.09	106.0 \pm 8.7	5.14	120.9 \pm 8.9	5.54	6.67
Fe 1	4250.787	1.56	-0.714	—	—	134.0 \pm 9.5	5.04	—	—	—
Fe 1	4388.407	3.60	-0.682	—	—	—	—	—	—	84.9 \pm 5.2
Fe 1	4415.122	1.61	-0.615	—	—	139.9 \pm 8.7	5.01	—	—	—
Fe 1	4430.614	2.22	-1.659	99.4 \pm 7.6	6.29	70.0 \pm 5.3	5.22	—	—	—
Fe 1	4442.339	2.20	-1.255	128.3 \pm 7.5	6.34	92.8 \pm 6.0	5.32	115.9 \pm 7.0	5.87	—
Fe 1	4443.194	2.86	-1.043	—	—	63.0 \pm 4.0	5.24	—	—	—
Fe 1	4447.717	2.22	-1.342	123.2 \pm 8.5	6.39	85.8 \pm 5.7	5.28	110.2 \pm 6.5	5.88	—
Fe 1	4459.117	2.18	-1.279	150.7 \pm 12.5	6.59	106.9 \pm 7.0	5.61	135.6 \pm 8.9	6.17	—
Fe 1	4466.551	2.83	-0.600	—	—	93.2 \pm 5.8	5.56	111.6 \pm 8.6	6.10	—
Fe 1	4494.563	2.20	-1.136	143.7 \pm 9.4	6.39	94.0 \pm 5.8	5.21	116.3 \pm 7.5	5.74	—
Fe 1	4528.614	2.18	-0.822	—	—	115.9 \pm 6.8	5.29	—	—	—
Fe 1	4531.148	1.49	-2.155	—	—	93.7 \pm 6.7	5.43	109.9 \pm 9.8	5.90	—
Fe 1	4592.651	1.56	-2.449	111.3 \pm 8.4	6.67	78.9 \pm 5.8	5.42	102.7 \pm 7.6	6.09	—
Fe 1	4602.941	1.49	-2.209	93.0 \pm 10.0	5.90	94.1 \pm 5.2	5.47	108.0 \pm 7.0	5.88	159.1 \pm 9.4
Fe 1	4630.120	2.28	-2.587	76.5 \pm 6.1	6.70	26.3 \pm 2.0	5.26	48.3 \pm 4.8	5.80	—
Fe 1	4643.463	3.65	-1.147	49.4 \pm 5.5	6.18	—	—	37.7 \pm 4.1	5.76	—
Fe 1	4647.434	2.95	-1.351	85.0 \pm 5.1	6.55	46.2 \pm 3.0	5.25	71.4 \pm 5.0	5.88	—
Fe 1	4661.970	2.99	-2.502	35.5 \pm 3.4	6.50	—	—	—	—	57.2 \pm 3.6
Fe 1	4733.591	1.49	-2.988	89.9 \pm 6.0	6.54	55.5 \pm 3.8	5.30	—	—	135.1 \pm 9.6
Fe 1	4736.773	3.21	-0.752	103.2 \pm 8.4	6.53	64.7 \pm 3.8	5.33	84.3 \pm 5.0	5.84	130.4 \pm 8.2
Fe 1	4786.807	3.02	-1.606	—	—	32.3 \pm 2.8	5.29	—	—	—
Fe 1	4800.649	4.14	-1.029	—	—	—	—	—	66.1 \pm 4.7	6.69
Fe 1	4871.318	2.87	-0.363	126.2 \pm 9.6	6.09	99.9 \pm 5.4	5.27	122.4 \pm 8.7	5.79	—
Fe 1	4872.138	2.88	-0.567	—	—	83.1 \pm 5.4	5.13	112.1 \pm 8.2	5.83	—
Fe 1	4890.755	2.88	-0.394	134.6 \pm 9.4	6.24	90.3 \pm 6.0	5.11	121.1 \pm 7.7	5.81	—
Fe 1	4891.492	2.85	-0.112	152.5 \pm 8.2	6.13	104.3 \pm 6.4	5.09	132.7 \pm 8.6	5.68	—
Fe 1	4903.310	2.88	-0.926	127.2 \pm 9.7	6.68	72.2 \pm 5.9	5.25	99.9 \pm 7.1	5.94	155.1 \pm 9.7
Fe 1	4918.994	2.87	-0.342	134.9 \pm 12.2	6.18	—	—	128.0 \pm 7.9	5.85	—
Fe 1	4920.502	2.83	0.068	—	—	—	—	159.8 \pm 10.4	5.80	—
Fe 1	4924.770	2.28	-2.241	—	—	50.7 \pm 3.5	5.39	70.2 \pm 5.2	5.88	117.8 \pm 7.9
Fe 1	4938.814	2.88	-1.077	106.1 \pm 8.4	6.48	62.6 \pm 3.8	5.18	—	—	134.8 \pm 8.4
Fe 1	4966.088	3.33	-0.871	—	—	55.2 \pm 4.0	5.36	75.1 \pm 6.4	5.85	—
Fe 1	5001.863	3.88	0.010	99.6 \pm 8.9	6.40	50.0 \pm 3.3	5.03	—	—	117.2 \pm 7.6
Fe 1	5006.119	2.83	-0.638	105.4 \pm 8.3	5.97	92.9 \pm 6.5	5.34	—	—	—
Fe 1	5014.942	3.94	-0.303	—	—	—	—	62.3 \pm 7.6	5.72	111.1 \pm 6.9
Fe 1	5044.211	2.85	-2.038	—	—	—	—	—	—	91.6 \pm 5.9
Fe 1	5049.820	2.28	-1.355	—	—	78.5 \pm 7.7	5.09	—	—	—
Fe 1	5068.766	2.94	-1.042	—	—	60.0 \pm 5.5	5.15	—	—	135.4 \pm 12.2
Fe 1	5074.748	4.22	-0.200	89.9 \pm 13.5	6.73	—	—	—	—	115.3 \pm 8.9
Fe 1	5131.468	2.22	-2.515	—	—	37.8 \pm 4.4	5.33	54.8 \pm 4.1	5.74	—
Fe 1	5159.058	4.28	-0.820	—	—	—	—	28.9 \pm 4.0	5.94	—
Fe 1	5162.272	4.18	0.020	74.9 \pm 10.2	6.14	51.4 \pm 3.8	5.38	—	—	103.7 \pm 6.6
Fe 1	5165.410	4.22	-0.003	56.0 \pm 9.0	5.77	—	—	—	—	6.49
Fe 1	5171.596	1.49	-1.793	—	—	115.0 \pm 6.5	5.44	128.4 \pm 8.2	5.82	—
Fe 1	5191.455	3.04	-0.551	113.5 \pm 10.1	6.21	100.2 \pm 6.7	5.61	106.4 \pm 11.2	5.82	—
Fe 1	5192.344	3	-0.421	—	—	90.3 \pm 6.1	5.23	111.9 \pm 9.7	5.75	—
Fe 1	5194.941	1.56	-2.090	126.7 \pm 7.8	6.55	91.3 \pm 5.0	5.25	107.6 \pm 7.9	5.72	—
Fe 1	5198.711	2.22	-2.135	90.8 \pm 7.2	6.46	54.2 \pm 3.4	5.26	—	—	121.5 \pm 8.6
Fe 1	5202.336	2.18	-1.838	125.0 \pm 8.6	6.81	76.2 \pm 5.3	5.37	—	—	—
Fe 1	5215.180	3.27	-0.871	—	—	58.7 \pm 6.8	5.33	—	—	117.7 \pm 9.9
Fe 1	5217.389	3.21	-1.070	—	—	43.9 \pm 4.2	5.17	—	—	114.8 \pm 9.9
Fe 1	5232.940	2.94	-0.058	148.1 \pm 10.2	6.07	113.5 \pm 6.8	5.24	143.3 \pm 9.7	5.80	—
Fe 1	5242.491	3.63	-0.967	—	—	23.1 \pm 2.8	5.13	49.8 \pm 5.8	5.76	89.7 \pm 6.1
Fe 1	5266.555	3.00	-0.386	122.2 \pm 8.0	6.13	94.2 \pm 6.4	5.26	113.6 \pm 10.4	5.73	—
Fe 1	5281.790	3.04	-0.834	109.0 \pm 8.4	6.41	68.1 \pm 3.8	5.21	89.4 \pm 6.4	5.74	139.7 \pm 9.6
Fe 1	5283.621	3.24	-0.432	108.5 \pm 7.3	6.22	74.2 \pm 4.4	5.17	—	—	—
Fe 1	5288.525	3.69	-1.508	—	—	—	—	—	—	61.1 \pm 8.2
Fe 1	5302.300	3.28	-0.720	102.8 \pm 14.7	6.45	66.3 \pm 4.8	5.34	—	—	—
Fe 1	5307.361	1.61	-2.987	88.4 \pm 12.1	6.56	52.3 \pm 4.1	5.32	65.6 \pm 4.7	5.68	—
Fe 1	5322.041	2.28	-2.803	57.0 \pm 6.0	6.38	—	—	—	86.8 \pm 6.0	6.45
Fe 1	5324.179	3.21	-0.103	131.1 \pm 8.5	6.20	97.2 \pm 5.6	5.29	104.1 \pm 6.7	5.51	—
Fe 1	5328.531	1.56	-1.850	—	—	111.4 \pm 7.0	5.46	—	—	—
Fe 1	5332.899	1.56	-2.777	108.5 \pm 11.2	6.80	62.0 \pm 4.1	5.24	—	—	54.5 \pm 8.7
Fe 1	5339.929	3.27	-0.647	—	—	63.5 \pm 3.5	5.19	85.9 \pm 6.8	5.73	132.6 \pm 9.5
Fe 1	5364.871	4.45	0.228	76.8 \pm 7.7	6.24	42.0 \pm 3.1	5.29	55.5 \pm 5.7	5.60	103.1 \pm 6.3
Fe 1	5365.399	3.57	-1.020	58.4 \pm 7.9	6.11	22.7 \pm 3.1	5.10	—	85.9 \pm 7.3	6.37
Fe 1	5367.466	4.41	0.443	89.2 \pm 7.0	6.25	44.5 \pm 4.1	5.09	69.9 \pm 4.4	5.64	111.2 \pm 7.4
Fe 1	5369.961	4.37	0.536	—	—	56.2 \pm 3.9	5.17	—	—	—

Table 7. continued.

El.	λ	χ_{ex}	$\log(gf)$	EW $\pm\sigma$ (EW) $\log \varepsilon(X) + 12$ [dex]						
				08	09	10	11	12		
Fe 1	5379.574	3.69	-1.514	-	-	-	67.7 \pm 5.1	6.54	-	-
Fe 1	5383.369	4.31	0.645	103.9 \pm 11.0	6.23	58.0 \pm 4.3	5.03	96.0 \pm 7.0	5.87	117.1 \pm 7.9
Fe 1	5393.167	3.24	-0.715	-	-	-	98.0 \pm 9.1	6.02	-	-
Fe 1	5400.501	4.37	-0.160	70.2 \pm 5.3	6.40	24.4 \pm 2.6	5.21	50.4 \pm 5.5	5.81	-
Fe 1	5410.910	4.47	0.398	75.1 \pm 10.0	6.06	37.9 \pm 3.1	5.07	72.5 \pm 6.0	5.81	111.1 \pm 8.5
Fe 1	5415.199	4.39	0.642	104.0 \pm 6.5	6.30	57.3 \pm 3.7	5.11	76.8 \pm 4.5	5.55	124.6 \pm 7.0
Fe 1	5424.068	4.32	0.520	110.9 \pm 9.4	6.47	64.5 \pm 4.3	5.29	76.3 \pm 5.0	5.59	125.7 \pm 10.0
Fe 1	5445.042	4.39	-0.020	79.3 \pm 9.3	6.48	30.8 \pm 2.8	5.24	-	102.4 \pm 6.0	6.72
Fe 1	5560.211	4.43	-1.190	-	-	-	-	-	48.8 \pm 3.9	6.69
Fe 1	5569.618	3.42	-0.486	94.9 \pm 6.3	6.16	60.7 \pm 5.6	5.13	-	137.2 \pm 9.5	6.57
Fe 1	5572.842	3.40	-0.275	119.7 \pm 10.8	6.37	73.9 \pm 4.1	5.16	-	-	-
Fe 1	5576.089	3.43	-1.000	80.2 \pm 8.0	6.38	45.5 \pm 3.5	5.37	-	114.0 \pm 6.8	6.71
Fe 1	5586.755	3.37	-0.120	132.3 \pm 9.0	6.35	88.9 \pm 5.0	5.28	105.9 \pm 6.9	5.70	-
Fe 1	5615.644	3.33	0.050	-	-	-	-	112.8 \pm 6.6	5.62	-
Fe 1	5618.632	4.21	-1.276	-	-	-	-	-	44.1 \pm 3.0	6.38
Fe 1	5701.544	2.56	-2.216	62.5 \pm 5.7	6.20	30.0 \pm 3.1	5.23	59.2 \pm 5.4	5.88	110.6 \pm 6.5
Fe 1	5753.122	4.26	-0.688	-	-	-	-	-	75.9 \pm 4.5	6.59
Fe 1	5775.081	4.22	-1.298	-	-	-	-	-	61.1 \pm 4.4	6.77
Fe 1	5816.373	4.55	-0.601	33.1 \pm 3.4	6.22	-	-	-	68.4 \pm 6.0	6.67
Fe 1	6003.011	3.88	-1.120	46.6 \pm 3.2	6.26	-	-	36.0 \pm 2.5	5.88	84.6 \pm 4.8
Fe 1	6024.058	4.55	-0.120	71.8 \pm 4.1	6.55	26.6 \pm 1.8	5.41	53.1 \pm 3.8	5.99	87.1 \pm 7.4
Fe 1	6027.051	4.08	-1.089	35.3 \pm 3.6	6.22	-	-	-	69.5 \pm 3.8	5.57
Fe 1	6056.004	4.73	-0.460	-	-	-	-	-	58.5 \pm 4.5	6.53
Fe 1	6065.482	2.61	-1.530	102.8 \pm 6.9	6.45	63.4 \pm 3.9	5.23	98.1 \pm 6.1	6.03	142.0 \pm 7.8
Fe 1	6078.491	4.80	-0.321	33.1 \pm 5.7	6.20	-	-	-	63.2 \pm 4.2	6.57
Fe 1	6079.008	4.65	-1.120	-	-	-	-	-	36.5 \pm 2.6	6.59
Fe 1	6082.710	2.22	-3.573	-	-	-	-	-	64.9 \pm 4.0	6.50
Fe 1	6136.615	2.45	-1.400	-	-	82.2 \pm 4.7	5.30	101.1 \pm 5.9	5.77	-
Fe 1	6137.691	2.59	-1.403	109.6 \pm 9.1	6.42	74.3 \pm 4.4	5.29	-	157.7 \pm 9.4	6.64
Fe 1	6151.617	2.18	-3.299	39.4 \pm 5.1	6.33	-	-	26.1 \pm 3.0	5.83	86.9 \pm 4.6
Fe 1	6157.728	4.08	-1.260	44.1 \pm 3.3	6.57	-	-	21.7 \pm 3.9	5.92	-
Fe 1	6165.360	4.14	-1.474	-	-	-	-	-	46.4 \pm 3.2	6.51
Fe 1	6173.334	2.22	-2.880	59.5 \pm 4.8	6.37	-	-	-	101.7 \pm 5.7	6.59
Fe 1	6180.203	2.73	-2.586	38.7 \pm 4.6	6.24	-	-	24.2 \pm 2.7	5.73	81.7 \pm 4.9
Fe 1	6187.989	3.94	-1.720	-	-	-	-	-	51.1 \pm 3.5	6.60
Fe 1	6191.558	2.43	-1.417	112.2 \pm 7.4	6.31	85.3 \pm 4.5	5.35	102.4 \pm 6.1	5.78	-
Fe 1	6200.312	2.61	-2.437	53.6 \pm 7.5	6.26	-	-	37.6 \pm 2.6	5.72	99.1 \pm 7.5
Fe 1	6213.429	2.22	-2.482	66.5 \pm 4.6	6.12	31.0 \pm 2.5	5.08	55.7 \pm 3.4	5.63	114.0 \pm 6.5
Fe 1	6219.280	2.20	-2.433	74.8 \pm 5.2	6.22	42.8 \pm 2.5	5.23	-	122.1 \pm 6.6	6.51
Fe 1	6229.226	2.85	-2.805	20.6 \pm 2.6	6.18	-	-	-	50.1 \pm 3.4	6.22
Fe 1	6230.722	2.56	-1.281	125.6 \pm 8.2	6.54	92.8 \pm 5.0	5.52	101.4 \pm 7.0	5.76	-
Fe 1	6246.318	3.60	-0.733	89.3 \pm 5.8	6.44	42.3 \pm 2.6	5.21	-	113.0 \pm 6.5	6.52
Fe 1	6252.555	2.40	-1.687	103.4 \pm 5.8	6.35	70.0 \pm 4.0	5.26	95.4 \pm 5.5	5.85	146.0 \pm 8.9
Fe 1	6265.132	2.18	-2.550	73.5 \pm 5.5	6.28	40.0 \pm 2.4	5.27	63.7 \pm 4.4	5.79	130.1 \pm 6.9
Fe 1	6297.792	2.22	-2.740	68.2 \pm 4.7	6.40	27.6 \pm 1.9	5.26	-	108.9 \pm 6.2	6.58
Fe 1	6301.500	3.65	-0.718	79.7 \pm 5.2	6.28	-	-	-	110.6 \pm 6.1	6.51
Fe 1	6302.494	3.69	-0.973	-	-	-	-	-	99.2 \pm 5.1	6.58
Fe 1	6311.500	2.83	-3.141	-	-	-	-	-	45.1 \pm 3.6	6.44
Fe 1	6322.685	2.59	-2.426	64.9 \pm 4.5	6.45	-	-	44.3 \pm 3.0	5.80	103.6 \pm 6.1
Fe 1	6335.330	2.20	-2.177	87.7 \pm 7.5	6.23	51.3 \pm 2.9	5.12	77.6 \pm 5.3	5.71	129.2 \pm 7.8
Fe 1	6344.148	2.43	-2.923	33.7 \pm 4.3	6.12	-	-	32.2 \pm 3.1	5.88	94.1 \pm 5.1
Fe 1	6355.028	2.85	-2.350	42.7 \pm 3.7	6.21	-	-	-	100.3 \pm 5.6	6.86
Fe 1	6380.743	4.19	-1.376	-	-	-	-	-	49.3 \pm 3.3	6.52
Fe 1	6392.538	2.28	-4.030	-	-	-	-	-	37.9 \pm 2.6	6.44
Fe 1	6393.601	2.43	-1.432	118.1 \pm 6.3	6.39	77.9 \pm 4.2	5.19	102.5 \pm 5.8	5.76	-
Fe 1	6400.000	3.60	-0.290	-	-	61.6 \pm 3.3	5.12	-	-	-
Fe 1	6408.018	3.69	-1.018	60.1 \pm 4.4	6.19	24.1 \pm 2.3	5.21	39.5 \pm 6.8	5.60	99.8 \pm 6.9
Fe 1	6411.648	3.65	-0.595	90.6 \pm 5.7	6.36	47.7 \pm 3.0	5.23	60.6 \pm 3.6	5.53	120.7 \pm 7.3
Fe 1	6419.949	4.73	-0.240	50.4 \pm 3.2	6.41	-	-	22.3 \pm 4.1	5.67	71.3 \pm 5.8
Fe 1	6421.350	2.28	-2.027	98.8 \pm 6.3	6.46	64.8 \pm 3.7	5.33	91.7 \pm 5.6	5.96	150.8 \pm 8.3
Fe 1	6430.845	2.18	-2.006	105.0 \pm 8.7	6.39	73.4 \pm 4.5	5.34	93.2 \pm 5.5	5.81	153.4 \pm 8.3
Fe 1	6494.980	2.40	-1.273	122.8 \pm 8.5	6.27	90.1 \pm 5.1	5.24	115.8 \pm 6.5	5.82	-
Fe 1	6518.366	2.83	-2.460	36.6 \pm 3.6	6.17	-	-	-	81.5 \pm 5.3	6.51
Fe 1	6581.209	1.49	-4.679	-	-	-	-	-	54.8 \pm 3.1	6.34
Fe 1	6592.913	2.73	-1.473	99.7 \pm 6.2	6.40	56.4 \pm 3.2	5.15	78.6 \pm 4.2	5.65	135.9 \pm 7.8
Fe 1	6593.870	2.43	-2.422	79.1 \pm 5.3	6.55	30.5 \pm 1.6	5.24	55.3 \pm 3.5	5.80	122.5 \pm 6.4
Fe 1	6608.025	2.28	-4.030	-	-	-	-	-	33.0 \pm 3.0	6.33
Fe 1	6609.110	2.56	-2.692	44.1 \pm 2.8	6.24	-	-	29.8 \pm 3.1	5.74	-
Fe 1	6677.985	2.69	-1.418	108.0 \pm 6.6	6.46	67.6 \pm 4.0	5.26	93.8 \pm 5.4	5.85	156.8 \pm 9.2
Fe 1	6750.151	2.42	-2.621	62.1 \pm 4.3	6.37	20.6 \pm 2.0	5.19	44.0 \pm 4.0	5.77	104.6 \pm 6.6
Fe 2	4178.854	2.58	-2.500	78.4 \pm 10.7	6.12	66.0 \pm 5.6	5.30	85.1 \pm 5.9	5.88	-
Fe 2	4491.397	2.86	-2.700	75.1 \pm 6.1	6.47	41.9 \pm 2.9	5.24	71.0 \pm 6.1	5.96	-
Fe 2	4515.333	2.84	-2.450	-	-	55.3 \pm 3.5	5.26	76.1 \pm 5.8	5.82	-
Fe 2	4576.333	2.84	-2.920	55.1 \pm 4.4	6.14	-	-	49.4 \pm 5.0	5.67	-

Table 7. continued.

El.	λ	χ_{ex}	$\log(gf)$	EW $\pm\sigma$ (EW) $\log \varepsilon(X) + 12$ [dex]							
				08	09	10	11	12	13	14	15
Fe 2	4583.829	2.81	-1.860	108.2 \pm 9.2	6.31	85.5 \pm 6.1	5.32	102.9 \pm 6.3	5.80	-	-
Fe 2	4620.513	2.83	-3.240	-	-	-	-	33.2 \pm 3.5	5.63	55.2 \pm 3.7	6.50
Fe 2	4923.921	2.89	-1.320	129.0 \pm 8.2	6.15	105.5 \pm 6.6	5.27	124.8 \pm 8.8	5.72	136.2 \pm 7.5	6.32
Fe 2	5018.436	2.89	-1.220	-	-	-	-	153.5 \pm 12.9	6.00	-	-
Fe 2	5197.567	3.23	-2.100	82.7 \pm 6.0	6.38	51.1 \pm 3.3	5.21	-	-	-	88.6 \pm 21.5
Fe 2	5234.623	3.22	-2.230	79.3 \pm 8.3	6.41	47.9 \pm 4.1	5.26	85.0 \pm 9.3	6.14	91.3 \pm 5.1	6.86
Fe 2	5264.802	3.23	-3.120	42.7 \pm 6.3	6.44	-	-	38.0 \pm 6.4	6.04	42.8 \pm 3.6	6.53
Fe 2	5275.997	3.20	-1.940	-	-	-	-	85.5 \pm 7.2	5.83	-	-
Fe 2	5284.103	2.89	-2.990	52.5 \pm 6.5	6.15	29.5 \pm 3.3	5.25	-	-	-	-
Fe 2	5325.552	3.22	-3.120	31.0 \pm 6.7	6.16	-	-	34.3 \pm 4.4	5.95	-	-
Fe 2	5425.249	3.20	-3.160	47.1 \pm 6.2	6.54	-	-	22.7 \pm 2.8	5.68	41.6 \pm 4.1	6.51
Fe 2	5534.838	3.24	-2.730	-	-	24.8 \pm 1.7	5.28	-	-	62.5 \pm 3.8	6.68
Fe 2	5991.371	3.15	-3.540	-	-	-	-	22.4 \pm 2.3	5.99	30.1 \pm 4.5	6.52
Fe 2	6149.246	3.89	-2.720	-	-	-	-	-	-	28.3 \pm 2.8	6.54
Fe 2	6238.386	3.89	-2.754	21.4 \pm 4.0	6.25	-	-	-	-	36.8 \pm 2.9	6.82
Fe 2	6247.557	3.89	-2.310	33.1 \pm 3.6	6.12	20.3 \pm 1.7	5.48	-	-	42.9 \pm 2.4	6.55
Fe 2	6369.459	2.89	-4.160	-	-	-	-	-	-	23.9 \pm 1.9	6.65
Fe 2	6416.919	3.89	-2.650	30.7 \pm 3.7	6.40	-	-	-	-	32.4 \pm 2.2	6.60
Fe 2	6432.676	2.89	-3.520	33.0 \pm 3.7	6.21	-	-	27.8 \pm 3.5	5.78	43.4 \pm 2.6	6.54
Fe 2	6456.379	3.90	-2.100	58.4 \pm 3.7	6.50	25.9 \pm 2.0	5.42	41.9 \pm 3.8	5.84	55.9 \pm 3.2	6.69
Fe 2	6516.077	2.89	-3.320	-	-	-	-	-	-	56.6 \pm 4.4	6.66
Co 1	3995.307	0.92	-0.220	108.9 \pm 16.7	3.03	82.0 \pm 7.2	2.03	91.6 \pm 9.5	2.31	-	-
Co 1	4121.318	0.92	-0.320	-	-	93.4 \pm 6.9	2.61	-	-	140.3 \pm 13.3	3.73
Ni 1	4604.987	3.48	-0.240	51.3 \pm 5.9	4.86	-	-	-	-	-	-
Ni 1	4904.412	3.54	-0.170	-	-	29.1 \pm 2.7	4.11	37.5 \pm 3.0	4.35	83.3 \pm 5.9	5.32
Ni 1	5081.110	3.85	0.300	-	-	33.6 \pm 3.4	4.09	51.2 \pm 6.4	4.50	-	-
Ni 1	5084.096	3.68	0.030	-	-	-	-	40.0 \pm 3.3	4.35	74.1 \pm 5.5	5.04
Ni 1	5115.392	3.83	-0.110	48.0 \pm 7.2	5.01	-	-	-	-	-	-
Ni 1	5155.764	3.90	0.074	33.0 \pm 4.1	4.57	-	-	-	-	-	-
Ni 1	6128.973	1.68	-3.430	-	-	-	-	-	-	50.3 \pm 3.4	5.20
Ni 1	6176.812	4.09	-0.260	29.0 \pm 2.9	4.98	-	-	-	-	50.1 \pm 3.2	5.16
Ni 1	6177.242	1.83	-3.460	21.3 \pm 2.1	5.41	-	-	-	-	24.6 \pm 2.2	4.87
Ni 1	6327.599	1.68	-3.170	26.1 \pm 3.1	5.06	-	-	-	-	66.8 \pm 3.9	5.26
Ni 1	6482.798	1.93	-2.630	54.8 \pm 3.7	5.41	-	-	-	-	64.3 \pm 4.2	5.00
Ni 1	6586.310	1.95	-2.780	26.9 \pm 5.4	5.00	-	-	-	-	67.0 \pm 3.8	5.22
Ni 1	6643.630	1.68	-2.220	76.4 \pm 4.2	5.14	41.2 \pm 2.4	4.06	55.3 \pm 3.6	4.41	130.0 \pm 7.2	5.60
Ni 1	6767.772	1.83	-2.140	68.3 \pm 3.8	5.05	29.8 \pm 1.7	3.93	-	-	108.2 \pm 7.5	5.28
Cu 1	5105.537	1.39	-1.542	53.4 \pm 9.8	2.51	-	-	-	-	122.2 \pm 8.2	3.04
Cu 1	5700.237	1.64	-2.583	-	-	-	-	-	-	27.0 \pm 2.9	2.64
Zn 1	4722.153	4.03	-0.338	-	-	31.5 \pm 2.6	2.61	-	-	66.1 \pm 5.2	3.86
Zn 1	4810.528	4.08	-0.137	51.2 \pm 4.8	3.23	34.1 \pm 2.3	2.51	43.7 \pm 4.3	2.79	68.1 \pm 4.5	3.77
Sr 2	4215.519	0	-0.145	-	-	152.7 \pm 8.3	0.63	-	-	-	-
Y 2	4883.682	1.08	0.070	-	-	32.5 \pm 3.7	-0.33	55.5 \pm 4.7	0.29	-	-
Y 2	5087.419	1.08	-0.170	-	-	-	-	25.3 \pm 2.5	-0.13	-	-
Y 2	5200.410	0.99	-0.570	49.2 \pm 5.8	1.09	-	-	-	-	-	-
Y 2	5205.722	1.03	-0.340	-	-	17.8 \pm 3.6	-0.37	-	-	-	-
Zr 2	4149.198	0.80	-0.040	-	-	-	-	-	-	0.0 \pm 0.0	1.30
Zr 2	4161.200	0.71	-0.590	-	-	30.7 \pm 4.6	0.38	-	-	0.0 \pm 0.0	1.42
Zr 2	4208.980	0.71	-0.510	-	-	33.2 \pm 4.4	0.35	-	-	-	-
Ba 2	4554.029	0	0.170	-	-	139.0 \pm 8.3	0.26	-	-	-	-
Ba 2	4934.076	0	-0.150	-	-	142.9 \pm 8.6	0.02	-	-	-	-
Ba 2	5853.668	0.60	-1.000	79.8 \pm 7.8	1.28	39.9 \pm 3.1	-0.34	69.6 \pm 5.7	0.46	117.2 \pm 6.5	2.05
Ba 2	6141.713	0.70	-0.076	118.8 \pm 8.2	1.30	83.0 \pm 4.6	-0.24	121.0 \pm 7.1	0.76	-	58.5 \pm 3.8
Ba 2	6496.897	0.60	-0.377	115.5 \pm 9.3	1.35	-	-	118.3 \pm 7.2	0.80	-	44.7 \pm 6.7
La 2	3988.520	0.40	0.170	70.1 \pm 8.7	0.91	-	-	-	-	-	-
La 2	4748.730	0.93	-0.540	-	-	-	-	-	-	25.1 \pm 2.3	0.44
La 2	4804.040	0.23	-1.490	-	-	-	-	-	-	33.2 \pm 2.4	0.73
La 2	6390.480	0.32	-1.410	18.6 \pm 2.1	0.63	-	-	-	-	33.2 \pm 3.4	0.65
La 2	6774.268	0.13	-1.820	-	-	-	-	-	-	23.0 \pm 2.5	0.52
Ce 2	4562.359	0.48	0.210	41.0 \pm 5.3	0.66	-	-	-	-	-	-
Ce 2	4628.161	0.52	0.140	-	-	-	-	20.4 \pm 1.7	-0.17	64.8 \pm 4.1	1.16
Ce 2	5274.229	1.04	0.130	20.6 \pm 3.8	0.81	-	-	-	-	-	-
Pr 2	4143.112	0.37	0.609	-	-	-	-	32.9 \pm 5.8	-0.59	-	-
Pr 2	4179.393	0.20	0.477	81.4 \pm 10.2	1.27	-	-	-	-	-	-
Pr 2	5206.555	0.95	-0.060	-	-	-	-	-	-	-	30.5 \pm 6.0
Pr 2	5322.771	0.48	-0.319	-	-	-	-	-	-	38.3 \pm 4.1	0.52
Nd 2	4061.080	0.47	0.550	-	-	-	-	58.7 \pm 5.7	0.17	-	-
Nd 2	4446.380	0.20	-0.350	-	-	-	-	-	-	80.6 \pm 5.8	1.69
Nd 2	4462.980	0.56	0.040	36.0 \pm 6.6	0.61	-	-	-	-	-	-
Nd 2	4706.540	0.00	-0.710	36.4 \pm 5.4	0.69	-	-	26.3 \pm 4.1	-0.01	73.1 \pm 5.8	1.38
Nd 2	5249.580	0.98	0.200	-	-	-	-	-	-	48.0 \pm 4.6	0.85
Nd 2	5319.810	0.55	-0.140	35.0 \pm 5.6	0.67	-	-	-	-	-	-
Sm 2	4424.340	0.49	0.140	-	-	-	-	28.6 \pm 6.1	-0.45	-	-
Sm 2	4536.510	0.10	-1.280	-	-	-	-	-	-	39.6 \pm 3.0	0.81

Table 7. continued.

El.	λ	χ_{ex}	$\log(gf)$	EW $\pm\sigma(\text{EW})$ log $\varepsilon(X) + 12$ [dex]							
				08	09	10	11	12	13	14	15
Sm 2	4566.200	0.33	-0.590	—	—	—	—	—	46.8 ± 4.3	0.62	—
Sm 2	4642.228	0.38	-0.460	—	—	—	—	—	57.8 ± 4.4	0.89	—
Sm 2	4704.400	0	-0.860	—	—	—	—	—	55.5 ± 5.0	0.70	—
Eu 2	4129.708	0.00	0.220	115.1 ± 15.6	-0.53	29.8 ± 3.8	-1.88	—	—	—	—
Eu 2	4205.042	0	0.210	—	—	36.4 ± 3.0	-1.79	—	—	—	—
Eu 2	6645.103	1.38	0.121	—	—	—	—	52.9 ± 4.0	0.57	—	—

Table 8. Line parameters, observed equivalent widths and corresponding abundances of stars 13, 14, 15, 16, and 17 observed with MIKE.

El.	λ	χ_{ex}	$\log(gf)$	EW $\pm\sigma(\text{EW})$ log $\varepsilon(X) + 12$ [dex]							
				13	14	15	16	17	13	14	15
O I	6300.304	0.00	-9.750	65.5 ± 4.9	8.11	—	—	—	40.6 ± 2.8	7.74	44.4 ± 6.0
O I	6363.776	0.02	-10.260	24.9 ± 1.7	8.03	21.4 ± 1.7	8.15	—	—	—	—
Na 1	5682.633	2.10	-0.706	69.5 ± 4.6	4.98	30.4 ± 3.5	4.60	30.3 ± 3.1	4.64	—	38.8 ± 4.3
Na 1	5688.205	2.10	-0.452	—	—	—	—	56.6 ± 6.0	4.85	—	—
Na 1	6160.747	2.10	-1.246	35.3 ± 3.3	4.96	—	—	—	21.6 ± 3.5	4.70	—
Mg 1	4167.271	4.35	-0.745	—	—	—	—	143.7 ± 10.0	6.64	—	—
Mg 1	4571.096	0	-5.623	—	—	—	—	142.0 ± 9.4	6.56	—	138.7 ± 9.1
Mg 1	4702.991	4.35	-0.440	—	—	—	—	152.2 ± 10.2	6.40	—	153.7 ± 9.0
Mg 1	5528.405	4.35	-0.498	—	—	—	—	154.3 ± 10.5	6.42	—	—
Mg 1	5711.088	4.35	-1.724	115.6 ± 6.2	6.75	—	—	79.3 ± 5.8	6.50	106.8 ± 6.9	6.65
Al 1	6696.023	3.14	-1.347	25.0 ± 2.0	5.10	—	—	—	—	—	—
Al 1	6698.673	3.14	-1.647	15.4 ± 1.3	5.15	—	—	—	—	—	—
Si 1	4102.936	1.91	-3.140	—	—	—	—	139.9 ± 9.3	6.56	—	—
Si 1	5665.555	4.92	-2.040	31.6 ± 2.5	6.68	—	—	24.5 ± 5.1	6.58	—	—
Si 1	5690.425	4.93	-1.870	40.9 ± 3.1	6.71	27.1 ± 2.5	6.47	29.5 ± 2.2	6.54	—	38.2 ± 5.3
Si 1	5701.104	4.93	-2.050	31.5 ± 2.0	6.70	—	—	—	—	—	—
Si 1	5772.146	5.08	-1.750	41.4 ± 2.5	6.79	—	—	25.3 ± 2.5	6.50	—	32.5 ± 3.6
Si 1	5948.541	5.08	-1.230	73.2 ± 4.3	6.84	62.8 ± 3.7	6.72	67.0 ± 3.8	6.79	73.4 ± 5.0	6.85
Si 1	6244.465	5.62	-1.091	27.2 ± 2.4	6.50	18.8 ± 2.5	6.28	18.1 ± 2.0	6.27	—	22.3 ± 2.6
Ca 1	4425.437	1.88	-0.358	—	—	116.2 ± 6.1	5.25	—	—	—	—
Ca 1	4455.887	1.90	-0.518	—	—	—	—	125.8 ± 8.2	5.61	—	—
Ca 1	5581.965	2.52	-0.555	116.4 ± 6.7	5.39	91.5 ± 5.7	5.45	82.5 ± 5.9	5.27	104.8 ± 6.8	5.25
Ca 1	5588.749	2.53	0.358	—	—	131.5 ± 7.7	5.41	135.8 ± 8.4	5.50	—	—
Ca 1	5590.114	2.52	-0.571	115.2 ± 6.8	5.38	83.5 ± 7.3	5.27	86.5 ± 4.9	5.37	99.9 ± 7.0	5.15
Ca 1	5601.277	2.53	-0.523	118.3 ± 6.7	5.40	89.0 ± 6.2	5.36	—	—	115.5 ± 8.1	5.44
Ca 1	5857.451	2.93	0.240	—	—	—	—	—	—	—	—
Ca 1	6102.723	1.88	-0.793	159.4 ± 9.0	5.31	131.3 ± 6.9	5.50	126.7 ± 7.9	5.46	156.1 ± 9.0	5.35
Ca 1	6122.217	1.89	-0.316	—	—	155.7 ± 8.5	5.38	154.8 ± 8.8	5.40	—	151.6 ± 8.6
Ca 1	6161.297	2.52	-1.266	91.6 ± 5.8	5.52	53.0 ± 2.8	5.25	49.8 ± 3.8	5.24	79.9 ± 5.3	5.37
Ca 1	6166.439	2.52	-1.142	95.4 ± 5.2	5.46	61.5 ± 5.0	5.29	—	—	81.2 ± 5.8	5.27
Ca 1	6169.042	2.52	-0.797	113.1 ± 6.1	5.44	82.5 ± 5.2	5.39	82.5 ± 4.6	5.42	103.7 ± 6.0	5.35
Ca 1	6169.563	2.53	-0.478	134.0 ± 7.6	5.51	96.3 ± 6.8	5.37	101.2 ± 5.5	5.50	123.0 ± 7.8	5.40
Ca 1	6439.075	2.53	0.390	—	—	147.8 ± 7.8	5.50	—	—	—	152.9 ± 10.1
Ca 1	6455.598	2.52	-1.340	77.4 ± 4.7	5.32	—	—	47.3 ± 4.5	5.25	67.7 ± 4.2	5.21
Ca 1	6499.650	2.52	-0.818	112.3 ± 6.0	5.40	85.8 ± 5.4	5.46	86.4 ± 5.4	5.51	—	76.7 ± 4.9
Ca 1	6717.681	2.71	-0.524	—	—	—	—	—	—	—	90.8 ± 4.9
Sc 2	4415.557	0.60	-0.668	—	—	—	—	—	—	139.6 ± 13.0	2.05
Sc 2	5526.790	1.77	0.024	—	—	99.0 ± 5.6	2.17	—	—	111.3 ± 8.0	2.12
Sc 2	5657.896	1.51	-0.603	108.5 ± 7.7	2.24	—	—	—	—	—	—
Sc 2	6309.920	1.50	-1.618	33.1 ± 2.3	1.85	—	—	—	—	32.3 ± 3.1	1.80
Sc 2	6604.601	1.36	-1.309	72.0 ± 3.9	2.02	54.5 ± 3.4	1.92	53.2 ± 4.0	1.91	70.3 ± 4.0	1.97
Ti 1	4512.734	0.84	-0.400	—	—	—	—	88.7 ± 8.0	3.86	121.1 ± 9.4	3.86
Ti 1	4534.776	0.84	0.350	—	—	—	—	114.8 ± 8.5	3.79	141.3 ± 10.0	3.56
Ti 1	4548.764	0.83	-0.280	132.4 ± 8.9	3.85	—	—	91.2 ± 7.0	3.78	—	89.0 ± 7.2
Ti 1	4555.483	0.85	-0.400	—	—	—	—	84.3 ± 7.5	3.74	—	—
Ti 1	4623.097	1.74	0.160	—	—	—	—	—	—	—	60.3 ± 4.0
Ti 1	4645.188	1.73	-0.510	90.6 ± 6.8	4.33	—	—	—	—	62.7 ± 4.4	3.81
Ti 1	4840.874	0.90	-0.430	—	—	90.2 ± 4.8	3.85	80.5 ± 6.6	3.66	—	—
Ti 1	4999.503	0.83	0.320	—	—	—	—	130.0 ± 8.0	3.97	—	—
Ti 1	5016.161	0.85	-0.480	—	—	—	—	—	—	—	90.5 ± 7.0
Ti 1	5039.958	0.02	-1.080	155.5 ± 8.9	3.91	111.9 ± 8.8	3.85	114.9 ± 11.1	4.00	153.1 ± 12.7	4.04
Ti 1	5113.440	1.44	-0.700	—	—	43.4 ± 6.8	3.68	—	—	—	40.3 ± 4.9
Ti 1	5192.969	0.02	-0.950	—	—	—	—	118.3 ± 8.3	3.89	—	—
Ti 1	5210.384	0.05	-0.820	—	—	123.6 ± 8.8	3.89	117.2 ± 8.3	3.76	—	122.0 ± 7.6
Ti 1	5490.147	1.46	-0.840	—	—	—	—	27.5 ± 4.3	3.56	58.8 ± 7.3	3.54
Ti 1	5978.541	1.87	-0.496	68.0 ± 3.9	3.83	—	—	—	—	52.9 ± 4.9	3.63
Ti 1	6126.216	1.07	-1.425	86.9 ± 5.1	3.85	—	—	31.0 ± 2.6	3.67	69.4 ± 4.4	3.64
Ti 1	6258.102	1.44	-0.390	—	—	66.3 ± 5.3	3.69	64.6 ± 3.8	3.74	107.7 ± 5.8	3.77
Ti 1	6554.223	1.44	-1.150	63.4 ± 3.4	3.73	—	—	25.6 ± 1.9	3.73	54.1 ± 3.1	3.63
Ti 1	6556.062	1.46	-1.060	83.5 ± 5.1	3.96	—	—	—	—	—	—
Ti 1	6743.122	0.90	-1.630	85.9 ± 4.8	3.70	35.2 ± 2.6	3.59	31.1 ± 2.0	3.61	72.3 ± 4.0	3.56

Table 8. continued.

El.	λ	χ_{ex}	$\log(gf)$	EW $\pm\sigma$ (EW) log $\varepsilon(X) + 12$ [dex]							
				13	14	15	16	17	18	19	20
Ti 2	4399.765	1.24	-1.200	-	-	131.5 \pm 6.6	4.10	-	-	157.0 \pm 9.3	4.17
Ti 2	4417.713	1.16	-1.190	-	-	-	-	137.2 \pm 10.3	4.21	-	127.9 \pm 9.5
Ti 2	4443.801	1.08	-0.710	-	-	153.8 \pm 8.4	3.84	158.6 \pm 10.7	3.90	-	-
Ti 2	4493.522	1.08	-2.780	102.0 \pm 7.0	4.47	78.1 \pm 4.2	4.27	-	-	-	72.2 \pm 5.3
Ti 2	4563.757	1.22	-0.690	-	-	145.8 \pm 7.3	3.85	-	-	-	147.7 \pm 9.0
Ti 2	4583.409	1.16	-2.840	80.7 \pm 6.5	4.13	64.5 \pm 4.0	4.06	-	-	-	59.9 \pm 4.9
Ti 2	4636.320	1.16	-3.230	73.1 \pm 4.8	4.33	50.5 \pm 3.4	4.09	-	-	-	73.9 \pm 4.8
Ti 2	4708.663	1.24	-2.350	-	-	81.4 \pm 4.9	4.09	-	-	-	78.1 \pm 5.7
Ti 2	4865.610	1.12	-2.700	90.1 \pm 6.3	4.07	69.4 \pm 5.2	3.93	-	-	-	87.2 \pm 8.2
Ti 2	5154.068	1.57	-1.750	-	-	98.9 \pm 10.6	4.25	-	-	-	3.95
Ti 2	5185.902	1.89	-1.410	105.2 \pm 6.7	4.10	-	-	-	-	-	-
Ti 2	5381.021	1.57	-1.970	-	-	91.1 \pm 5.1	4.23	88.1 \pm 6.1	4.15	-	90.9 \pm 5.3
Ti 2	5418.768	1.58	-2.130	92.2 \pm 6.0	4.08	78.5 \pm 5.2	4.10	74.7 \pm 4.8	4.00	87.3 \pm 6.1	4.01
Ti 2	6559.563	2.05	-2.175	58.5 \pm 3.1	4.03	59.2 \pm 3.5	4.20	-	-	-	-
Cr 1	4545.953	0.94	-1.370	139.5 \pm 9.0	4.74	101.8 \pm 6.6	4.60	85.7 \pm 5.7	4.14	119.8 \pm 9.4	4.31
Cr 1	4646.162	1.03	-0.740	-	-	-	-	117.5 \pm 8.6	4.54	-	90.2 \pm 8.1
Cr 1	4651.284	0.98	-1.460	-	-	89.3 \pm 4.7	4.30	-	-	-	-
Cr 1	5296.691	0.98	-1.360	151.7 \pm 9.9	4.49	96.4 \pm 9.8	4.13	-	-	132.4 \pm 7.4	4.19
Cr 1	5345.796	1	-0.896	-	-	-	-	120.8 \pm 8.1	4.34	-	-
Cr 1	5348.314	1.00	-1.210	149.9 \pm 8.7	4.30	-	-	108.0 \pm 7.5	4.35	137.1 \pm 8.2	4.15
Cr 1	5409.784	1.03	-0.670	-	-	130.2 \pm 7.6	4.29	-	-	-	-
Cr 1	6330.091	0.94	-2.920	76.6 \pm 4.5	4.21	-	-	30.1 \pm 3.4	4.16	65.9 \pm 4.0	4.11
Cr 2	4588.199	4.07	-0.627	-	-	55.2 \pm 4.5	4.30	51.0 \pm 3.5	4.16	-	-
Mn 1	4754.040	2.28	-0.088	151.6 \pm 10.0	3.97	-	-	-	-	-	-
Mn 1	5407.417	2.14	-1.743	95.5 \pm 7.1	3.82	-	-	-	-	69.8 \pm 6.5	3.66
Mn 1	5420.351	2.14	-1.462	118.7 \pm 6.2	3.63	-	-	-	-	-	40.7 \pm 5.2
Mn 1	5432.539	0.00	-3.795	143.3 \pm 7.8	3.57	-	-	-	-	-	3.53
Mn 1	5516.766	2.18	-1.847	-	-	-	-	-	-	-	24.4 \pm 3.5
Mn 1	6013.510	3.07	-0.352	88.4 \pm 4.8	3.85	44.0 \pm 3.8	3.64	37.6 \pm 3.7	3.61	69.8 \pm 3.7	3.66
Mn 1	6021.820	3.08	-0.054	102.9 \pm 5.5	3.93	53.8 \pm 3.5	3.57	55.4 \pm 3.9	3.66	-	59.2 \pm 3.8
Fe 1	4067.978	3.21	-0.472	-	-	-	-	-	-	123.8 \pm 10.2	6.17
Fe 1	4114.445	2.83	-1.303	-	-	92.3 \pm 6.2	6.31	-	-	-	-
Fe 1	4157.780	3.42	-0.403	-	-	-	-	-	-	128.3 \pm 14.4	6.50
Fe 1	4175.636	2.85	-0.827	131.1 \pm 9.8	6.24	114.4 \pm 6.0	6.43	-	-	-	-
Fe 1	4176.566	3.37	-0.805	112.4 \pm 10.8	6.38	-	-	-	-	-	98.5 \pm 8.2
Fe 1	4182.382	3.02	-1.180	-	-	90.4 \pm 4.9	6.36	92.2 \pm 7.1	6.41	-	-
Fe 1	4195.329	3.33	-0.492	140.5 \pm 9.3	6.59	-	-	-	-	-	-
Fe 1	4388.407	3.60	-0.682	95.4 \pm 8.9	6.05	77.4 \pm 10.0	6.06	-	-	-	-
Fe 1	4442.339	2.20	-1.255	-	-	153.0 \pm 7.7	6.09	157.2 \pm 10.1	6.18	-	-
Fe 1	4447.717	2.22	-1.342	-	-	144.0 \pm 7.2	6.11	142.7 \pm 9.9	6.15	-	140.8 \pm 10.2
Fe 1	4602.000	1.61	-3.154	131.8 \pm 8.2	6.55	-	-	92.9 \pm 6.6	6.36	-	-
Fe 1	4602.941	1.49	-2.209	-	-	136.2 \pm 7.1	6.18	-	-	-	131.3 \pm 8.6
Fe 1	4630.120	2.28	-2.587	136.6 \pm 8.9	6.78	88.5 \pm 5.9	6.41	-	-	110.8 \pm 7.0	6.39
Fe 1	4661.970	2.99	-2.502	79.9 \pm 4.9	6.57	43.9 \pm 3.4	6.16	-	-	-	-
Fe 1	4733.591	1.49	-2.988	-	-	-	-	-	-	143.7 \pm 9.3	6.40
Fe 1	4736.773	3.21	-0.752	152.3 \pm 9.4	6.69	118.3 \pm 6.1	6.54	-	-	136.6 \pm 8.3	6.50
Fe 1	4800.649	4.14	-1.029	78.4 \pm 4.8	6.60	36.1 \pm 4.2	5.94	-	-	60.6 \pm 5.0	6.23
Fe 1	4890.755	2.88	-0.394	-	-	152.6 \pm 7.6	6.13	149.6 \pm 9.7	6.12	-	-
Fe 1	4903.310	2.88	-0.926	-	-	-	-	125.4 \pm 8.6	6.32	156.1 \pm 9.8	6.37
Fe 1	4924.770	2.28	-2.241	141.6 \pm 8.2	6.60	-	-	-	-	-	-
Fe 1	4938.814	2.88	-1.077	-	-	107.9 \pm 5.5	6.11	114.8 \pm 7.2	6.26	-	-
Fe 1	5001.863	3.88	0.010	122.9 \pm 8.6	6.16	-	-	95.7 \pm 7.0	6.03	117.6 \pm 8.0	6.13
Fe 1	5006.119	2.83	-0.638	-	-	140.5 \pm 7.2	6.15	127.7 \pm 8.2	5.98	-	-
Fe 1	5028.126	3.57	-1.123	-	-	-	-	71.4 \pm 10.0	6.16	-	-
Fe 1	5049.820	2.28	-1.355	-	-	-	-	140.7 \pm 8.8	6.25	-	143.4 \pm 8.1
Fe 1	5068.766	2.94	-1.042	159.7 \pm 9.5	6.50	-	-	113.6 \pm 7.3	6.25	-	-
Fe 1	5074.748	4.22	-0.200	116.0 \pm 7.3	6.61	91.2 \pm 7.9	6.50	-	-	-	-
Fe 1	5131.468	2.22	-2.515	-	-	92.7 \pm 5.6	6.29	-	-	-	-
Fe 1	5141.739	2.42	-1.964	-	-	-	-	96.5 \pm 6.7	6.13	125.3 \pm 13.3	6.21
Fe 1	5162.272	4.18	0.020	118.4 \pm 9.4	6.36	93.1 \pm 7.8	6.26	92.7 \pm 6.9	6.25	95.5 \pm 7.6	5.95
Fe 1	5194.941	1.56	-2.090	-	-	144.1 \pm 10.5	6.40	138.7 \pm 8.4	6.29	-	-
Fe 1	5196.059	4.26	-0.493	-	-	-	-	54.2 \pm 6.4	5.94	-	-
Fe 1	5198.711	2.22	-2.135	149.1 \pm 9.3	6.42	-	-	-	-	-	-
Fe 1	5215.180	3.27	-0.871	129.6 \pm 8.0	6.26	105.3 \pm 7.1	6.28	88.9 \pm 7.2	5.91	117.3 \pm 8.5	6.09
Fe 1	5216.274	1.61	-2.150	-	-	-	-	130.7 \pm 9.3	6.21	-	-
Fe 1	5217.389	3.21	-1.070	127.7 \pm 10.5	6.35	-	-	-	-	-	-
Fe 1	5242.491	3.63	-0.967	-	-	71.0 \pm 5.4	6.03	-	-	100.0 \pm 7.9	6.34
Fe 1	5266.555	3.00	-0.386	-	-	149.9 \pm 9.7	6.15	-	-	-	152.9 \pm 9.5
Fe 1	5281.790	3.04	-0.834	158.0 \pm 9.1	6.34	122.2 \pm 8.3	6.25	112.2 \pm 7.2	6.08	135.7 \pm 10.1	6.06
Fe 1	5283.621	3.24	-0.432	-	-	137.6 \pm 7.6	6.36	128.6 \pm 9.5	6.24	-	134.0 \pm 7.9
Fe 1	5288.525	3.69	-1.508	72.0 \pm 5.4	6.24	-	-	-	-	-	43.8 \pm 3.1
Fe 1	5302.300	3.28	-0.720	-	-	-	-	-	-	-	120.7 \pm 7.7
Fe 1	5307.361	1.61	-2.987	-	-	-	-	104.4 \pm 9.5	6.30	-	104.8 \pm 7.4
Fe 1	5322.041	2.28	-2.803	106.8 \pm 7.0	6.29	79.2 \pm 6.2	6.27	65.3 \pm 4.3	5.99	-	-

Table 8. continued.

El.	λ	χ_{ex}	$\log(gf)$	EW $\pm\sigma$ (EW) log $\varepsilon(X) + 12$ [dex]							
				13	14	15	16	17	—	—	—
Fe 1	5324.179	3.21	-0.103	—	—	147.3 \pm 9.0	6.12	143.7 \pm 8.0	6.08	—	—
Fe 1	5339.929	3.27	-0.647	144.1 \pm 9.5	6.27	—	—	117.5 \pm 6.6	6.28	143.9 \pm 8.5	6.33
Fe 1	5364.871	4.45	0.228	120.3 \pm 7.4	6.50	80.1 \pm 7.2	6.04	90.3 \pm 5.4	6.27	100.4 \pm 6.5	6.17
Fe 1	5365.399	3.57	-1.020	91.0 \pm 6.5	5.99	73.6 \pm 4.6	6.05	—	—	85.8 \pm 5.5	5.94
Fe 1	5367.466	4.41	0.443	117.4 \pm 9.1	6.19	94.2 \pm 8.9	6.11	92.6 \pm 5.6	6.08	103.7 \pm 7.9	5.99
Fe 1	5379.574	3.69	-1.514	77.4 \pm 4.8	6.34	46.7 \pm 5.6	6.05	46.0 \pm 3.3	6.08	64.3 \pm 5.9	6.11
Fe 1	5383.369	4.31	0.645	146.1 \pm 8.3	6.35	116.2 \pm 7.3	6.23	108.2 \pm 7.2	6.08	128.7 \pm 9.1	6.13
Fe 1	5393.167	3.24	-0.715	—	—	—	—	119.6 \pm 7.9	6.34	—	—
Fe 1	5400.501	4.37	-0.160	—	—	—	—	76.7 \pm 5.2	6.26	102.1 \pm 5.6	6.49
Fe 1	5410.910	4.47	0.398	—	—	—	—	—	—	—	99.3 \pm 5.9
Fe 1	5415.199	4.39	0.642	132.7 \pm 7.5	6.23	115.6 \pm 7.9	6.29	108.0 \pm 6.7	6.15	122.8 \pm 7.0	6.12
Fe 1	5424.068	4.32	0.520	155.4 \pm 11.3	6.59	119.3 \pm 9.2	6.40	116.4 \pm 7.8	6.34	—	—
Fe 1	5445.042	4.39	-0.020	112.6 \pm 6.6	6.51	84.4 \pm 5.1	6.31	76.9 \pm 4.3	6.14	—	—
Fe 1	5560.211	4.43	-1.190	47.8 \pm 3.4	6.41	—	—	28.8 \pm 3.4	6.28	—	21.5 \pm 2.9
Fe 1	5569.618	3.42	-0.486	147.9 \pm 9.4	6.30	106.8 \pm 7.2	6.03	109.0 \pm 7.2	6.08	—	109.2 \pm 8.0
Fe 1	5576.089	3.43	-1.000	127.5 \pm 7.3	6.47	95.7 \pm 5.9	6.32	93.7 \pm 6.3	6.29	118.8 \pm 7.0	6.38
Fe 1	5586.755	3.37	-0.120	—	—	141.3 \pm 8.6	6.18	141.3 \pm 7.3	6.19	—	—
Fe 1	5618.632	4.21	-1.276	53.8 \pm 3.6	6.31	—	—	—	—	48.5 \pm 3.9	6.22
Fe 1	5701.544	2.56	-2.216	130.4 \pm 7.9	6.48	84.5 \pm 6.3	6.10	84.3 \pm 6.1	6.14	—	92.1 \pm 6.1
Fe 1	5753.122	4.26	-0.688	83.3 \pm 4.7	6.36	69.5 \pm 5.2	6.43	60.3 \pm 3.6	6.24	—	—
Fe 1	5775.081	4.22	-1.298	62.5 \pm 3.7	6.49	43.4 \pm 4.4	6.39	37.6 \pm 2.3	6.30	54.0 \pm 3.5	6.35
Fe 1	5816.373	4.55	-0.601	—	—	45.0 \pm 2.8	6.14	—	—	58.7 \pm 3.7	6.19
Fe 1	6003.011	3.88	-1.120	93.8 \pm 5.8	6.46	54.5 \pm 3.4	6.01	67.5 \pm 4.3	6.33	—	72.1 \pm 4.5
Fe 1	6024.058	4.55	-0.120	99.6 \pm 5.5	6.48	78.2 \pm 5.0	6.40	83.7 \pm 5.2	6.53	89.7 \pm 5.4	6.33
Fe 1	6027.051	4.08	-1.089	71.7 \pm 4.1	6.25	—	—	55.0 \pm 3.7	6.27	58.2 \pm 4.2	6.02
Fe 1	6056.004	4.73	-0.460	66.7 \pm 3.7	6.41	44.8 \pm 3.5	6.21	40.6 \pm 3.0	6.15	60.3 \pm 3.8	6.31
Fe 1	6065.482	2.61	-1.530	—	—	—	—	119.2 \pm 7.5	6.23	—	127.3 \pm 7.9
Fe 1	6078.491	4.80	-0.321	63.8 \pm 3.4	6.30	44.3 \pm 4.8	6.14	—	—	56.1 \pm 4.1	6.17
Fe 1	6079.008	4.65	-1.120	35.3 \pm 2.3	6.36	24.4 \pm 2.7	6.31	—	—	32.3 \pm 2.8	6.31
Fe 1	6082.710	2.22	-3.573	—	—	42.6 \pm 3.8	6.06	37.8 \pm 4.6	6.04	72.9 \pm 4.9	6.21
Fe 1	6136.615	2.45	-1.400	—	—	—	—	—	—	—	—
Fe 1	6137.691	2.59	-1.403	—	—	130.9 \pm 7.6	6.24	130.7 \pm 8.0	6.27	—	126.9 \pm 8.1
Fe 1	6151.617	2.18	-3.299	103.1 \pm 6.7	6.36	54.5 \pm 3.1	5.95	56.5 \pm 3.6	6.06	86.6 \pm 4.8	6.10
Fe 1	6157.728	4.08	-1.260	89.2 \pm 5.3	6.75	47.4 \pm 5.6	6.24	45.4 \pm 3.3	6.23	65.5 \pm 3.8	6.32
Fe 1	6165.360	4.14	-1.474	49.3 \pm 3.3	6.30	—	—	—	—	—	—
Fe 1	6173.334	2.22	-2.880	124.0 \pm 7.3	6.39	77.3 \pm 6.7	6.07	—	—	114.8 \pm 6.6	6.30
Fe 1	6180.203	2.73	-2.586	96.5 \pm 5.5	6.32	67.3 \pm 4.3	6.24	57.4 \pm 3.6	6.08	81.6 \pm 4.6	6.08
Fe 1	6187.989	3.94	-1.720	48.7 \pm 2.9	6.26	29.3 \pm 3.8	6.13	27.1 \pm 3.3	6.13	43.1 \pm 2.8	6.17
Fe 1	6200.312	2.61	-2.437	120.3 \pm 6.6	6.46	81.7 \pm 5.2	6.25	75.1 \pm 4.3	6.15	104.7 \pm 5.9	6.23
Fe 1	6213.429	2.22	-2.482	145.1 \pm 8.1	6.35	97.4 \pm 6.4	6.10	97.3 \pm 5.2	6.15	—	—
Fe 1	6219.280	2.20	-2.433	152.7 \pm 8.1	6.39	107.1 \pm 7.9	6.23	99.7 \pm 6.3	6.12	131.7 \pm 8.8	6.12
Fe 1	6229.226	2.85	-2.805	71.3 \pm 4.5	6.23	—	—	31.8 \pm 3.4	5.93	57.0 \pm 3.3	6.00
Fe 1	6230.722	2.56	-1.281	—	—	155.4 \pm 9.2	6.43	146.7 \pm 8.1	6.35	—	—
Fe 1	6240.646	2.22	-3.233	95.4 \pm 5.3	6.23	59.0 \pm 4.6	6.04	—	—	—	—
Fe 1	6246.318	3.60	-0.733	125.6 \pm 6.9	6.26	96.9 \pm 5.8	6.18	96.6 \pm 5.8	6.19	118.0 \pm 7.1	6.18
Fe 1	6252.555	2.40	-1.687	—	—	127.9 \pm 7.1	6.21	128.6 \pm 7.4	6.26	—	120.8 \pm 6.7
Fe 1	6265.132	2.18	-2.550	153.2 \pm 8.3	6.47	104.2 \pm 5.7	6.24	106.6 \pm 6.2	6.34	137.3 \pm 7.4	6.29
Fe 1	6290.965	4.73	-0.774	46.8 \pm 2.7	6.33	—	—	—	—	—	—
Fe 1	6297.792	2.22	-2.740	129.1 \pm 7.4	6.32	—	—	—	—	110.9 \pm 6.6	6.06
Fe 1	6301.500	3.65	-0.718	130.8 \pm 7.0	6.40	101.4 \pm 5.8	6.32	98.4 \pm 5.2	6.27	120.9 \pm 6.8	6.29
Fe 1	6302.494	3.69	-0.973	100.8 \pm 5.5	6.13	71.5 \pm 5.5	5.96	84.7 \pm 5.2	6.28	—	86.8 \pm 6.5
Fe 1	6311.500	2.83	-3.141	52.9 \pm 3.6	6.22	25.4 \pm 2.8	6.04	—	—	46.1 \pm 3.8	6.12
Fe 1	6322.685	2.59	-2.426	121.1 \pm 6.8	6.42	88.6 \pm 5.6	6.35	—	—	109.8 \pm 6.7	6.27
Fe 1	6335.330	2.20	-2.177	—	—	117.2 \pm 7.1	6.14	116.2 \pm 6.5	6.17	150.2 \pm 9.4	6.13
Fe 1	6344.148	2.43	-2.923	113.3 \pm 6.6	6.54	75.4 \pm 4.3	6.34	—	—	100.1 \pm 5.3	6.35
Fe 1	6355.028	2.85	-2.350	116.7 \pm 6.0	6.61	70.3 \pm 5.1	6.20	64.0 \pm 4.3	6.12	—	70.0 \pm 4.1
Fe 1	6380.743	4.19	-1.376	56.1 \pm 3.0	6.37	26.8 \pm 2.1	6.03	28.9 \pm 2.6	6.12	41.3 \pm 3.0	6.11
Fe 1	6392.538	2.28	-4.030	53.5 \pm 3.3	6.34	—	—	—	—	44.6 \pm 2.9	6.21
Fe 1	6393.601	2.43	-1.432	—	—	133.2 \pm 7.7	6.05	131.6 \pm 7.8	6.06	—	131.5 \pm 7.3
Fe 1	6408.018	3.69	-1.018	112.0 \pm 6.4	6.37	78.3 \pm 5.9	6.14	76.4 \pm 4.4	6.13	—	85.9 \pm 5.0
Fe 1	6411.648	3.65	-0.595	137.1 \pm 7.5	6.36	102.9 \pm 5.8	6.21	104.2 \pm 6.1	6.25	123.8 \pm 8.2	6.20
Fe 1	6419.949	4.73	-0.240	78.0 \pm 4.2	6.38	49.9 \pm 4.0	6.08	54.5 \pm 3.3	6.20	64.9 \pm 3.9	6.16
Fe 1	6421.350	2.28	-2.027	—	—	126.1 \pm 6.8	6.41	120.1 \pm 6.7	6.30	158.7 \pm 8.3	6.47
Fe 1	6430.845	2.18	-2.006	—	—	135.3 \pm 8.2	6.24	129.7 \pm 7.2	6.19	—	125.6 \pm 7.2
Fe 1	6494.980	2.40	-1.273	—	—	—	—	149.8 \pm 7.8	6.14	—	—
Fe 1	6518.366	2.83	-2.460	97.3 \pm 5.3	6.31	54.2 \pm 4.9	5.94	—	—	—	51.2 \pm 3.0
Fe 1	6581.209	1.49	-4.679	72.8 \pm 4.3	6.16	—	—	29.5 \pm 2.1	5.99	—	—
Fe 1	6592.913	2.73	-1.473	—	—	111.8 \pm 7.7	6.04	117.3 \pm 6.8	6.18	149.0 \pm 7.9	6.18
Fe 1	6593.870	2.43	-2.422	145.0 \pm 8.0	6.57	98.4 \pm 6.3	6.31	92.7 \pm 5.1	6.24	123.5 \pm 7.0	6.26
Fe 1	6608.025	2.28	-4.030	52.7 \pm 3.2	6.31	23.6 \pm 2.2	6.15	—	—	41.0 \pm 2.8	6.13
Fe 1	6609.110	2.56	-2.692	115.3 \pm 6.4	6.48	76.0 \pm 4.5	6.26	71.5 \pm 4.2	6.22	104.0 \pm 5.4	6.33
Fe 1	6677.985	2.69	-1.418	—	—	130.2 \pm 7.0	6.27	132.4 \pm 7.0	6.34	158.1 \pm 9.0	6.20

Table 8. continued.

El.	λ	χ_{ex}	$\log(gf)$	EW $\pm\sigma$ (EW) $\log \varepsilon(X) + 12$ [dex]						
				13	14	15	16	17		
Fe 2	4491.397	2.86	-2.700	-	-	76.6 \pm 4.4	6.38	74.3 \pm 4.5	6.27	-
Fe 2	4515.333	2.84	-2.450	-	-	81.5 \pm 4.6	6.25	-	-	-
Fe 2	4576.333	2.84	-2.920	-	-	66.3 \pm 3.6	6.27	66.4 \pm 4.9	6.24	-
Fe 2	4620.513	2.83	-3.240	64.0 \pm 3.8	6.40	-	-	60.3 \pm 4.0	6.37	-
Fe 2	4923.921	2.89	-1.320	158.6 \pm 9.2	6.27	147.0 \pm 7.6	6.22	143.6 \pm 8.3	6.17	-
Fe 2	5197.567	3.23	-2.100	-	-	70.1 \pm 6.2	5.96	-	-	-
Fe 2	5234.623	3.22	-2.230	95.1 \pm 6.1	6.57	-	-	82.1 \pm 5.5	6.34	-
Fe 2	5264.802	3.23	-3.120	-	-	-	-	-	-	30.8 \pm 4.4
Fe 2	5284.103	2.89	-2.990	-	-	-	-	-	-	5.94
Fe 2	5325.552	3.22	-3.120	43.0 \pm 3.3	6.27	-	-	-	-	34.2 \pm 4.2
Fe 2	5425.249	3.20	-3.160	37.5 \pm 2.8	6.14	32.7 \pm 4.0	6.02	36.0 \pm 3.1	6.10	6.02
Fe 2	5534.838	3.24	-2.730	66.7 \pm 4.9	6.46	44.7 \pm 5.9	5.95	-	-	6.17
Fe 2	5991.371	3.15	-3.540	35.6 \pm 2.4	6.43	31.2 \pm 2.3	6.30	24.6 \pm 1.9	6.12	-
Fe 2	6149.246	3.89	-2.720	28.7 \pm 2.9	6.35	-	-	-	-	-
Fe 2	6238.386	3.89	-2.754	40.3 \pm 2.8	6.70	29.0 \pm 3.0	6.34	36.0 \pm 2.9	6.51	-
Fe 2	6247.557	3.89	-2.310	45.8 \pm 3.0	6.39	44.8 \pm 4.2	6.31	42.4 \pm 2.8	6.23	6.25
Fe 2	6369.459	2.89	-4.160	19.5 \pm 1.4	6.28	-	-	-	-	43.9 \pm 3.4
Fe 2	6416.919	3.89	-2.650	35.8 \pm 2.7	6.49	-	-	-	-	23.5 \pm 2.3
Fe 2	6432.676	2.89	-3.520	48.3 \pm 2.8	6.37	37.1 \pm 3.0	6.10	41.9 \pm 3.4	6.21	6.07
Fe 2	6456.379	3.90	-2.100	58.9 \pm 3.2	6.50	62.0 \pm 4.1	6.53	56.5 \pm 3.4	6.37	6.41
Fe 2	6516.077	2.89	-3.320	62.1 \pm 3.3	6.46	51.7 \pm 3.2	6.24	47.1 \pm 3.3	6.12	6.29
Co 1	3842.049	0.92	-0.770	-	-	-	-	-	-	97.2 \pm 28.7
Co 1	4121.318	0.92	-0.320	-	-	136.4 \pm 7.0	3.63	-	-	-
Co 1	5647.234	2.28	-1.560	32.6 \pm 3.9	3.48	-	-	-	-	-
Ni 1	4604.987	3.48	-0.240	-	-	62.7 \pm 3.3	4.79	74.8 \pm 5.0	5.13	-
Ni 1	4686.213	3.60	-0.590	-	-	44.2 \pm 4.5	4.81	41.9 \pm 3.8	4.78	-
Ni 1	4904.412	3.54	-0.170	106.3 \pm 6.6	5.40	-	-	-	-	-
Ni 1	5084.096	3.68	0.030	82.4 \pm 5.7	4.82	67.3 \pm 6.3	4.81	-	-	66.4 \pm 5.5
Ni 1	5115.392	3.83	-0.110	71.8 \pm 5.5	4.93	74.1 \pm 6.0	5.34	-	-	39.5 \pm 7.2
Ni 1	6128.973	1.68	-3.430	67.8 \pm 3.6	5.08	-	-	-	-	-
Ni 1	6176.812	4.09	-0.260	54.3 \pm 2.8	4.98	-	-	-	-	-
Ni 1	6177.242	1.83	-3.460	43.4 \pm 2.8	4.90	-	-	-	-	-
Ni 1	6327.599	1.68	-3.170	87.9 \pm 4.8	5.15	48.3 \pm 3.7	4.86	-	-	-
Ni 1	6482.798	1.93	-2.630	85.2 \pm 4.8	4.91	-	-	53.8 \pm 4.0	4.81	51.0 \pm 2.9
Ni 1	6586.310	1.95	-2.780	86.1 \pm 4.9	5.10	-	-	44.6 \pm 2.7	4.80	-
Ni 1	6643.630	1.68	-2.220	-	-	117.6 \pm 6.1	5.32	103.5 \pm 5.6	5.08	107.2 \pm 7.0
Ni 1	6767.772	1.83	-2.140	137.1 \pm 7.3	5.16	95.9 \pm 5.6	4.98	88.5 \pm 4.8	4.86	89.0 \pm 5.3
Cu 1	5105.537	1.39	-1.542	141.9 \pm 9.1	2.85	-	-	-	-	-
Cu 1	5700.237	1.64	-2.583	-	-	19.6 \pm 3.7	2.48	-	-	-
Cu 1	5782.127	1.64	-1.905	110.9 \pm 6.0	2.54	-	-	43.1 \pm 2.4	2.28	-
Zn 1	4722.153	4.03	-0.338	74.4 \pm 5.0	3.72	52.7 \pm 4.5	3.29	51.2 \pm 5.7	3.22	65.8 \pm 5.1
Zn 1	4810.528	4.08	-0.137	75.1 \pm 5.1	3.59	62.4 \pm 3.4	3.41	65.8 \pm 4.8	3.47	65.5 \pm 5.4
Zr 2	4149.198	0.80	-0.040	-	-	0.0 \pm 0.0	1.15	-	-	-
Zr 2	4161.200	0.71	-0.590	-	-	0.0 \pm 0.0	0.94	-	-	-
Zr 2	4208.980	0.71	-0.510	-	-	0.0 \pm 0.0	1.52	-	-	-
Ba 2	5853.668	0.60	-1.000	148.3 \pm 8.3	1.85	111.3 \pm 8.0	1.69	97.4 \pm 9.1	1.30	111.8 \pm 6.0
Ba 2	6141.713	0.70	-0.076	-	-	154.8 \pm 9.4	1.58	137.5 \pm 8.5	1.30	1.10
Ba 2	6496.897	0.60	-0.377	-	-	147.3 \pm 8.6	1.56	-	-	143.4 \pm 8.2
La 2	4748.730	0.93	-0.540	32.8 \pm 3.2	0.25	-	-	-	-	-
La 2	4804.040	0.23	-1.490	40.5 \pm 3.8	0.44	-	-	-	-	-
La 2	5303.530	0.32	-1.350	36.2 \pm 3.9	0.28	-	-	-	-	-
La 2	6320.376	0.17	-1.610	40.4 \pm 2.4	0.35	-	-	-	-	-
La 2	6390.480	0.32	-1.410	41.9 \pm 3.5	0.38	26.5 \pm 3.8	0.29	-	-	-
La 2	6774.268	0.13	-1.820	39.0 \pm 2.2	0.44	-	-	-	-	-
Ce 2	4562.359	0.48	0.210	-	-	-	-	49.7 \pm 5.2	0.40	-
Ce 2	4628.161	0.52	0.140	93.4 \pm 5.9	1.22	54.5 \pm 3.7	0.64	50.3 \pm 3.3	0.52	5.21 \pm 3.5
Ce 2	5330.556	0.87	-0.400	24.6 \pm 1.3	0.49	22.8 \pm 4.3	0.67	-	-	0.56
Pr 2	4510.152	0.42	-0.023	-	-	-	-	-	-	-
Pr 2	5322.771	0.48	-0.319	43.3 \pm 3.8	0.12	-	-	-	-	-
Nd 2	4061.080	0.47	0.550	-	-	-	-	-	-	-
Nd 2	4446.380	0.20	-0.350	93.4 \pm 6.2	1.14	-	-	51.4 \pm 6.3	0.47	-
Nd 2	4706.540	0	-0.710	-	-	49.8 \pm 3.1	0.43	42.5 \pm 3.4	0.27	77.8 \pm 5.1
Nd 2	4825.480	0.18	-0.420	-	-	-	-	53.9 \pm 3.6	0.50	82.2 \pm 4.7
Nd 2	5249.580	0.98	0.200	70.6 \pm 5.1	0.81	51.6 \pm 4.0	0.76	34.5 \pm 3.7	0.34	41.2 \pm 4.2
Nd 2	5306.460	0.86	-0.970	16.9 \pm 1.5	0.61	-	-	-	-	-
Nd 2	5319.810	0.55	-0.140	-	-	-	-	46.1 \pm 3.2	0.42	-
Nd 2	5431.520	1.12	-0.470	30.9 \pm 2.5	0.82	-	-	-	-	-
Nd 2	5533.820	0.56	-1.230	26.8 \pm 1.6	0.72	-	-	-	-	-
Sm 2	4467.340	0.66	0.150	-	-	-	-	41.3 \pm 3.6	0.01	-
Sm 2	4536.510	0.10	-1.280	49.6 \pm 4.1	0.50	-	-	-	-	-
Sm 2	4577.690	0.25	-0.650	-	-	-	-	25.1 \pm 2.7	-0.16	-
Sm 2	4642.228	0.38	-0.460	64.8 \pm 4.8	0.39	38.6 \pm 2.7	0.13	-	-	33.4 \pm 2.4
Sm 2	4704.400	0	-0.860	-	-	42.7 \pm 3.3	0.15	-	-	41.0 \pm 3.1
Eu 2	6645.103	1.38	0.121	41.9 \pm 5.2	-0.01	-	-	-	-	27.9 \pm 2.4
Eu 2						-	-	-	-	-0.16

Table 9. Line parameters, observed equivalent widths and corresponding abundances of star 18 observed with MIKE.

El.	λ	χ_{ex}	$\log(gf)$	EW $\pm\sigma(\text{EW})$	$\log \epsilon(X) + 12 [\text{dex}]$
				18	
O 1	6300.304	0.00	-9.750	42.5 \pm 2.3	7.89
O 1	6363.776	0.02	-10.260	19.9 \pm 1.7	8.00
Na 1	6160.747	2.10	-1.246	26.7 \pm 3.8	4.90
Mg 1	5711.088	4.35	-1.724	88.5 \pm 5.9	6.44
Si 1	5701.104	4.93	-2.050	26.5 \pm 2.7	6.60
Si 1	5772.146	5.08	-1.750	28.0 \pm 2.7	6.52
Si 1	5948.541	5.08	-1.230	72.2 \pm 5.3	6.84
Si 1	6244.465	5.62	-1.091	21.6 \pm 2.6	6.35
Ca 1	5581.965	2.52	-0.555	94.9 \pm 5.0	5.19
Ca 1	5601.277	2.53	-0.523	100.8 \pm 5.7	5.29
Ca 1	6161.297	2.52	-1.266	61.9 \pm 3.8	5.18
Ca 1	6166.439	2.52	-1.142	71.9 \pm 4.1	5.24
Ca 1	6455.598	2.52	-1.340	56.6 \pm 3.8	5.14
Ca 1	6499.650	2.52	-0.818	97.8 \pm 5.9	5.38
Sc 2	5526.790	1.77	0.024	91.7 \pm 5.4	1.86
Sc 2	6604.601	1.36	-1.309	59.9 \pm 3.4	1.90
Ti 1	4512.734	0.84	-0.400	101.4 \pm 7.5	3.61
Ti 1	4645.188	1.73	-0.510	58.3 \pm 4.3	3.91
Ti 1	5210.384	0.05	-0.820	157.8 \pm 9.4	4.16
Ti 1	6126.216	1.07	-1.425	54.7 \pm 3.7	3.64
Ti 1	6258.102	1.44	-0.390	89.5 \pm 5.4	3.70
Ti 1	6556.062	1.46	-1.060	51.1 \pm 3.2	3.72
Ti 2	4493.522	1.08	-2.780	79.4 \pm 4.8	4.08
Ti 2	4583.409	1.16	-2.840	68.2 \pm 6.0	3.97
Ti 2	4636.320	1.16	-3.230	64.3 \pm 3.7	4.25
Ti 2	4865.610	1.12	-2.700	81.3 \pm 5.4	4.02
Cr 1	4545.953	0.94	-1.370	112.0 \pm 7.3	4.34
Cr 1	5345.796	1.00	-0.896	151.4 \pm 9.1	4.42
Cr 1	6330.091	0.94	-2.920	52.3 \pm 3.3	4.11
Cr 2	4588.199	4.07	-0.627	58.3 \pm 4.0	4.34
Mn 1	6013.510	3.07	-0.352	67.1 \pm 3.7	3.74
Mn 1	6021.820	3.08	-0.054	80.7 \pm 4.6	3.76
Fe 1	4602.000	1.61	-3.154	107.9 \pm 7.6	6.28
Fe 1	4630.120	2.28	-2.587	110.3 \pm 7.2	6.54
Fe 1	4903.310	2.88	-0.926	155.7 \pm 9.4	6.49
Fe 1	5159.058	4.28	-0.820	61.0 \pm 4.1	6.24
Fe 1	5198.711	2.22	-2.135	126.1 \pm 7.3	6.25
Fe 1	5242.491	3.63	-0.967	93.4 \pm 6.2	6.30
Fe 1	5281.790	3.04	-0.834	131.7 \pm 7.9	6.13
Fe 1	5283.621	3.24	-0.432	152.9 \pm 16.7	6.35
Fe 1	5307.361	1.61	-2.987	132.6 \pm 7.5	6.54
Fe 1	5364.871	4.45	0.228	110.4 \pm 7.4	6.47
Fe 1	5365.399	3.57	-1.020	93.4 \pm 6.2	6.24
Fe 1	5367.466	4.41	0.443	106.1 \pm 6.8	6.13
Fe 1	5560.211	4.43	-1.190	39.2 \pm 5.6	6.33
Fe 1	5569.618	3.42	-0.486	134.7 \pm 7.5	6.27
Fe 1	5753.122	4.26	-0.688	80.7 \pm 5.1	6.45
Fe 1	5775.081	4.22	-1.298	54.5 \pm 3.3	6.44
Fe 1	6003.011	3.88	-1.120	83.4 \pm 5.7	6.41
Fe 1	6024.058	4.55	-0.120	93.2 \pm 5.1	6.49
Fe 1	6027.051	4.08	-1.089	60.4 \pm 3.2	6.15
Fe 1	6056.004	4.73	-0.460	52.8 \pm 3.9	6.23
Fe 1	6065.482	2.61	-1.530	149.2 \pm 8.0	6.37
Fe 1	6078.491	4.80	-0.321	57.2 \pm 3.3	6.26
Fe 1	6079.008	4.65	-1.120	34.2 \pm 2.6	6.41
Fe 1	6137.691	2.59	-1.403	158.0 \pm 8.8	6.33
Fe 1	6151.617	2.18	-3.299	86.9 \pm 4.8	6.28
Fe 1	6157.728	4.08	-1.260	64.3 \pm 3.7	6.39
Fe 1	6165.360	4.14	-1.474	42.5 \pm 2.7	6.27
Fe 1	6173.334	2.22	-2.880	107.0 \pm 5.7	6.32
Fe 1	6180.203	2.73	-2.586	79.4 \pm 4.9	6.18
Fe 1	6187.989	3.94	-1.720	47.4 \pm 2.5	6.34
Fe 1	6200.312	2.61	-2.437	98.9 \pm 5.5	6.27
Fe 1	6213.429	2.22	-2.482	124.1 \pm 7.0	6.24
Fe 1	6219.280	2.20	-2.433	134.0 \pm 8.1	6.34
Fe 1	6229.226	2.85	-2.805	49.0 \pm 3.2	5.98
Fe 1	6252.555	2.40	-1.687	149.2 \pm 7.8	6.21
Fe 1	6265.132	2.18	-2.550	130.8 \pm 7.5	6.35
Fe 1	6290.965	4.73	-0.774	38.2 \pm 3.2	6.24
Fe 1	6297.792	2.22	-2.740	126.2 \pm 7.7	6.52
Fe 1	6322.685	2.59	-2.426	105.9 \pm 6.0	6.35
Fe 1	6335.330	2.20	-2.177	131.8 \pm 7.5	6.01
Fe 1	6344.148	2.43	-2.923	94.1 \pm 5.7	6.39

Table 9. continued.

El.	λ	χ_{ex}	$\log(gf)$	EW± σ (EW) 18	$\log \varepsilon(X) + 12$ [dex]
Fe 1	6355.028	2.85	-2.350	95.9 ± 5.0	6.42
Fe 1	6392.538	2.28	-4.030	35.4 ± 2.4	6.18
Fe 1	6408.018	3.69	-1.018	94.0 ± 5.1	6.20
Fe 1	6411.648	3.65	-0.595	116.7 ± 7.1	6.19
Fe 1	6419.949	4.73	-0.240	68.7 ± 4.4	6.30
Fe 1	6430.845	2.18	-2.006	158.2 ± 9.4	6.20
Fe 1	6593.870	2.43	-2.422	122.0 ± 6.6	6.40
Fe 1	6608.025	2.28	-4.030	36.9 ± 2.7	6.19
Fe 1	6677.985	2.69	-1.418	156.2 ± 8.9	6.33
Fe 1	6750.151	2.42	-2.621	108.0 ± 6.1	6.31
Fe 2	4491.397	2.86	-2.700	81.5 ± 6.7	6.40
Fe 2	4620.513	2.83	-3.240	52.8 ± 4.5	6.14
Fe 2	5991.371	3.15	-3.540	30.0 ± 2.6	6.27
Fe 2	6149.246	3.89	-2.720	29.5 ± 2.2	6.34
Fe 2	6238.386	3.89	-2.754	31.2 ± 2.5	6.42
Fe 2	6247.557	3.89	-2.310	43.6 ± 2.8	6.31
Fe 2	6369.459	2.89	-4.160	20.1 ± 2.1	6.29
Fe 2	6516.077	2.89	-3.320	57.0 ± 3.4	6.35
Ni 1	6128.973	1.68	-3.430	46.6 ± 2.6	4.86
Ni 1	6586.310	1.95	-2.780	60.6 ± 3.7	4.80
Ni 1	6643.630	1.68	-2.220	131.1 ± 7.1	5.19
Ni 1	6767.772	1.83	-2.140	113.7 ± 6.5	4.97
Ba 2	5853.668	0.60	-1.000	115.1 ± 6.4	1.38
Ba 2	6496.897	0.60	-0.377	159.0 ± 8.5	1.48
La 2	6390.480	0.32	-1.410	18.1 ± 2.5	-0.08
Ce 2	4628.161	0.52	0.140	55.2 ± 4.0	0.38
Nd 2	4706.540	0.00	-0.710	65.1 ± 4.9	0.55
Nd 2	5249.580	0.98	0.200	50.5 ± 3.6	0.51
Sm 2	4536.510	0.10	-1.280	22.6 ± 3.8	0.01
Sm 2	4642.228	0.38	-0.460	44.1 ± 3.2	0.06
Eu 2	6645.103	1.38	0.121	29.8 ± 2.0	-0.20

Table 10. Line parameters, observed equivalent widths and corresponding abundances of stars 19, 20, 21, 22, and 23 observed with UVES.

El.	λ	χ_{ex}	$\log(gf)$	$\log \varepsilon(X) + 12$ [dex]				
				19	20	21	22	23
O I	6300.304	0	-9.750	—	—	—	31.7 ± 2.2	8.07
Na 1	5682.633	2.10	-0.706	—	—	49.0 ± 3.0	5.15	35.0 ± 2.8
Na 1	5688.205	2.10	-0.452	—	—	71.6 ± 3.8	5.29	49.6 ± 2.9
Na 1	5889.951	0.00	0.108	148.0 ± 7.9	3.34	167.2 ± 9.7	3.40	—
Na 1	5895.924	0.00	-0.194	128.9 ± 7.0	3.32	145.5 ± 7.6	3.40	—
Mg 1	3829.355	2.71	-0.227	—	—	166.1 ± 12.8	4.85	—
Mg 1	3832.304	2.71	0.125	176.0 ± 10.0	4.85	—	—	—
Mg 1	5172.684	2.71	-0.450	162.3 ± 9.5	4.76	190.0 ± 11.5	4.82	—
Mg 1	5183.604	2.72	-0.239	184.1 ± 11.6	4.80	213.3 ± 14.4	4.80	—
Mg 1	5528.405	4.35	-0.498	—	—	61.5 ± 3.6	4.98	167.8 ± 10.0
Mg 1	5711.088	4.35	-1.724	—	—	—	6.71	154.3 ± 8.5
Al 1	3961.520	0.01	-0.323	121.5 ± 7.1	2.90	—	—	—
Si 1	5665.555	4.92	-2.040	—	—	—	29.3 ± 2.0	6.92
Si 1	5684.484	4.95	-1.650	—	—	—	46.9 ± 2.6	6.94
Si 1	5690.425	4.93	-1.870	—	—	—	32.8 ± 2.1	6.84
Si 1	5948.541	5.08	-1.230	—	—	—	61.9 ± 3.6	6.96
Si 1	6244.465	5.62	-1.091	—	—	—	25.7 ± 1.5	6.65
Ca 1	5349.465	2.71	-0.310	—	—	—	91.1 ± 4.8	5.88
Ca 1	5581.965	2.52	-0.555	—	—	—	93.0 ± 4.9	5.87
Ca 1	5588.749	2.53	0.358	44.1 ± 2.5	3.64	45.9 ± 2.6	3.58	130.8 ± 7.0
Ca 1	5590.114	2.52	-0.571	—	—	—	5.72	122.8 ± 6.7
Ca 1	5601.277	2.53	-0.523	—	—	—	97.2 ± 5.6	5.94
Ca 1	5857.451	2.93	0.240	23.7 ± 1.6	3.82	21.5 ± 2.0	3.69	121.3 ± 6.3
Ca 1	6102.723	1.88	-0.793	32.3 ± 1.9	3.75	35.0 ± 2.1	3.70	100.3 ± 5.1
Ca 1	6122.217	1.89	-0.316	57.9 ± 3.1	3.73	60.2 ± 3.4	3.65	119.0 ± 6.4
Ca 1	6161.297	2.52	-1.266	—	—	—	—	147.1 ± 7.6
Ca 1	6162.173	1.90	-0.090	73.0 ± 3.9	3.78	73.0 ± 4.0	3.65	5.40
Ca 1	6166.439	2.52	-1.142	—	—	—	—	142.8 ± 8.2
Ca 1	6169.042	2.52	-0.797	—	—	—	67.8 ± 4.2	5.75
Ca 1	6169.563	2.53	-0.478	—	—	—	88.9 ± 5.0	5.88
Ca 1	6439.075	2.53	0.390	51.9 ± 2.7	3.70	53.0 ± 2.9	3.62	73.8 ± 3.8
Ca 1	6455.598	2.52	-1.340	—	—	—	55.8 ± 3.0	5.69
Ca 1	6499.650	2.52	-0.818	—	—	—	87.5 ± 4.8	5.89
Ca 1	6717.681	2.71	-0.524	—	—	—	—	91.7 ± 4.8
Sc 2	4246.822	0.31	0.242	114.1 ± 6.6	0.06	132.5 ± 7.4	0.36	5.44
Sc 2	4400.389	0.61	-0.536	57.0 ± 3.8	-0.01	73.8 ± 4.7	0.25	51.3 ± 2.8
						—	—	104.3 ± 5.7
						—	—	118.8 ± 6.4
						—	—	121.5 ± 1.4
						—	—	142.8 ± 8.2
						—	—	1.21

Table 10. continued.

El.	λ	χ_{ex}	$\log(gf)$	EW $\pm\sigma$ (EW) $\log \varepsilon(X) + 12$ [dex]							
				19		20		21		22	
Sc 2	4415.557	0.60	-0.668	50.8 \pm 3.9	-0.02	-	-	-	-	-	-
Sc 2	5031.021	1.36	-0.400	-	-	33.3 \pm 2.1	0.26	-	-	-	67.7 \pm 3.1
Sc 2	5526.790	1.77	0.024	21.6 \pm 1.5	0.08	33.5 \pm 2.0	0.33	-	-	-	-
Sc 2	6604.601	1.36	-1.309	-	-	-	-	49.4 \pm 2.6	2.43	-	-
Ti 1	3989.758	0.02	-0.130	-	-	62.2 \pm 3.6	1.92	-	-	-	-
Ti 1	3998.636	0.05	0.020	55.1 \pm 3.5	1.84	-	-	-	-	-	-
Ti 1	4512.734	0.84	-0.400	-	-	-	-	-	-	88.8 \pm 5.6	4.13
Ti 1	4840.874	0.90	-0.430	-	-	-	-	82.4 \pm 4.3	4.30	79.5 \pm 4.2	3.91
Ti 1	4913.613	1.87	0.220	-	-	-	-	-	-	48.3 \pm 2.8	3.70
Ti 1	4981.730	0.85	0.570	44.4 \pm 2.5	1.94	50.3 \pm 2.9	1.89	128.4 \pm 7.5	4.26	129.2 \pm 7.0	3.97
Ti 1	4991.066	0.84	0.450	-	-	49.7 \pm 2.9	1.98	-	-	-	-
Ti 1	4997.097	0	-2.070	-	-	-	-	-	-	53.6 \pm 3.0	3.75
Ti 1	4999.503	0.83	0.320	33.8 \pm 2.1	1.96	45.1 \pm 2.6	2.01	136.8 \pm 7.3	4.62	-	-
Ti 1	5016.161	0.85	-0.480	-	-	-	-	88.6 \pm 5.1	4.38	78.2 \pm 4.4	3.81
Ti 1	5039.958	0.02	-1.080	-	-	25.3 \pm 1.7	2.00	102.5 \pm 5.5	4.40	97.5 \pm 5.8	3.87
Ti 1	5064.653	0.05	-0.940	-	-	28.4 \pm 2.0	1.96	111.2 \pm 6.0	4.54	106.6 \pm 5.8	4.00
Ti 1	5113.440	1.44	-0.700	-	-	-	-	-	-	26.9 \pm 1.6	3.61
Ti 1	5173.743	0	-1.060	-	-	28.8 \pm 1.6	2.01	-	-	-	-
Ti 1	5192.969	0.02	-0.950	20.5 \pm 1.5	1.91	33.8 \pm 1.9	2.03	-	-	-	69.9 \pm 3.7
Ti 1	5210.384	0.05	-0.820	23.5 \pm 1.5	1.89	36.9 \pm 2.1	1.99	118.0 \pm 6.5	4.54	111.7 \pm 6.4	3.96
Ti 1	5490.147	1.46	-0.840	-	-	-	-	36.4 \pm 2.4	4.11	-	-
Ti 1	5978.541	1.87	-0.496	-	-	-	-	34.5 \pm 2.0	4.19	-	-
Ti 1	6126.216	1.07	-1.425	-	-	-	-	42.3 \pm 2.4	4.29	31.2 \pm 2.1	3.89
Ti 1	6258.102	1.44	-0.390	-	-	-	-	69.3 \pm 3.9	4.29	58.9 \pm 3.4	3.86
Ti 1	6556.062	1.46	-1.060	-	-	-	-	35.2 \pm 1.9	4.23	23.5 \pm 1.5	3.81
Ti 2	3759.292	0.61	0.280	162.7 \pm 10.7	2.05	-	-	-	-	-	-
Ti 2	3761.321	0.57	0.180	-	-	174.9 \pm 10.1	2.11	-	-	-	-
Ti 2	4028.338	1.89	-0.920	-	-	55.7 \pm 4.8	2.40	-	-	-	-
Ti 2	4337.914	1.08	-0.960	-	-	99.9 \pm 6.0	2.34	-	-	-	-
Ti 2	4399.765	1.24	-1.200	73.4 \pm 7.0	2.19	87.7 \pm 5.3	2.46	-	-	-	-
Ti 2	4417.713	1.16	-1.190	83.1 \pm 5.6	2.31	-	-	-	-	132.8 \pm 8.6	4.28
Ti 2	4418.331	1.24	-1.990	-	-	-	-	-	-	98.9 \pm 6.9	4.42
Ti 2	4443.801	1.08	-0.710	107.2 \pm 5.7	2.30	120.8 \pm 7.1	2.52	157.7 \pm 8.7	4.43	-	130.1 \pm 7.8
Ti 2	4444.554	1.12	-2.200	-	-	46.6 \pm 3.0	2.46	-	-	-	-
Ti 2	4450.482	1.08	-1.520	-	-	81.3 \pm 5.4	2.43	-	-	-	-
Ti 2	4865.610	1.12	-2.700	-	-	22.3 \pm 1.8	2.42	63.5 \pm 3.7	4.45	64.1 \pm 3.4	3.99
Ti 2	5129.156	1.89	-1.340	25.9 \pm 2.0	2.12	-	-	-	-	-	-
Ti 2	5154.068	1.57	-1.750	24.5 \pm 1.9	2.09	36.4 \pm 2.2	2.32	-	-	88.0 \pm 5.2	4.15
Ti 2	5185.902	1.89	-1.410	-	-	33.4 \pm 2.1	2.33	83.3 \pm 4.7	4.56	85.3 \pm 4.6	4.12
Ti 2	5188.687	1.58	-1.050	-	-	78.0 \pm 4.8	2.38	-	-	-	-
Ti 2	5226.539	1.57	-1.260	-	-	67.2 \pm 3.7	2.36	-	-	-	90.4 \pm 5.0
Ti 2	5336.786	1.58	-1.600	33.6 \pm 2.4	2.14	47.9 \pm 2.7	2.37	92.3 \pm 4.7	4.60	91.4 \pm 5.7	4.07
Ti 2	5381.021	1.57	-1.970	-	-	28.0 \pm 1.8	2.35	-	-	-	-
Ti 2	5418.768	1.58	-2.130	-	-	23.5 \pm 1.4	2.43	67.2 \pm 3.7	4.47	68.8 \pm 4.0	4.04
Ti 2	6559.563	2.05	-2.175	-	-	-	-	40.5 \pm 3.2	4.36	-	-
V 1	4379.230	0.30	0.580	-	-	-	-	131.4 \pm 8.0	3.83	-	66.3 \pm 4.8
V 1	6216.364	0.28	-1.330	-	-	-	-	38.5 \pm 2.2	3.13	-	1.92
V 2	4005.702	1.82	-0.450	-	-	33.3 \pm 2.2	1.28	-	-	-	-
Cr 1	4254.352	0.00	-0.090	109.4 \pm 6.2	2.38	107.8 \pm 6.1	2.08	-	-	-	-
Cr 1	4274.812	0.00	-0.220	100.6 \pm 6.1	2.28	100.4 \pm 5.7	2.02	-	-	-	-
Cr 1	5206.023	0.94	0.020	77.4 \pm 4.0	2.41	74.0 \pm 4.1	2.16	-	-	-	-
Cr 1	5296.691	0.98	-1.360	-	-	-	-	104.0 \pm 5.7	5.00	92.2 \pm 5.4	4.38
Cr 1	5300.745	0.98	-2.016	-	-	-	-	72.5 \pm 4.0	4.81	-	-
Cr 1	5345.796	1.00	-0.896	27.9 \pm 1.8	2.44	24.7 \pm 2.0	2.22	121.6 \pm 6.5	4.93	109.3 \pm 5.8	4.35
Cr 1	5348.314	1	-1.210	-	-	-	-	109.2 \pm 5.9	4.99	97.3 \pm 5.1	4.37
Cr 1	5409.784	1.03	-0.670	-	-	37.7 \pm 2.4	2.29	-	-	-	88.5 \pm 4.6
Cr 1	6330.091	0.94	-2.920	-	-	-	-	37.4 \pm 2.3	4.71	21.6 \pm 1.9	4.18
Mn 1	4030.750	0.00	-0.494	125.5 \pm 7.4	2.04	125.1 \pm 6.8	1.73	-	-	-	-
Mn 1	4033.060	0.00	-0.644	111.0 \pm 6.3	1.94	-	-	-	-	-	-
Mn 1	4034.480	0.00	-0.842	103.8 \pm 6.1	2.05	-	-	-	-	-	-
Mn 1	4041.350	2.11	0.277	42.6 \pm 3.2	2.16	-	-	-	-	-	-
Mn 1	5407.417	2.14	-1.743	-	-	-	-	-	-	-	7.1 \pm 0.8
Mn 1	5420.351	2.14	-1.462	-	-	-	-	52.9 \pm 3.5	4.00	28.3 \pm 2.3	3.56
Mn 1	5432.539	0	-3.795	-	-	-	-	70.0 \pm 3.9	4.03	39.4 \pm 2.4	3.44
Mn 1	5516.766	2.18	-1.847	-	-	-	-	26.1 \pm 2.2	4.09	-	-
Fe 1	3902.945	1.56	-0.466	119.5 \pm 6.9	4.44	126.7 \pm 8.3	4.32	-	-	-	-
Fe 1	4005.242	1.56	-0.610	-	-	127.1 \pm 7.2	4.45	-	-	-	-
Fe 1	4062.441	2.85	-0.862	37.3 \pm 2.8	4.38	34.9 \pm 7.6	4.21	-	-	101.3 \pm 6.6	6.38
Fe 1	4063.594	1.56	0.062	149.9 \pm 8.3	4.37	-	-	-	-	-	-
Fe 1	4136.998	3.41	-0.453	26.2 \pm 2.0	4.41	-	-	-	-	-	-
Fe 1	4156.799	2.83	-0.809	49.8 \pm 3.8	4.56	-	-	-	-	-	-
Fe 1	4157.780	3.42	-0.403	-	-	30.3 \pm 1.9	4.35	-	-	-	-
Fe 1	4175.636	2.85	-0.827	-	-	-	-	-	-	-	87.6 \pm 5.6
Fe 1	4176.566	3.37	-0.805	-	-	-	-	-	-	90.7 \pm 7.1	6.45

Table 10. continued.

El.	λ	χ_{ex}	$\log(gf)$	EW $\pm\sigma$ (EW) $\log \varepsilon(X) + 12$ [dex]						
				19	20	21	22	23		
Fe 1	4182.382	3.02	-1.180	-	-	-	-	-	63.7 ± 3.8	5.63
Fe 1	4184.892	2.83	-0.869	46.4 ± 3.0	4.55	-	-	-	85.4 ± 5.5	5.72
Fe 1	4187.039	2.45	-0.548	-	-	80.9 ± 5.4	4.37	-	-	-
Fe 1	4187.795	2.42	-0.554	-	-	92.6 ± 5.5	4.61	-	-	-
Fe 1	4195.329	3.33	-0.492	-	-	31.1 ± 2.6	4.35	-	-	-
Fe 1	4199.095	3.05	0.155	76.6 ± 4.1	4.50	-	-	-	-	-
Fe 1	4202.029	1.49	-0.708	120.1 ± 6.9	4.50	123.4 ± 6.7	4.31	-	-	-
Fe 1	4217.545	3.43	-0.484	-	-	-	-	-	67.8 ± 4.1	5.49
Fe 1	4222.213	2.45	-0.967	67.7 ± 4.4	4.62	-	-	-	96.5 ± 6.1	5.53
Fe 1	4227.426	3.33	0.266	-	-	75.6 ± 4.8	4.53	-	-	-
Fe 1	4238.810	3.40	-0.233	-	-	-	-	104.0 ± 6.1	6.20	-
Fe 1	4250.119	2.47	-0.405	89.6 ± 4.9	4.61	-	-	-	-	126.5 ± 7.8
Fe 1	4250.787	1.56	-0.714	117.9 ± 7.3	4.53	124.1 ± 7.2	4.40	-	-	155.0 ± 9.0
Fe 1	4260.474	2.40	0.109	111.4 ± 6.3	4.50	100.3 ± 5.6	4.06	-	-	-
Fe 1	4271.153	2.45	-0.349	93.8 ± 5.6	4.63	94.4 ± 5.3	4.45	-	-	-
Fe 1	4388.407	3.60	-0.682	-	-	-	-	85.0 ± 5.6	6.40	-
Fe 1	4442.339	2.20	-1.255	-	-	-	-	-	-	119.7 ± 6.5
Fe 1	4447.717	2.22	-1.342	65.7 ± 3.8	4.62	65.9 ± 3.9	4.47	160.1 ± 9.0	6.69	135.7 ± 7.7
Fe 1	4494.563	2.20	-1.136	80.2 ± 4.5	4.70	82.6 ± 4.8	4.58	-	-	117.1 ± 6.7
Fe 1	4800.649	4.14	-1.029	-	-	-	-	56.2 ± 3.1	6.79	-
Fe 1	4871.318	2.87	-0.363	67.9 ± 4.0	4.42	68.1 ± 3.8	4.28	-	-	107.7 ± 5.5
Fe 1	4872.138	2.88	-0.567	54.0 ± 3.8	4.37	54.7 ± 3.2	4.25	-	-	96.7 ± 5.1
Fe 1	4890.755	2.88	-0.394	70.7 ± 3.7	4.52	74.1 ± 4.5	4.44	-	-	110.0 ± 6.1
Fe 1	4891.492	2.85	-0.112	82.2 ± 4.5	4.46	83.8 ± 4.6	4.33	-	-	121.9 ± 6.9
Fe 1	4903.310	2.88	-0.926	-	-	41.8 ± 3.0	4.37	131.0 ± 7.0	6.76	122.5 ± 6.9
Fe 1	4918.994	2.87	-0.342	72.4 ± 4.3	4.48	69.7 ± 3.7	4.28	-	-	108.2 ± 6.0
Fe 1	4920.502	2.83	0.068	90.2 ± 4.9	4.42	-	-	-	-	-
Fe 1	4924.770	2.28	-2.241	-	-	20.9 ± 1.4	4.48	102.9 ± 5.7	7.01	91.4 ± 5.0
Fe 1	4938.814	2.88	-1.077	39.0 ± 2.2	4.58	35.7 ± 2.2	4.39	113.0 ± 6.1	6.64	104.2 ± 5.8
Fe 1	5001.863	3.88	0.010	-	-	27.4 ± 1.6	4.38	105.7 ± 5.8	6.59	92.9 ± 5.0
Fe 1	5006.119	2.83	-0.638	65.5 ± 3.6	4.59	63.7 ± 3.5	4.41	-	-	131.6 ± 7.9
Fe 1	5014.942	3.94	-0.303	-	-	-	-	99.4 ± 5.4	6.86	86.3 ± 4.5
Fe 1	5028.126	3.57	-1.123	-	-	-	-	80.0 ± 4.4	6.82	-
Fe 1	5044.211	2.85	-2.038	-	-	-	-	-	-	36.5 ± 2.0
Fe 1	5049.820	2.28	-1.355	60.0 ± 3.4	4.51	-	-	-	-	34.9 ± 2.3
Fe 1	5068.766	2.94	-1.042	-	-	-	-	-	-	97.8 ± 5.2
Fe 1	5074.748	4.22	-0.200	-	-	-	-	117.5 ± 6.2	6.72	100.7 ± 5.5
Fe 1	5141.739	2.42	-1.964	-	-	-	-	100.3 ± 5.2	7.01	78.8 ± 4.4
Fe 1	5145.094	2.20	-2.876	-	-	-	-	90.0 ± 4.9	6.54	-
Fe 1	5162.272	4.18	0.020	-	-	18.7 ± 1.7	4.50	106.6 ± 5.8	6.85	53.9 ± 2.9
Fe 1	5171.596	1.49	-1.793	97.5 ± 5.3	4.75	99.8 ± 5.2	4.57	-	-	151.3 ± 8.4
Fe 1	5191.455	3.04	-0.551	46.6 ± 2.7	4.37	50.5 ± 2.9	4.32	-	-	-
Fe 1	5192.344	3.00	-0.421	60.8 ± 3.2	4.46	-	-	-	-	-
Fe 1	5194.941	1.56	-2.090	72.4 ± 3.8	4.57	77.9 ± 4.3	4.49	-	-	128.0 ± 7.0
Fe 1	5196.059	4.26	-0.493	-	-	-	-	63.8 ± 3.8	6.48	-
Fe 1	5198.711	2.22	-2.135	26.1 ± 1.7	4.55	26.0 ± 2.1	4.41	103.9 ± 5.8	6.77	-
Fe 1	5202.336	2.18	-1.838	41.6 ± 2.3	4.50	42.6 ± 2.7	4.38	-	-	96.3 ± 5.3
Fe 1	5215.180	3.27	-0.871	26.9 ± 1.7	4.58	21.9 ± 1.4	4.35	107.9 ± 6.2	6.74	92.7 ± 5.0
Fe 1	5216.274	1.61	-2.150	67.8 ± 3.6	4.60	71.4 ± 4.2	4.49	-	-	123.9 ± 6.9
Fe 1	5217.389	3.21	-1.070	-	-	19.6 ± 1.4	4.42	101.1 ± 5.5	6.75	90.5 ± 5.0
Fe 1	5232.940	2.94	-0.058	82.2 ± 4.5	4.45	81.0 ± 4.3	4.27	-	-	151.8 ± 9.6
Fe 1	5242.491	3.63	-0.967	-	-	-	-	-	-	58.8 ± 4.1
Fe 1	5253.021	2.28	-3.940	-	-	-	-	-	-	-
Fe 1	5266.555	3.00	-0.386	58.0 ± 3.2	4.36	63.4 ± 3.4	4.33	-	-	140.6 ± 8.4
Fe 1	5281.790	3.04	-0.834	40.0 ± 2.2	4.53	32.8 ± 1.8	4.27	121.8 ± 6.7	6.64	110.2 ± 6.2
Fe 1	5283.621	3.24	-0.432	45.9 ± 3.0	4.48	-	-	-	-	87.8 ± 5.1
Fe 1	5302.300	3.28	-0.720	-	-	-	-	118.0 ± 6.7	6.76	102.8 ± 5.4
Fe 1	5307.361	1.61	-2.987	23.6 ± 1.7	4.57	-	-	105.2 ± 5.4	7.04	97.4 ± 5.2
Fe 1	5322.041	2.28	-2.803	-	-	-	-	73.1 ± 4.1	6.71	60.9 ± 3.3
Fe 1	5324.179	3.21	-0.103	62.9 ± 3.4	4.43	61.2 ± 3.3	4.27	-	-	106.3 ± 5.8
Fe 1	5332.899	1.56	-2.777	32.2 ± 2.1	4.48	36.6 ± 2.2	4.41	-	-	100.0 ± 5.7
Fe 1	5339.929	3.27	-0.647	29.7 ± 1.8	4.41	30.3 ± 1.9	4.31	119.9 ± 6.8	6.69	103.8 ± 5.7
Fe 1	5364.871	4.45	0.228	-	-	-	-	99.6 ± 5.2	6.77	-
Fe 1	5365.399	3.57	-1.020	-	-	-	-	77.0 ± 4.2	6.59	65.6 ± 3.5
Fe 1	5367.466	4.41	0.443	23.4 ± 1.7	4.56	22.2 ± 1.8	4.45	105.7 ± 5.5	6.63	80.7 ± 4.4
Fe 1	5369.961	4.37	0.536	29.6 ± 1.9	4.56	23.0 ± 1.5	4.32	-	-	93.5 ± 4.9
Fe 1	5379.574	3.69	-1.514	-	-	-	-	54.9 ± 3.0	6.64	-
Fe 1	5383.369	4.31	0.645	30.5 ± 1.8	4.40	28.4 ± 1.6	4.27	113.9 ± 6.0	6.47	99.5 ± 5.6
Fe 1	5389.479	4.41	-0.410	-	-	-	-	74.0 ± 4.0	6.84	57.1 ± 3.0
Fe 1	5393.167	3.24	-0.715	32.1 ± 2.4	4.49	27.5 ± 1.6	4.28	-	-	78.5 ± 4.3
Fe 1	5400.501	4.37	-0.160	-	-	-	-	-	-	72.6 ± 3.9
Fe 1	5410.910	4.47	0.398	21.2 ± 1.3	4.62	-	-	98.9 ± 5.1	6.62	84.3 ± 4.5
Fe 1	5415.199	4.39	0.642	-	-	26.6 ± 1.7	4.32	113.6 ± 5.9	6.53	97.9 ± 5.6
Fe 1	5424.068	4.32	0.520	-	-	34.8 ± 1.9	4.54	126.6 ± 6.8	6.76	108.3 ± 5.7

Table 10. continued.

El.	λ	χ_{ex}	$\log(gf)$	EW $\pm\sigma$ (EW) $\log \varepsilon(X) + 12$ [dex]							
				19	20	21	22	23			
Fe 1	5445.042	4.39	-0.020	—	—	92.2 \pm 4.8	6.82	75.0 \pm 4.2	6.21	49.2 \pm 2.7	5.60
Fe 1	5560.211	4.43	-1.190	—	—	43.5 \pm 2.5	6.87	—	—	—	—
Fe 1	5569.618	3.42	-0.486	—	—	28.3 \pm 1.9	4.28	123.9 \pm 6.5	6.70	103.0 \pm 5.4	6.10
Fe 1	5572.842	3.40	-0.275	42.4 \pm 2.7	4.43	43.0 \pm 2.4	4.33	—	—	78.6 \pm 4.1	5.50
Fe 1	5576.089	3.43	-1	—	—	—	—	106.9 \pm 5.7	6.97	92.4 \pm 5.2	6.41
Fe 1	5586.755	3.37	-0.120	52.1 \pm 2.8	4.42	53.8 \pm 3.0	4.32	—	—	131.9 \pm 7.3	6.15
Fe 1	5615.644	3.33	0.050	62.0 \pm 3.3	4.38	62.0 \pm 3.2	4.25	—	—	140.8 \pm 7.4	6.05
Fe 1	5618.632	4.21	-1.276	—	—	—	—	46.7 \pm 2.5	6.77	28.6 \pm 1.8	6.19
Fe 1	5662.516	4.18	-0.573	—	—	—	—	84.8 \pm 4.5	6.87	65.3 \pm 3.5	6.24
Fe 1	5701.544	2.56	-2.216	—	—	—	—	91.6 \pm 4.9	6.86	81.0 \pm 4.2	6.29
Fe 1	5753.122	4.26	-0.688	—	—	—	—	71.2 \pm 3.9	6.85	47.0 \pm 2.6	6.07
Fe 1	6003.011	3.88	-1.120	—	—	—	—	74.3 \pm 4.6	6.88	57.3 \pm 3.1	6.25
Fe 1	6024.058	4.55	-0.120	—	—	—	—	89.6 \pm 5.3	6.99	75.0 \pm 4.3	6.45
Fe 1	6027.051	4.08	-1.089	—	—	—	—	61.3 \pm 3.4	6.75	41.7 \pm 2.4	6.12
Fe 1	6056.004	4.73	-0.460	—	—	—	—	59.0 \pm 3.2	6.83	38.4 \pm 2.1	6.21
Fe 1	6065.482	2.61	-1.530	36.5 \pm 1.9	4.57	34.1 \pm 2.1	4.39	122.9 \pm 6.7	6.82	112.5 \pm 6.0	6.32
Fe 1	6078.491	4.80	-0.321	—	—	—	—	59.4 \pm 3.2	6.76	—	—
Fe 1	6079.008	4.65	-1.120	—	—	—	—	34.0 \pm 2.0	6.81	—	—
Fe 1	6082.710	2.22	-3.573	—	—	—	—	47.4 \pm 2.7	6.68	33.7 \pm 2.0	6.16
Fe 1	6136.615	2.45	-1.400	54.6 \pm 2.9	4.57	51.6 \pm 3.1	4.37	137.6 \pm 7.1	6.75	123.3 \pm 6.5	6.20
Fe 1	6137.691	2.59	-1.403	45.6 \pm 2.4	4.58	44.1 \pm 2.4	4.41	135.5 \pm 8.0	6.84	119.8 \pm 7.0	6.29
Fe 1	6151.617	2.18	-3.299	—	—	—	—	62.9 \pm 3.4	6.69	49.6 \pm 2.9	6.14
Fe 1	6157.728	4.08	-1.260	—	—	—	—	60.6 \pm 3.3	6.90	37.2 \pm 2.6	6.19
Fe 1	6165.360	4.14	-1.474	—	—	—	—	37.6 \pm 2.4	6.64	—	—
Fe 1	6173.334	2.22	-2.880	—	—	—	—	81.3 \pm 4.3	6.78	72.7 \pm 3.9	6.27
Fe 1	6180.203	2.73	-2.586	—	—	—	—	66.2 \pm 3.5	6.74	—	—
Fe 1	6187.989	3.94	-1.720	—	—	—	—	44.0 \pm 2.4	6.80	23.4 \pm 1.7	6.16
Fe 1	6191.558	2.43	-1.417	51.4 \pm 2.7	4.50	50.0 \pm 2.9	4.33	135.8 \pm 7.7	6.70	122.4 \pm 6.3	6.16
Fe 1	6200.312	2.61	-2.437	—	—	—	—	82.4 \pm 4.7	6.85	70.4 \pm 3.9	6.27
Fe 1	6213.429	2.22	-2.482	—	—	—	—	98.9 \pm 5.2	6.77	86.6 \pm 4.7	6.18
Fe 1	6219.280	2.20	-2.433	20.5 \pm 1.1	4.61	21.9 \pm 1.8	4.50	105.6 \pm 6.0	6.83	97.0 \pm 5.1	6.33
Fe 1	6229.226	2.85	-2.805	—	—	—	—	46.5 \pm 2.7	6.63	27.8 \pm 2.0	6.02
Fe 1	6230.722	2.56	-1.281	52.6 \pm 2.9	4.54	55.1 \pm 3.3	4.44	—	—	133.6 \pm 7.6	6.34
Fe 1	6240.646	2.22	-3.233	—	—	—	—	65.4 \pm 3.5	6.76	52.0 \pm 2.8	6.18
Fe 1	6246.318	3.60	-0.733	—	—	—	—	102.8 \pm 5.4	6.73	—	56.2 \pm 2.9
Fe 1	6252.555	2.40	-1.687	41.5 \pm 2.3	4.55	41.7 \pm 2.6	4.41	126.5 \pm 6.9	6.77	118.9 \pm 6.5	6.31
Fe 1	6265.132	2.18	-2.550	—	—	—	—	103.3 \pm 5.6	6.87	85.8 \pm 4.6	6.16
Fe 1	6297.792	2.22	-2.740	—	—	—	—	—	—	89.0 \pm 5.3	6.48
Fe 1	6301.500	3.65	-0.718	—	—	—	—	97.0 \pm 5.1	6.66	86.7 \pm 4.5	6.19
Fe 1	6302.494	3.69	-0.973	—	—	—	—	77.8 \pm 4.3	6.54	57.8 \pm 3.1	5.85
Fe 1	6322.685	2.59	-2.426	—	—	—	—	84.0 \pm 4.5	6.84	70.6 \pm 3.9	6.22
Fe 1	6335.330	2.20	-2.177	—	—	27.1 \pm 1.9	4.36	108.7 \pm 5.9	6.61	104.0 \pm 5.5	6.19
Fe 1	6344.148	2.43	-2.923	—	—	—	—	—	—	—	22.6 \pm 1.7
Fe 1	6355.028	2.85	-2.350	—	—	—	—	—	—	63.4 \pm 3.6	6.31
Fe 1	6380.743	4.19	-1.376	—	—	—	—	45.5 \pm 2.7	6.77	28.1 \pm 2.0	6.22
Fe 1	6393.601	2.43	-1.432	47.0 \pm 2.6	4.42	46.3 \pm 3.3	4.26	133.8 \pm 7.1	6.63	122.0 \pm 6.2	6.12
Fe 1	6400	3.60	-0.290	—	—	—	—	—	—	110.9 \pm 5.7	6.15
Fe 1	6408.018	3.69	-1.018	—	—	—	—	89.0 \pm 5.2	6.82	—	—
Fe 1	6411.648	3.65	-0.595	—	—	—	—	109.3 \pm 5.8	6.74	95.1 \pm 5.3	6.22
Fe 1	6419.949	4.73	-0.240	—	—	—	—	—	—	54.5 \pm 2.9	6.31
Fe 1	6421.350	2.28	-2.027	—	—	35.5 \pm 2.2	4.47	120.8 \pm 6.7	6.95	113.5 \pm 6.0	6.42
Fe 1	6430.845	2.18	-2.006	40.1 \pm 2.3	4.55	44.2 \pm 2.5	4.47	127.7 \pm 6.9	6.72	117.7 \pm 6.3	6.24
Fe 1	6494.980	2.40	-1.273	62.7 \pm 3.3	4.49	68.7 \pm 3.6	4.44	153.2 \pm 8.5	6.67	141.8 \pm 8.0	6.23
Fe 1	6518.366	2.83	-2.460	—	—	—	—	66.3 \pm 3.5	6.71	—	—
Fe 1	6581.209	1.49	-4.679	—	—	—	—	35.7 \pm 2.3	6.58	—	—
Fe 1	6592.913	2.73	-1.473	—	—	—	—	117.4 \pm 6.4	6.73	107.4 \pm 5.7	6.22
Fe 1	6593.870	2.43	-2.422	—	—	—	—	95.8 \pm 5.0	6.88	89.0 \pm 4.9	6.41
Fe 1	6609.110	2.56	-2.692	—	—	—	—	73.8 \pm 4.5	6.79	60.5 \pm 3.4	6.21
Fe 1	6677.985	2.69	-1.418	38.7 \pm 2.2	4.56	42.2 \pm 2.4	4.49	129.4 \pm 7.6	6.81	117.9 \pm 6.2	6.31
Fe 1	6750.151	2.42	-2.621	—	—	—	—	87.5 \pm 5.0	6.89	72.1 \pm 4.5	6.21
Fe 2	4178.854	2.58	-2.500	53.0 \pm 3.7	4.69	—	—	—	—	—	81.7 \pm 5.0
Fe 2	4515.333	2.84	-2.450	42.0 \pm 2.7	4.69	—	—	—	—	—	—
Fe 2	4923.921	2.89	-1.320	94.8 \pm 5.3	4.68	—	134.7 \pm 8.8	6.54	131.9 \pm 8.0	6.13	117.5 \pm 6.6
Fe 2	5197.567	3.23	-2.100	33.2 \pm 2.0	4.58	26.3 \pm 1.9	4.46	—	—	72.3 \pm 4.0	6.09
Fe 2	5234.623	3.22	-2.230	37.5 \pm 2.4	4.78	33.1 \pm 2.0	4.72	—	—	77.8 \pm 4.2	6.35
Fe 2	5264.802	3.23	-3.120	—	—	—	43.0 \pm 2.9	6.76	37.5 \pm 2.3	6.24	26.7 \pm 1.5
Fe 2	5275.997	3.20	-1.940	44.1 \pm 2.8	4.59	39.5 \pm 2.4	4.52	—	—	—	—
Fe 2	5284.103	2.89	-2.990	—	—	—	—	—	—	—	39.2 \pm 2.3
Fe 2	5325.552	3.22	-3.120	—	—	—	38.6 \pm 2.3	6.63	30.7 \pm 1.6	6.05	—
Fe 2	5425.249	3.20	-3.160	—	—	—	38.4 \pm 2.3	6.64	—	—	—
Fe 2	5534.838	3.24	-2.730	—	—	—	—	—	50.4 \pm 2.9	6.18	41.9 \pm 2.3
Fe 2	5991.371	3.15	-3.540	—	—	—	30.1 \pm 2.3	6.74	—	—	—
Fe 2	6149.246	3.89	-2.720	—	—	—	28.4 \pm 2.3	6.70	—	—	—
Fe 2	6247.557	3.89	-2.310	—	—	—	48.7 \pm 2.7	6.86	37.8 \pm 2.1	6.20	29.0 \pm 1.9

Table 10. continued.

El.	λ	χ_{ex}	$\log(gf)$	EW $\pm\sigma$ (EW) log $\varepsilon(X) + 12$ [dex]				
				19	20	21	22	23
Fe 2	6369.459	2.89	-4.160	-	-	23.7 \pm 1.6	6.87	-
Fe 2	6416.919	3.89	-2.650	-	-	35.0 \pm 2.1	6.83	23.6 \pm 1.6
Fe 2	6432.676	2.89	-3.520	-	-	41.5 \pm 2.3	6.72	34.9 \pm 2.1
Fe 2	6456.379	3.90	-2.100	-	-	58.9 \pm 3.3	6.92	52.9 \pm 3.3
Fe 2	6516.077	2.89	-3.320	-	-	52.3 \pm 3.8	6.79	44.5 \pm 2.5
Co 1	3842.049	0.92	-0.770	-	-	48.4 \pm 3.9	1.85	-
Co 1	3845.468	0.92	0.010	-	-	78.8 \pm 6.1	1.67	-
Co 1	3995.307	0.92	-0.220	71.1 \pm 4.7	1.64	82.9 \pm 5.2	1.64	-
Co 1	4118.773	1.05	-0.490	55.8 \pm 4.5	1.90	-	-	101.6 \pm 5.8
Co 1	4121.318	0.92	-0.320	79.7 \pm 4.6	2.01	-	-	-
Co 1	5483.354	1.71	-1.490	-	-	-	-	97.8 \pm 6.1
Ni 1	3807.144	0.42	-1.230	98.0 \pm 7.0	3.12	113.7 \pm 7.1	3.26	-
Ni 1	3858.297	0.42	-0.960	-	-	110.0 \pm 6.8	2.84	-
Ni 1	4904.412	3.54	-0.170	-	-	-	-	-
Ni 1	5081.110	3.85	0.300	-	-	-	-	39.4 \pm 2.4
Ni 1	5084.096	3.68	0.030	-	-	-	-	34.1 \pm 2.0
Ni 1	5115.392	3.83	-0.110	-	-	-	-	-
Ni 1	5155.764	3.90	0.074	-	-	-	-	-
Ni 1	5476.904	1.83	-0.780	60.7 \pm 3.4	3.06	68.8 \pm 3.8	3.06	-
Ni 1	6128.973	1.68	-3.430	-	-	-	-	100.4 \pm 5.3
Ni 1	6176.812	4.09	-0.260	-	-	-	-	-
Ni 1	6327.599	1.68	-3.170	-	-	-	-	-
Ni 1	6482.798	1.93	-2.630	-	-	-	-	-
Ni 1	6586.310	1.95	-2.780	-	-	-	-	-
Ni 1	6643.630	1.68	-2.220	-	-	-	-	-
Ni 1	6767.772	1.83	-2.140	-	-	-	-	-
Cu 1	5105.537	1.39	-1.542	-	-	-	-	-
Zn 1	4810.528	4.08	-0.137	-	-	18.3 \pm 1.5	1.92	61.9 \pm 3.6
Sr 2	4077.709	0.00	0.167	101.7 \pm 6.3	-1.10	154.1 \pm 8.4	-0.14	-
Sr 2	4215.519	0.00	-0.145	95.9 \pm 5.5	-1.03	145.7 \pm 7.8	-0.02	-
Y 2	3600.732	0.18	0.280	-	-	-	-	-
Y 2	3774.330	0.13	0.210	-	-	83.6 \pm 5.8	-0.68	-
Y 2	4883.682	1.08	0.070	-	-	23.6 \pm 1.7	-0.92	80.5 \pm 4.1
Y 2	4900.119	1.03	-0.090	-	-	-	-	-
Y 2	5087.419	1.08	-0.170	-	-	16.6 \pm 1.1	-0.89	62.8 \pm 3.6
Y 2	5200.410	0.99	-0.570	-	-	-	-	58.0 \pm 3.2
Y 2	5402.774	1.84	-0.630	-	-	-	-	46.3 \pm 2.8
Zr 2	4149.198	0.80	-0.040	-	-	0.0 \pm 0.0	-0.36	-
Zr 2	4161.200	0.71	-0.590	-	-	0.0 \pm 0.0	-0.24	-
Zr 2	4208.980	0.71	-0.510	-	-	0.0 \pm 0.0	-0.23	-
Ba 2	4934.076	0.00	-0.150	54.6 \pm 3.6	-2.05	161.9 \pm 8.6	-0.27	-
Ba 2	5853.668	0.60	-1	-	-	43.5 \pm 2.6	-0.73	97.5 \pm 5.8
Ba 2	6141.713	0.70	-0.076	23.6 \pm 1.3	-1.89	93.0 \pm 5.0	-0.63	145.6 \pm 7.8
Ba 2	6496.897	0.60	-0.377	25.8 \pm 1.6	-1.69	92.4 \pm 4.9	-0.54	137.9 \pm 7.5
La 2	4086.710	0	-0.070	-	-	39.2 \pm 3.3	-1.46	-
La 2	6390.480	0.32	-1.410	-	-	-	-	-
Ce 2	3999.237	0.29	0.060	-	-	20.8 \pm 1.5	-0.91	-
Ce 2	5274.229	1.04	0.130	-	-	-	-	-
Nd 2	4109.450	0.32	0.350	-	-	-	-	-
Nd 2	4825.480	0.18	-0.420	-	-	-	-	44.3 \pm 3.5
Nd 2	5249.580	0.98	0.200	-	-	-	-	-
Nd 2	5319.810	0.55	-0.140	-	-	-	-	-
Eu 2	4129.708	0	0.220	-	-	68.3 \pm 4.4	-1.93	-
Eu 2	6645.103	1.38	0.121	-	-	-	-	-
						33.1 \pm 2.0	0.57	-

Table 11. Line parameters, observed equivalent widths and corresponding abundances of stars 24, 25, 26, 27, and 28 observed with UVES.

El.	λ	χ_{ex}	$\log(gf)$	EW $\pm\sigma$ (EW) log $\varepsilon(X) + 12$ [dex]				
				24	25	26	27	28
O 1	6300.304	0	-9.750	-	-	-	30.8 \pm 2.2	8.70
O 1	6363.776	0.02	-10.260	-	-	-	-	-
Na 1	5682.633	2.10	-0.706	-	-	54.0 \pm 3.0	4.81	-
Na 1	5688.205	2.10	-0.452	-	-	75.2 \pm 4.0	4.89	28.4 \pm 2.1
Na 1	5889.951	0.00	0.108	183.1 \pm 9.7	3.84	-	-	-
Na 1	5895.924	0.00	-0.194	165.2 \pm 9.2	3.92	-	-	-
Na 1	6154.226	2.10	-1.547	-	-	-	-	-
Na 1	6160.747	2.10	-1.246	-	-	20.9 \pm 1.4	4.72	32.7 \pm 2.2
Mg 1	4167.271	4.35	-0.745	69.5 \pm 3.9	5.53	-	-	-
Mg 1	5172.684	2.71	-0.450	205.1 \pm 15.6	5.20	-	-	-
Mg 1	5183.604	2.72	-0.239	203.9 \pm 13.2	4.98	-	-	-
Mg 1	5528.405	4.35	-0.498	81.1 \pm 4.6	5.39	190.4 \pm 10.8	6.55	126.5 \pm 6.8
Mg 1	5711.088	4.35	-1.724	-	-	99.0 \pm 5.3	6.56	53.3 \pm 3.0
						6.19	113.6 \pm 6.4	7.27
						-	82.8 \pm 4.2	6.38

Table 11. continued.

El.	λ	χ_{ex}	$\log(gf)$	EW $\pm\sigma$ (EW) log $\varepsilon(X) + 12$ [dex]					28
				24	25	26	27	28	
Al 1	6698.673	3.14	-1.647	-	-	-	-	31.7 \pm 2.2	5.98
Si 1	5645.613	4.93	-2.140	-	-	-	-	37.0 \pm 2.4	7.29
Si 1	5665.555	4.92	-2.040	-	-	-	-	37.2 \pm 2.3	7.19
Si 1	5684.484	4.95	-1.650	-	-	42.8 \pm 2.5	6.56	20.0 \pm 1.6	6.17
Si 1	5690.425	4.93	-1.870	-	-	32.4 \pm 1.8	6.55	-	-
Si 1	5701.104	4.93	-2.050	-	-	-	-	37.2 \pm 2.6	7.21
Si 1	5708.399	4.95	-1.470	-	-	-	-	-	-
Si 1	5948.541	5.08	-1.230	-	-	63.3 \pm 3.4	6.68	33.2 \pm 1.7	6.20
Si 1	6243.814	5.62	-1.244	-	-	-	-	77.8 \pm 4.8	7.37
Ca 1	5349.465	2.71	-0.310	-	-	104.8 \pm 5.5	5.40	58.3 \pm 3.3	4.92
Ca 1	5581.965	2.52	-0.555	-	-	108.2 \pm 5.6	5.39	59.2 \pm 3.1	4.94
Ca 1	5588.749	2.53	0.358	58.9 \pm 3.3	3.93	155.2 \pm 8.4	5.40	99.0 \pm 5.3	4.95
Ca 1	5590.114	2.52	-0.571	20.8 \pm 1.8	4.07	101.7 \pm 5.5	5.26	56.3 \pm 2.9	4.89
Ca 1	5601.277	2.53	-0.523	23.2 \pm 1.6	4.09	-	-	60.6 \pm 3.2	4.94
Ca 1	5857.451	2.93	0.240	35.0 \pm 2.3	4.06	128.5 \pm 7.1	5.39	79.4 \pm 4.5	5.01
Ca 1	6102.723	1.88	-0.793	47.6 \pm 2.7	4.03	153.1 \pm 8.4	5.38	93.1 \pm 5.0	5.03
Ca 1	6122.217	1.89	-0.316	77.0 \pm 3.9	4.09	181.0 \pm 9.8	5.30	121.3 \pm 6.9	5.04
Ca 1	6161.297	2.52	-1.266	-	-	73.0 \pm 4.5	5.31	25.0 \pm 1.6	4.88
Ca 1	6162.173	1.90	-0.090	92.4 \pm 4.6	4.18	198.4 \pm 11.5	5.27	134.6 \pm 7.4	5.01
Ca 1	6166.439	2.52	-1.142	-	-	83.4 \pm 4.6	5.38	30.6 \pm 1.9	4.89
Ca 1	6169.042	2.52	-0.797	-	-	102.4 \pm 5.5	5.39	50.4 \pm 2.6	4.95
Ca 1	6169.563	2.53	-0.478	-	-	119.7 \pm 6.5	5.41	68.6 \pm 3.8	5.00
Ca 1	6439.075	2.53	0.390	67.0 \pm 3.4	3.99	173.4 \pm 9.3	5.45	116.3 \pm 6.1	5.16
Ca 1	6455.598	2.52	-1.340	-	-	69.8 \pm 3.8	5.31	-	-
Ca 1	6499.650	2.52	-0.818	-	-	102.6 \pm 5.6	5.38	-	-
Sc 2	4246.822	0.31	0.242	130.2 \pm 7.3	0.55	-	-	153.8 \pm 8.7	1.59
Sc 2	4415.557	0.60	-0.668	-	-	-	-	90.4 \pm 6.0	1.47
Sc 2	5031.021	1.36	-0.400	-	-	102.1 \pm 5.5	1.94	70.1 \pm 4.2	1.57
Sc 2	5526.790	1.77	0.024	38.5 \pm 2.2	0.47	-	-	-	-
Sc 2	6604.601	1.36	-1.309	-	-	-	-	29.3 \pm 2.2	1.53
Ti 1	3998.636	0.05	0.020	-	-	-	-	94.3 \pm 6.5	3.23
Ti 1	4840.874	0.90	-0.430	-	-	114.3 \pm 6.1	3.80	49.0 \pm 3.1	3.24
Ti 1	4913.613	1.87	0.220	-	-	80.2 \pm 4.5	3.68	26.6 \pm 2.0	3.27
Ti 1	4981.730	0.85	0.570	-	-	167.5 \pm 9.1	3.75	98.4 \pm 5.5	3.37
Ti 1	4997.097	0	-2.070	-	-	107.3 \pm 5.8	3.86	-	-
Ti 1	4999.503	0.83	0.320	52.8 \pm 2.9	2.31	172.8 \pm 9.6	4.04	93.4 \pm 5.3	3.47
Ti 1	5016.161	0.85	-0.480	-	-	119.3 \pm 6.7	3.78	49.2 \pm 2.8	3.20
Ti 1	5039.958	0.02	-1.080	-	-	149.2 \pm 7.9	4.06	72.9 \pm 3.9	3.33
Ti 1	5064.653	0.05	-0.940	-	-	161.5 \pm 9.1	4.27	79.5 \pm 4.3	3.39
Ti 1	5145.460	1.46	-0.540	-	-	-	-	-	-
Ti 1	5192.969	0.02	-0.950	39.2 \pm 2.2	2.30	183.0 \pm 10.0	4.62	81.2 \pm 4.9	3.38
Ti 1	5210.384	0.05	-0.820	43.0 \pm 2.4	2.27	-	-	123.4 \pm 6.6	4.83
Ti 1	5490.147	1.46	-0.840	-	-	56.8 \pm 3.3	3.61	-	-
Ti 1	5978.541	1.87	-0.496	-	-	57.5 \pm 3.1	3.81	-	-
Ti 1	6126.216	1.07	-1.425	-	-	73.7 \pm 4.1	3.84	-	-
Ti 1	6258.102	1.44	-0.390	-	-	102.7 \pm 5.9	3.81	32.8 \pm 2.0	3.40
Ti 1	6554.223	1.44	-1.150	-	-	51.3 \pm 2.8	3.70	-	-
Ti 1	6556.062	1.46	-1.060	-	-	63.8 \pm 3.5	3.83	-	-
Ti 1	6743.122	0.90	-1.630	-	-	68.7 \pm 3.8	3.65	-	-
Ti 2	3761.321	0.57	0.180	168.9 \pm 10.0	2.26	-	-	-	-
Ti 2	4417.713	1.16	-1.190	102.2 \pm 6.2	2.91	-	-	-	-
Ti 2	4418.331	1.24	-1.990	-	-	-	-	71.3 \pm 4.8	3.63
Ti 2	4443.801	1.08	-0.710	119.4 \pm 6.8	2.71	-	-	138.5 \pm 8.3	3.68
Ti 2	4444.554	1.12	-2.200	49.0 \pm 3.2	2.59	-	-	75.5 \pm 5.0	3.82
Ti 2	4468.493	1.13	-0.630	-	-	-	-	-	-
Ti 2	4798.531	1.08	-2.660	27.6 \pm 1.7	2.53	-	-	-	-
Ti 2	4865.610	1.12	-2.700	22.8 \pm 1.8	2.50	93.6 \pm 4.7	4.26	50.8 \pm 2.7	3.61
Ti 2	5129.156	1.89	-1.340	-	-	-	-	78.2 \pm 4.2	3.82
Ti 2	5154.068	1.57	-1.750	45.3 \pm 2.4	2.54	-	-	71.9 \pm 3.8	3.68
Ti 2	5185.902	1.89	-1.410	40.6 \pm 2.4	2.52	-	-	68.4 \pm 3.6	3.64
Ti 2	5336.786	1.58	-1.600	-	-	112.9 \pm 5.9	4.12	80.2 \pm 4.3	3.73
Ti 2	5381.021	1.57	-1.970	35.3 \pm 2.0	2.56	101.5 \pm 5.4	4.21	64.4 \pm 3.5	3.69
Ti 2	5418.768	1.58	-2.130	30.0 \pm 1.9	2.62	84.8 \pm 4.7	4.02	54.1 \pm 3.2	3.63
Ti 2	6559.563	2.05	-2.175	-	-	51.5 \pm 2.8	3.94	-	-
V 1	4379.230	0.30	0.580	-	-	-	-	-	-
V 1	6216.364	0.28	-1.330	-	-	80.2 \pm 4.2	2.69	-	-
V 1	6233.164	0.28	-2.070	-	-	27.7 \pm 4.6	2.58	-	-
Cr 1	4254.352	0.00	-0.090	117.4 \pm 6.3	2.65	-	-	-	-
Cr 1	5206.023	0.94	0.020	85.0 \pm 4.4	2.62	-	-	-	-
Cr 1	5296.691	0.98	-1.360	-	-	137.1 \pm 7.5	4.42	61.4 \pm 3.2	3.70
Cr 1	5298.271	0.98	-1.140	-	-	-	-	83.5 \pm 5.1	5.22
Cr 1	5300.745	0.98	-2.016	-	-	101.8 \pm 5.4	4.25	26.9 \pm 2.1	3.59
Cr 1	5345.796	1.00	-0.896	-	-	157.6 \pm 8.3	4.39	82.3 \pm 4.7	3.77
Cr 1	5348.314	1	-1.210	24.9 \pm 1.6	2.67	140.6 \pm 7.6	4.35	67.5 \pm 3.7	3.71
								116.1 \pm 6.1	5.18
								127.1 \pm 6.7	4.21

Table 11. continued.

El.	λ	χ_{ex}	$\log(gf)$	EW±σ(EW) log ε(X) + 12 [dex]				
				24	25	26	27	28
Cr I	5409.784	1.03	-0.670	50.7 ± 3.1	2.67	-	94.6 ± 5.3	3.88
Cr I	6330.091	0.94	-2.920	-	-	63.8 ± 3.4	4.20	-
Mn I	4033.060	0.00	-0.644	119.0 ± 6.5	2.21	-	-	45.6 ± 2.7
Mn I	5420.351	2.14	-1.462	-	-	87.8 ± 5.6	3.58	-
Mn I	5432.539	0	-3.795	-	-	126.0 ± 6.5	3.51	84.7 ± 5.3
Mn I	5516.766	2.18	-1.847	-	-	-	-	4.19
Fe I	3753.611	2.18	-0.890	81.0 ± 4.5	4.86	-	-	-
Fe I	4032.627	1.49	-2.377	59.8 ± 3.5	4.73	-	-	-
Fe I	4067.978	3.21	-0.472	52.3 ± 3.5	4.77	-	-	-
Fe I	4114.445	2.83	-1.303	36.7 ± 2.6	4.80	-	-	-
Fe I	4147.668	1.49	-2.104	81.2 ± 5.3	5.00	-	-	-
Fe I	4154.805	3.37	-0.400	50.8 ± 3.1	4.84	-	-	-
Fe I	4156.799	2.83	-0.809	61.6 ± 5.9	4.87	-	-	-
Fe I	4175.636	2.85	-0.827	58.4 ± 3.2	4.82	-	-	-
Fe I	4181.754	2.83	-0.371	80.6 ± 4.9	4.94	-	-	-
Fe I	4182.382	3.02	-1.180	27.9 ± 1.9	4.69	-	-	-
Fe I	4184.892	2.83	-0.869	51.6 ± 3.6	4.68	-	84.5 ± 5.2	5.88
Fe I	4187.039	2.45	-0.548	97.8 ± 5.4	5.02	-	-	-
Fe I	4199.095	3.05	0.155	80.0 ± 4.6	4.67	-	-	-
Fe I	4202.029	1.49	-0.708	129.2 ± 8.1	4.75	-	-	-
Fe I	4217.545	3.43	-0.484	39.0 ± 2.7	4.74	-	-	-
Fe I	4222.213	2.45	-0.967	76.9 ± 5.0	4.91	-	-	-
Fe I	4233.603	2.48	-0.604	84.2 ± 4.9	4.77	-	-	-
Fe I	4443.194	2.86	-1.043	49.8 ± 4.1	4.81	-	-	-
Fe I	4447.717	2.22	-1.342	-	-	-	108.4 ± 6.5	5.85
Fe I	4786.807	3.02	-1.606	-	-	-	53.3 ± 2.8	5.76
Fe I	4789.651	3.55	-0.958	-	-	-	52.6 ± 3.3	5.71
Fe I	4859.741	2.88	-0.764	-	-	146.7 ± 8.6	6.13	-
Fe I	4871.318	2.87	-0.363	79.0 ± 4.5	4.71	-	-	-
Fe I	4872.138	2.88	-0.567	67.0 ± 3.7	4.66	-	111.9 ± 6.1	5.62
Fe I	4890.755	2.88	-0.394	81.8 ± 4.6	4.81	-	100.6 ± 5.4	5.64
Fe I	4891.492	2.85	-0.112	93.5 ± 5.8	4.77	-	119.9 ± 6.8	5.78
Fe I	4903.310	2.88	-0.926	55.8 ± 3.0	4.77	-	-	-
Fe I	4918.994	2.87	-0.342	84.2 ± 4.8	4.79	-	91.6 ± 5.0	5.80
Fe I	4920.502	2.83	0.068	105.5 ± 6.4	4.81	-	113.9 ± 6.4	5.62
Fe I	4924.770	2.28	-2.241	34.0 ± 2.3	4.91	128.2 ± 7.1	6.50	-
Fe I	4938.814	2.88	-1.077	48.9 ± 3.0	4.78	135.0 ± 7.1	6.23	-
Fe I	4966.088	3.33	-0.871	-	-	-	78.2 ± 4.5	5.97
Fe I	5001.863	3.88	0.010	38.7 ± 2.2	4.71	-	-	-
Fe I	5006.119	2.83	-0.638	73.3 ± 4.2	4.79	165.3 ± 10.1	6.14	-
Fe I	5014.942	3.94	-0.303	-	-	-	63.7 ± 3.4	5.78
Fe I	5044.211	2.85	-2.038	-	-	-	45.7 ± 2.8	5.76
Fe I	5049.820	2.28	-1.355	74.9 ± 4.0	4.85	-	-	-
Fe I	5068.766	2.94	-1.042	46.5 ± 3.1	4.76	130.4 ± 7.2	6.15	-
Fe I	5074.748	4.22	-0.200	-	-	-	82.0 ± 4.4	5.74
Fe I	5079.223	2.20	-2.067	-	-	-	60.4 ± 3.5	5.90
Fe I	5131.468	2.22	-2.515	23.0 ± 1.7	4.85	-	-	-
Fe I	5141.739	2.42	-1.964	25.2 ± 1.9	4.60	118.8 ± 6.2	6.14	-
Fe I	5162.272	4.18	0.020	32.0 ± 2.5	4.91	-	71.3 ± 4.1	5.89
Fe I	5171.596	1.49	-1.793	100.9 ± 5.5	4.88	-	-	-
Fe I	5191.455	3.04	-0.551	62.0 ± 3.3	4.68	-	-	-
Fe I	5192.344	3.00	-0.421	68.9 ± 4.1	4.65	-	-	-
Fe I	5194.941	1.56	-2.090	83.3 ± 4.4	4.85	-	104.8 ± 5.9	5.73
Fe I	5198.711	2.22	-2.135	36.2 ± 2.2	4.75	-	75.6 ± 4.3	5.80
Fe I	5202.336	2.18	-1.838	57.9 ± 3.2	4.81	177.5 ± 10.0	6.55	-
Fe I	5215.180	3.27	-0.871	36.8 ± 2.4	4.79	124.8 ± 6.9	6.29	-
Fe I	5216.274	1.61	-2.150	78.8 ± 4.7	4.86	-	-	-
Fe I	5217.389	3.21	-1.070	29.9 ± 1.9	4.77	116.4 ± 6.2	6.25	112.6 ± 6.4
Fe I	5232.940	2.94	-0.058	90.6 ± 5.4	4.69	-	71.5 ± 3.8	5.81
Fe I	5242.491	3.63	-0.967	-	-	-	108.5 ± 5.7	6.90
Fe I	5253.021	2.28	-3.940	-	-	47.2 ± 2.6	5.67	-
Fe I	5266.555	3.00	-0.386	73.6 ± 4.2	4.71	-	-	-
Fe I	5281.790	3.04	-0.834	49.3 ± 2.7	4.71	144.8 ± 7.9	6.25	125.4 ± 7.1
Fe I	5283.621	3.24	-0.432	55.4 ± 3.3	4.67	-	-	6.24
Fe I	5288.525	3.69	-1.508	-	-	112.6 ± 6.4	6.82	-
Fe I	5302.300	3.28	-0.720	40.6 ± 2.3	4.72	-	-	-
Fe I	5307.361	1.61	-2.987	-	-	75.1 ± 4.2	5.88	128.8 ± 6.9
Fe I	5322.041	2.28	-2.803	-	-	108.7 ± 6.1	5.62	-
Fe I	5324.179	3.21	-0.103	76.6 ± 4.2	4.75	-	110.4 ± 6.1	6.68
Fe I	5332.899	1.56	-2.777	39.7 ± 2.5	4.62	-	82.7 ± 4.6	6.82
Fe I	5339.929	3.27	-0.647	43.5 ± 2.5	4.68	134.0 ± 7.3	6.20	-
Fe I	5364.871	4.45	0.228	26.3 ± 1.7	4.88	106.2 ± 5.6	6.32	106.4 ± 6.2
Fe I	5365.399	3.57	-1.020	-	-	92.1 ± 5.2	6.13	89.5 ± 4.9
Fe I	5367.466	4.41	0.443	32.6 ± 2.2	4.77	111.4 ± 6.4	6.17	105.4 ± 6.8

Table 11. continued.

El.	λ	χ_{ex}	$\log(gf)$	EW $\pm\sigma$ (EW) log $\varepsilon(X) + 12$ [dex]							
				24	25	26	27	28	29	30	31
Fe 1	5369.961	4.37	0.536	37.7 \pm 2.7	4.73	120.7 \pm 6.5	6.20	76.8 \pm 4.4	5.69	—	—
Fe 1	5379.574	3.69	-1.514	—	—	66.2 \pm 3.5	6.20	—	—	59.5 \pm 3.7	6.13
Fe 1	5383.369	4.31	0.645	43.3 \pm 2.6	4.66	124.6 \pm 6.6	6.09	79.9 \pm 4.2	5.59	—	130.7 \pm 7.0
Fe 1	5389.479	4.41	-0.410	—	—	81.9 \pm 4.3	6.39	—	—	69.8 \pm 3.6	6.80
Fe 1	5393.167	3.24	-0.715	41.9 \pm 2.5	4.69	132.0 \pm 7.3	6.19	81.6 \pm 4.7	5.71	—	—
Fe 1	5410.910	4.47	0.398	26.9 \pm 1.7	4.76	102.9 \pm 5.6	6.11	65.6 \pm 4.0	5.69	—	—
Fe 1	5415.199	4.39	0.642	—	—	124.8 \pm 6.6	6.18	75.8 \pm 4.3	5.58	—	105.6 \pm 5.8
Fe 1	5424.068	4.32	0.520	—	—	—	—	84.3 \pm 4.5	5.82	—	121.3 \pm 6.7
Fe 1	5445.042	4.39	-0.020	—	—	—	—	56.8 \pm 3.1	5.81	—	135.0 \pm 7.2
Fe 1	5560.211	4.43	-1.190	—	—	39.9 \pm 2.3	6.31	—	—	46.2 \pm 3.0	7.00
Fe 1	5569.618	3.42	-0.486	—	—	138.9 \pm 7.6	6.25	83.9 \pm 4.4	5.71	—	—
Fe 1	5572.842	3.40	-0.275	54.3 \pm 3.1	4.66	150.3 \pm 7.8	6.19	—	—	—	—
Fe 1	5576.089	3.43	-1	28.5 \pm 2.3	4.92	124.1 \pm 6.5	6.52	—	—	—	119.5 \pm 6.3
Fe 1	5586.755	3.37	-0.120	67.0 \pm 3.7	4.72	166.1 \pm 9.4	6.20	106.3 \pm 5.6	5.73	—	166.9 \pm 9.2
Fe 1	5615.644	3.33	0.050	73.9 \pm 4.4	4.65	172.8 \pm 10.0	6.05	—	—	—	—
Fe 1	5618.632	4.21	-1.276	—	—	44.1 \pm 2.5	6.18	—	—	52.2 \pm 2.9	6.98
Fe 1	5662.516	4.18	-0.573	—	—	92.8 \pm 5.0	6.40	44.9 \pm 2.4	5.82	83.4 \pm 4.5	6.87
Fe 1	5701.544	2.56	-2.216	—	—	117.4 \pm 6.2	6.37	57.5 \pm 3.3	5.79	95.5 \pm 5.5	7.06
Fe 1	5753.122	4.26	-0.688	—	—	72.7 \pm 3.8	6.22	34.5 \pm 1.8	5.82	69.7 \pm 4.1	6.89
Fe 1	6003.011	3.88	-1.120	—	—	84.6 \pm 4.8	6.37	34.5 \pm 2.2	5.78	78.1 \pm 4.2	7.05
Fe 1	6024.058	4.55	-0.120	—	—	—	—	48.7 \pm 2.6	5.89	91.7 \pm 4.8	7.07
Fe 1	6027.051	4.08	-1.089	—	—	64.9 \pm 3.6	6.19	—	—	64.0 \pm 3.6	6.90
Fe 1	6056.004	4.73	-0.460	—	—	56.2 \pm 3.1	6.26	—	—	63.8 \pm 3.7	7.01
Fe 1	6065.482	2.61	-1.530	50.8 \pm 2.9	4.83	153.7 \pm 8.9	6.35	86.9 \pm 4.5	5.82	—	150.8 \pm 7.9
Fe 1	6078.491	4.80	-0.321	—	—	58.4 \pm 3.1	6.25	—	—	—	—
Fe 1	6079.008	4.65	-1.120	—	—	31.1 \pm 1.9	6.32	—	—	39.0 \pm 2.4	6.98
Fe 1	6082.710	2.22	-3.573	—	—	66.7 \pm 3.9	6.17	—	—	52.0 \pm 3.1	6.88
Fe 1	6136.615	2.45	-1.400	66.9 \pm 3.4	4.81	167.8 \pm 9.5	6.23	99.5 \pm 5.4	5.78	141.0 \pm 7.8	6.82
Fe 1	6137.691	2.59	-1.403	57.2 \pm 3.1	4.79	—	—	96.1 \pm 5.3	5.87	—	—
Fe 1	6151.617	2.18	-3.299	—	—	89.4 \pm 4.7	6.24	—	—	63.0 \pm 3.7	6.81
Fe 1	6157.728	4.08	-1.260	—	—	65.1 \pm 3.8	6.36	—	—	63.8 \pm 3.6	7.06
Fe 1	6165.360	4.14	-1.474	—	—	37.6 \pm 2.2	6.13	—	—	44.2 \pm 2.6	6.86
Fe 1	6173.334	2.22	-2.880	—	—	108.2 \pm 6.1	6.25	46.6 \pm 2.9	5.77	83.8 \pm 4.7	6.97
Fe 1	6180.203	2.73	-2.586	—	—	80.9 \pm 4.2	6.14	—	—	—	76.8 \pm 4.2
Fe 1	6187.989	3.94	-1.720	—	—	46.2 \pm 2.7	6.28	—	—	48.0 \pm 2.6	6.97
Fe 1	6191.558	2.43	-1.417	67.3 \pm 3.5	4.80	170.3 \pm 9.6	6.22	103.5 \pm 5.8	5.84	—	—
Fe 1	6200.312	2.61	-2.437	—	—	107.3 \pm 5.7	6.36	41.0 \pm 2.4	5.68	—	103.0 \pm 5.4
Fe 1	6213.429	2.22	-2.482	23.1 \pm 1.7	4.74	129.1 \pm 7.0	6.24	—	—	—	123.6 \pm 6.5
Fe 1	6219.280	2.20	-2.433	30.2 \pm 1.8	4.82	134.5 \pm 7.5	6.25	72.0 \pm 4.1	5.84	105.7 \pm 5.4	6.95
Fe 1	6229.226	2.85	-2.805	—	—	59.5 \pm 3.4	6.11	—	—	48.2 \pm 2.5	6.75
Fe 1	6240.646	2.22	-3.233	—	—	85.2 \pm 4.9	6.17	—	—	—	80.0 \pm 4.7
Fe 1	6246.318	3.60	-0.733	—	—	117.1 \pm 6.3	6.22	65.3 \pm 3.5	5.70	—	114.8 \pm 6.4
Fe 1	6252.555	2.40	-1.687	58.3 \pm 3.0	4.86	161.2 \pm 8.5	6.30	91.5 \pm 5.0	5.81	—	156.2 \pm 8.2
Fe 1	6265.132	2.18	-2.550	24.1 \pm 1.7	4.77	132.5 \pm 7.0	6.29	65.0 \pm 3.5	5.76	99.4 \pm 5.2	6.91
Fe 1	6290.965	4.73	-0.774	—	—	—	—	—	—	48.5 \pm 3.1	6.94
Fe 1	6297.792	2.22	-2.740	—	—	—	—	—	—	—	124.9 \pm 6.9
Fe 1	6301.500	3.65	-0.718	28.8 \pm 2.2	4.87	113.0 \pm 5.9	6.18	—	—	—	124.4 \pm 6.4
Fe 1	6302.494	3.69	-0.973	—	—	88.5 \pm 4.7	5.99	—	—	—	—
Fe 1	6322.685	2.59	-2.426	—	—	110.7 \pm 6.0	6.36	—	—	87.0 \pm 4.9	7.04
Fe 1	6335.330	2.20	-2.177	39.7 \pm 2.3	4.74	—	—	79.3 \pm 4.2	5.74	112.3 \pm 5.8	6.79
Fe 1	6344.148	2.43	-2.923	—	—	—	—	31.2 \pm 1.9	5.74	—	—
Fe 1	6355.028	2.85	-2.350	—	—	—	—	37.0 \pm 2.3	5.79	72.4 \pm 5.0	6.90
Fe 1	6380.743	4.19	-1.376	—	—	44.9 \pm 2.6	6.22	—	—	46.9 \pm 2.5	6.87
Fe 1	6392.538	2.28	-4.030	—	—	42.6 \pm 2.6	6.25	—	—	27.8 \pm 1.9	6.79
Fe 1	6393.601	2.43	-1.432	59.7 \pm 3.2	4.65	167.2 \pm 9.0	6.12	97.8 \pm 5.1	5.70	134.0 \pm 7.5	6.68
Fe 1	6400	3.60	-0.290	46.8 \pm 2.5	4.73	—	—	—	—	—	—
Fe 1	6408.018	3.69	-1.018	—	—	—	—	43.1 \pm 2.7	5.60	86.4 \pm 4.6	6.83
Fe 1	6411.648	3.65	-0.595	28.4 \pm 1.8	4.73	124.8 \pm 6.8	6.26	67.7 \pm 3.6	5.67	113.7 \pm 6.3	6.83
Fe 1	6419.949	4.73	-0.240	—	—	67.3 \pm 3.5	6.24	—	—	73.1 \pm 3.9	6.98
Fe 1	6421.350	2.28	-2.027	47.4 \pm 2.7	4.83	—	—	88.4 \pm 4.8	5.92	—	155.1 \pm 8.2
Fe 1	6430.845	2.18	-2.006	56.0 \pm 2.9	4.83	165.3 \pm 9.1	6.21	96.0 \pm 5.1	5.89	124.4 \pm 6.8	6.76
Fe 1	6494.980	2.40	-1.273	78.5 \pm 4.0	4.81	190.4 \pm 10.9	6.19	111.7 \pm 6.0	5.77	—	189.5 \pm 10.8
Fe 1	6518.366	2.83	-2.460	—	—	83.6 \pm 4.5	6.17	27.3 \pm 2.1	5.66	69.8 \pm 3.9	6.91
Fe 1	6581.209	1.49	-4.679	—	—	61.9 \pm 3.3	6.11	—	—	34.9 \pm 2.4	6.63
Fe 1	6592.913	2.73	-1.473	40.2 \pm 2.2	4.69	—	—	80.5 \pm 4.4	5.71	—	147.0 \pm 7.8
Fe 1	6593.870	2.43	-2.422	—	—	123.7 \pm 6.5	6.34	59.3 \pm 3.4	5.81	100.8 \pm 5.5	7.11
Fe 1	6608.025	2.28	-4.030	—	—	42.3 \pm 2.4	6.23	—	—	29.4 \pm 2.0	6.82
Fe 1	6609.110	2.56	-2.692	—	—	98.6 \pm 5.4	6.30	35.3 \pm 2.4	5.73	78.2 \pm 4.4	7.02
Fe 1	6677.985	2.69	-1.418	58.3 \pm 3.1	4.92	160.9 \pm 8.9	6.31	—	—	131.6 \pm 7.6	6.90
Fe 1	6750.151	2.42	-2.621	—	—	113.3 \pm 6.3	6.33	47.5 \pm 3.1	5.74	85.1 \pm 4.6	6.97
Fe 2	4178.854	2.58	-2.500	57.7 \pm 3.9	4.86	—	—	—	—	—	—
Fe 2	4923.921	2.89	-1.320	96.0 \pm 5.3	4.82	—	—	116.1 \pm 6.9	5.82	—	—
Fe 2	5018.436	2.89	-1.220	103.2 \pm 5.9	4.86	—	—	—	—	—	—
Fe 2	5197.567	3.23	-2.100	38.8 \pm 3.3	4.73	—	—	—	—	—	—

Table 11. continued.

El.	λ	χ_{ex}	$\log(gf)$	EW $\pm\sigma$ (EW) $\log \varepsilon(X) + 12$ [dex]							
				24	25	26	27	28	24	25	26
Fe 2	5234.623	3.22	-2.230	45.3 \pm 2.6	4.98	86.2 \pm 4.7	6.41	-	-	76.9 \pm 4.6	7.06
Fe 2	5264.802	3.23	-3.120	-	-	43.1 \pm 2.7	6.29	-	-	-	-
Fe 2	5284.103	2.89	-2.990	-	-	-	-	38.7 \pm 2.4	5.66	-	-
Fe 2	5414.070	3.22	-3.540	-	-	22.0 \pm 1.8	6.14	-	-	-	-
Fe 2	5534.838	3.24	-2.730	-	-	-	-	41.2 \pm 2.3	5.87	-	-
Fe 2	5991.371	3.15	-3.540	-	-	-	-	-	-	22.6 \pm 1.6	6.75
Fe 2	6149.246	3.89	-2.720	-	-	25.9 \pm 1.9	6.27	-	-	23.4 \pm 1.7	6.78
Fe 2	6247.557	3.89	-2.310	-	-	-	-	28.8 \pm 1.9	5.89	41.1 \pm 3.1	6.92
Fe 2	6416.919	3.89	-2.650	-	-	31.6 \pm 2.1	6.37	-	-	29.5 \pm 1.9	6.91
Fe 2	6432.676	2.89	-3.520	-	-	39.5 \pm 2.6	6.18	24.3 \pm 1.8	5.80	-	-
Fe 2	6456.379	3.90	-2.100	-	-	53.2 \pm 3.3	6.37	39.6 \pm 2.3	5.96	48.4 \pm 3.0	6.92
Fe 2	6516.077	2.89	-3.320	-	-	-	-	32.4 \pm 2.3	5.80	46.4 \pm 2.8	6.92
Co 1	3845.468	0.92	0.010	90.8 \pm 5.4	2.22	-	-	-	-	-	-
Co 1	3995.307	0.92	-0.220	86.9 \pm 4.7	1.93	-	-	-	-	-	-
Co 1	4121.318	0.92	-0.320	-	-	-	-	113.7 \pm 8.8	3.25	144.6 \pm 9.8	4.39
Co 1	5483.354	1.71	-1.490	-	-	104.3 \pm 5.4	3.98	-	-	85.5 \pm 4.7	4.77
Co 1	5647.234	2.28	-1.560	-	-	29.7 \pm 1.6	3.50	-	-	30.1 \pm 1.8	4.28
Ni 1	3858.297	0.42	-0.960	111.5 \pm 7.4	3.24	-	-	-	-	-	-
Ni 1	4904.412	3.54	-0.170	-	-	83.3 \pm 4.8	4.97	43.8 \pm 2.6	4.45	-	-
Ni 1	5081.110	3.85	0.300	-	-	-	-	47.6 \pm 2.5	4.42	-	-
Ni 1	5084.096	3.68	0.030	-	-	76.8 \pm 4.2	4.78	41.2 \pm 2.7	4.34	-	-
Ni 1	5115.392	3.83	-0.110	-	-	64.7 \pm 3.5	4.84	28.6 \pm 1.7	4.38	65.0 \pm 3.9	5.60
Ni 1	5476.904	1.83	-0.780	75.6 \pm 4.0	3.39	-	-	111.8 \pm 6.3	4.51	-	-
Ni 1	6128.973	1.68	-3.430	-	-	56.3 \pm 3.4	4.97	-	-	37.8 \pm 2.5	5.57
Ni 1	6176.812	4.09	-0.260	-	-	49.6 \pm 2.9	4.93	-	-	57.8 \pm 3.4	5.75
Ni 1	6177.242	1.83	-3.460	-	-	30.9 \pm 2.0	4.74	-	-	26.5 \pm 2.1	5.49
Ni 1	6327.599	1.68	-3.170	-	-	75.4 \pm 3.9	5.04	-	-	62.5 \pm 4.0	5.91
Ni 1	6482.798	1.93	-2.630	-	-	74.7 \pm 3.9	4.83	-	-	62.6 \pm 3.5	5.67
Ni 1	6586.310	1.95	-2.780	-	-	70.5 \pm 4.0	4.92	-	-	56.6 \pm 3.6	5.68
Ni 1	6643.630	1.68	-2.220	25.8 \pm 1.7	3.56	142.0 \pm 7.6	5.29	66.8 \pm 3.8	4.59	114.6 \pm 6.1	6.09
Ni 1	6767.772	1.83	-2.140	-	-	119.7 \pm 6.3	5.00	56.2 \pm 3.1	4.46	90.1 \pm 5.5	5.69
Cu 1	5105.537	1.39	-1.542	-	-	-	-	28.3 \pm 1.6	1.76	-	-
Zn 1	4810.528	4.08	-0.137	18.1 \pm 1.4	1.94	56.3 \pm 3.4	3.15	46.5 \pm 2.7	2.97	65.0 \pm 4.2	4.09
Sr 2	4215.519	0.00	-0.145	139.6 \pm 8.1	0.22	-	-	-	-	-	-
Y 2	3600.732	0.18	0.280	66.2 \pm 6.4	-0.84	-	-	87.8 \pm 9.6	0.61	-	-
Y 2	3774.330	0.13	0.210	66.2 \pm 5.8	-0.96	-	-	-	-	-	-
Y 2	4883.682	1.08	0.070	24.3 \pm 2.1	-0.83	90.6 \pm 5.0	0.94	58.7 \pm 3.3	0.55	74.9 \pm 4.2	1.91
Y 2	5087.419	1.08	-0.170	-	-	75.4 \pm 3.9	0.78	44.3 \pm 2.5	0.39	58.2 \pm 4.0	1.65
Y 2	5200.410	0.99	-0.570	-	-	-	-	38.3 \pm 2.3	0.52	-	-
Y 2	5205.722	1.03	-0.340	-	-	-	-	45.2 \pm 2.9	0.51	-	-
Y 2	5402.774	1.84	-0.630	-	-	24.1 \pm 1.7	1.03	-	-	-	-
Ba 2	4934.076	0.00	-0.150	118.3 \pm 6.6	-0.81	-	-	170.4 \pm 10.7	0.82	-	-
Ba 2	5853.668	0.60	-1	-	-	114.0 \pm 6.6	1.24	72.9 \pm 4.1	0.80	80.0 \pm 5.0	2.05
Ba 2	6141.713	0.70	-0.076	61.8 \pm 3.2	-1.08	169.0 \pm 9.6	1.47	113.5 \pm 6.1	0.90	123.7 \pm 6.9	1.94
Ba 2	6496.897	0.60	-0.377	55.9 \pm 3.0	-1.06	168.1 \pm 9.0	1.51	114.1 \pm 6.6	0.99	112.9 \pm 6.3	1.93
La 2	3988.520	0.40	0.170	-	-	-	-	-	-	82.6 \pm 10.2	1.97
La 2	4804.040	0.23	-1.490	-	-	-	-	-	-	-	33.0 \pm 2.6
La 2	4920.980	0.13	-0.580	-	-	-	-	-	-	-	-
La 2	5290.820	0	-1.650	-	-	-	-	32.7 \pm 3.6	-0.34	-	-
La 2	5303.530	0.32	-1.350	-	-	24.1 \pm 1.7	0.07	-	-	-	-
La 2	6320.376	0.17	-1.610	-	-	25.2 \pm 2.0	0.09	-	-	-	-
La 2	6390.480	0.32	-1.410	-	-	22.9 \pm 1.6	0.03	-	-	-	-
La 2	6774.268	0.13	-1.820	-	-	19.9 \pm 1.5	0.07	-	-	-	-
Ce 2	5187.458	1.21	0.170	-	-	28.0 \pm 2.1	0.53	-	-	-	-
Ce 2	5274.229	1.04	0.130	-	-	25.7 \pm 1.7	0.29	-	-	-	-
Ce 2	5330.556	0.87	-0.400	-	-	-	-	-	-	-	-
Pr 2	5322.771	0.48	-0.319	-	-	32.2 \pm 1.7	-0.03	-	-	-	-
Nd 2	4061.080	0.47	0.550	-	-	-	-	57.7 \pm 4.5	0.40	-	-
Nd 2	5249.580	0.98	0.200	-	-	49.7 \pm 3.0	0.45	-	-	-	-
Nd 2	5319.810	0.55	-0.140	-	-	-	-	-	-	30.3 \pm 2.3	0.96
Eu 2	4129.708	0	0.220	-	-	-	-	122.4 \pm 6.6	-0.92	-	-
Eu 2	6645.103	1.38	0.121	-	-	34.8 \pm 2.0	-0.12	-	-	-	-